This is to certify that the
dissertation entitled

COUPLED-CLUSTER METHODS FOR OPEN-SHELL
MOLECULAR AND OTHER MANY-FERMION SYSTEMS

presented by

JEFFREY R. GOUR

has been accepted towards fulfillment
of the requirements for the

Ph.D. degree in Chemistry

Major Professor's Signature

5/3/2010

Date

DATE DUE	DATE DUE	DATE DUE

5/08 K:/Proj/Acc&Pres/CIRC/DateDue.indd

COUPLED-CLUSTER METHODS FOR OPEN-SHELL MOLECULAR AND OTHER MANY-FERMION SYSTEMS

By

Jeffrey R. Gour

A DISSERTATION

Submitted to
Michigan State University
in partial fulfillment of the requirements
for the degree of

DOCTOR OF PHILOSOPHY

Chemistry

2010

one of the best methods in this category, termed CR-CC(2,3) or CR-EOMCC(2,3), in which a noniterative correction due to triple excitations is added to the CCSD or EOMCCSD energy, and its higher-order CR-CC(2,4)/CR-EOMCC(2,4) approach, in which a noniterative correction due to triple and quadruple excitations is added to the CCSD/EOMCCSD energy, to open-shell systems. In this thesis the theoretical details of all of these new methodologies as well as a sample of benchmark examples that illustrate their performance in studies of ground and excited states of open-shell molecular systems are discussed. In addition, since there is nothing in the underlying theoretical framework specific to electronic structure, the CC approaches developed in this thesis are not restricted to molecular cases and can be applied to other many-fermion systems, such as atomic nuclei. Representative examples of applications of the new CC methods developed in this thesis research in the context of quantum chemistry to studies of nuclear structure are given as well.

ABSTRACT

COUPLED-CLUSTER METHODS FOR OPEN-SHELL MOLECULAR AND OTHER MANY-FERMION SYSTEMS

By

Jeffrey R. Gour

The description of the electronic structure of radicals and other open-shell molecular systems represents a significant challenge for current theoretical methodologies. Since the low-lying electronic states of open-shell species often possess a manifestly multi-determinantal character, it is difficult to perform calculations for these systems that are both highly accurate and practical enough to be applied to a wide range of chemical problems of interest. To overcome these difficulties, we have developed two new classes of coupled-cluster (CC) methods, which are capable of accounting for the high-level electron correlation effects that characterize open-shell systems at a relatively low computational cost. The first class of methods, the active-space variants of the electron-attached (EA) and ionized (IP) equation-of-motion CC (EOMCC) theories, utilize the idea of applying a linear electron-attaching or ionizing operator to the correlated, ground-state CC wave function of an N-electron closed-shell system in order to generate the ground and excited states of the related $(N \pm 1)$-electron radical species. Furthermore, these approaches use a physically motivated set of active orbitals to *a priori* select the dominant higher-order correlation effects to be included in the calculation, which significantly reduces the costs of the high-level approximations needed for obtaining accurate results for open-shell species without sacrificing accuracy. The second class consists of the size extensive, left-eigenstate completely-renormalized (CR) CC approaches based on the biorthogonal formulation of the method of moments of CC equations, in which noniterative corrections due to higher-order excitations are added to the energies obtained with the standard CC approximations, such as CCSD (CC with singles and doubles). We have extended

ACKNOWLEDGMENT

First and foremost, I wish to thank my Ph.D. advisor, Professor Piotr Piecuch for his teaching and guidance. Thanks to his constant support and his desire to see me become the best that I can be, I not only learned a great deal about electronic structure theory, but also about how to be a better scientist. His inspiration, expectations, and patience have been key components in my growth and success as a researcher, and I am deeply grateful for all he has done for me.

I would also like to thank the rest of my guidance committee, namely Professor Katharine C. Hunt, Professor Robert Cukier, and Professor James K. McCusker, for their advice, support, and patience in overseeing my graduate study.

I also owe a great deal of gratitude to Professor Marta Włoch, a former postdoctoral research associate in the Piecuch group. When I first joined the group, it was her that took me under her wing and helped introduce me to various details regarding the research to be done. Without her I would have been lost in the beginning. Not only that, but as I grew into my own and became more independent, she turned from mentor to valuable collaborator. I was able to overcome many difficulties in my research thanks to discussions with her. Without her help, most of this research would not have been possible. I would also like to thank other members of the Piecuch group, both past and present, for the help they provided me, including Dr. Karol Kowalski, Dr. Maricris Lodriguito, Dr. Wei Li, Mr. Jesse Lutz, and Ms. Janelle Bradley.

Finally, I would like to acknowledge the National Science foundation for providing me with a Graduate Research Fellowship that supported most of my research. Additional support was also provided through several fellowships from Michigan State University (including some from the Department of Chemistry), and from the US Department of Energy. I would also like to acknowledge the MSU High Performance Computing Center for providing resources utilized for much of this research.

TABLE OF CONTENTS

LIST OF TABLES

LIST OF FIGURES

Images in this dissertation are presented in color

Chapter 1

Introduction

The single-reference coupled-cluster (CC) theory [1–5] is widely regarded as the pre-eminent *ab initio* approach for studying chemical systems. The success of the CC methodology, and its extension to excited states through the equation-of-motion (EOM) CC formalism [6–10] or its symmetry-adapted-cluster configuration-interaction (SAC-CI) [11–15] and linear response CC [16–20] analogs, lies in its ability to efficiently account for the many-electron correlation effects, the consideration of which is essential for obtaining an accurate description of a molecular system. As is true of other single-reference quantum theories based on the idea of expanding the many-electron wave function in a basis of molecular orbitals, the conventional CC methodology builds correlations into the wave function through excitations out of a single reference determinant. The advantage of the CC theory over other formalisms is that it uses an exponential excitation operator to describe these correlation effects, and so it is able to account for additional excitations, not explicitly included in the calculation, through the product or so-called 'disconnected' excitations. For instance, if one were to include only operators that create singly and doubly excited configurations out of the reference in the CC calculations, the various products of these components that result from expanding the exponential in a Taylor series lead to some triple,

quadruple, pentuple, etc. excitations also being accounted for without increasing the computer costs. As a result, the CC formalism provides an optimum balance between high accuracy and relatively low computer effort, making it an ideal theory for studying many molecular systems, and for further electronic structure theory advances.

Despite the success of approaches based on the CC theory over the years, there are a number of open issues in the CC methodology, one of which is the adequate description of open-shell systems. Due to their high reactivity and importance as chemical intermediates and magnetic systems, open-shell molecular systems, such as radicals and biradicals, play a significant role in chemistry, and as such a theoretical understanding of such species would be invaluable for many areas of chemical research. Unfortunately, such systems still represent a major challenge for modern electronic structure theories, and the CC theory is no exception. The source of the difficulty stems from the types of many-electron correlation effects that define the electronic structure of open-shell systems, particularly those where chemical bonds are stretched or broken. In general, the many-electron correlations can be classified into two types, dynamical and nondynamical. The former refers to the correlations that result from the short-range interactions whereby electrons instantaneously avoid each other, and are mathematically included in the wave function via excitations out of a reference state. As indicated by the above explanation, the CC theory has few problems with this type of correlation effects. The nondynamical (sometimes referred to as static) correlation effects, on the other hand, are long-range effects stemming from the multi-configurational character of systems having quasidegenerate electronic states (i.e. states that are close in energy). This means that for states characterized by large nondynamic correlations, a single Slater determinant is not a good reference for the many-electron wave function, and so multiple determinants must be used to create a reference function on top of which dynamical correlations can be

built. As it turns out, the majority of open-shell systems, particularly when they undergo chemical transformations or when they are electronically excited, display such a multi-reference character, and so methodologies that are capable of providing an accurate and balanced description of both dynamical and nondynamical many-electron correlation effects are needed to accurately describe them.

Unfortunately, the basic, low-order CC approaches, including the CCSD (CC with singles and doubles) approach [21–24], and its excited-state EOMCCSD [7–9], SAC-CI-SD-R [11–15], and linear response CCSD [19,20] analogs, have difficulty balancing these types of correlation effects, and thus the accurate description of the low-lying states of open-shell systems is a major challenge for such approaches. Even the popular CCSD(T) approach [25], in which a noniterative, quasiperturbative correction due to triply excited clusters is added to the energy obtained with CCSD, has problems describing such systems. Though it is known to offer an excellent description of dynamical correlation effects, which provide a near perfect description of closed-shell systems near the equilibrium geometry, CCSD(T) fails to properly account for nondynamical correlation effects. The full CCSDT (CC with singles, doubles, and triples) [26,27] and EOMCCSDT [28–30] approaches, which were recently extended to open-shell systems [31], are able to better balance the dynamical and nondynamical correlation effects, and thus are capable of producing high quality results for many open-shell situations, but the computational costs of such schemes are extremely high, restricting their use to small systems with only a few light atoms (a dozen or so correlated electrons). In contrast, CCSD(T) can nowadays be routinely applied to systems with up to about 100 correlated electrons and a few hundred basis functions within a canonical formulation, and one can go to systems with hundreds of correlated electrons and thousands of basis functions when one uses the local correlation formulation [32–44]. Thus in order to accurately study a wide range of open-shell problems of interest, alternatives to the standard single-reference CC methods that

are not much more expensive than CCSD(T) are needed.

One of the main reasons that properly accounting for both dynamical and nondynamical correlations within the standard CC truncation hierarchy requires high-level, and computationally expensive, approximations is the single-reference nature of these schemes. Indeed single determinants are bad starting points for the description of manifestly multi-reference states, such as those found in open-shell systems. As a result, the only way to properly describe such systems within the standard CC truncations is to compensate for the bad start and account for nondynamical correlations dynamically, i.e. through the inclusion of higher-order excitation effects. Based on this analysis, an obvious solution is to simply start from a better reference state that accurately accounts for the nondynamical correlations in the system, leaving only the remaining dynamical correlations to be described by the exponential excitation operator. This is the basic idea behind the genuine multi-reference (MR) CC theories of either the valence-universal [45,46] or state-universal [47] type, for which an exponential excitation operator is applied to a multi-determinantal reference in order to generate the wave functions for the desired many-electron states. At first glance, this would seem like the ideal solution for open-shell systems, as it properly balances nondynamical (through the multi-determinantal reference state) and dynamical (through the exponential ansatz) correlations without the use of high-order excitations in the wave operator that transforms the zero-order reference states into the target wave functions. Unfortunately, these formalisms are not without their own problems. In particular, the genuine MRCC approaches of the above two types face issues related to unphysical [48–50] and singular [48,49,51–54] solutions, intruder states [48,49,52], and intruder solutions [48,50], all of which can cause convergence problems as well as other complications in the MRCC calculations and the ensuing analysis of the results. Furthermore, there are potential difficulties related to the size and choice of the multi-dimensional reference space for certain types of systems. Indeed, the

configurations included in the complete multi-dimensional reference space are generally determined via all possible rearrangements of the occupancies of a selected set of molecular orbitals composing what is referred to as the *active space*. Unfortunately, the size of such a reference space grows factorially with the number of active orbitals and electrons, and so choosing a proper active space for a given system can be a difficult task requiring a great deal of expertise. In fact, it is possible that for some systems, such as those containing transition metal atoms that have a large degree of quasidegeneracy due to the open f or g shells, the appropriate active space may result in the MRCC calculation being prohibitively expensive. In addition, the complicated formalism associated with the genuine MRCC theories makes it difficult to implement highly-efficient, general-purpose computer codes that can be applied to a wide range of open-shell problems. Recently, there has been a great deal of progress and renewed interest in overcoming the above issues and further developing both the valence-universal and state-universal MRCC approaches [48,55–67]. However, despite these developments, we feel that, due to the complications arising from a genuine MR formalism, it would be ideal to investigate the possibility of overcoming the difficulties facing the standard single-reference CC schemes in calculations involving open-shell systems within the formally simpler single-reference framework.

One methodology that may provide a mechanism by which to address the challenges posed by open-shell systems within a single-reference formalism is that of the electron-attached (EA) [68–70] and ionized (IP) [71–77] EOMCC theories, and the analogous and historically older EA and IP SAC-CI methods [78–84]. The basic idea behind these methodologies is to construct the ground- and excited-state wave functions of an $(N \pm 1)$-electron system by applying a linear electron-attaching or ionizing operator to the correlated CC ground state of an N-electron closed-shell system. This wave function definition leads to a natural and computationally convenient formalism for studying ground and excited states of open-shell systems, such

as radicals, that differ from the corresponding closed-shell species by one electron. Furthermore, the use of the closed-shell N-electron reference state in calculations for the $(N \pm 1)$-electron systems ensures that the resulting wave functions are automatically orthogonally spin-adapted, and thus EA- and IP-EOMCC approaches do not suffer from the spin contamination issues that may arise in the traditional open-shell implementations of the conventional CC or EOMCC approximations that rely on the unrestricted Hartree-Fock (UHF) or restricted open-shell HF (ROHF) reference determinants. Unfortunately, as was the case for the regular CC and EOMCC methodologies, the basic, low-order EA- and IP-EOMCC approaches, which include the EA-EOMCCSD [68,69] and IP-EOMCCSD [71–74] approximations, and their EA and IP SAC-CI analogs truncated at 2-particle-1-hole ($2p$-$1h$) and 2-hole-1-particle ($2h$-$1p$) excitations [78–84], have significant difficulties with describing the excitation spectra of most radicals [68, 84–89]. One can address these deficiencies through the inclusion of higher-order components of the electron-attaching or ionizing operators, such as the $3p$-$2h$ or $3h$-$2p$ excitations, which gives rise to schemes such as EA-EOMCCSDT [70], IP-EOMCCSDT [75, 76], EA-EOMCCSD($3p$-$2h$) [85–87], IP-EOMCCSD($3h$-$2p$) [85–87], EA-EOMCCSDTQ [90] and IP-EOMCCSDTQ [90] as well as their less complete SAC-CI analogs [81–83, 88]. Though these schemes are all capable of providing high quality results for radical systems, the associate computational costs are usually prohibitively high, restricting their use to relatively small systems.

Given how well suited the EA- and IP-EOMCC methodologies, as well as their multiply-attached and multiply-ionized counterparts (e.g., the doubly electron-attached (DEA) and doubly ionized (DIP) EOMCC approaches [91–93]) are for studying radicals and other open-shell systems, it has been our goal to develop a new formulation of these schemes that maintains all the good attributes of such methods while avoiding the high computer costs associated with including higher-than $2p$-$1h/2h$-$1p$

effects. An idea for how to develop such a formulation is provided by the so-called active-space CC [94–108] and EOMCC [28, 29, 109–111] approaches. In these and related schemes [112–119], the multi-reference concept of active orbitals is used to *a priori* select the dominant triply and other higher-than-doubly excited clusters in the standard CC/EOMCC calculations. In this way, the computational costs associated with the high-order CC/EOMCC approximations are greatly reduced, since the vast majority of the higher-than-double excitations are not included in the calculations, and the characteristic high accuracy of the high-order CC/EOMCC schemes is maintained at the same time. Indeed, the lowest-order active-space CC methods, such as SSMRCCSD(T) (state-selective MRCC with singles doubles and active-space triples) [97–105] or CCSDt [106–108], and their excited-state EOMCCSDt analog [28, 29, 109], have shown promising results, even for challenging cases involving bond breaking [95, 96, 100, 101, 104–108] or excited states dominated by two-electron transitions [28, 29, 109–111]. Thus, it would seem that combining the active-space CC methodology with the EA- and IP-EOMCC formalisms is a natural mechanism for developing an approach capable of performing highly accurate calculations for radicals at a relatively low computational cost. The development and benchmarking of such active-space EA- and IP-EOMCC approaches, in which higher-than $2p$-$1h$ and higher-than $2h$-$1p$ components of the electron-attaching and ionizing operators, respectively, are selected through the use of a suitably defined set of active orbitals, is one of the primary goals of this dissertation, and is discussed in Chapter 2.

Despite the initial successes and considerable promise of the active-space EA- and IP-EOMCC formalisms in studies of the excitation spectra of open-shell systems developed as part of this work, we must remember that no method is bullet-proof. Indeed, the use of the multi-reference concept of active orbitals means that these methods are not 'black-box'; they require some *a priori* analysis by the user of the nature of the electronic states of interest before performing the calculation. Though

this difficulty is not nearly as severe in the active-space methods as it is in the genuine MRCC theories, primarily due to the fact that the computer costs of the active-space schemes, including the EA- and IP-EOMCC approaches developed in this thesis research, scale polynomially with the size of the active space rather than exponentially, they are still somewhat more difficult to use than the conventional single-reference CC methods. Furthermore, the structure of these theories is such that they are not generally applicable to all types of open-shell systems. Indeed if one wants to study open-shell systems that are M-electrons away from some closed-shell system, then a different hierarchy of methods must be used for each value of M. The EA-EOMCC and IP-EOMCC schemes described in this dissertation are applicable to the case of $M = 1$, which includes the majority of radicals and positively or negatively charged ions of closed-shell atoms and molecules. If one wants to examine systems that are two electrons away from a closed-shell, including biradicals, schemes such as the DEA- and DIP-EOMCC methods and their active-space variants [85] must be implemented and applied, etc. Furthermore, the applicability of approaches based on adding or removing M electrons from a closed-shell species to open-shell systems where $M > 2$ may become questionable since as one moves further away from the closed-shell system, the electronic similarities between the two decrease. As a result of these potential complications, alternative, and perhaps even complimentary, methods for studying open-shell systems would be useful. Indeed, part of the success and popularity of the CCSD(T) approach is that it is able to produce highly accurate results for systems primarily described by dynamical correlations with both reasonably low computational costs and an easy-to-use black-box nature. It is this nature that has allowed CCSD(T) to be so easily accessible to both experts and non-experts alike. Given these remarks, the development of a robust formalism that maintains the computational costs and ease-of-use of CCSD(T) while better balancing both dynamical and nondynamical correlation effects than CCSD(T) would be a good alternative to

active-space EA- and IP-EOMCC methods for accurate studies of open-shell systems.

An excellent candidate for such a methodology is presented by the completely renormalized (CR) CC and EOMCC methods [120–140], particularly the recent variants based on the so-called biorthogonal method of moments of coupled-cluster (MMCC) equations [133–140]. These approaches represent a new class of CC schemes based on adding noniterative corrections to the standard CC or EOMCC energies, which are designed to improve on the performance of CCSD, CCSD(T), and EOMCCSD in situations involving larger nondynamical correlations while maintaining similar costs and ease of use. Furthermore, these methods have a natural hierarchy for constructing corrections for truncations besides CCSD and due to higher-than-triple excitations, as well as a natural extension to excited states. One of the most promising methods of this type is the CR-CC(2,3) approach [133–140], which, in analogy to CCSD(T), is based on adding a noniterative correction due to triple excitations to the ground-state CCSD energy. Various applications of this scheme have revealed that it is capable of producing high quality results in studies of single bond breaking and biradical structures on singlet potential energy surfaces [133–135, 137, 141–147], while offering excellent values for activation barriers in thermochemical kinetics studies [148, 149]. Indeed, for situations where the structure is dominated by dynamical correlations, CR-CC(2,3) is as accurate as CCSD(T), but, unlike CCSD(T), it maintains these high accuracies as one moves onto structures characterized by stronger nondynamical correlation effects, such as biradicals or the bond-breaking regions of a potential energy surface. This success for singlet states characterized by large nondynamic correlation effects begs the question of whether CR-CC(2,3), and its excited-state CR-EOMCC(2,3) analog, would perform equally well in calculations involving open-shell systems, such as bond breaking and excited states of radicals, and singlet-triplet gaps in biradicals. In addition the question as to how well higher-level CR-CC schemes, such as the CR-CC(2,4) approach which corrects the CCSD energy

for the effects of both triples and quadruples, would perform. To address these questions, the CR-CC(2,3) scheme was extended to general open-shell systems [138] and excited states [135, 140], and a general purpose CR-CC(2,4) code, applicable to both closed- and open-shell systems, was implemented as part of this research. The details of these methodologies as well as the results of selected applications to open-shell systems, reported in [138–140, 150, 151], are presented in Chapter 3.

Up until this point, all of the discussion regarding the CC theory and its applications to open-shell systems has been in the context of quantum chemistry. However, there is nothing intrinsic in the CC wave function ansatz, nor in the formulation of the various CC methods studied in this work, that restricts their use to chemical systems. Indeed, the underlying physics governing any many-fermion problem, whether they be chemical, nuclear, or condensed matter to name a few, is fundamentally the same, and it is only the form of the potential in which the fermions move that varies. In fact, though the major developments of the methodology have occurred in the context of quantum chemistry, the CC theory was actually first suggested within the field of nuclear physics [1, 2], and it is our belief that a reintroduction of CC approaches within nuclear physics would benefit the study of the structure of nuclei. Indeed, two of the main techniques for studying nuclear structure, namely the Green's function Monte Carlo [152] and no-core shell-model [153–156], though successful in providing highly accurate results, suffer from extremely high computational costs and so are limited to light nuclei with a dozen or so nucleons at best. In order to study medium-mass and heavy nuclei, methods that better balance accuracy and computational cost are needed, and, as discussed above, such a balance is precisely the origin of the success of the CC theory in quantum chemistry. Furthermore, due to the fact that the shell structure of nuclei is very similar to that of atoms and thus displays a large amount of degeneracy, the majority of nuclei are open-shell many-fermion systems characterized by large nondynamical correlation effects. As a result, the

methods developed and studied in this work, which are designed specifically for properly describing open-shell systems while requiring reasonably low computer costs, are particularly well-suited for studies of nuclear structure. Thus, as a final component of this dissertation, selected results of CC studies of the ground- and excited-state energies of various nuclei [157–171], with a focus on the results obtained by the author of this thesis [157, 161–170], are presented and discussed in Chapter 4.

Chapter 2

Active-Space Coupled-Cluster Methods for Open-Shell Systems

In this chapter, the extension of the active-space CC methodology to the EA- and IP-EOMCC formalisms, which results in new classes of low-cost, highly accurate *ab initio* approaches for ground- and excited states of open-shell systems, is discussed. Section 2.1 provides the theoretical details of these approaches, including an overview of the original EA- and IP-EOMCC theories and the details of the new active-space extensions of these methods, as described in [85–87], as well as a description of our recently developed highly efficient computer implementations of the most basic active-space EA- and IP-EOMCC schemes [87]. Section 2.2 provides examples of several benchmark calculations, taken from [85–89,140], in order to illustrate the performance of the active-space EA- and IP-EOMCC approximations developed in this work.

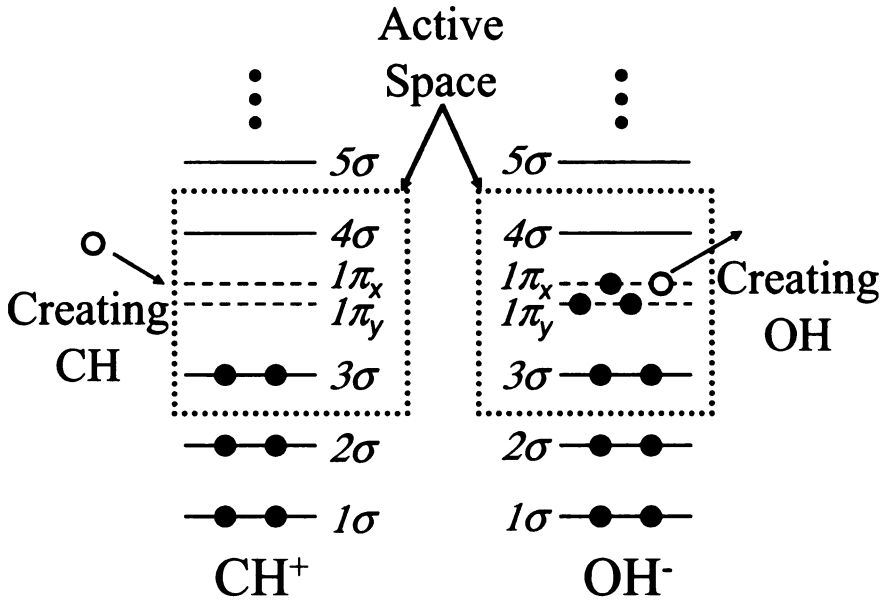

Figure 2.1: Pictorial illustration of the generation of the CH and OH radicals from the closed-shell CH^+ and OH^- ions, respectively.

2.1 Theory and Computer Implementation

2.1.1 The Electron-Attached and Ionized Equation-of-Motion Coupled-Cluster Theories

The key idea behind the EA- and IP-EOMCC methodologies is that, rather than treating the open-shell molecular $(N \pm 1)$-electron system of interest directly, one instead generates the ground and excited states of it by adding an electron to or removing an electron from the related N-electron closed-shell system. This idea is illustrated in Figure 2.1, which gives a schematic representation of generating the CH and OH radicals from the closed-shell CH^+ and OH^- ions, respectively.

This idea can be expressed more rigorously by using the following form for the electronic wave function of the μth state of an $(N+1)$- or $(N-1)$-electron system (where $\mu = 0$ corresponds to the ground state and $\mu > 0$ corresponds to the excited

states):

$$|\Psi_\mu^{(N\pm1)}\rangle = R_\mu^{(N\pm1)}|\Psi_0\rangle. \tag{2.1}$$

In this equation, $R_\mu^{(N+1)}$ and $R_\mu^{(N-1)}$ are the electron-attaching and ionizing operators, respectively, whereas $|\Psi_0\rangle$ is the correlated ground-state wave function of the N-electron closed-shell system, which is defined through the exponential ansatz of the single-reference CC theory,

$$|\Psi_0\rangle = e^T|\Phi\rangle. \tag{2.2}$$

In the above equation, $|\Phi\rangle$ is a closed-shell N-electron reference determinant (e.g., the restricted Hartree Fock (RHF) reference) and T is the cluster operator of the standard single-reference CC theory,

$$T = \sum_{n=1}^{M_T} T_n, \quad T_n = \left(\frac{1}{n!}\right)^2 t_{a_1\ldots a_n}^{i_1\ldots i_n} a^{a_1}\ldots a^{a_n} a_{i_n}\ldots a_{i_1}, \tag{2.3}$$

where in the exact case $M_T = N$ while in the approximate approaches $M_T < N$. For instance, in the basic CCSD approach $M_T = 2$, so the cluster operator $T^{(\mathrm{CCSD})}$ is given by

$$T^{(\mathrm{CCSD})} = T_1 + T_2 = t_a^i a^a a_i + \tfrac{1}{4} t_{ab}^{ij} a^a a^b a_j a_i. \tag{2.4}$$

Throughout this paper we employ the usual notation where $i, j, \ldots$ $(a, b, \ldots)$ refer to the spin-orbitals occupied (unoccupied) in the reference determinant $|\Phi\rangle$, a^p (a_p) are the creation (annihilation) operators associated with the spin-orbital basis set $\{|p\rangle\}$, and the coefficients $t_{a_1\ldots a_n}^{i_1\ldots i_n}$ entering Eq. (2.3) are the usual cluster amplitudes. In addition, whenever possible, we make use of the Einstein summation notation over repeated upper and lower indices.

The electron-attaching and ionizing operators introduced in Eq. (2.1), $R_\mu^{(N+1)}$

and $R_\mu^{(N-1)}$, respectively, are defined as

$$R_\mu^{(N+1)} = \sum_{n=0}^{M_R} R_{\mu,(n+1)p\text{-}nh} \tag{2.5}$$

and

$$R_\mu^{(N-1)} = \sum_{n=0}^{M_R} R_{\mu,(n+1)h\text{-}np} \tag{2.6}$$

where the $((n+1)p\text{-}nh)$ component of $R_\mu^{(N+1)}$ and the $((n+1)h\text{-}np)$ component of $R_\mu^{(N-1)}$ are given by

$$R_{\mu,(n+1)p\text{-}nh} = \frac{1}{n!(n+1)!} r_{aa_1\ldots a_n}^{i_1\ldots i_n} a^a a^{a_1} \ldots a^{a_n} a_{i_n} \ldots a_{i_1} \tag{2.7}$$

and

$$R_{\mu,(n+1)h\text{-}np} = \frac{1}{n!(n+1)!} r_{a_1\ldots a_n}^{ii_1\ldots i_n} a^{a_1} \ldots a^{a_n} a_{i_n} \ldots a_{i_1} a_i, \tag{2.8}$$

and where $M_R = N$ in the exact case and $M_R < N$ in the approximate schemes. Equation (2.7) reveals that the $((n+1)p\text{-}nh)$-components of $R_\mu^{(N+1)}$ can be viewed as operators which create a particle in an unoccupied spin-orbital and, for $n > 0$, simultaneously cause an excitation of n electrons from occupied spin-orbitals into unoccupied spin-orbitals. Similarly, from Eq. (2.8) we see that the $((n+1)h\text{-}np)$-components of $R_\mu^{(N-1)}$ can be viewed as operators which remove one of the electrons from an occupied spin-orbital and, for $n > 0$, simultaneously excite n of the remaining electrons.

By substituting the EA- and IP-EOMCC wave function ansätze, Eqs. (2.1) and (2.2) in which $M_R \leq M_T$, into the time-independent Schrödinger equation, one obtains the following non-Hermitian eigenvalue problem:

$$(\bar{H}_{N,\text{open}} R_\mu^{(N\pm1)})_C|\Phi\rangle = \omega_\mu^{(N\pm1)} R_\mu^{(N\pm1)}|\Phi\rangle. \tag{2.9}$$

Here

$$\bar{H}_{N,\text{open}} = (H_N e^T)_{C,\text{open}} = e^{-T} H_N e^T - (H_N e^T)_{C,\text{closed}} \tag{2.10}$$

is the similarity-transformed Hamiltonian of the CC theory in the normal-ordered form relative to the Fermi vacuum $|\Phi\rangle$, the subscripts "open", "closed", and C refer to the open (i.e., having external lines), closed (i.e. having no external lines), and connected parts of a given operator expression, and the eigenvalues obtained from solving Eq. (2.9) are the energy differences given by

$$\omega_\mu^{(N\pm1)} = E_\mu^{(N\pm1)} - E_0^{(N)}, \tag{2.11}$$

where $E_\mu^{(N\pm1)}$ is the total energy of the μth state of the $(N \pm 1)$-electron system and $E_0^{(N)}$ is the ground-state energy of the N-electron reference system. Thus in the EA- and IP-EOMCC formalisms, the energies of the ground- and excited-state wave functions of an $(N \pm 1)$-electron system are obtained by diagonalizing the similarity-transformed Hamiltonian $\bar{H}_{N,\text{open}}$, calculated using the cluster operator of the related N-electron closed-shell system, in the subspace of $\mathscr{H}^{(N+1)}$ spanned by the determinants $|\Phi^a\rangle = a^a|\Phi\rangle$ and $|\Phi^{aa_1\ldots a_n}_{i_1\ldots i_n}\rangle = a^a a^{a_1}\ldots a^{a_n} a_{i_n}\ldots a_{i_1}|\Phi\rangle$ $(n = 1,\ldots,M_R)$ in the EA-EOMCC case, and in the subspace of $\mathscr{H}^{(N-1)}$ spanned by the determinants $|\Phi_i\rangle = a_i|\Phi\rangle$ and $|\Phi_{ii_1\ldots i_n}^{a_1\ldots a_n}\rangle = a^{a_1}\ldots a^{a_n} a_{i_n}\ldots a_{i_1} a_i|\Phi\rangle$ $(n = 1,\ldots,M_R)$ in the IP-EOMCC case. Here, $\mathscr{H}^{(N+1)}$ and $\mathscr{H}^{(N-1)}$ are the relevant $(N+1)$- and $(N-1)$-electron subspaces of the Fock space, respectively.

There are several advantages to using this hierarchical approach for studying open-shell systems, in which we construct the $(N \pm 1)$-electron wave functions by adding an electron to or removing an electron from the N-electron closed-shell species, over the more traditional idea of performing calculations directly on the $(N \pm 1)$-electron system of interest. Since the EA- and IP-EOMCC formalisms start from a closed-shell reference system, for which the correlation effects are much easier to describe and are

trivial to capture with the CC theory, these methodologies are able to account for the high-level correlation effects needed to describe the low-lying states of valence systems such as radicals in a much more efficient manner. For example, consider an $(N+1)$-electron radical (e.g., the CH radical shown in Figure 2.1). As illustrated later, if one were to perform the traditional CC calculations, which do not change the number of electrons, directly for this radical, one would have to include the effects of triple excitations in the calculation in order to obtain an accurate description of the corresponding low-lying states. It can be shown, however, that some of the triple excitations relative to the $(N+1)$-electron reference determinant are $3p$-$2h$ excitations relative to the N-electron reference $|\Phi\rangle$, while the remaining triple excitations correspond to $4p$-$3h$ excitations from $|\Phi\rangle$. It turns out that as long as the N-electron system is a good closed-shell, then most of the important triples, at least within the spectroscopic region, are of the $3p$-$2h$ type. Since the number of $3p$-$2h$ terms is less than the number of triples ($3p$-$3h$ terms), the use of the EA-EOMCC formalism allows us to essentially describe the same correlation effects at a reduced computational effort. Similar statements also apply to the IP-EOMCC methodology.

Another advantage of the EA- and IP-EOMCC approaches is that they are based on diagonalizing the similarity-transformed Hamiltonian of a closed-shell system, which commutes with the S^2 and S_z operators. Because of this, the resulting eigenstates are automatically orthogonally spin-adapted, and so by using the EA-EOMCC and IP-EOMCC formalisms one can avoid the spin-contamination issues that may plague the standard spin-orbital based open-shell CC/EOMCC implementations that utilize the ROHF or UHF references (particularly, the latter ones).

When constructing approximate EA-EOMCC and IP-EOMCC schemes, special attention must be given to the relationship between the truncation in the cluster operator T and the truncation in the electron-attaching and ionizing operators $R_\mu^{(N+1)}$ and $R_\mu^{(N-1)}$, respectively. For the approximate EA-EOMCC and IP-EOMCC meth-

ods, the connected form of the eigenvalue problem displayed in Eq. (2.9), which guarantees the size intensivity [20] of the eigenvalues, is only valid when the condition that $M_R \leq M_T$ is satisfied [10]. Thus, if we wish to retain the size intensivity of the "excitation" energies $\omega_\mu^{(N\pm1)}$, Eq. (2.11), we must ensure that any truncation scheme applied to the EA-EOMCC and IP-EOMCC theories satisfies this restriction on M_R and M_T. Currently, the most common EA-EOMCC and IP-EOMCC approximations, as implemented in [68, 70, 75, 90], satisfy this criterion by setting $M_R = M_T - 1$. The most basic examples in this category are the conventional EA-EOMCCSD [68, 69] and IP-EOMCCSD [71–74] methods (referred to in this work as EA-EOMCCSD($2p$-$1h$) and IP-EOMCCSD($2h$-$1p$)), where $M_R = 1$ and $M_T = 2$. Other examples include the higher-order EA-EOMCCSDT [70] and IP-EOMCCSDT [75, 76] schemes, for which $M_R = 2$ and $M_T = 3$, and the recently implemented EA- and IP-EOMCCSDTQ approaches [90], for which $M_R = 3$ and $M_T = 4$. As part of this work, we developed implementations of the EA-EOMCC and IP-EOMCC methodologies that make use of an alternate truncation scheme utilizing the less limiting condition $M_R = M_T$, which still satisfies the more general condition of Piecuch and Bartlett [10], i.e. $M_R \leq M_T$. The recently developed EA-EOMCCSD($3p$-$2h$) and IP-EOMCCSD($3h$-$2p$) approaches [85–87], in which $M_R = M_T = 2$, belong to this class of approximations.

The advantage of the EA-EOMCCSD($3p$-$2h$) and IP-EOMCCSD($3h$-$2p$) methods of [85–87] over the EA-EOMCCSDT and IP-EOMCCSDT methods of [70, 75, 76] is that they include the important $3p$-$2h$ and $3h$-$2p$ components in the electron-attaching and ionizing operators, respectively, without suffering from the expensive $n_o^3 n_u^5$ scaling characterizing the ground-state CCSDT calculations required by EA-EOMCCSDT and IP-EOMCCSDT. Here, n_o (n_u) is the number of spin-orbitals occupied (unoccupied) in the reference determinant $|\Phi\rangle$. As it turns out, in most cases the $3p$-$2h$ and $3h$-$2p$ effects in $R_\mu^{(N+1)}$ and $R_\mu^{(N-1)}$, respectively, play a much more

significant role than the triply excited (T_3) components of the cluster operator T, and it is usually not necessary to include the T_3 clusters in T until the $4p$-$3h$ and $4h$-$3p$ effects become important (see [85–88, 172] for further discussion, analysis, and several numerical examples). Thus, in many situations, particularly those involving electronic excitations in radicals [85–88], there is a lesser need for using T_3 in the EA-EOMCC/IP-EOMCC calculations at the $3p$-$2h$/$3h$-$2p$ level of theory. In all these cases, one can safely rely on our EA-EOMCCSD($3p$-$2h$) and IP-EOMCCSD($3h$-$2p$) approaches, in which $T = T_1 + T_2$, rather than their more expensive EA-EOMCCSDT and IP-EOMCCSDT counterparts of [70, 75, 76], in which $T = T_1 + T_2 + T_3$. On the other hand, even the simplified EA- and IP-EOMCC models with $3p$-$2h$ and $3h$-$2p$ excitations, such as the EA-EOMCCSD($3p$-$2h$) and IP-EOMCCSD($3h$-$2p$) approaches of [85–87], have limited use due to the $n_o^2 n_u^5$ or $n_o^3 n_u^4$ iterative steps involved in the diagonalization of the similarity-transformed Hamiltonian in the space of $|\Phi^a\rangle$, $|\Phi^{ab}_{j}\rangle$, and $|\Phi^{abc}_{jk}\rangle$ or $|\Phi_i\rangle$, $|\Phi_{ij}^{b}\rangle$, and $|\Phi_{ijk}^{bc}\rangle$ determinants, respectively. This prompts the need for the development of EA- and IP-EOMCC approaches in which the computer costs of incorporating the $3p$-$2h$, $3h$-$2p$, and other higher than $2p$-$1h$ and $2h$-$1p$ excitations are substantially reduced. The key idea is to reduce the computer costs of EA- and IP-EOMCC methods with higher than $2p$-$1h$ and $2h$-$1p$ excitations without sacrificing the accuracy characterizing these higher-level schemes, which is the basis for the active-space EA- and IP-EOMCC approaches discussed in the next section.

Before moving on, it should be emphasized that, up to some details with respect to approximations and computer implementation, the above equations also describe the historically older electron-attached and ionized variants of the SAC-CI approach of Nakatsuji et al. [78–83]. As a result of these mathematical similarities, the developments in this work, including the extension of the active-space CC/EOMCC methodologies to electron-attached and ionized states, apply to the SAC-CI approach as well as the EA- and IP-EOMCC methods. Furthermore, as will be seen in Section (2.2),

we make direct use of the SAC-CI scheme in order to study the effects of higher-than $3p$-$2h$ and higher-than $3h$-$2p$ correlation effects in studies of radical systems [88].

2.1.2 The Active-Space EA- and IP-EOMCC Methodologies

The EA-EOMCC and IP-EOMCC theories provide a convenient formalism for studying radicals and other open-shell systems around closed shells, but they are not without their limitations. It has been shown, for example, that in order to get an accurate description of the excitation spectra [85–88, 172] and the ground- and excited-state potential energy surfaces [86,88] of radical species, one must include higher than $2p$-$1h$ and higher than $2h$-$1p$ components in the electron-attaching and ionizing operators (see, e.g., [82, 88] for similar findings within the context of SAC-CI). Unfortunately, as mentioned in Section 2.1.1, the inclusion of such terms can significantly increase the computational costs involved, restricting the use of the resulting schemes to relatively small systems. One approach for reducing the costs of including the higher than $2p$-$1h$ and higher than $2h$-$1p$ effects, without sacrificing the accuracy associated with such terms, is to use the active-space variants of the EA-EOMCC and IP-EOMCC methodologies, which were developed as part of this work [85–87], and which are particularly well suited for calculations of the electronic excitations in radicals.

It is well-known that the radical formation process is generally dominated by a small subset of orbitals. Indeed a radical can often be obtained, at least at the zero-order level, by attaching an electron to one of the lowest-energy unoccupied orbitals or removing an electron from one of the highest-energy occupied orbitals of the related closed-shell system (see Figure 2.1). The fundamental idea of the active-space EA- and IP-EOMCC approaches is to use these dominant orbitals (which in analogy to the genuine multi-reference approaches can be viewed as active orbitals) to *a priori* select the most important higher than $2p$-$1h$ and higher than $2h$-$1p$ components of the electron-attaching and ionizing operators that enter into the EA-EOMCC

and IP-EOMCC formalisms, neglecting the rest in the calculation. In this way, one considerably reduces to the dimension of the resulting eigenvalue problem while still maintaining the high accuracy characterizing the higher-level EA- and IP-EOMCC approximations.

We begin our formal discussion of the active-space EA-EOMCC and IP-EOMCC methods by dividing the available spin-orbitals into four disjoint groups: core spin-orbitals (**i**, **j**, **k**, ...), active spin-orbitals occupied in the reference determinant $|\Phi\rangle$ (**I**, **J**, **K**, ...), active spin-orbitals unoccupied in the reference $|\Phi\rangle$ (**A**, **B**, **C**, ...), and virtual spin-orbitals (**a**, **b**, **c**, ...). We continue to label occupied and unoccupied spin-orbitals by the italic characters i, j, k, ...and a, b, c, ...respectively, if their active/inactive character is not specified. This orbital classification scheme can be used to redefine the electron-attaching and ionizing operators, $R_\mu^{(N+1)}$ and $R_\mu^{(N-1)}$, respectively, in order to restrict the excitations that are included in the active-space calculations. For example, in the most basic active-space EA- and IP-EOMCC approximations, which can be thought of as the active-space variants of the EA-EOMCCSD(3p-2h) and IP-EOMCCSD(3h-2p) schemes discussed in Section 2.1.1 and which we refer to as EA-EOMCCSDt and IP-EOMCCSDt, we define the electron-attaching and ionizing operators as

$$R_\mu^{(N+1)}(\text{CCSDt}) = R_{\mu,1p} + R_{\mu,2p\text{-}1h} + r_{\mu,3p\text{-}2h}, \tag{2.12}$$

and

$$R_\mu^{(N-1)}(\text{CCSDt}) = R_{\mu,1h} + R_{\mu,2h\text{-}1p} + r_{\mu,3h\text{-}2p}. \tag{2.13}$$

Here the $R_{\mu,(n+1)p-nh}$ and $R_{\mu,(n+1)h-np}$ terms with $n = 0$ or 1 are defined as in Eqs. (2.7) and (2.8) while the "little r" 3p-2h and 3h-2p components are defined by:

$$r_{\mu,3p\text{-}2h} = \sum_{j>k,\mathbf{A}<b<c} r_{\mathbf{A}bc}^{jk} a^{\mathbf{A}} a^b a^c a_k a_j \tag{2.14}$$

and

$$r_{\mu,3h\text{-}2p} = \sum_{\mathbf{I}>j>k,b<c} r^{\mathbf{I}jk}_{bc} a^b a^c a_k a_j a_{\mathbf{I}}. \tag{2.15}$$

Using these definitions of $R_\mu^{(N+1)}$ and $R_\mu^{(N-1)}$, we solve Eq. (2.9) in the subspace of $\mathscr{H}^{(N+1)}$ spanned by the $|\Phi^a\rangle$, $|\Phi^{ab}_j\rangle$, and $|\Phi^{\mathbf{A}bc}_{jk}\rangle$ determinants (the EA-EOMCC case) or in the subspace of $\mathscr{H}^{(N-1)}$ spanned by the $|\Phi_i\rangle$, $|\Phi_{ij}{}^b\rangle$, and $|\Phi_{\mathbf{I}jk}{}^{bc}\rangle$ determinants (the IP-EOMCC case). As immediately implied by the above definitions, the EA- and IP-EOMCCSDt schemes provide significant computational savings relative to the full inclusion of the $3p$-$2h$ and $3h$-$2p$ components in the electron-attaching and ionizing operators. In particular, the EA-EOMCCSDt approach reduces the expensive $n_o^2 n_u^5$ steps required to diagonalize $\bar{H}_{N,\text{open}}$ in the EA-EOMCCSDT and EA-EOMCCSD($3p$-$2h$) approximations to the CCSD-like $N_u n_o^2 n_u^4$ steps, where N_u ($< n_u$) is the number of active orbitals unoccupied in the reference determinant $|\Phi\rangle$. Similarly, the IP-EOMCCSDt method reduces the $n_o^3 n_u^4$ steps required to diagonalize $\bar{H}_{N,\text{open}}$ in the IP-EOMCCSDT and IP-EOMCCSD($3p$-$2h$) approximations to the CCSD-like $N_o n_o^2 n_u^4$ steps, where N_o ($< n_o$) is the number of active orbitals occupied in $|\Phi\rangle$.

The actual form of the similarity-transformed Hamiltonian, $\bar{H}_{N,\text{open}}$, that is diagonalized in the active-space EA-EOMCC and IP-EOMCC methods depends on the truncation scheme for the cluster operator T used in the parent approximation. For instance, if one were to derive the EA-EOMCCSDt and IP-EOMCCSDt methods from the EA-EOMCCSDT and IP-EOMCCSDT schemes of [70,75,76], than the similarity-transformed Hamiltonian of the underlying CCSDt approach [95–98, 101, 106–108], $\bar{H}^{(\text{CCSDt})}_{N,\text{open}} = (H_N e^{T^{(\text{CCSDt})}})_{C,\text{open}}$, would be used. The cluster operator defining the CCSDt approximation is given by

$$T^{(\text{CCSDt})} = T_1 + T_2 + t_3, \tag{2.16}$$

with

$$t_3 = \sum_{\mathbf{I}>j>k,\mathbf{A}<b<c} t^{\mathbf{I}jk}_{\mathbf{A}bc}\, a^{\mathbf{A}} a^b a^c a_k a_j a_{\mathbf{I}}. \tag{2.17}$$

This approach reduces the costly $n_o^3 n_u^5$ steps characterizing the underlying CCSDT calculation required by the EA-EOMCCSDT and IP-EOMCCSDT approximations to the much more manageable $N_o N_u n_o^2 n_u^4$ steps of CCSDt. However, since there are many cases where there is little need for including T_3 at the $3p$-$2h$/$3h$-$2p$ level of the EA/IP EOMCC theory (as discussed in Section 2.1.1), it is possible to further reduce these costs by using the simpler and less expensive EA-EOMCCSD($3p$-$2h$) and IP-EOMCCSD($3h$-$2p$) schemes as parent approximations for the active-space work, as is done throughout this thesis. The resulting EA-EOMCCSDt and IP-EOMCCSDt methods, the efficient implementation of which is discussed in the next section, diagonalize the similarity-transformed Hamiltonian of the CCSD approach,

$$\bar{H}^{(\mathrm{CCSD})}_{N,\mathrm{open}} = (H_N e^{T_1+T_2})_{C,\mathrm{open}} = e^{-T_1-T_2} H_N e^{T_1+T_2}. \tag{2.18}$$

As a result, the underlying ground-state calculation for the N-electron system, which generates the cluster amplitudes used in constructing $\bar{H}^{(\mathrm{CCSD})}_{N,\mathrm{open}}$, requires only the inexpensive $n_o^2 n_u^4$ steps associated with the standard CCSD method. Given that it is generally true that $N_o < n_o$ and $N_u \ll n_u$, the final result is that the EA- and IP-EOMCCSDt schemes developed in this work have computer costs that are only a small prefactor times those of the relatively inexpensive CCSD approach. For example, one can obtain excellent EA-EOMCCSDt results for the ground and excited states of the CH radical using only the $1\pi_x$, $1\pi_y$, and 4σ valence orbitals of CH^+ as active orbitals ($N_u = 3$), which is much less than the typical numbers of unoccupied orbitals that one would have to use in the parent EA-EOMCCSD($3p$-$2h$) calculations for CH. Similarly, one obtains the excellent IP-EOMCCSDt results for OH using only the valence orbitals of OH^- as active orbitals, which are fewer in number than all

occupied orbitals. This reflects on the simple physical picture shown in Figure 2.1 where the low-lying states of CH and OH are dominated by attaching an electron to or removing an electron from one of the valence orbitals of the corresponding CH^+ and OH^- closed-shell species while relaxing the remaining electrons through single ($1p$-$1h$) and double ($2p$-$2h$) excitations.

The above process of selecting higher than $2p$-$1h$ and $2h$-$1p$ excitations via active orbitals can be used to define higher-order active-space EA- and IP-EOMCC approximations. For instance, in the EA-EOMCCSDtq and IP-EOMCCSDtq approaches we define [85]

$$R_\mu^{(N+1)}(\text{CCSDtq}) = R_{\mu,1p} + R_{\mu,2p\text{-}1h} + r_{\mu,3p\text{-}2h} + r_{\mu,4p\text{-}3h} \tag{2.19}$$

and

$$R_\mu^{(N-1)}(\text{CCSDtq}) = R_{\mu,1h} + R_{\mu,2h\text{-}1p} + r_{\mu,3h\text{-}2p} + r_{\mu,4h\text{-}3p}, \tag{2.20}$$

where $r_{\mu,3p\text{-}2h}$ and $r_{\mu,3h\text{-}2p}$ have the same mathematical form as in Eqs. (2.14) and (2.15), and

$$r_{\mu,4p\text{-}3h} = \sum_{\mathbf{J}>k>l,\mathbf{A}<\mathbf{B}<c<d} r_{\mathbf{AB}cd}^{\mathbf{J}kl}\, a^{\mathbf{A}} a^{\mathbf{B}} a^c a^d a_l a_k a_{\mathbf{J}}, \tag{2.21}$$

and

$$r_{\mu,4h\text{-}3p} = \sum_{\mathbf{I}>\mathbf{J}>k>l,\mathbf{B}<c<d} r_{\mathbf{B}cd}^{\mathbf{IJ}kl}\, a^{\mathbf{B}} a^c a^d a_l a_k a_{\mathbf{J}} a_{\mathbf{I}}. \tag{2.22}$$

We then diagonalize the similarity-transformed Hamiltonian of either the CCSDtq [97–100, 103, 106] or CCSDt [95–98, 101, 106–108] theory in the subspace of $\mathscr{H}^{(N+1)}$ spanned by the $|\Phi^a\rangle$, $|\Phi^{ab}_j\rangle$, $|\Phi^{\mathbf{A}bc}_{jk}\rangle$, and $|\Phi^{\mathbf{AB}cd}_{\mathbf{J}kl}\rangle$ determinants (the EA-EOMCC case) or in the subspace of $\mathscr{H}^{(N-1)}$ spanned by the $|\Phi_i\rangle$, $|\Phi_{ij}^{\ b}\rangle$, $|\Phi_{\mathbf{I}jk}^{\ bc}\rangle$, and $|\Phi_{\mathbf{IJ}kl}^{\ \mathbf{B}cd}\rangle$ determinants (the IP-EOMCC case). One can also extend the active-space ideas to the multiply attached and multiply ionized EOMCC schemes (cf., e.g., [91–93]) where we diagonalize the similarity-transformed Hamiltonian of an N-electron, closed

shell system in the suitably defined $(N \pm \nu)$-electron subspaces of the Fock space, where $\nu \geq 2$. For example, the active-space DIP-EOMCC approximations, where $\nu = 2$, can be obtained by considering the various truncations of the following ionizing operator [85]:

$$\begin{aligned} R_{\mu}^{(N-2)} = & \tfrac{1}{2} r^{ij} a_j a_i + \tfrac{1}{6} r^{ijk}_{c} a^c a_k a_j a_i \\ & + \sum_{\mathbf{I}>\mathbf{J}>k>l,c<d} r^{\mathbf{IJ}kl}_{cd} a^c a^d a_l a_k a_{\mathbf{J}} a_{\mathbf{I}} \\ & + \sum_{\mathbf{I}>\mathbf{J}>\mathbf{K}>l>m,\mathbf{C}<d<e} r^{\mathbf{IJK}lm}_{\mathbf{C}de} a^{\mathbf{C}} a^d a^e a_m a_l a_{\mathbf{K}} a_{\mathbf{J}} a_{\mathbf{I}} \\ & + \cdots , \end{aligned} \tag{2.23}$$

A similar operator can be constructed for the active-space DEA-EOMCC methods. All of the resulting approaches offer considerable reduction in the CPU timings and numbers of r amplitudes that define the corresponding $R_{\mu}^{(N\pm\nu)}$ operators, when compared to the corresponding parent methods. At the same time, the active-space EA, DEA, IP, DIP, etc. EOMCC approaches are systematic in a sense that they naturally reduce to the parent EA, DEA, IP, DIP, etc. EOMCC schemes when all orbitals in the molecular orbital basis are active. This natural and straightforward relationship between the parent CC/EOMCC approach and its active-space variant is characteristic of all active-space CC/EOMCC methods [28,29,97–101,103–111].

2.1.3 Key Details of the Efficient Computer Implementation of the Active-Space EA-EOMCCSDt and IP-EOMCCSDt Approaches

In this section, we discuss our highly efficient implementations of the active-space EA-EOMCCSDt and IP-EOMCCSDt schemes discussed in Section 2.1.2, and the corresponding factorized equations in terms of recursively generated intermediates

that lead to the vectorized computer codes through the use of fast matrix multiplication routines from the BLAS library. Our EA- and IP-EOMCCSDt codes, which are interfaced with the RHF/ROHF and integral routines available in the GAMESS software package [173], can be broken down into three major components. In the first step, we solve the usual CCSD equations for the ground state of the N-electron reference system in order to obtain the singly and doubly excited cluster amplitudes, t_a^i and t_{ab}^{ij}, respectively. In this work, we usually use the RHF-based CCSD closed-shell codes described in [174], which are included in GAMESS, since our main focus is on applications of the EA/IP-EOMCCSDt methods to open-shell species that are obtained by the attachment of one electron to or removal of one electron from the N-electron closed-shell species. However, we also have an option of using the more general CCSD codes for both the closed-shell and open-shell systems using the ROHF reference, also included in GAMESS [138], in case we want to perform the EA/IP-EOMCCSDt calculations for cases where the N-electron reference system is an open-shell itself. In the next step, we use the converged t_a^i and t_{ab}^{ij} amplitudes to construct the one- and two-body matrix elements of the CCSD similarity-transformed Hamiltonian $\bar{H}_{N,\mathrm{open}}^{(\mathrm{CCSD})}$, $\bar{h}_p^q$ and $\bar{h}_{pq}^{rs}$, respectively, which define the one- and two-body components of $\bar{H}_{N,\mathrm{open}}^{(\mathrm{CCSD})}$ within the second quantized formalism,

$$\bar{H}_1^{(\mathrm{CCSD})} = \bar{h}_p^q a^p a_q, \tag{2.24}$$

and

$$\bar{H}_2^{(\mathrm{CCSD})} = \bar{h}_{pq}^{rs} N[a^p a^q a_s a_r], \tag{2.25}$$

respectively ($N[\ldots]$ is the normal product of the operators between the brackets). The explicit equations defining these matrix elements in terms of the one- and two-electron molecular integrals of the Hamiltonian, $f_p^q = \langle p|f|q\rangle$ (f is the Fock operator) and $v_{pq}^{rs} = \langle pq|v|rs\rangle - \langle pq|v|sr\rangle$ (v is the electron-electron interaction), respectively, and

the CCSD cluster amplitudes, which have also been presented in [9, 10, 132, 140, 175], can be found in Table 2.1.

In the final step, which is the focus of this section, we use the converged CCSD cluster amplitudes and the one- and two-body matrix elements of $\bar{H}_{N,\mathrm{open}}^{(\mathrm{CCSD})}$ to construct the EA-EOMCCSDt and IP-EOMCCSDt equations, which are then solved using the Hirao-Nakatsuji generalization [176] of the Davidson diagonalization algorithm [177] to non-Hermitian eigenvalue problems of the type represented by Eq. (2.9). Let us recall that the EA-EOMCCSDt equations are obtained by replacing $\bar{H}_{N,\mathrm{open}}$ and $R_\mu^{(N+1)}$ in Eq. (2.9) by $\bar{H}_{N,\mathrm{open}}^{(\mathrm{CCSD})}$, Eq. (2.18), and $R_\mu^{(N+1)}$(CCSDt), Eq. (2.12), and projecting the resulting equation on the $|\Phi^a\rangle$, $|\Phi^{ab}_{\ j}\rangle$, and $|\Phi^{\mathbf{A}bc}_{\ jk}\rangle$ determinants. Similarly, the IP-EOMCCSDt equations are obtained by replacing $\bar{H}_{N,\mathrm{open}}$ and $R_\mu^{(N-1)}$ in Eq. (2.9) by $\bar{H}_{N,\mathrm{open}}^{(\mathrm{CCSD})}$, Eq. (2.18), and $R_\mu^{(N-1)}$(CCSDt), Eq. (2.13), and projecting the resulting equation on the $|\Phi_i\rangle$, $|\Phi_{ij}^{\ b}\rangle$, and $|\Phi_{\mathbf{I}jk}^{\ bc}\rangle$ determinants. In this step, we make use of the explicit, factorized form of the equations defining the EA-EOMCCSDt and IP-EOMCCSDt eigenvalue problems in terms of the molecular integrals of the Hamiltonian f_p^q and v_{pq}^{rs}, the CCSD cluster amplitudes t_a^i and t_{ab}^{ij}, and the r_a, $r_{ab}^{\ j}$, and $r_{\mathbf{A}bc}^{\ jk}$ amplitudes defining the relevant electron-attaching operator or the r^i, $r^{ij}_{\ b}$ and $r^{\mathbf{I}jk}_{\ bc}$ amplitudes defining the relevant ionizing operator (cf. Eqs. (2.12)-(2.15)). These equations, along with the formalism by which they are derived, following [87], will be discussed next. Following this discussion, the details of the computer implementation of these equations will be described in detail.

In order to derive the EA- and IP-EOMCCSDt equations, we begin with the working equations defining the parent EA-EOMCCSD($3p$-$2h$) and IP-EOMCCSD($3h$-$2p$) approximations, which are presented in Appendix A. It is worth noting that these equations were also presented in an alternative form in [85]. It should be emphasized that the equations found in [85] are mathematically equivalent to the analogous equations found in Appendix A. The differences are the result of the fact that

Table 2.1: Explicit algebraic expressions for the one- and two-body matrix elements of $\bar{H}^{(\mathrm{CCSD})}_{N,\mathrm{open}}$ ($\bar{h}^q_p$ and $\bar{h}^{rs}_{pq}$, respectively) taken from [132, 140].

Intermediate	Expression[a]
$\bar{h}^a_i$	$f^a_i + v^{ae}_{im} t^m_e$
$\bar{h}^j_i$	$f^j_i + v^{je}_{im} t^m_e + \frac{1}{2} v^{ef}_{mi} t^{mj}_{ef} + \bar{h}^e_i t^j_e$
$\bar{h}^b_a$	$I^b_a - \bar{h}^b_m t^m_a$
$\bar{h}^{bc}_{ai}$	$v^{bc}_{ai} - v^{bc}_{mi} t^m_a$
$\bar{h}^{ka}_{ij}$	$v^{ka}_{ij} + v^{ea}_{ij} t^k_e$
$\bar{h}^{cd}_{ab}$	$v^{cd}_{ab} + \frac{1}{2} v^{cd}_{mn} t^{mn}_{ab} - \bar{h}^{cd}_{am} t^m_b + v^{cd}_{bm} t^m_a$
$\bar{h}^{kl}_{ij}$	$v^{kl}_{ij} + \frac{1}{2} v^{ef}_{ij} t^{kl}_{ef} - \bar{h}^{le}_{ij} t^k_e + v^{ke}_{ij} t^l_e$
$\bar{h}^{jb}_{ia}$	$I'^{jb}_{ia} - v^{eb}_{im} t^{jm}_{ea} - \bar{h}^{jb}_{im} t^m_a$
$\bar{h}^{ic}_{ab}$	$v^{ic}_{ab} + v^{ec}_{ab} t^i_e - \bar{h}^{ic}_{mb} t^m_a + I'^{ic}_{ma} t^m_b - \bar{h}^c_m t^{im}_{ab} + \bar{h}^{ce}_{bm} t^{im}_{ae} - v^{ce}_{am} t^{im}_{be} + \frac{1}{2} \bar{h}^{ic}_{nm} t^{nm}_{ab}$
$\bar{h}^{jk}_{ia}$	$v^{jk}_{ia} + \bar{h}^{jk}_{mi} t^m_a - v^{ke}_{ia} t^j_e + \mathscr{A}^{jk} \bar{h}^{je}_{im} t^{km}_{ae} + \bar{h}^e_i t^{jk}_{ea} + I'^{je}_{ia} t^k_e - \frac{1}{2} v^{ef}_{ai} t^{jk}_{ef}$
I'^b_a	$f^b_a + v^{be}_{am} t^m_e$
I^b_a	$I'^b_a - \frac{1}{2} v^{eb}_{mn} t^{mn}_{ea}$
I'^{jb}_{ia}	$v^{jb}_{ia} + v^{eb}_{ia} t^j_e$

[a] Summation over repeated upper and lower indices is assumed. $f^q_p = \langle p|f|q\rangle$ and $v^{rs}_{pq} = \langle pq|v|rs\rangle - \langle pq|v|sr\rangle$ are the one- and two-body matrix elements of the Hamiltonian in the normal-ordered form (one- and two-electron integrals), and the t^i_a and t^{ij}_{ab} are the singly and doubly excited cluster amplitudes defining the ground-state CCSD wave function of the N-electron reference system. The antisymmetrizer $\mathscr{A}^{jk} = 1 - (jk)$, where (jk) is the transposition of indices j and k (see, also Eq. (2.94)).

the equations presented in [85] are in a form that is ideal for implementing the full EA-EOMCCSD(3p-2h) and IP-EOMCCSD(3h-2p) schemes, while the equations presented in Appendix A are in a form which is a good starting point for deriving the computationally efficient form for the equations defining the active-space EA-EOMCCSDt and IP-EOMCCSDt approaches that in the majority of applications use small subsets of the r_{abc}^{jk} and r_{bc}^{ijk} amplitudes defining the 3p-2h and 3h-2p components of $R_{\mu}^{(N+1)}$ and $R_{\mu}^{(N+1)}$, respectively.

Generally, the explicit EA-EOMCCSDt and IP-EOMCCSDt equations are obtained by applying the active-space restrictions on the spin-orbital indices defining the $|\Phi_{jk}^{abc}\rangle$ and $|\Phi_{ijk}^{bc}\rangle$ determinants and on the indices defining the corresponding r_{abc}^{jk} and r_{bc}^{ijk} amplitudes, as described in Section 2.1.2, to each term of the parent EA-EOMCCSD(3p-2h) and IP-EOMCCSD(3h-2p) equations, as presented in Appendix A. In order to illustrate the inner workings of this procedure, which is based on the general principles laid down in [97], we derive a few typical terms which enter into the EA-EOMCCSDt equations. We begin by analyzing the following contribution to Eq. (A.3) in Appendix A, corresponding to the projection on $|\Phi_{jk}^{abc}\rangle$, which we label as $D_{jk}^{abc}(1)$:

$$D_{jk}^{abc}(1) = \tfrac{1}{8}\bar{h}_{bc}^{ef} r_{aef}^{jk}. \tag{2.26}$$

In the EA-EOMCCSDt approach, we only consider 3p-2h projections of the type $|\Phi_{jk}^{\mathbf{A}bc}\rangle$, and so we must restrict the indices in Eq. (2.26) as follows:

$$D_{jk}^{\mathbf{A}bc}(1) = \tfrac{1}{8}\bar{h}_{bc}^{ef} r_{\mathbf{A}ef}^{jk}. \tag{2.27}$$

As one can see, we replaced the generic unoccupied index a in Eq. (2.26) corresponding to the projection on $|\Phi_{jk}^{abc}\rangle$ by the active label $\mathbf{A}$. Since the $r_{\mathbf{A}ef}^{jk}$ amplitude which enters Eq. (2.27) contains an active unoccupied index (and thus already has the proper form required by Eq. (2.14)), no further restrictions to the indices defining the

$D^{abc}_{jk}(1)$ term are required. This completes the derivation of the final formula for this particular contribution to the EA-EOMCCSDt equations. Unfortunately, the majority of the terms which enter the active-space equations are not so easily obtained, and so it is useful to examine more difficult cases. For example, let us consider the following contribution to Eq. (A.3) in Appendix A, which we label as $D^{abc}_{jk}(2)$:

$$D^{abc}_{jk}(2) = -\tfrac{1}{2}\bar{h}^{je}_{ma} r^{mk}_{bce}. \tag{2.28}$$

If we exploit the same approach as used in the previous example, we obtain the following expression:

$$D^{\mathbf{A}bc}_{jk}(2) = -\tfrac{1}{2}\bar{h}^{je}_{m\mathbf{A}} r^{mk}_{bce}. \tag{2.29}$$

Again, we replaced the generic unoccupied index a in Eq. (2.28) by the active index $\mathbf{A}$ defining the $|\Phi^{\mathbf{A}bc}_{jk}\rangle$ determinant. Unlike in the previous case, however, the r^{mk}_{bce} amplitude that enters the above equation does not necessarily have at least one active unoccupied index, and so it is not automatically of the form required by Eq. (2.14). Furthermore, whether or not this amplitude satisfies the active-space restrictions depends on whether the indices b and c correspond to active unoccupied or inactive virtual spin-orbitals. As a result, instead of the generic projection $|\Phi^{\mathbf{A}bc}_{jk}\rangle$, that converts Eq. (2.28) into the less useful Eq. (2.29), we must consider four more specialized and distinct classes of the restricted 3*p*-2*h* projections that belong to the general $|\Phi^{\mathbf{A}bc}_{jk}\rangle$ type, given in Table 2.2.

When we apply the 3*p*-2*h* projection of type 1 in Table 2.2 to the term given in Eq. (2.28) (i.e., the projection on the $|\Phi^{\mathbf{ABC}}_{jk}\rangle$ determinant), we obtain

$$D^{\mathbf{ABC}}_{jk}(2) = -\tfrac{1}{2}\bar{h}^{je}_{m\mathbf{A}} r^{mk}_{\mathbf{BC}e}. \tag{2.30}$$

Because the 3*p*-2*h* amplitude $r^{mk}_{\mathbf{BC}e}$ has at least two active unoccupied indices, it

Table 2.2: The various classes of restricted projections that must be considered when generating the computationally efficient form of the equations defining the EA-EOMCCSDt and IP-EOMCCSDt eigenvalue problems.

	EA-EOMCC			IP-EOMCC		
Projection Type	$1p$	$2p$-$1h$	$3p$-$2h$	$1h$	$2h$-$1p$	$3h$-$2p$
1	$\langle\Phi^{\mathbf{A}}\vert$	$\langle\Phi^{\mathbf{AB}}_{j}\vert$	$\langle\Phi^{\mathbf{ABC}}_{jk}\vert$	$\langle\Phi_{\mathbf{I}}\vert$	$\langle\Phi^{b}_{\mathbf{IJ}}\vert$	$\langle\Phi^{bc}_{\mathbf{IJK}}\vert$
2	$\langle\Phi^{\mathbf{a}}\vert$	$\langle\Phi^{\mathbf{Ab}}_{j}\vert$	$\langle\Phi^{\mathbf{ABc}}_{jk}\vert$	$\langle\Phi_{\mathbf{i}}\vert$	$\langle\Phi^{b}_{\mathbf{Ij}}\vert$	$\langle\Phi^{bc}_{\mathbf{IJk}}\vert$
3		$\langle\Phi^{\mathbf{aB}}_{j}\vert$	$\langle\Phi^{\mathbf{AbC}}_{jk}\vert$		$\langle\Phi^{b}_{\mathbf{iJ}}\vert$	$\langle\Phi^{bc}_{\mathbf{IjK}}\vert$
4		$\langle\Phi^{\mathbf{ab}}_{j}\vert$	$\langle\Phi^{\mathbf{Abc}}_{jk}\vert$		$\langle\Phi^{b}_{\mathbf{ij}}\vert$	$\langle\Phi^{bc}_{\mathbf{Ijk}}\vert$

satisfies the active-space requirements of Eq. (2.14) and so no further constraints on the indices defining this term have to be imposed. Similarly, if we consider the projection on $\langle\Phi^{\mathbf{ABc}}_{jk}\vert$ (projection type 2 in Table 2.2), we obtain

$$D^{\mathbf{ABc}}_{jk}(2) = -\tfrac{1}{2}\bar{h}^{je}_{m\mathbf{A}} r^{mk}_{\mathbf{Bc}e}, \tag{2.31}$$

which also requires no additional restrictions on the spin-orbital indices, since the $3p$-$2h$ amplitude $r^{mk}_{\mathbf{Bc}e}$ has at least one active unoccupied index, as required by Eq. (2.14). Furthermore, comparing Eqs. (2.30) and (2.31) reveals that the only difference between these two terms is in the restriction on the index c, which in Eq. (2.30) is restricted to active unoccupied spin-orbitals and in Eq. (2.31) to inactive virtual spin-orbitals. This straightforward relationship between Eqs. (2.30) and (2.31) allows us to recombine these two contributions into one, somewhat more general term of the form

$$D^{\mathbf{AB}c}_{jk}(2) = -\tfrac{1}{2}\bar{h}^{je}_{m\mathbf{A}} r^{mk}_{\mathbf{B}ce}, \tag{2.32}$$

where the unoccupied index c can be active or inactive. When we consider projection type 3 from Table 2.2 (the projection on $\langle\Phi^{\mathbf{AbC}}_{jk}\vert$), we obtain

$$D^{\mathbf{AbC}}_{jk}(2) = \tfrac{1}{2}\bar{h}^{je}_{m\mathbf{A}} r^{mk}_{\mathbf{C}b\mathbf{e}}, \tag{2.33}$$

where we have made use of the antisymmetric properties of the $3p$-$2h$ amplitudes to maintain the ordering of the spin-orbital labels employed in Eq. (2.14) (i.e., the index restricted to active spin-orbitals is the leftmost of the unoccupied spin-orbital labels). We have moved the index $\mathbf{C}$ in $r_{\mathbf{Cbe}}^{mk}$ to the leftmost position because it is more convenient to have a consistent placement of the active spin-orbital labels when implementing the EA-EOMCCSDt and IP-EOMCCSDt schemes. As with the previous two cases, no further restrictions on the spin-orbital indices defining this term are required. Finally, we consider the projection on $|\Phi_{jk}^{\mathbf{Abc}}\rangle$ (projection type 4 in Table 2.2). The resulting expression for this contribution is

$$D_{jk}^{\mathbf{Abc}}(2) = -\tfrac{1}{2}\bar{h}_{m\mathbf{A}}^{je} r_{\mathbf{bce}}^{mk}, \tag{2.34}$$

where, unlike in the previous cases, the $r_{\mathbf{bce}}^{mk}$ amplitude which enters this term does not automatically have at least one unoccupied index constrained to active unoccupied spin-orbitals. In order to impose such a condition, we must restrict the summation over all particle spin-orbitals e in Eq. (2.34) to active spin-orbital labels only since $\mathbf{b}$ and $\mathbf{c}$ are virtual (i.e., inactive) indices. The resulting expression is given by

$$\tilde{D}_{jk}^{\mathbf{Abc}}(2) = -\tfrac{1}{2}\bar{h}_{m\mathbf{A}}^{j\mathbf{E}} r_{\mathbf{Ebc}}^{mk}, \tag{2.35}$$

where the overtilde denotes the fact that we imposed restrictions on the summations appearing in $D_{jk}^{\mathbf{Abc}}(2)$ and where once again we have made use of the antisymmetric nature of the $3p$-$2h$ amplitudes to maintain the order of unoccupied indices used in Eq. (2.14) (active indices precede the generic or inactive ones). Equations (2.32), (2.33), and (2.35) represent all contributions to the EA-EOMCCSDt working equations which result from the single term in the EA-EOMCCSD($3p$-$2h$) equations projected on $3p$-$2h$ excited determinants given by Eq. (2.28).

By applying the above procedure to each term which enters the explicit form of

the equations defining the EA-EOMCCSD($3p$-$2h$) and IP-EOMCCSD($3h$-$2p$) methods (Eqs. (A.1),(A.2), (A.3),(A.7),(A.8) and (A.9) in Appendix A) and by making use of the projection types given in Table 2.2, one can derive the explicit form of all contributions to the EA- and IP-EOMCCSDt equations. After combining all of these contributions together, we obtain the final form of the fully factorized, computationally efficient EA-EOMCCSDt and IP-EOMCCSDt equations, which are presented below. We begin with the expressions for the EA-EOMCCSDt scheme. The factorized equations defining the projections of the EA-EOMCCSDt eigenvalue problem on the $1p$ determinants $|\Phi^a\rangle$ are

$$\langle\Phi^a|(\bar{H}^{(\mathrm{CCSD})}_{N,\mathrm{open}} R^{(N+1)}_\mu)_C|\Phi\rangle = \mathfrak{T}_a = \omega^{(N+1)}_\mu r_a, \tag{2.36}$$

where

$$\mathfrak{T}_{\mathbf{A}} = \chi_{\mathbf{A}} + \tfrac{1}{4} v^{ef}_{mn} r^{mn}_{\mathbf{A}ef} \tag{2.37}$$

and

$$\mathfrak{T}_{\mathbf{a}} = \chi_{\mathbf{a}} + \tfrac{1}{2} \sum_{\mathbf{E}<f} v^{\mathbf{E}f}_{mn} r^{mn}_{\mathbf{E}f\mathbf{a}}, \tag{2.38}$$

with

$$\chi_a = \bar{h}^e_a r_e + \bar{h}^e_m r^m_{ae} + \tfrac{1}{2} \bar{h}^{ef}_{am} r^m_{ef}. \tag{2.39}$$

The EA-EOMCCSDt equations defining the projections on the $2p$-$1h$ determinants $|\Phi^{ab}_j\rangle$ are given by

$$\langle\Phi^{ab}_j|(\bar{H}^{(\mathrm{CCSD})}_{N,\mathrm{open}} R^{(N+1)}_\mu)_C|\Phi\rangle = \mathscr{A}_{ab} \mathfrak{T}^{\ j}_{ab} = \omega^{(N+1)}_\mu r^{\ j}_{ab}, \tag{2.40}$$

where

$$\mathfrak{T}^{\ j}_{\mathbf{A}b} = \chi^{\ j}_{\mathbf{A}b} + \alpha^{\ j}_{\mathbf{A}b} + \tfrac{1}{2} \bar{h}^{ef}_{bm} r^{jm}_{\mathbf{A}ef}, \tag{2.41}$$

$$\mathfrak{T}^{\ j}_{\mathbf{a}\mathbf{B}} = \Delta^{\ j}_{\mathbf{a}\mathbf{B}} - \alpha^{\ j}_{\mathbf{B}\mathbf{a}}, \tag{2.42}$$

and

$$\mathfrak{T}_{\mathbf{ab}}^{\ j} = \Delta_{\mathbf{ab}}^{\ j}, \tag{2.43}$$

with

$$\alpha_{\mathbf{A}b}^{\ j} = \tfrac{1}{2}\bar{h}_m^e r_{\mathbf{A}be}^{\ jm} - \tfrac{1}{4}\bar{h}_{mn}^{je} r_{\mathbf{A}be}^{\ mn}, \tag{2.44}$$

$$\begin{aligned}\chi_{ab}^{\ j} &= -\tfrac{1}{2}\bar{h}_{ab}^{je} r_e + \bar{h}_a^e r_{eb}^{\ j} - \tfrac{1}{2}\bar{h}_m^j r_{ab}^{\ m} \\ &\quad + \tfrac{1}{4}\bar{h}_{ab}^{ef} r_{ef}^{\ j} - \bar{h}_{ma}^{je} r_{eb}^{\ m} - \tfrac{1}{2} I_m t_{ab}^{mj},\end{aligned} \tag{2.45}$$

$$\Delta_{\mathbf{aB}}^{\ j} = \chi_{\mathbf{aB}}^{\ j} + \sum_{\mathbf{E}<f} \bar{h}_{\mathbf{B}m}^{\mathbf{E}f} r_{\mathbf{E}f\mathbf{a}}^{\ jm}, \tag{2.46}$$

and

$$\Delta_{\mathbf{ab}}^{\ j} = \chi_{\mathbf{ab}}^{\ j} + \sum_{\mathbf{E}<f} \bar{h}_{\mathbf{b}m}^{\mathbf{E}f} r_{\mathbf{E}f\mathbf{a}}^{\ jm} + \tfrac{1}{2}\bar{h}_m^{\mathbf{E}} r_{\mathbf{E}\mathbf{ab}}^{\ jm} - \tfrac{1}{4}\bar{h}_{mn}^{j\mathbf{E}} r_{\mathbf{E}\mathbf{ab}}^{\ mn}. \tag{2.47}$$

Finally, the EA-EOMCCSDt equations defining the projections on the selected $3p$-$2h$ determinants $|\Phi_{jk}^{\mathbf{A}bc}\rangle$ have the following computationally efficient form:

$$\langle \Phi_{jk}^{\mathbf{A}bc} | (\bar{H}_{N,\mathrm{open}}^{(\mathrm{CCSD})} R_\mu^{(N+1)})_C | \Phi \rangle = \mathscr{A}_{bc}\mathscr{A}^{jk}\mathfrak{T}_{\mathbf{A}bc}^{\ jk} = \omega_\mu^{(N+1)} r_{\mathbf{A}bc}^{\ jk}, \tag{2.48}$$

where

$$\mathfrak{T}_{\mathbf{AB}c}^{\ jk} = \chi_{\mathbf{AB}c}^{\ jk} + \beta_{\mathbf{B}c\mathbf{A}}^{\ jk} + \tfrac{1}{4}\gamma_{\mathbf{B}c\mathbf{A}}^{\ jk}, \tag{2.49}$$

$$\mathfrak{T}_{\mathbf{AbC}}^{\ jk} = \Delta_{\mathbf{AbC}}^{\ jk} - \beta_{\mathbf{CbA}}^{\ jk}, \tag{2.50}$$

and

$$\mathfrak{T}_{\mathbf{Abc}}^{\ jk} = \Delta_{\mathbf{Abc}}^{\ jk}, \tag{2.51}$$

with

$$\gamma_{\mathbf{A}bc}^{\ jk} = \bar{h}_{bc}^{ef} r_{\mathbf{A}ef}^{\ jk}, \tag{2.52}$$

$$\beta_{\mathbf{A}bc}^{\ jk} = \tfrac{1}{4}\bar{h}_c^e r_{\mathbf{A}be}^{\ jk} - \tfrac{1}{2}\bar{h}_{mc}^{je} r_{\mathbf{A}be}^{\ mk}, \tag{2.53}$$

$$\begin{aligned}\chi_{\mathbf{A}bc}^{\;\;jk} &= -\tfrac{1}{2}\bar{h}_{bc}^{ke} r_{\mathbf{A}e}^{\;\;j} + \bar{h}_{\mathbf{A}c}^{ke} r_{be}^{\;\;j} - \tfrac{1}{4}\bar{h}_{m\mathbf{A}}^{jk} r_{bc}^{\;\;m} \\ &\quad -\tfrac{1}{2}\bar{h}_{mc}^{jk} r_{\mathbf{A}b}^{\;\;m} + \tfrac{1}{2}\bar{h}_{m}^{j} r_{\mathbf{A}bc}^{\;\;km} + \tfrac{1}{8}\bar{h}_{mn}^{jk} r_{\mathbf{A}bc}^{\;\;mn} \\ &\quad -\tfrac{1}{2} I_{\mathbf{A}m}^{\;\;j} t_{bc}^{mk} + I_{bm}^{\;\;j} t_{\mathbf{A}c}^{mk} - \tfrac{1}{4} I_{bc}^{\;\;f} t_{\mathbf{A}f}^{jk} \\ &\quad +\tfrac{1}{2} I_{\mathbf{A}c}^{\;\;f} t_{bf}^{jk} + \tfrac{1}{8}\gamma_{\mathbf{A}bc}^{\;\;jk} + 2\beta_{\mathbf{A}bc}^{\;\;jk}, \end{aligned} \tag{2.54}$$

$$\Delta_{\mathbf{AbC}}^{\;\;jk} = \chi_{\mathbf{AbC}}^{\;\;jk} - \tfrac{1}{2}\sum_{\mathbf{E}<f} \bar{h}_{\mathbf{AC}}^{\mathbf{E}f} r_{\mathbf{E}f\mathbf{b}}^{\;\;jk}, \tag{2.55}$$

and

$$\Delta_{\mathbf{Abc}}^{\;\;jk} = \chi_{\mathbf{Abc}}^{\;\;jk} - \tfrac{1}{2}\sum_{\mathbf{E}<f} \bar{h}_{\mathbf{Ac}}^{\mathbf{E}f} r_{\mathbf{E}f\mathbf{b}}^{\;\;jk} + \tfrac{1}{4}\bar{h}_{\mathbf{A}}^{\mathbf{E}} r_{\mathbf{E}bc}^{\;\;jk} - \tfrac{1}{2}\bar{h}_{m\mathbf{A}}^{j\mathbf{E}} r_{\mathbf{E}bc}^{\;\;mk}. \tag{2.56}$$

In addition, the above equations for the EA-EOMCCSDt approximation make use of the following recursively generated intermediates:

$$I_m = \tfrac{1}{2} v_{mn}^{ef} r_{ef}^{\;\;n}, \tag{2.57}$$

$$I_{\mathbf{A}m}^{\;\;j} = \tilde{I}_{\mathbf{A}m}^{\;\;j} + \tfrac{1}{2} v_{mn}^{ef} r_{\mathbf{A}ef}^{\;\;jn}, \tag{2.58}$$

and

$$I_{\mathbf{a}m}^{\;\;j} = \tilde{I}_{\mathbf{a}m}^{\;\;j} + \sum_{\mathbf{E}<f} v_{mn}^{\mathbf{E}f} r_{\mathbf{E}f\mathbf{a}}^{\;\;jn}, \tag{2.59}$$

where

$$\tilde{I}_{am}^{\;\;j} = \bar{h}_{ma}^{je} r_e + \tfrac{1}{2}\bar{h}_{am}^{ef} r_{ef}^{\;\;j} + \bar{h}_{mn}^{je} r_{ae}^{\;\;n}, \tag{2.60}$$

and

$$I_{\mathbf{A}b}^{\;\;f} = \tilde{I}_{\mathbf{A}b}^{\;\;f} - \tfrac{1}{2} v_{mn}^{ef} r_{\mathbf{A}eb}^{\;\;mn}, \tag{2.61}$$

$$I_{\mathbf{aB}}^{\;\;f} = \tilde{I}_{\mathbf{aB}}^{\;\;f} - \tfrac{1}{2} v_{mn}^{ef} r_{\mathbf{Ba}e}^{\;\;mn}, \tag{2.62}$$

and

$$I_{\mathbf{ab}}^{\;\;f} = \tilde{I}_{\mathbf{ab}}^{\;\;f} + \tfrac{1}{2} v_{mn}^{\mathbf{E}f} r_{\mathbf{Eab}}^{\;\;mn}, \tag{2.63}$$

where

$$\tilde{I}_{ab}^{\ f} = \bar{h}_{ab}^{ef} r_e - \mathscr{A}_{ab} \bar{h}_{bm}^{ef} r_{ae}^{\ m}. \tag{2.64}$$

A similar set of expressions can also be written for the IP-EOMCCSDt scheme. The final, factorized equations defining the projections of the IP-EOMCCSDt eigenvalue problem on the $1h$ determinants $|\Phi_i\rangle$ are

$$\langle \Phi_i | (\bar{H}^{(\mathrm{CCSD})}_{N,\mathrm{open}} R^{(N-1)}_{\mu})_C | \Phi \rangle = \mathfrak{T}^i = \omega^{(N-1)}_{\mu} r^i, \tag{2.65}$$

where

$$\mathfrak{T}^{\mathbf{I}} = \chi^{\mathbf{I}} + \tfrac{1}{4} v_{mn}^{ef} r^{\mathbf{I}mn}_{\ \ ef} \tag{2.66}$$

and

$$\mathfrak{T}^{\mathbf{i}} = \chi^{\mathbf{i}} + \tfrac{1}{2} \sum_{\mathbf{M}>n} v_{\mathbf{M}n}^{ef} r^{\mathbf{M}n\mathbf{i}}_{\ \ ef}, \tag{2.67}$$

with

$$\chi^i = -\bar{h}_m^i r^m + \bar{h}_m^e r^{im}_{\ \ e} - \tfrac{1}{2} \bar{h}_{mn}^{ie} r^{mn}_{\ \ e}. \tag{2.68}$$

The IP-EOMCCSDt equations defining the projections on the $2p$-$1h$ determinants $|\Phi_{ij}^{\ b}\rangle$ are given by

$$\langle \Phi_{ij}^{\ b} | (\bar{H}^{(\mathrm{CCSD})}_{N,\mathrm{open}} R^{(N-1)}_{\mu})_C | \Phi \rangle = \mathscr{A}^{ij} \mathfrak{T}^{ij}_{\ b} = \omega^{(N-1)}_{\mu} r^{ij}_{\ b}, \tag{2.69}$$

where

$$\mathfrak{T}^{\mathbf{I}j}_{\ b} = \chi^{\mathbf{I}j}_{\ b} + \alpha^{\mathbf{I}j}_{\ b} + \tfrac{1}{2} \bar{h}_{mn}^{je} r^{\mathbf{I}mn}_{\ \ eb}, \tag{2.70}$$

$$\mathfrak{T}^{\mathbf{i}\mathbf{J}}_{\ b} = \Delta^{\mathbf{i}\mathbf{J}}_{\ b} - \alpha^{\mathbf{J}\mathbf{i}}_{\ b}, \tag{2.71}$$

and

$$\mathfrak{T}^{\mathbf{i}\mathbf{j}}_{\ b} = \Delta^{\mathbf{i}\mathbf{j}}_{\ b}, \tag{2.72}$$

with

$$\chi^{ij}_{b} = -\tfrac{1}{2}\bar{h}^{ij}_{mb}r^{m} - \bar{h}^{i}_{m}r^{mj}_{b} + \tfrac{1}{2}\bar{h}^{e}_{b}r^{ij}_{e} + \tfrac{1}{4}\bar{h}^{ij}_{mn}r^{mn}_{b} - \bar{h}^{ie}_{mb}r^{mj}_{e} + \tfrac{1}{2}I^{e}t^{ij}_{eb}, \tag{2.73}$$

$$\alpha^{\mathbf{I}j}_{b} = \tfrac{1}{2}\bar{h}^{e}_{m}r^{\mathbf{I}jm}_{be} + \tfrac{1}{4}\bar{h}^{ef}_{bm}r^{\mathbf{I}jm}_{ef}, \tag{2.74}$$

$$\Delta^{\mathbf{iJ}}_{b} = \chi^{\mathbf{iJ}}_{b} + \sum_{\mathbf{M}>n}\bar{h}^{\mathbf{Je}}_{\mathbf{M}n}r^{\mathbf{M}n\mathbf{i}}_{eb}, \tag{2.75}$$

and

$$\Delta^{\mathbf{ij}}_{b} = \chi^{\mathbf{ij}}_{b} + \sum_{\mathbf{M}>n}\bar{h}^{\mathbf{je}}_{\mathbf{M}n}r^{\mathbf{M}n\mathbf{i}}_{eb} + \tfrac{1}{2}\bar{h}^{e}_{\mathbf{M}}r^{\mathbf{Mij}}_{be} + \tfrac{1}{4}\bar{h}^{ef}_{b\mathbf{M}}r^{\mathbf{Mij}}_{ef}. \tag{2.76}$$

Finally, the IP-EOMCCSDt equations defining the projections on the selected $3h$-$2p$ determinants $|\Phi^{bc}_{\mathbf{I}jk}\rangle$ have the following computationally efficient form:

$$\langle\Phi^{bc}_{\mathbf{I}jk}|(\bar{H}^{(\mathrm{CCSD})}_{N,\mathrm{open}}R^{(N-1)}_{\mu})_{C}|\Phi\rangle = \mathscr{A}_{bc}\mathscr{A}^{jk}\mathfrak{T}^{\mathbf{I}jk}_{bc}, = \omega^{(N-1)}_{\mu}r^{\mathbf{I}jk}_{bc}, \tag{2.77}$$

where

$$\mathfrak{T}^{\mathbf{IJ}k}_{bc} = \chi^{\mathbf{IJ}k}_{bc} - \beta^{\mathbf{J}k\mathbf{I}}_{bc} + \tfrac{1}{4}\gamma^{\mathbf{J}k\mathbf{I}}_{bc}, \tag{2.78}$$

$$\mathfrak{T}^{\mathbf{IjK}}_{bc} = \Delta^{\mathbf{IjK}}_{bc} + \beta^{\mathbf{Kj}\mathbf{I}}_{bc}, \tag{2.79}$$

and

$$\mathfrak{T}^{\mathbf{Ijk}}_{bc} = \Delta^{\mathbf{Ijk}}_{bc}, \tag{2.80}$$

with

$$\gamma^{\mathbf{I}jk}_{bc} = \bar{h}^{jk}_{mn}r^{\mathbf{I}mn}_{bc}, \tag{2.81}$$

$$\beta^{\mathbf{I}jk}_{bc} = \tfrac{1}{4}\bar{h}^{k}_{m}r^{\mathbf{I}jm}_{bc} + \tfrac{1}{2}\bar{h}^{ke}_{mc}r^{\mathbf{I}jm}_{be}, \tag{2.82}$$

$$\begin{aligned}\chi_{bc}^{\mathbf{I}jk} &= \tfrac{1}{2}\bar{h}_{mb}^{jk} r_{c}^{\mathbf{I}m} + \bar{h}_{mb}^{\mathbf{I}j} r_{c}^{km} - \tfrac{1}{4}\bar{h}_{bc}^{\mathbf{I}e} r_{e}^{jk} - \tfrac{1}{2}\bar{h}_{bc}^{ke} r_{e}^{\mathbf{I}j} \\ &+ \tfrac{1}{2}\bar{h}_{c}^{e} r_{be}^{\mathbf{I}jk} + \tfrac{1}{8}\bar{h}_{bc}^{ef} r_{ef}^{\mathbf{I}jk} + \tfrac{1}{4} I_{n}^{jk} t_{bc}^{\mathbf{I}n} - \tfrac{1}{2} I_{n}^{\mathbf{I}k} t_{bc}^{jn} \\ &+ \tfrac{1}{2} I_{c}^{\mathbf{I}f} t_{bf}^{jk} + I_{c}^{kf} t_{bf}^{\mathbf{I}j} + \tfrac{1}{8}\gamma_{bc}^{\mathbf{I}jk} - 2\beta_{bc}^{\mathbf{I}jk}, \end{aligned} \tag{2.83}$$

$$\Delta_{bc}^{\mathbf{IjK}} = \chi_{bc}^{\mathbf{IjK}} - \tfrac{1}{2} \sum_{\mathbf{M}>n} \bar{h}_{\mathbf{M}n}^{\mathbf{IK}} r_{bc}^{\mathbf{M}n\mathbf{j}}, \tag{2.84}$$

and

$$\Delta_{bc}^{\mathbf{Ijk}} = \chi_{bc}^{\mathbf{Ijk}} - \tfrac{1}{2} \sum_{\mathbf{M}>n} \bar{h}_{\mathbf{M}n}^{\mathbf{Ik}} r_{bc}^{\mathbf{M}n\mathbf{j}} - \tfrac{1}{4}\bar{h}_{\mathbf{M}}^{\mathbf{I}} r_{bc}^{\mathbf{Mjk}} - \tfrac{1}{2}\bar{h}_{\mathbf{M}c}^{\mathbf{I}e} r_{be}^{\mathbf{Mjk}}. \tag{2.85}$$

As was the case with the EA-EOMCCSDt scheme, the IP-EOMCCSDt equations utilize several additional recursively generated intermediates which are as follows:

$$I^{e} = -\tfrac{1}{2} v_{mn}^{ef} r_{f}^{mn}, \tag{2.86}$$

$$I_{c}^{\mathbf{I}f} = \tilde{I}_{c}^{\mathbf{I}f} - \tfrac{1}{2} v_{mn}^{ef} r_{ec}^{\mathbf{I}mn}, \tag{2.87}$$

and

$$I_{c}^{\mathbf{i}f} = \tilde{I}_{c}^{\mathbf{i}f} - \sum_{\mathbf{M}>n} v_{\mathbf{M}n}^{ef} r_{ec}^{\mathbf{M}n\mathbf{i}}, \tag{2.88}$$

where

$$\tilde{I}_{c}^{if} = -\bar{h}_{mc}^{if} r^{m} + \tfrac{1}{2}\bar{h}_{mn}^{if} r_{c}^{mn} - \bar{h}_{cm}^{ef} r_{e}^{im}, \tag{2.89}$$

and

$$I_{n}^{\mathbf{J}k} = \tilde{I}_{n}^{\mathbf{J}k} + \tfrac{1}{2} v_{mn}^{ef} r_{ef}^{\mathbf{J}mk}, \tag{2.90}$$

$$I_{n}^{\mathbf{jK}} = \tilde{I}_{n}^{\mathbf{jK}} + \tfrac{1}{2} v_{mn}^{ef} r_{ef}^{\mathbf{K}jm}, \tag{2.91}$$

and

$$I_{n}^{\mathbf{jk}} = \tilde{I}_{n}^{\mathbf{jk}} - \tfrac{1}{2} v_{\mathbf{M}n}^{ef} r_{ef}^{\mathbf{Mjk}}, \tag{2.92}$$

where

$$\tilde{I}_n^{jk} = -\bar{h}_{mn}^{jk} r^m - \mathscr{A}^{jk} \bar{h}_{mn}^{ke} r_e^{jm}. \tag{2.93}$$

The antisymmetrizer $\mathscr{A}_{pq} = \mathscr{A}^{pq}$, which enters the above equations is defined as

$$\mathscr{A}_{pq} \equiv \mathscr{A}^{pq} = 1 - (pq), \tag{2.94}$$

respectively, with (pq) representing a transposition of indices p and q.

We now consider the most important details of the efficient computer implementation of the EA-EOMCCSDt and IP-EOMCCSDt eigenvalue equations, Eqs. (2.36)-(2.93). Figures 2.2 and 2.3 give the key elements of the algorithms that are used to compute the projections of the EA- and IP-EOMCCSDt eigenvalue problems on the selected $3p$-$2h$ and $3h$-$2p$ determinants, $|\Phi_{jk}^{\mathbf{A}bc}\rangle$ and $|\Phi_{\mathbf{I}jk}^{bc}\rangle$, respectively, which are the most expensive and difficult parts of the EA-EOMCCSDt and IP-EOMCCSDt calculations (see Eqs. (2.48)-(2.56) and (2.58)-(2.64) for the EA-EOMCCSDt case and Eqs. (2.77)-(2.85) and (2.87)-(2.93) for the IP-EOMCCSDt case). The algorithms for calculating the remaining $1p$, $2p$-$1h$, $1h$, and $2h$-$1p$ projections are similar and are not discussed here.

One of the key features of our algorithm is the fact that the explicit loops that are used to construct the EA-EOMCCSDt and IP-EOMCCSDt equations projected on $|\Phi_{jk}^{\mathbf{A}bc}\rangle$ and $|\Phi_{\mathbf{I}jk}^{bc}\rangle$, Eqs. (2.48) and (2.77), respectively, range over active indices only, as indicated in Figures 2.2 and 2.3 by the use of bold, uppercase letters for the looping variables. Within these usually short loops, thanks to the use of the one- and two-body matrix elements of $\bar{H}_{N,\mathrm{open}}^{(\mathrm{CCSD})}$, $\bar{h}_p^q$ and $\bar{h}_{pq}^{rs}$, respectively, and the recursively generated intermediates defined above, our code possesses a high degree of vectorization, allowing us to exploit highly efficient, fast matrix multiplication routines from the BLAS library to perform the necessary computations. To avoid confusion with the summations performed by the explicit loops over active indices, all of the remaining

summations which are performed by the fast matrix multiplication routines are explicitly labeled in Figures 2.2 and 2.3 using the traditional summation symbol Σ, rather than relying on the Einstein summation convention used in the rest of this dissertation. By incorporating the short loops over one or at most two active indices at a time, we are able to make the full use of the computational benefits offered by the fast matrix multiplication routines while simultaneously ensuring that any unnecessary overcomputation of terms of the EA-EOMCCSD($3p$-$2h$) and IP-EOMCCSD($3h$-$2p$) methods that vanish in the active space EA-EOMCCSDt and IP-EOMCCSDt schemes is avoided. As a result, the EA-EOMCCSDt and IP-EOMCCSDt codes described in this work take full advantage of the low $N_u n_o^2 n_u^4$ and $N_o n_o^2 n_u^4$ CPU operation counts characterizing these approaches. In addition, although our current implementation is a serial code, the explicit loops over active indices used in our algorithm can easily be parallelized without altering the encompassed fast matrix multiplications, further improving the efficiency. Finally, it should be noted that the explicit loops over active indices make it possible to avoid storing the $N_u n_o^2 n_u^2$ (the EA-EOMCCSDt case) and $N_o n_o^2 n_u^2$ (the IP-EOMCCSDt case) objects in memory. As a result, the memory requirements for the present implementations of the EA- and IP-EOMCCSDt methods are $\sim 2 n_o n_u^3$ words, i.e., similar to the memory requirements of the conventional CCSD or EOMCCSD approaches. These memory requirements are solely defined by the construction of the matrix elements of $\bar{H}^{(\mathrm{CCSD})}_{N,\mathrm{open}}$ (see Table 2.1) and are the same as the memory requirements characterizing the low-order EA-EOMCCSD($2p$-$1h$) and IP-EOMCCSD($2h$-$1p$) schemes. The highly efficient computer programs based on the above algorithms for the EA-EOMCCSDt and IP-EOMCCSDt methods and the corresponding EA-EOMCCSD($2p$-$1h$), IP-EOMCCSD($2h$-$1p$), EA-EOMCCSD($3p$-$2h$), and IP-EOMCCSD($3h$-$2p$) codes were interfaced with the RHF/ROHF and integral routines available in GAMESS. The EA-EOMCCSD($2p$-$1h$), IP-EOMCCSD($2h$-$1p$), EA-EOMCCSD($3p$-$2h$), and EA-EOMCCSDt GAMESS options will be released to

the world within the next few weeks. The release of the IP-EOMCCSD($3h$-$2p$) and IP-EOMCCSDt options will follow in the not-too-distant future.

Figure 2.2: The key elements of the algorithm used to compute $\langle \Phi^{\mathbf{A}bc}_{jk} | (\bar{H}^{(\mathrm{CCSD})}_{N,\mathrm{open}} R^{(N+1)}_{\mu})_C | \Phi \rangle$, Eq. (2.48), in the efficient implementation of the EA-EOMCCSDt method.

Calculate $\tilde{I}_{ab}^{\ f}$ for all values of a, b, f, Eq.(2.64)

Calculate $\tilde{I}_{am}^{\ j}$ for all values of a, m, j, Eq.(2.60)

Set $I_{ab}^{\ f} = \tilde{I}_{ab}^{\ f}$ for all values of a, b, f

Set $I_{am}^{\ j} = \tilde{I}_{am}^{\ j}$ for all values of a, m, j

LOOP OVER **D**

Calculate $I_{\mathbf{D}b}^{\ f} = I_{\mathbf{D}b}^{\ f} - \frac{1}{2} \sum_{e,m,n} v_{mn}^{ef} r_{\mathbf{D}eb}^{\ mn}$ for all values of b, f, Eq.(2.61)

Calculate $I_{\mathbf{aD}}^{\ f} = I_{\mathbf{aD}}^{\ f} - \frac{1}{2} \sum_{e,m,n} v_{mn}^{ef} r_{\mathbf{Da}e}^{\ mn}$ for all values of $\mathbf{a}, f$, Eq.(2.62)

Calculate $I_{\mathbf{ab}}^{\ f} = I_{\mathbf{ab}}^{\ f} + \frac{1}{2} \sum_{m,n} v_{mn}^{\mathbf{D}f} r_{\mathbf{Dab}}^{\ mn}$ for all values of $\mathbf{a}, \mathbf{b}, f$, Eq.(2.63)

Calculate $I_{\mathbf{D}m}^{\ j} = I_{\mathbf{D}m}^{\ j} + \frac{1}{2} \sum_{e,f,n} v_{mn}^{ef} r_{\mathbf{D}ef}^{\ jn}$ for all values of m, j, Eq.(2.58)

Calculate $I_{\mathbf{a}m}^{\ j} = I_{\mathbf{a}m}^{\ j} + \sum_{n} \sum_{f(>\mathbf{D})} v_{mn}^{\mathbf{D}f} r_{\mathbf{D}f\mathbf{a}}^{\ jn}$ for all values of $\mathbf{a}, m, j$, Eq.(2.59)

END OF LOOP OVER **D**

LOOP OVER **A**

Calculate $\gamma_{\mathbf{A}bc}^{\ jk}$, $\beta_{\mathbf{A}bc}^{\ jk}$, and $\chi_{\mathbf{A}bc}^{\ jk}$ for all values of b, c, j, k,

Eqs.(2.52)-(2.54)

Set $\Delta_{\mathbf{A}bc}^{\ jk} = \chi_{\mathbf{A}bc}^{\ jk}$ for all values of $\mathbf{b}, c, j, k$

LOOP OVER **E**

Calculate $\Delta_{\mathbf{AbC}}^{\ jk} = \Delta_{\mathbf{AbC}}^{\ jk} - \frac{1}{2} \sum_{f(>\mathbf{E})} \bar{h}_{\mathbf{AC}}^{\mathbf{E}f} r_{\mathbf{E}f\mathbf{b}}^{\ jk}$ for all values of $\mathbf{b}, \mathbf{C}, j, k$,

Eq.(2.55)

Calculate $\Delta_{\mathbf{Abc}}^{\ jk} = \Delta_{\mathbf{Abc}}^{\ jk} - \frac{1}{2} \sum_{f(>\mathbf{E})} \bar{h}_{\mathbf{Ac}}^{\mathbf{E}f} r_{\mathbf{E}f\mathbf{b}}^{\ jk} + \frac{1}{4} \bar{h}_{\mathbf{A}}^{\mathbf{E}} r_{\mathbf{Ebc}}^{\ jk} - \frac{1}{2} \sum_{m} \bar{h}_{m\mathbf{A}}^{j\mathbf{E}} r_{\mathbf{Ebc}}^{\ mk}$

for all values of $\mathbf{b}, \mathbf{c}, j, k$, Eq.(2.56)

END OF LOOP OVER **E**

Set $\mathfrak{T}_{\mathbf{Abc}}^{\ jk} = \Delta_{\mathbf{Abc}}^{\ jk}$, Eq.(2.51)

END OF LOOP OVER **A**

LOOP OVER **A**

LOOP OVER **D**

Calculate $\mathfrak{T}_{\mathbf{AD}c}^{\ jk}$ for all values of c, j, k, Eq.(2.49)

Calculate $\mathfrak{T}_{\mathbf{AbD}}^{\ jk}$ for all values of $\mathbf{b}, j, k$, Eq.(2.50)

END OF LOOP OVER **D**

Calculate $\langle \Phi_{jk}^{\mathbf{A}bc} | (\bar{H}_{N,\mathrm{open}}^{(\mathrm{CCSD})} R_{\mu}^{(N+1)})_C | \Phi \rangle$ by antisymmetrizing $\mathfrak{T}_{\mathbf{A}bc}^{\ jk}$, Eq.(2.48)

END OF LOOP OVER **A**

Figure 2.3: The key elements of the algorithm used to compute $\langle \Phi^{bc}_{\mathbf{I}jk} | (\bar{H}^{(\mathrm{CCSD})}_{N,\mathrm{open}} R^{(N-1)}_{\mu})_C | \Phi \rangle$ Eq. (2.77), in the efficient implementation of the IP-EOMCCSDt method.

Calculate $\tilde{I}^{jk}_{n}$ for all values of j,k,n, Eq.(2.93)

Calculate $\tilde{I}^{if}_{c}$ for all values of i,c,f, Eq.(2.89)

Set $I^{jk}_{n} = \tilde{I}^{jk}_{n}$ for all values of j,k,n

Set $I^{if}_{c} = \tilde{I}^{if}_{c}$ for all values of i,c,f

LOOP OVER **L**

Calculate $I^{\mathbf{L}k}_{n} = I^{\mathbf{L}k}_{n} + \frac{1}{2}\sum_{m,e,f} v^{ef}_{mn} r^{\mathbf{L}mk}_{ef}$ for all values of k,n, Eq.(2.90)

Calculate $I^{\mathbf{jL}}_{n} = I^{\mathbf{jL}}_{n} + \frac{1}{2}\sum_{m,e,f} v^{ef}_{mn} r^{\mathbf{Lj}m}_{ef}$ for all values of $\mathbf{j},n$, Eq.(2.91)

Calculate $I^{\mathbf{jk}}_{n} = I^{\mathbf{jk}}_{n} - \frac{1}{2}\sum_{e,f} v^{ef}_{\mathbf{L}n} r^{\mathbf{Ljk}}_{ef}$ for all values of $\mathbf{j},\mathbf{k},n$, Eq.(2.92)

Calculate $I^{\mathbf{L}f}_{c} = I^{\mathbf{L}f}_{c} - \frac{1}{2}\sum_{m,n,e} v^{ef}_{mn} r^{\mathbf{L}mn}_{ec}$ for all values of c,f, Eq.(2.87)

Calculate $I^{\mathbf{i}f}_{c} = I^{\mathbf{i}f}_{c} - \sum_{e}\sum_{n<(\mathbf{L})} v^{ef}_{\mathbf{L}n} r^{\mathbf{L}n\mathbf{i}}_{ec}$ for all values of $\mathbf{i},c,f$, Eq.(2.88)

END OF LOOP OVER **L**

LOOP OVER **I**

Calculate $\gamma^{\mathbf{I}jk}_{bc}$, $\beta^{\mathbf{I}jk}_{bc}$, and $\chi^{\mathbf{I}jk}_{bc}$ for all values of j,k,b,c, Eqs.(2.81)-(2.83)

Set $\Delta^{\mathbf{I}jk}_{bc} = \chi^{\mathbf{I}jk}_{bc}$ for all values of $\mathbf{j},k,b,c$

LOOP OVER **M**

Calculate $\Delta^{\mathbf{IjK}}_{bc} = \Delta^{\mathbf{IjK}}_{bc} - \frac{1}{2}\sum_{n(<\mathbf{M})} \bar{h}^{\mathbf{IK}}_{\mathbf{M}n} r^{\mathbf{M}n\mathbf{j}}_{bc}$ for all values of $\mathbf{j},\mathbf{K},b,c$, Eq.(2.84)

Calculate $\Delta^{\mathbf{Ijk}}_{bc} = \Delta^{\mathbf{Ijk}}_{bc} - \frac{1}{2}\sum_{n(<\mathbf{M})} \bar{h}^{\mathbf{Ik}}_{\mathbf{M}n} r^{\mathbf{M}n\mathbf{j}}_{bc} - \frac{1}{4}\bar{h}^{\mathbf{I}}_{\mathbf{M}} r^{\mathbf{Mjk}}_{bc} - \frac{1}{2}\sum_{e} \bar{h}^{\mathbf{I}e}_{\mathbf{M}c} r^{\mathbf{Mjk}}_{be}$ for all values of $\mathbf{j},\mathbf{k},b,c$, Eq.(2.85)

END OF LOOP OVER **M**

Set $\mathfrak{T}^{\mathbf{Ijk}}_{bc} = \Delta^{\mathbf{Ijk}}_{bc}$, Eq.(2.80)

END OF LOOP OVER **I**

LOOP OVER **I**

LOOP OVER **L**

Calculate $\mathfrak{T}^{\mathbf{IL}k}_{bc}$ for all values of k,b,c, Eq.(2.78)

Calculate $\mathfrak{T}^{\mathbf{IjL}}_{bc}$ for all values of $\mathbf{j},b,c$, Eq.(2.79)

END OF LOOP OVER **L**

Calculate $\langle \Phi^{bc}_{\mathbf{I}jk} | (\bar{H}^{(\mathrm{CCSD})}_{N,\mathrm{open}} R^{(N-1)}_{\mu})_C | \Phi \rangle$ by antisymmetrizing $\mathfrak{T}^{\mathbf{I}jk}_{bc}$, Eq.(2.77)

END OF LOOP OVER **I**

2.2 Applications

To illustrate the accuracy of the EA- and IP-EOMCCSDt methods as well as the performance of the highly efficient computer codes that we developed for these methods using the algorithms discussed in Section 2.1.3, several benchmark calculations for small open-shell systems, for which the exact full configuration interaction (CI) or other reliable theoretical and experimental data are available, are examined. One of our main goals is to demonstrate the ability of EA- and IP-EOMCCSDt approaches to provide results of the same accuracy as their parent EA-EOMCCSD($3p$-$2h$) and IP-EOMCCSD($3h$-$2p$) schemes, while maintaining computational costs on the order of the much less expensive CCSD approach.

2.2.1 Excitation Energies of Diatomic Radicals: CH and SH

In this section we consider benchmark calculations for the low-lying excited states of the CH and SH radicals [85, 87]. We begin by considering CH, for which we performed the EA-EOMCCSD($2p$-$1h$), EA-EOMCCSD($3p$-$2h$), and EA-EOMCCSDt calculations of the adiabatic excitation energies T_e corresponding to four low-lying excited states using the aug-cc-pVxZ (x=D, T, and Q) basis sets [178–180] (see Tables 2.3 and 2.4). These results are compared with the UHF-based EOMCCSD and EOMCCSDT calculations reported in [31] and our own complete-active-space self-consistent field theory (CASSCF) based MRCI(Q) calculations using the internally contracted MRCI approach with quasidegenerate Davidson corrections [181, 182], as implemented in MOLPRO [183] (see [184] for more information). In all EA-EOMCC calculations for CH, the RHF determinant for the closed-shell CH^+ ion was employed as a reference, and two separate sets of EA-EOMCCSDt calculations, which differed in the size of the active space considered, were carried out. In the first set of the EA-EOMCCSDt calculations for CH, the active space consisted of the $1\pi_x$ and $1\pi_y$

orbitals of CH^+, while the second set used a slightly larger active space composed of the $1\pi_x$, $1\pi_y$, and 4σ orbitals. The relevant experimental data, including adiabatic excitation energies and the equilibrium bond lengths used in the CC/EOMCC and MRCI(Q) calculations, were taken from [185–189] (the same values were used in [31]). The lowest-energy core orbital (which correlates with the $1s$ orbitals of C) was kept frozen, and the spherical components of the d and (where present in the basis set) f functions were used. The C_{2v} symmetry was exploited.

The CH radical is quite challenging for the basic, low-order CC/EOMCC methods due to the strong multi-reference or doubly excited character of several of the low-lying excited states (cf., e.g., [132,190,191]). Indeed, an analysis of Table 2.3 reveals that the basic EA-EOMCCSD($2p$-$1h$) approach has severe difficulty describing the excited states of CH, producing errors relative to the highly accurate EOMCCSDT and MRCI(Q) results for these states which range from 1.50 to 3.18 eV and 1.53 to 3.29 eV, respectively. The UHF-based EOMCCSD approach is better, but only slightly. For the $B\ ^2\Sigma^-$ and $C\ ^2\Sigma^+$ states, which have a significant doubly excited character, the errors in the EOMCCSD values of T_e relative to the highly accurate EOMCCSDT data of [31] are 1.14-1.35 and 1.22-1.45 eV, respectively. Furthermore, the EA-EOMCCSD($2p$-$1h$) method predicts an incorrect ordering of excited states by placing the $B\ ^2\Sigma^-$ state higher in energy than the $C\ ^2\Sigma^+$ state. These major failures of the EA-EOMCCSD($2p$-$1h$) approximation and the EOMCCSD approach point to the need for including the higher-order $3p$-$2h$ effects in the EA-EOMCC formalism in order to accurately describe the excitation spectrum of CH. Indeed, the EA-EOMCCSD($3p$-$2h$) method greatly improves the poor EA-EOMCCSD($2p$-$1h$) and EOMCCSD results, restoring the correct ordering of states and reducing the large errors relative to EOMCCSDT and MRCI(Q) down to $\sim 0.01 - 0.12$ and $0.02 - 0.15$ eV, respectively. Unfortunately, this success comes at a high price. For instance, as shown in Table 2.4, the average time per iteration for the EA-EOMCCSD($3p$-$2h$)

calculations is, depending on the basis set, anywhere from 56 to 69 times longer than the iteration time for the corresponding EA-EOMCCSD(2p-1h) calculation. Such a dramatic increase in the computational costs makes the EA-EOMCCSD(3p-2h) approach impractical for most realistic applications.

In order to avoid the large computational costs of the EA-EOMCCSD(3p-2h) method, while accurately including the most important 3p-2h correlation effects, we consider the active-space EA-EOMCCSDt approximation. Table 2.3 reveals that for both active spaces considered in this work the EA-EOMCCSDt approach is capable of reproducing the highly accurate EA-EOMCCSD(3p-2h) results almost perfectly. In fact, the EA-EOMCCSDt scheme produces excitation energies for these states and basis sets which differ from the EA-EOMCCSD(3p-2h) values by $\sim 0.01 - 0.05$ eV, regardless of which of the two active spaces is used. The real success of the EA-EOMCCSDt approximation, however, is the fact that it produces these high accuracies at a small fraction of the large costs needed by the full EA-EOMCCSD(3p-2h) method. As shown in Table 2.4, the computer times required by the EA-EOMCCSDt approach are on the order of those characterizing the inexpensive EA-EOMCCSD(2p-1h) and CCSD/EOMCCSD calculations. This is particularly true for the aug-cc-pVQZ basis set, for which the average time per iteration for the EA-EOMCCSDt calculations is only around 3 times longer than the EA-EOMCCSD(2p-1h) iteration time. This is a factor of 20 speed-up relative to the EA-EOMCCSD(3p-2h) scheme. The results in Tables 2.3 and 2.4 clearly illustrate the ability of the EA-EOMCCSDt method to balance accuracy and computational cost when studying the excited states of radicals, producing accuracies equivalent to the very expensive EA-EOMCCSD(3p-2h) approximation at the relatively low costs characterizing the standard EA-EOMCCSD(2p-1h) and CCSD/EOMCCSD approaches.

We now consider the SH radical (Tables 2.5 and 2.6). In this case, we performed the IP-EOMCCSD(2h-1p), IP-EOMCCSD(3h-2p), and IP-EOMCCSDt calculations

Table 2.3: The ground-state energies and the adiabatic excitation energies corresponding to the low-lying excited states of the CH radical, as obtained with the aug-cc-pVxZ (x=D, T, and Q) basis sets [178–180]. Units are hartree for the ground-state energy and eV for the excitation energies. Experimental excitation energies and nuclear geometries used in the CC/EOMCC calculations[a] are taken from [185–189]. In all correlated calculations the lowest energy core orbital was frozen.

	CCSD/	CCSDT/	EA-EOM					
State	EOMCCSD[b]	EOMCCSDT[b]	CCSD(2p-1h)	CCSD(3p-2h)	CCSDt[c]	CCSDt[d]	MRCI(Q)[e]	Exp.
aug-cc-pVDZ								
$X\ ^2\Pi$	-38.384 805	-37.387 721	-38.385 027	-38.386 710	-38.384 594	-38.385 058	-38.388 014	
$a\ ^4\Sigma^-$	0.95	0.66	2.369	0.666	0.635	0.641	0.648	0.74 [189]
$A\ ^2\Delta$	3.33	3.02	4.898	3.037	3.008	3.015	3.002	2.87 [185]
$B\ ^2\Sigma^-$	4.41	3.27	6.105	3.377	3.349	3.357	3.258	3.23 [187]
$C\ ^2\Sigma^+$	5.29	4.07	5.570	4.100	4.088	4.092	4.038	3.94 [188]
aug-cc-pVTZ								
$X\ ^2\Pi$	-38.409 320	-38.413 493	-38.409 823	-38.412 070	-38.409 013	-38.409 413	-38.413 811	
$a\ ^4\Sigma^-$	1.03	0.74	2.661	0.743	0.697	0.704	0.718	0.74 [189]
$A\ ^2\Delta$	3.28	2.94	5.120	2.964	2.925	2.931	2.911	2.87 [185]
$B\ ^2\Sigma^-$	4.62	3.27	6.453	3.393	3.353	3.359	3.251	3.23 [187]
$C\ ^2\Sigma^+$	5.48	4.03	5.815	4.053	4.036	4.040	3.980	3.94 [188]
aug-cc-pVQZ								
$X\ ^2\Pi$	-38.415 848	-	-38.416 559	-38.418 732	-38.415 489	-38.415 905	-38.420 576	
$a\ ^4\Sigma^-$	1.06	-	2.741	0.766	0.717	0.724	0.741	0.74 [189]
$A\ ^2\Delta$	3.27	-	5.181	2.952	2.911	2.917	2.896	2.87 [185]
$B\ ^2\Sigma^-$	4.67	-	6.538	3.390	3.347	3.355	3.245	3.23 [187]
$C\ ^2\Sigma^+$	5.52	-	5.878	4.037	4.019	4.021	3.962	3.94 [188]

[a] The equilibrium bond lengths used in the CC/EOMCC calculations were taken from experiment and are the same as those used by Hirata in [31]. They are: r_e = 1.1197868 Å for the $X\ ^2\Pi$ state [185], r_0 = 1.0977 Å for the $a\ ^4\Sigma^-$ state [186], r_e = 1.1031 Å for the $A\ ^2\Delta$ state [185], r_e = 1.1640 Å for the $B\ ^2\Sigma^-$ state [187], and r_e = 1.1143 Å for the $C\ ^2\Sigma^+$ state [188].

[b] The UHF-based results reported in [31].

[c] The active space consisted of the $1\pi_x$ and $1\pi_y$ orbitals of CH^+.

[d] The active space consisted of the $1\pi_x$, $1\pi_y$, and 4σ orbitals of CH^+.

[e] The active space consisted of 14 orbitals; see [184] for further information.

Table 2.4: The average time per iteration for the EA-EOMCCSD($3p$-$2h$) and EA-EOMCCSDt calculations[a] performed for the CH radical with the aug-cc-pVxZ (x=D, T, and Q) basis sets [178–180]. The average times T are reported as $T/T_{2p\text{-}1h}$, where $T_{2p\text{-}1h}$ is the average time per iteration for the corresponding EA-EOMCCSD($2p$-$1h$) calculation. In all correlated calculations the lowest energy core orbital was kept frozen.

Method	aug-cc-pVDZ	aug-cc-pVTZ	aug-cc-pVQZ
EA-EOMCCSD($3p$-$2h$)	68.67	61.42	56.42
EA-EOMCCSDt[b]	7.39	4.18	3.00
EA-EOMCCSDt[c]	9.44	5.57	3.45
CCSD[d]	8.56	5.86	4.68
EOMCCSD[e]	1.72	1.00	1.19

[a] For consistency purposes, the average iteration time is computed using the first 10 iterations of the calculation for the ground state of the CH radical. The excited state calculations show essentially identical timings.
[b] The active space consisted of the $1\pi_x$ and $1\pi_y$ orbitals of CH^+.
[c] The active space consisted of the $1\pi_x$, $1\pi_y$, and 4σ orbitals of CH^+.
[d] ROHF-based CCSD calculation for the ground state using codes described in [132].
[e] ROHF-based EOMCCSD calculation for the $a\,^4\Sigma^-$ state using codes described in [132].

of the vertical excitation energies corresponding to six low-lying excited states, as well as the CASSCF-based MRCI(Q) calculations for comparison purposes (see [184] for further information). The equilibrium geometry for SH used in these calculations was taken from [192] and the basis sets considered consisted of the aug-cc-pV(x+d)Z basis [180, 193] for the S atom and the aug-cc-pVxZ basis [178, 180] for the H atom (x = D and T). The RHF determinant of the closed-shell SH^- ion was used as a reference in all IP-EOMCC calculations and the active-space for the IP-EOMCCSDt calculations consisted of the $2\pi_x$ and $2\pi_y$ orbitals of SH^-. The lowest-energy core orbital (which correlates with the $1s$ orbital of S) was kept frozen, and the spherical components of the d and (where present in the basis set) f functions were utilized. In analogy to CH, the C_{2v} symmetry was exploited.

As was the case for the CH radical, the SH system is very difficult to describe with the standard, low-order CC/EOMCC methods, such as the basic IP-EOMCCSD($2h$-$1p$)

Table 2.5: The ground-state energies and the vertical excitation energies corresponding to the low-lying excited states of the SH radical, as obtained with the aug-cc-pV(x+d)Z basis set for S [180, 193] and the aug-cc-pVxZ basis set for H [178, 180], where x=D and T. Units are hartree for the ground-state energy and eV for the excitation energies.[a]

	IP-EOM			
State	CCSD(2h-1p)	CCSD(3h-2p)	CCSDt[b]	MRCI(Q)[c]
	aug-cc-pV(D+d)Z/aug-cc-pVDZ			
$X\ ^2\Pi$	-398.287 215	-398.294 398	-398.294 167	-398.299 262
$A\ ^2\Sigma^+$	4.002	3.936	3.926	3.962
$1\ ^4\Sigma^-$	9.168	5.830	5.824	5.437
$1\ ^2\Sigma^-$	10.575	6.567	6.561	6.034
$1\ ^2\Delta$	10.713	7.383	7.378	7.001
$B\ ^2\Sigma^+$	10.341	8.191	8.210	7.862
$1\ ^4\Pi$	11.738	8.425	8.420	8.079
	aug-cc-pV(T+d)Z/aug-cc-pVTZ			
$X\ ^2\Pi$	-398.378 344	-398.388 242	-398.387 932	-398.395 274
$A\ ^2\Sigma^+$	3.987	3.926	3.912	3.949
$1\ ^4\Sigma^-$	11.252	5.994	5.986	5.527
$1\ ^2\Sigma^-$	10.878	6.766	6.758	6.175
$1\ ^2\Delta$	12.565	7.405	7.398	6.992
$B\ ^2\Sigma^+$	12.197	8.265	8.284	7.863
$1\ ^4\Pi$	12.028	8.561	8.554	8.103

[a] All calculations were performed at the experimental equilibrium geometry, r_e = 1.3409 Å, taken from [192]. In all correlated calculations the lowest energy core orbital was kept frozen.

[b] The active space consisted of the $2\pi_x$ and $2\pi_y$ orbitals of SH^-.

[c] The active space consisted of 10 orbitals; see [184] for further information.

Table 2.6: The average time per iteration for the IP-EOMCCSD($3h$-$2p$) and IP-EOMCCSDt calculations[a] performed for the SH radical with the aug-cc-pV(x+d)Z basis set for S [180, 193] and the aug-cc-pVxZ basis set for H [178, 180] where n=D and T. The average times T are reported as $T/T_{2h\text{-}1p}$, where $T_{2h\text{-}1p}$ is the average time per iteration for the corresponding IP-EOMCCSD($2h$-$1p$) calculation. In all correlated calculations the lowest energy core orbital was kept frozen.

Method	aug-cc-pV(D+d)Z	aug-cc-pV(T+d)Z
IP-EOMCCSD($3h$-$2p$)	332	1144
IP-EOMCCSDt[b]	118	280
CCSD[c]	44	342
EOMCCSD[d]	17	71

[a] For consistency purposes, the average iteration time is computed using the first 10 iterations of the calculation for the ground state of the SH radical. The excited state calculations show essentially identical timings.
[b] The active space consisted of the $2\pi_x$ and $2\pi_y$ orbitals of SH^-.
[c] ROHF-based CCSD calculation for the ground state using codes described in [132].
[d] ROHF-based EOMCCSD calculation for the $A\,^2\Sigma^+$ state using codes described in [132].

approach. Table 2.5 reveals that, with the exception of the $A\,^2\Sigma^+$ state, the IP-EOMCCSD($2h$-$1p$) approximation completely fails for the low-lying excited states studied in this work, producing errors relative to MRCI(Q) of $3.93 - 5.73$ eV when the aug-cc-pV(T+d)Z basis set is employed. This dramatic failure illustrates how essential the higher-order correlation effects, such as the $3h$-$2p$ component of the ionizing operator $R_\mu^{(N-1)}$, are when describing the excited states of SH. By explicitly including the $3h$-$2p$ contributions in the IP-EOMCC formalism, we can significantly improve these poor results. As shown in Table 2.5, the IP-EOMCCSD($3h$-$2p$) method reduces the huge errors relative to MRCI(Q) produced by the IP-EOMCCSD($2h$-$1p$) calculations to $\sim 0.40 - 0.59$ eV. These errors are still larger than one would like, possibly indicating a need for incorporating $4h$-$3p$ effects in the calculation, but clearly the IP-EOMCCSD($3h$-$2p$) results represent a major improvement over the poor performance of the IP-EOMCCSD($2h$-$1p$) method. Again, as was the case for CH, this improvement comes with a significant increase in the computational costs compared

to the IP-EOMCCSD($2h$-$1p$) calculations. As shown in Table 2.6, the average time per iteration required by the IP-EOMCCSD($3h$-$2p$) calculations with the aug-cc-pV(T+d)Z basis set is approximately 1100 times longer than that characterizing the IP-EOMCCSD($2h$-$1p$) calculations.

In order to reduce these high costs of the IP-EOMCCSD($3h$-$2p$) calculations we turn to the active-space IP-EOMCCSDt method. An analysis of the excitation energies in Table 2.5 shows that the IP-EOMCCSDt results are practically identical to those generated by the full IP-EOMCCSD($3h$-$2p$) method. In fact, the differences between the excitation energies produced by these two approaches do not exceed 0.02 eV for all states listed in Table 2.5. Most importantly, the IP-EOMCCSDt approach offers this excellent performance at a fraction of the high costs characterizing the IP-EOMCCSD($3h$-$2p$) calculations. This is shown in Table 2.6, where one can see that the average time per iteration required by the IP-EOMCCSDt approach is about four times smaller than the average time per iteration characterizing the IP-EOMCCSD($3h$-$2p$) calculation, when the aug-cc-pV(T+d)Z basis set is employed. The smaller degree of the savings in the computer effort in this case, compared to the EA-EOMCCSDt calculations for CH, is related to the fact that the ratio of the number of all occupied orbitals to active occupied orbitals in the SH/SH^- system is not as large as the ratio of the number of all unoccupied orbitals to active unoccupied orbitals in the CH/CH^+ system. The computational savings offered by the active-space IP-EOMCC schemes would be much more dramatic for larger systems, as well as for the higher-order active-space approximations, such as the IP-EOMCCSDtq method discussed in Section 2.1.2, where both active occupied and unoccupied orbitals are considered in selecting the dominant $4h$-$3p$ excitations (see Eq. (2.22)). On the other hand, it is encouraging to observe that a factor of four speed-up compared to the IP-EOMCCSD($3h$-$2p$) approach offered by the IP-EOMCCSDt calculations for SH is not achieved at the expense of losing the relatively high accuracy of the

IP-EOMCCSD($3h$-$2p$) results.

2.2.2 Potential Energy Curves of OH

In this section, we discuss IP-EOMCC and SAC-CI calculations of the potential energy curves for the low-lying states of the OH radical [86,88], which were performed using the 6-31G** [180, 194, 195] basis set and compared to the full CI results that were obtained with GAMESS (Figure 2.4 and Tables 2.7 – 2.10). The equilibrium geometry of OH was taken from [192]. In all calculations the lowest core orbital was kept frozen, the spherical components of the d functions were employed, and the C_{2v} symmetry was exploited. The SAC-CI calculations were carried out using the development version of the Gaussian suite of programs that was made available to my advisor by Professor Masahiro Ehara.

Figure 2.4: Potential energy curves for the ground and low-lying excited states of the OH radical. Energies are in hartree and the O-H distance $R_{\text{O-H}}$ is in Å. (*a*) The full CI results. (*b*) The IP-EOMCCSD($2h$-$1p$) results. (*c*) The IP-EOMCCSD($3h$-$2p$) results. (*d*) The IP-EOMCCSDt results. (*e*) The SAC-CI($4h$-$3p$) results (doublet states only). (*f*) The SAC-CI($4h$-$3p$)$\{3,1\}$ results (doublet states only).

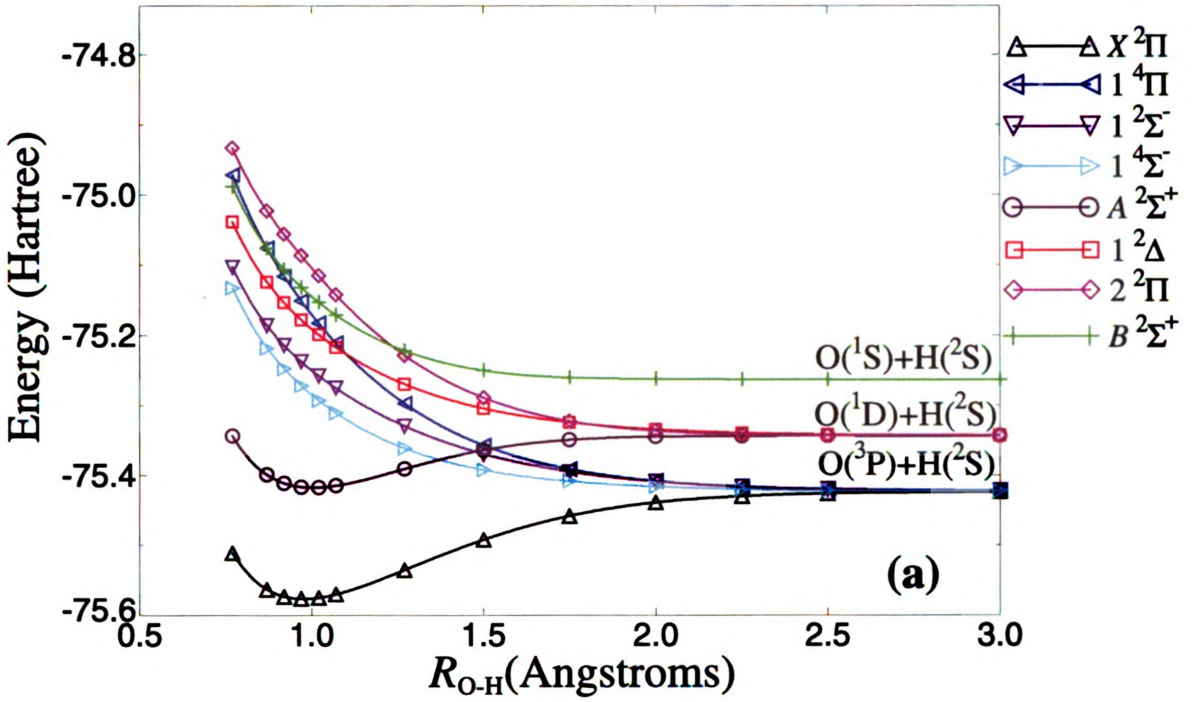
Energy (Hartree)
-74.8
-75.0
-75.2
-75.4
-75.6
0.5
1.0
1.5
2.0
2.5
3.0
$R_{O\text{-}H}$(Angstroms)
$X\,^2\Pi$
$1\,^4\Pi$
$1\,^2\Sigma^-$
$1\,^4\Sigma^-$
$A\,^2\Sigma^+$
$1\,^2\Delta$
$2\,^2\Pi$
$B\,^2\Sigma^+$
O(^{1}S)+H(^{2}S)
O(^{1}D)+H(^{2}S)
O(^{3}P)+H(^{2}S)
(a)

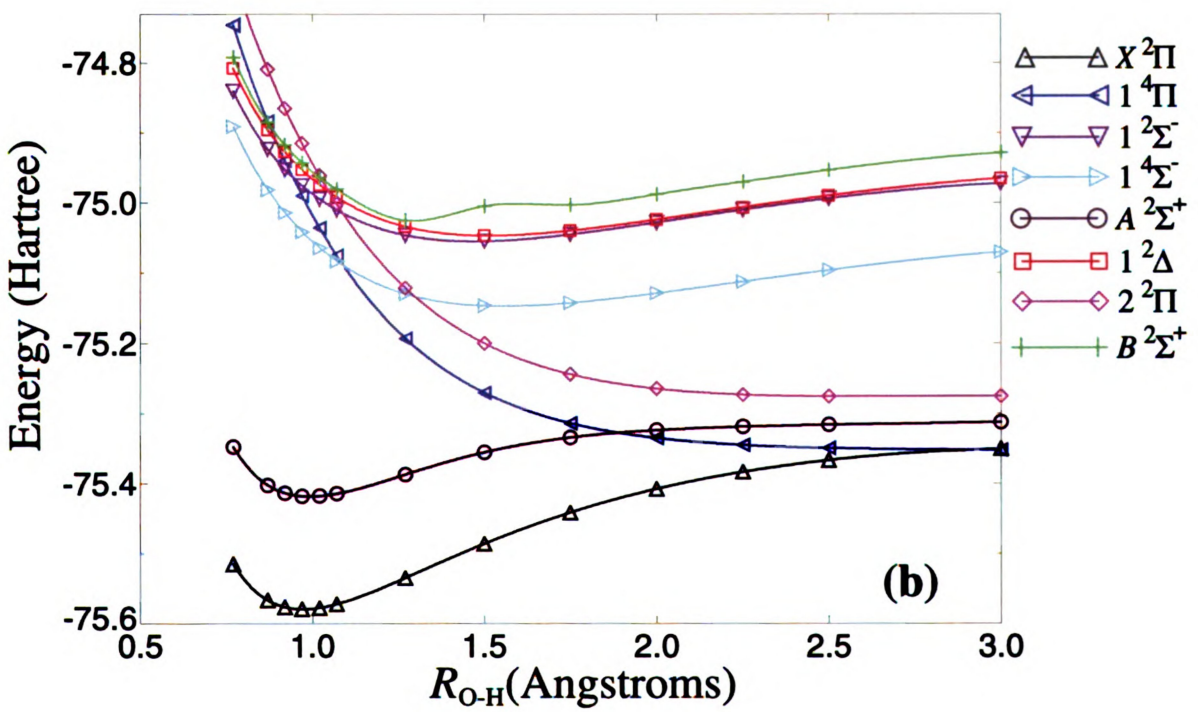
Energy (Hartree)
-74.8
-75.0
-75.2
-75.4
-75.6
0.5
1.0
1.5
2.0
2.5
3.0
$R_{O\text{-}H}$(Angstroms)
$X\,^2\Pi$
$1\,^4\Pi$
$1\,^2\Sigma^-$
$1\,^4\Sigma^-$
$A\,^2\Sigma^+$
$1\,^2\Delta$
$2\,^2\Pi$
$B\,^2\Sigma^+$
(b)

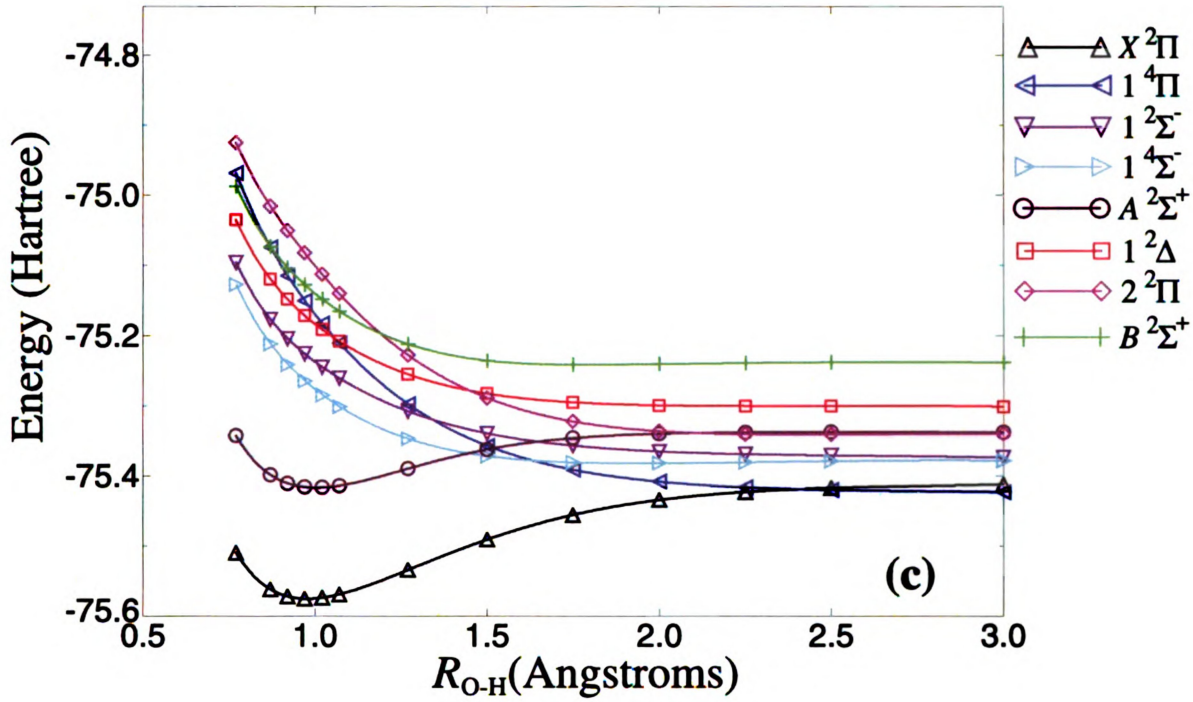

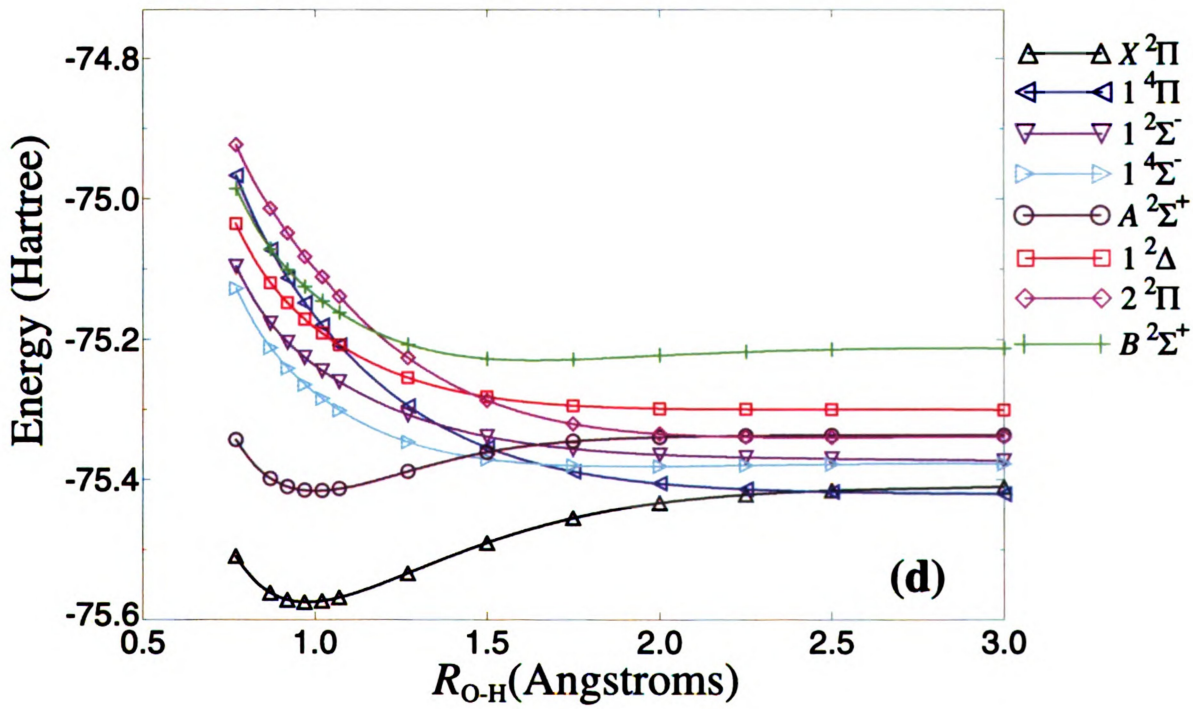

Figure 2.4 Continued

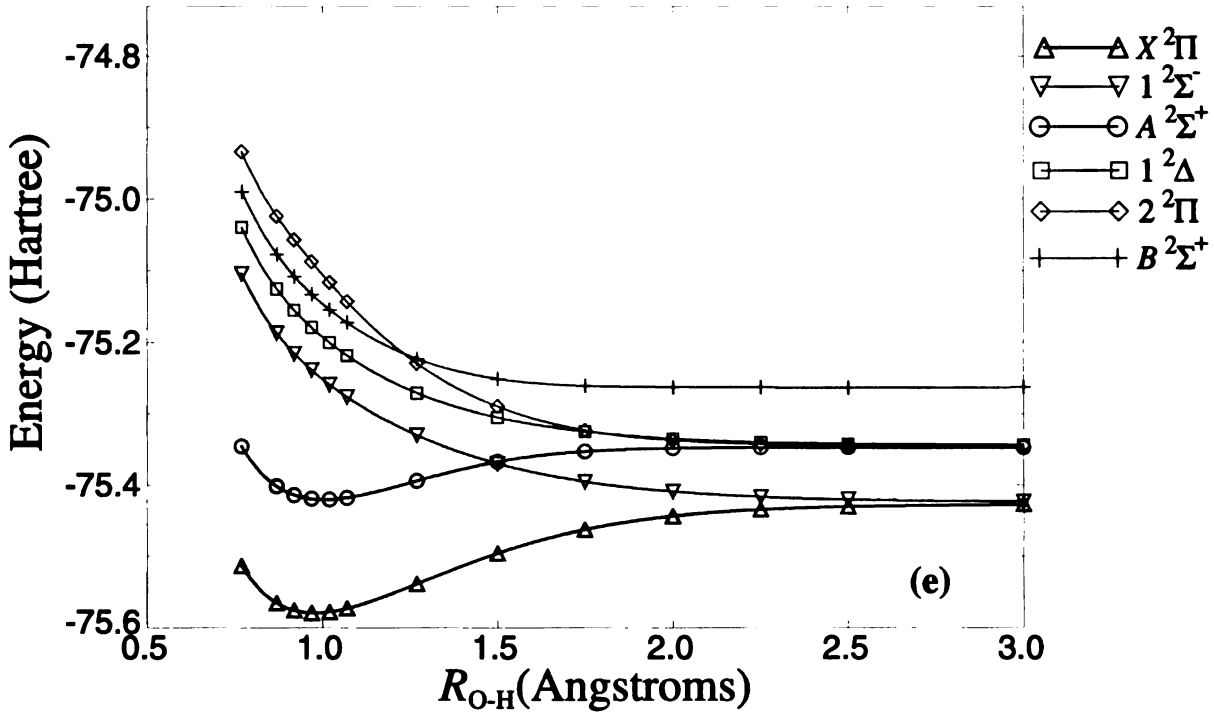

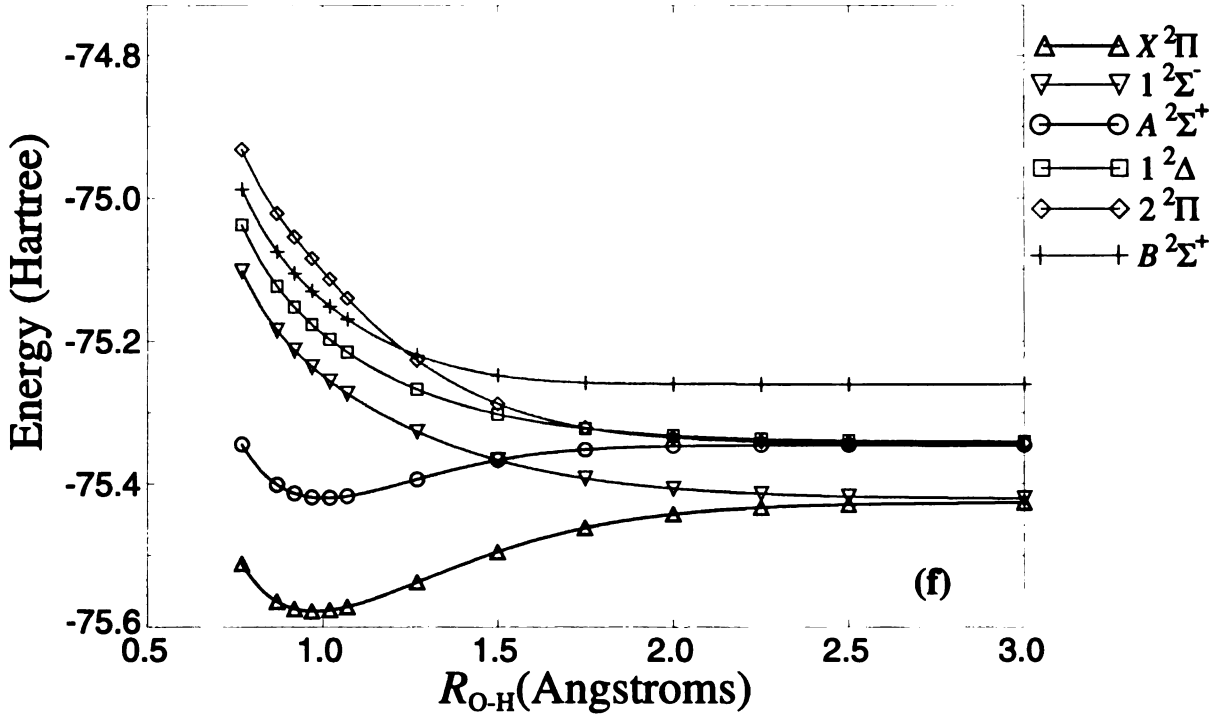

Figure 2.4 Continued

As was the case for the CH and SH radicals discussed in Section 2.2.1, many of the low-lying excited states of OH show a strong contribution from higher-order excitations or a significant multi-reference character (cf., e.g., [82, 196]). As a result, the OH radical is a challenging system to describe, especially for the low-order IP-EOMCCSD($2h$-$1p$) approach. In fact, if we look at the leading full CI configurations shown in Tables 2.7 and 2.8 we see that, with the exception of the $X\ ^2\Pi$ ground state and the $A\ ^2\Sigma^+$ excited state, the leading configuration for each state studied, at all four geometries analyzed in these tables, is at least a $2h$-$1p$ excitation relative to the ground-state reference configuration of OH^-. Just as the standard EOMCCSD approach fails for excited states dominated by doubles, the major contributions of $2h$-$1p$ excitations in the excited states of interest should cause a failure of the IP-EOMCCSD($2h$-$1p$) method, and, in fact, this is exactly what we observe. Tables 2.9 and 2.10 show that except for the $X\ ^2\Pi$ and $A\ ^2\Sigma^+$ states, the errors in the IP-EOMCCSD($2h$-$1p$) energies relative to full CI are huge, ranging from $\sim$ 70 to $\sim$ 450 millihartree. A comparison of Figures 2.4(a) and 2.4(b) reveals that these errors are not merely a quantitative concern, as this low-order approximation produces a qualitatively incorrect representation of the excited states of OH. The IP-EOMCCSD($2h$-$1p$) scheme shows some limited success only for the $X\ ^2\Pi$ and $A\ ^2\Sigma^+$ states, producing errors in the range of 0.6–4.3 millihartree for the O–H distances of 0.77–1.27 Å . However, it is important to notice that even in these two cases the relatively high accuracy of the IP-EOMCCSD($2h$-$1p$) results rapidly deteriorates as soon as the O–H distances become larger, with the errors in the IP-EOMCCSD($2h$-$1p$) results for the $X\ ^2\Pi$ and $A\ ^2\Sigma^+$ states steadily increasing to 73.5 and 31.6 millihartree, respectively, at the O–H separation of 3.0 Å. As is the case for the other states, this behavior is perfectly in sync with the nature of the leading configurations in the wave functions defining the $X\ ^2\Pi$ and $A\ ^2\Sigma^+$ states. Tables 2.7 and 2.8 show that at internuclear separations of 0.77 and 0.96966 Å, both states are predominantly single-reference states defined

by a $1h$ excitation, and as a result, the IP-EOMCCSD($2h$-$1p$) approach describes them well. As one moves out of the spectroscopic region, however, we see that the multi-reference character of the $X\ ^2\Pi$ and $A\ ^2\Sigma^+$ states increases, and $2h$-$1p$ (and even $3h$-$2p$) contributions become significant. In fact, for the $X\ ^2\Pi$ state, which of the two states analyzed here is the one that the IP-EOMCCSD($2h$-$1p$) approach has more difficulty with, a $2h$-$1p$ excitation actually becomes the dominant contribution.

The significant contributions of the $2h$-$1p$ excitations and the failure of the IP-EOMCCSD($2h$-$1p$) approach illustrate the importance of considering the $3h$-$2p$ components of the ionizing operator $R_\mu^{(N-1)}$ in calculations of the excited states of OH. Indeed, as shown in Tables 2.9 and 2.10, the inclusion of these effects through the IP-EOMCCSD($3h$-$2p$) approach does offer considerable improvements over the huge errors produced by IP-EOMCCSD($2h$-$1p$). The IP-EOMCCSD($3h$-$2p$) approach does a particularly good job of describing the $1\ ^4\Pi$ state, reducing the 225.443 millihartree maximum unsigned error (MUE) and 154.788 millihartree non-parallelity error (NPE value; defined as the difference between the most positive and most negative signed errors relative to full CI along a given potential energy curve) down to 2.674 and 2.374 millihartree, respectively. Since this state is strongly dominated by $2h$-$1p$ excitations and shows relatively small contributions from $3h$-$2p$ excitations, as shown in Table 2.7, it is not surprising that it is described so well at the $3h$-$2p$ level of theory. Though it does show somewhat larger contributions from the $3h$-$2p$ excitations than the $1\ ^4\Pi$ state, the $2\ ^2\Pi$ state is also described reasonably well by the IP-EOMCCSD($3h$-$2p$) method, producing the reasonable MUE and NPE values of 7.793 and 6.658 millihartree, respectively. The $X\ ^2\Pi$ and $A\ ^2\Sigma^+$ states are also well described by the IP-EOMCCSD($3h$-$2p$) scheme, especially in the spectroscopic region, where the errors relative to full CI are roughly 1.5 millihartree. Unfortunately the growing role of the $3h$-$2p$ excitations as the internuclear separation is increased results in errors that become as large as 11.777 and 6.272 millihartree, respectively, as the O-H distance

Table 2.7: An analysis of the major full CI configurations[a] for the low-lying Π and Δ states of the OH radical for a selected set of internuclear separations $R_{\text{O-H}}$.

State	Configuration Orbital Occupancy	Coefficients for Various Values of $R_{\text{O-H}}$				Excitation Type[c]
		0.77 Å	0.96966 Å[b]	1.50 Å	3.00 Å	
$X\ ^2\Pi$	$\|(1\sigma)^2(2\sigma)^2(3\sigma)^2(1\pi_x)^2(1\pi_y)^1\|$	0.961	0.951	0.873	-0.431	$1h$
	$\|(1\sigma)^2(2\sigma)^2(3\sigma)^1(1\pi_x)^2(1\pi_y)^1(4\sigma)^1\|$[d]	< 0.01, 0.070	0.017, 0.145	0.120, 0.356	0.472, 0.621	$2h$-$1p$
	$\|(1\sigma)^2(2\sigma)^2(1\pi_x)^2(1\pi_y)^1(4\sigma)^2\|$	< 0.01	-0.024	-0.144	0.356	$3h$-$2p$
$1\ ^2\Delta$	$\|(1\sigma)^2(2\sigma)^2(3\sigma)^2[(1\pi_x)^2-(1\pi_y)^2](4\sigma)^1\|$	-0.651	0.633	0.555	0.268	$2h$-$1p$
	$\|(1\sigma)^2(2\sigma)^2(3\sigma)^1[(1\pi_x)^2-(1\pi_y)^2](4\sigma)^2\|$	0.075	0.144	-0.367	-0.620	$3h$-$2p$
$1\ ^4\Pi$	$\|(1\sigma)^2(2\sigma)^2(3\sigma)^1(1\pi_x)^1(1\pi_y)^2(4\sigma)^1\|$	0.919	0.912	0.943	0.960	$2h$-$1p$
	$\|(1\sigma)^2(2\sigma)^2(3\sigma)^1(1\pi_x)^1(1\pi_y)^2(5\sigma)^1\|$	0.033	0.228	-0.191	0.049	$2h$-$1p$
	$\|(1\sigma)^2(2\sigma)^2(3\sigma)^1(1\pi_x)^1(1\pi_y)^1(4\sigma)^1(2\pi_y)^1\|$	-0.161	-0.135	-0.077	-0.029	$3h$-$2p$
	$\|(1\sigma)^2(2\sigma)^2(3\sigma)^1(1\pi_y)^2(4\sigma)^1(2\pi_x)^1\|$	-0.163	-0.140	-0.089	-0.048	$3h$-$2p$
$2\ ^2\Pi$	$\|(1\sigma)^2(2\sigma)^2(3\sigma)^2(1\pi_x)^2(1\pi_y)^1\|$	-0.040	0.027	-0.114	0.250	$1h$
	$\|(1\sigma)^2(2\sigma)^2(3\sigma)^1(1\pi_x)^2(1\pi_y)^1(4\sigma)^1\|$[d]	-0.528, 0.746	-0.407, 0.812	-0.086, 0.934	-0.352, 0.839	$2h$-$1p$
	$\|(1\sigma)^2(2\sigma)^2(3\sigma)^1(1\pi_x)^2(1\pi_y)^1(5\sigma)^1\|$	-0.027	0.178	-0.180	0.031	$2h$-$1p$
	$\|(1\sigma)^2(2\sigma)^2(1\pi_x)^2(1\pi_y)^1(4\sigma)^2\|$	0.124	-0.138	-0.047	-0.196	$3h$-$2p$

[a] All configurations with a coefficient of at least 0.15 for at least one of the selected values of $R_{\text{O-H}}$ are included.

[b] Equilibrium bond length taken from [192].

[c] Determined relative to the ground-state reference configuration of the closed-shell OH^- system, $|1\sigma^2 2\sigma^2 3\sigma^2 1\pi_x^2 1\pi_y^2|$.

[d] The two different coefficients shown are for the two doublet configuration state functions, each corresponding to a different intermediate spin state, that result from coupling the spins of the three unpaired electrons in this orbital occupation scheme.

Table 2.8: An analysis of the major full CI configurations[a] for the low-lying Σ states of the OH radical for a selected set of internuclear separations $R_{\text{O-H}}$.

State	Configuration Orbital Occupancy	Coefficients for Various Values of $R_{\text{O-H}}$ 0.77 Å	0.96966 Å[b]	1.50 Å	3.00 Å	Excitation Type[c]
$A\,^2\Sigma^+$	$\lvert(1\sigma)^2(2\sigma)^2(3\sigma)^1(1\pi_x)^2(1\pi_y)^2\rvert$	0.960	0.958	0.941	0.755	$1h$
	$\lvert(1\sigma)^2(2\sigma)^2(1\pi_x)^2(1\pi_y)^2(4\sigma)^1\rvert$	0.060	0.101	< 0.01	0.254	$2h$-$1p$
	$\lvert(1\sigma)^2(2\sigma)^2(3\sigma)^2[(1\pi_x)^2 + (1\pi_y)^2](4\sigma)^1\rvert$	< 0.01	< 0.01	0.115	-0.150	$2h$-$1p$
	$\lvert(1\sigma)^2(2\sigma)^2(3\sigma)^1[(1\pi_x)^2 + (1\pi_y)^2](4\sigma)^2\rvert$	< 0.01	0.012	-0.098	-0.356	$3h$-$2p$
$1\,^4\Sigma^-$	$\lvert(1\sigma)^2(2\sigma)^2(3\sigma)^2(1\pi_x)^1(1\pi_y)^1(5\sigma)^1\rvert$	0.039	0.189	-0.142	-0.021	$2h$-$1p$
	$\lvert(1\sigma)^2(2\sigma)^2(3\sigma)^2(1\pi_x)^1(1\pi_y)^1(4\sigma)^1\rvert$	0.915	0.893	0.803	-0.387	$2h$-$1p$
	$\lvert(1\sigma)^2(2\sigma)^2(3\sigma)^2\times$ $[(1\pi_x)^1(4\sigma)^1(2\pi_y)^1 - (1\pi_y)^1(4\sigma)^1(2\pi_x)^1]\rvert$	0.165	0.147	0.099	-0.026	$3h$-$2p$
	$\lvert(1\sigma)^2(2\sigma)^2(3\sigma)^1(1\pi_x)^1(1\pi_y)^1(4\sigma)^2\rvert$	0.104	0.193	0.487	0.874	$3h$-$2p$
$1\,^2\Sigma^-$	$\lvert(1\sigma)^2(2\sigma)^2(3\sigma)^2(1\pi_x)^1(1\pi_y)^1(4\sigma)^1\rvert$[d]	-0.459, 0.795	< 0.01, 0.892	-0.380, 0.658	0.185, -0.321	$2h$-$1p$
	$\lvert(1\sigma)^2(2\sigma)^2(3\sigma)^1(1\pi_x)^1(1\pi_y)^1(4\sigma)^2\rvert$[d]	-0.052, 0.091	-0.108, 0.186	-0.277, 0.479	-0.440, 0.763	$3h$-$2p$
$B\,^2\Sigma^+$	$\lvert(1\sigma)^2(2\sigma)^2(3\sigma)^1(1\pi_x)^2(1\pi_y)^2\rvert$	0.019	0.012	-0.207	0.524	$1h$
	$\lvert(1\sigma)^2(2\sigma)^2(3\sigma)^2[(1\pi_x)^2 + (1\pi_y)^2](4\sigma)^1\rvert$	0.636	0.613	0.527	0.217	$2h$-$1p$
	$\lvert(1\sigma)^2(2\sigma)^2(1\pi_x)^2(1\pi_y)^2(4\sigma)^1\rvert$	-0.148	-0.158	-0.169	0.166	$2h$-$1p$
	$\lvert(1\sigma)^2(3\sigma)^1(1\pi_x)^2(1\pi_y)^2(4\sigma)^2\rvert$	0.013	0.025	0.081	-0.173	$3h$-$2p$
	$\lvert(1\sigma)^2(2\sigma)^2(3\sigma)^1[(1\pi_x)^2 + (1\pi_y)^2](4\sigma)^2\rvert$	-0.072	0.139	-0.345	0.499	$3h$-$2p$

[a] All configurations with a coefficient of at least 0.15 for at least one of the selected values of $R_{\text{O-H}}$ are included.

[b] Equilibrium bond length taken from [192].

[c] Determined relative to the ground-state reference configuration of the closed-shell OH^- system, $\lvert 1\sigma^2 2\sigma^2 3\sigma^2 1\pi_x^2 1\pi_y^2\rvert$.

[d] The two different coefficients shown are for the two doublet configuration state functions, each corresponding to a different intermediate spin state, that result from coupling the spins of the three unpaired electrons in this orbital occupation scheme.

approaches 3.0 Å. The remaining $1\ ^2\Delta$, $1\ ^4\Sigma^-$, $1\ ^2\Sigma^-$, and $B\ ^2\Sigma^+$ states pose more of a challenge to the IP-EOMCCSD($3h$-$2p$) approach. An analysis of Tables 2.7 and 2.8 reveals that the role of the $3h$-$2p$ contributions in these states is very large, particularly at the significantly stretched geometries where several of the electronic states of OH become dominated by such excitations. This suggests a need for the explicit inclusion of the $4h$-$3p$ component in the ionizing operator $R_\mu^{(N-1)}$ in order to obtain an accurate description, as discussed below. Despite this, the IP-EOMCCSD($3h$-$2p$) method describes the $1\ ^2\Delta$, $1\ ^4\Sigma^-$, $1\ ^2\Sigma^-$, and $B\ ^2\Sigma^+$ states in the region around the ground-state equilibrium geometry reasonably well, producing errors for these four states of 4.203–12.392 millihartree at the equilibrium O–H distance of 0.96966 Å. As we move to larger distances, where the $3h$-$2p$ contributions begin to dominate the $1\ ^2\Delta$, $1\ ^4\Sigma^-$, $1\ ^2\Sigma^-$, and $B\ ^2\Sigma^+$ states, we see that the errors steadily increase toward 26.164–49.731 millihartree. It is worth noting that even though these errors are relatively large, they represent a significant improvement of the 335.385–450.090 millihartree errors obtained with the IP-EOMCCSD($2h$-$1p$) approach at 3.0 Å for the same four states. We can make similar qualitative observations by comparing Figures 2.4(a) and 2.4(c). This comparison shows that if we focus our attention on the spectroscopic (Franck-Condon) region, the IP-EOMCCSD($3h$-$2p$) method does a reasonable job of faithfully reproducing the full CI curves for all of the states of OH studied in this work. As we shift our attention to the larger O–H distances, we notice that while the success of the IP-EOMCCSD($3h$-$2p$) approach continues for the $X\ ^2\Pi$, $A\ ^2\Sigma^+$, $1\ ^4\Pi$, and $2\ ^2\Pi$ states, the results for the remaining states of OH show increasingly large deviations from the corresponding full CI data. Based on the above analysis it appears that one needs to incorporate the $4h$-$3p$ excitations in the IP-EOMCC calculations in order to obtain a better description of the bond-breaking region of the potential energy curves of OH. As discussed below, this is indeed the case.

Having analyzed the performance of the IP-EOMCCSD($3h$-$2p$) approach in detail, we now turn our attention to its active-space IP-EOMCCSDt variant. A comparison of Figures 2.4(c) and 2.4(d) reveals that, with the exception of the $B\ ^2\Sigma^+$ state, the IP-EOMCCSDt potential energy curves are almost a perfect match to the full IP-EOMCCSD($3h$-$2p$) curves. An analysis of Tables 2.9 and 2.10 confirms this observation. If we compare the errors in the two approaches, we find that for all states, except $B\ ^2\Sigma^+$, the differences between the IP-EOMCCSDt and IP-EOMCCSD($3h$-$2p$) results are less than 2.410 millihartree for all geometries considered. Furthermore, the corresponding NPE values differ by less than 1.570 millihartree for all of these states (in many cases, less than 0.01 millihartree). Unfortunately, the $B\ ^2\Sigma^+$ state is a problem for the IP-EOMCCSDt approach at larger O–H separations, where the IP-EOMCCSDt and IP-EOMCCSD($3h$-$2p$) results differ by as much as 25.770 millihartree at the O–H distance of 3.0 Å (for the O–H separations in the equilibrium region, the differences between the IP-EOMCCSDt and IP-EOMCCSD($3h$-$2p$) energies of the $B\ ^2\Sigma^+$ state are only 2–3 millihartree). This large discrepancy between the IP-EOMCCSDt and IP-EOMCCSD($3h$-$2p$) energies of the $B\ ^2\Sigma^+$ state at larger O–H separations is easily explainable by analyzing the data presented in Table 2.8. The second to the last configuration contributing to this state, shown in Table 2.8, is a $3h$-$2p$ excitation in which no electron is removed from the $1\pi_x$ or $1\pi_y$ orbitals. Since the active space used in the IP-EOMCCSDt calculations consisted of only those two orbitals, the amplitude that represents this particular $3h$-$2p$ configuration is not present in the IP-EOMCCSDt calculation, and since this is a relatively significant configuration for the proper description of the $B\ ^2\Sigma^+$ state at larger O–H distances, the accuracy of the IP-EOMCCSDt results for this state is hurt. One of the advantages of the active-space approaches, however, is that these kinds of problems can be dealt with by expanding the active space. The only problem with that strategy in the particular example of the OH radical is that with the core electrons frozen, expand-

ing the active space to include the 3σ orbital results in the IP-EOMCCSDt method becoming the full IP-EOMCCSD($3h$-$2p$) approach since no $3h$-$2p$ amplitudes are ignored when there is only one inactive orbital. In the end, these results show that with an appropriate choice of the active space the IP-EOMCCSDt approach is capable of accurately reproducing the results of the full IP-EOMCCSD($3h$-$2p$) calculations at the cost of the standard CCSD/EOMCCSD schemes.

We now return to the important issue of improving on the IP-EOMCCSD($3h$-$2p$) results. As mentioned above, the analysis of the dominant contributions to the full CI wave functions, along with the IP-EOMCCSD($3h$-$2p$) results, lead one to the conclusion that the inclusion of $4h$-$3p$ components of the $R_{\mu}^{(N-1)}$ operator in the IP-EOMCC calculations is necessary to accurately describe the entire potential energy curves of OH. In order to test this hypothesis, my advisor and I, in collaboration with Dr. Yuhki Ohtsuka, Professor Masahiro Ehara, and Professor Hiroshi Nakatsuji, performed SAC-CI($4h$-$3p$) calculations for the low-lying doublet states of OH [88]. As explained in Section 2.1.1, the IP SAC-CI methodology is equivalent, up to some implementational differences and unimportant terms, to IP-EOMCC and so can provide similar insight into the role of $4h$-$3p$ excitations as the corresponding IP-EOMCC method.

In order to verify the equivalence of the IP EOMCC and SAC-CI methodologies, we compare the SAC-CI($3h$-$2p$) results with those obtained with IP-EOMCCSD($3h$-$2p$). Examination of Tables 2.9 and 2.10 reveals that the two methods do in fact provide very similar results. This is particularly true in the spectroscopic region, where the differences between these two methods range from 0.022 – 4.755 millihartree. Past this range, particularly for states that become dominated by $3h$-$2p$ excitations (see Tables 2.7 and 2.8), the differences can become larger, but as these are the regions and states for which the $3h$-$2p$ methods have difficulties, this is not a major concern.

Table 2.9: A comparison of the total energies obtained with various IP EOMCC and SAC-CI methods for the low-lying Π and Δ states of the OH radical with the corresponding full CI results obtained for several internuclear separations $R_{\text{O-H}}$.[a]

		$R_{\text{O-H}}$(Å)										
State	Method	0.77	0.96966[b]	1.07	1.27	1.50	1.75	2.00	2.50	3.00	MUE	NPE
$X\ ^2\Pi$	IP-EOMCCSD($2h$-$1p$)	-4.293	-3.081	-2.165	0.592	6.231	16.711	31.180	59.437	73.473	73.473	77.766
	IP-EOMCCSD($3h$-$2p$)	1.483	1.433	1.381	1.323	1.621	2.842	4.955	9.188	11.777	11.777	10.454
	IP-EOMCCSDt[c]	1.608	1.587	1.549	1.509	1.835	3.153	5.466	10.170	13.104	13.104	11.595
	SAC-CI($3h$-$2p$)	-1.066	-1.542	-1.817	-2.437	-3.134	-3.350	-2.520	0.463	2.508	3.350	5.858
	SAC-CI($4h$-$3p$)	-2.217	-2.557	-2.724	-3.117	-3.732	-4.430	-4.776	-4.421	-3.841	4.776	2.559
	SAC-CI($4h$-$3p$)\{3,1\}[d]	-1.039	-1.363	-1.555	-2.003	-2.583	-3.159	-3.381	-2.895	-2.257	3.381	2.342
$1\ ^2\Delta$	IP-EOMCCSD($2h$-$1p$)	230.128	225.597	225.822	236.405	258.298	284.966	310.557	352.144	378.026	378.026	152.747
	IP-EOMCCSD($3h$-$2p$)	3.033	7.191	9.759	15.539	22.729	30.069	35.936	42.334	42.747	42.747	39.714
	IP-EOMCCSDt[c]	3.041	7.199	9.768	15.549	22.741	30.082	35.951	42.350	42.763	42.763	39.722
	SAC-CI($3h$-$2p$)	2.801	6.879	9.511	15.802	24.361	33.982	42.585	54.844	61.313	61.313	58.512
	SAC-CI($4h$-$3p$)	-0.781	-0.647	-0.554	-0.429	-0.388	-0.390	-0.385	-0.372	-0.497	0.781	0.409
	SAC-CI($4h$-$3p$)\{3,1\}[d]	0.440	1.485	2.021	2.577	2.559	2.381	2.283	2.246	2.129	2.577	2.137
$1\ ^4\Pi$	IP-EOMCCSD($2h$-$1p$)	225.443	160.850	135.830	104.690	87.228	78.300	74.106	71.462	70.655	225.443	154.788
	IP-EOMCCSD($3h$-$2p$)	2.674	1.061	0.823	0.911	1.062	1.081	1.024	0.683	-0.300	2.674	2.374
	IP-EOMCCSDt[c]	5.013	3.471	3.189	3.103	3.037	2.886	2.734	2.365	1.487	5.013	3.526
$2\ ^2\Pi$	IP-EOMCCSD($2h$-$1p$)	256.555	171.011	141.150	107.797	89.486	78.830	72.216	67.703	68.382	256.555	188.852
	IP-EOMCCSD($3h$-$2p$)	7.793	4.281	2.400	1.544	1.363	1.135	1.136	2.621	3.894	7.793	6.658
	IP-EOMCCSDt[c]	10.203	4.281	3.907	2.815	2.511	2.144	1.975	3.204	4.390	10.203	8.228
	SAC-CI($3h$-$2p$)	7.405	4.259	2.536	1.833	1.698	1.289	0.706	0.425	0.803	7.405	7.030
	SAC-CI($4h$-$3p$)	-0.857	-0.318	-0.157	-0.089	-0.144	-0.335	-0.727	-1.421	-1.531	1.531	1.442
	SAC-CI($4h$-$3p$)\{3,1\}[d]	0.536	1.699	2.107	2.270	1.996	1.563	1.028	0.258	0.158	2.270	2.112

[a] The various IP EOMCC and SAC-CI energies are reported in millihartree relative to the corresponding full CI energy values, which can be found in [86]. In all correlated calculations, the lowest occupied 1σ orbital was frozen.

[b] Equilibrium bond length taken from [192].

[c] The active space consisted of the $1\pi_x$ and $1\pi_y$ orbitals of OH^-.

[d] The active space consisted of the 3σ, $1\pi_x$, $1\pi_y$, and 4σ orbitals of OH^-.

Table 2.10: A comparison of the total energies obtained with various IP EOMCC and SAC-CI methods for the low-lying Σ states of the OH radical with the corresponding full CI results obtained for several internuclear separations $R_{\text{O-H}}$.[a]

		$R_{\text{O-H}}$(Å)										
State	Method	0.77	0.96966[b]	1.07	1.27	1.50	1.75	2.00	2.50	3.00	MUE	NPE
$A\ ^2\Sigma^+$	IP-EOMCCSD(2h-1p)	-4.256	-1.200	0.599	4.263	8.921	15.291	21.221	27.904	31.552	31.552	35.808
	IP-EOMCCSD(3h-2p)	1.295	1.387	1.460	1.682	2.312	3.872	5.613	7.065	6.272	7.065	5.770
	IP-EOMCCSDt[c]	0.659	1.197	1.589	2.345	2.930	3.927	5.378	7.002	6.636	7.002	6.343
	SAC-CI(3h-2p)	-1.359	-1.655	-1.758	-1.852	-1.409	0.438	2.874	5.895	6.905	6.905	8.757
	SAC-CI(4h-3p)	-2.317	-2.702	-2.878	-3.188	-3.439	-3.506	-3.460	-3.492	-3.651	3.651	1.334
	SAC-CI(4h-3p)\{3,1\}[d]	-1.330	-1.680	-1.900	-2.311	-2.505	-2.373	-2.183	-2.113	-2.237	2.505	1.175
$1\ ^4\Sigma^-$	IP-EOMCCSD(2h-1p)	241.228	231.421	228.426	232.233	246.606	266.731	287.982	326.146	352.758	352.758	124.332
	IP-EOMCCSD(3h-2p)	5.097	8.606	10.698	15.519	21.911	29.099	35.506	43.534	45.127	45.127	40.03
	IP-EOMCCSDt[c]	5.100	8.609	10.702	15.523	21.916	29.104	35.512	43.540	45.133	45.133	40.033
$1\ ^2\Sigma^-$	IP-EOMCCSD(2h-1p)	262.848	262.749	265.988	283.913	315.124	350.078	380.988	426.231	450.090	450.090	187.712
	IP-EOMCCSD(3h-2p)	7.410	12.392	15.535	22.612	31.064	38.914	44.518	49.731	49.263	49.731	42.321
	IP-EOMCCSDt[c]	7.411	12.394	15.538	22.616	31.068	38.919	44.524	49.737	49.269	49.737	42.326
	SAC-CI(3h-2p)	7.043	11.957	15.187	22.856	32.788	42.968	51.235	61.994	67.298	67.298	60.255
	SAC-CI(4h-3p)	-0.698	-0.564	-0.467	-0.318	-0.247	-0.237	-0.253	-0.340	-0.597	0.698	0.461
	SAC-CI(4h-3p)\{3,1\}[d]	0.821	1.939	2.510	3.107	3.093	2.899	2.763	2.603	2.338	3.107	2.286
$B\ ^2\Sigma^+$	IP-EOMCCSD(2h-1p)	196.170	188.632	190.368	197.080	245.827	257.391	274.583	310.450	335.385	335.385	146.753
	IP-EOMCCSD(3h-2p)	0.765	4.203	6.234	10.556	15.433	19.675	22.722	26.164	26.161	26.164	25.399
	IP-EOMCCSDt[c]	2.904	6.936	9.406	15.224	23.227	32.202	40.005	49.673	51.931	51.931	49.027
	SAC-CI(3h-2p)	0.515	3.851	5.945	10.732	16.702	22.512	27.370	34.916	39.324	39.324	38.809
	SAC-CI(4h-3p)	-0.946	-0.797	-0.668	-0.411	-0.159	0.075	0.352	1.021	1.464	1.464	2.410
	SAC-CI(4h-3p)\{3,1\}[d]	0.217	1.244	1.790	2.435	2.561	2.501	2.567	3.053	3.452	3.452	3.235

[a] The various IP EOMCC and SAC-CI energies are reported in millihartree relative to the corresponding full CI energy values, which can be found in [86]. In all correlated calculations, the lowest occupied 1σ orbital was frozen.

[b] Equilibrium bond length taken from [192].

[c] The active space consisted of the $1\pi_x$ and $1\pi_y$ orbitals of OH^-.

[d] The active space consisted of the 3σ, $1\pi_x$, $1\pi_y$, and 4σ orbitals of OH^-.

With the equivalency of the IP SAC-CI and EOMCC approaches verified, the results of the SAC-CI($4h$-$3p$) calculations can now be considered as a substitute for the IP-EOMCCSD($4h$-$3p$) calculations, which we were unable to perform since we do not have the corresponding IP-EOMCCSD($4h$-$3p$) codes. Comparison of Figures 2.4(a) and 2.4(e) shows that for the doublet states of OH, the SAC-CI($4h$-$3p$) scheme produces potential energy curves which are virtually identical to those obtained with full CI. In particular, it is worth noting that SAC-CI($4h$-$3p$) preserves, to a very good approximation, the asymptotic degeneracy of the $X\ ^2\Pi$ and $1\ ^2\Sigma^-$ states and the asymptotic degeneracy of the $A\ ^2\Sigma^+$, $1\ ^2\Delta$, and $2\ ^2\Pi$ states that were missing from the results obtained with the lower-order IP EOMCC and SAC-CI methods. The success of the SAC-CI($4h$-$3p$) approach can be verified quantitatively by examining Tables 2.9 and 2.10. The errors in the results relative to full CI do not exceed 4.776 millihartree for any of the states or geometries considered, and for several of the states the MUE values are less than 1.531 millihartree. Furthermore, the NPE values for all of the states of OH considered in this section range from 0.405 to 2.559 millihartree, illustrating that the SAC-CI($4h$-$3p$) approach provides a uniformly accurate description of the entire potential energy curves of the OH radical.

Unfortunately the high accuracy obtained with the SAC-CI($4h$-$3p$) approach comes at a heavy price. The number of $4h$-$3p$ amplitudes that enter the IP EOMCC or equivalent SAC-CI eigenvalue problem is given by $n_o^4 n_u^3$, which for any molecular system of reasonable size is a huge number (compare this to the $n_o^3 n_u^2$ $3h$-$2p$ amplitudes that enter the IP-EOMCCSD($3h$-$2p$) eigenvalue problem). As a result, the computational costs associated with solving the SAC-CI($4h$-$3p$) eigenvalue problem are very large; the corresponding CPU steps scale as $n_o^4 n_u^5$. As in the case of the IP-EOMCCSD($3h$-$2p$) calculations, one can overcome this difficulty by considering the active-space variant of SAC-CI($4h$-$3p$). Indeed, we considered the active-space SAC-CI($4h$-$3p$)\{3,1\} approach, which uses the definition for the $4h$-$3p$ operator given

by Eq. (2.22), and in which the {3,1} denotes that the active-space consisted of the three highest occupied molecular orbitals and the lowest unoccupied orbital of OH^- (cf., Figure 2.1). As can be seen from Tables 2.9 and 2.10, the active-space SAC-CI(4*h*-3*p*){3,1} calculations faithfully reproduce the full SAC-CI(4*h*-3*p*) results. The MUE values of the two schemes differ by less than 2.409 millihartree for all states considered, while the differences in the NPE values do not exceed 1.825 millihartree. Furthermore, comparing Figures 2.4(e) and 2.4(f) reveals the potential energy curves generated with the active-space SAC-CI(4*h*-3*p*){3,1} approach look essentially the same as those obtained with the parent SAC-CI(4*h*-3*p*) method in which all 3*h*-2*p* and 4*h*-3*p* excitations are considered. This includes the spectroscopic as well as asymptotic regions of the potential energy curves and all calculated electronic states. As in all other examples of active-space CC or EOMCC calculations, the SAC-CI(4*h*-3*p*){3,1} approach is capable of producing these high accuracies using a small fraction of the excitation amplitudes defining, in this case, the $R_{\mu,4h\text{-}3p}$ component of $R_\mu^{(N-1)}$. The active-space SAC-CI(4*h*-3*p*){3,1} calculations for the OH/6-31G(d) system use less than 30% of all 4*h*-3*p* excitations, which is a substantial saving in the computer effort compared to the full SAC-CI(4*h*-3*p*) scheme. For larger numbers of electrons and basis functions these savings would be even greater.

2.2.3 Excitation Energies of C_2N, CNC, N_3, and NCO

In this section, we consider benchmark EA- and IP-EOMCC calculations of the adiabatic excitation energies of several low-lying states of the C_2N, CNC, N_3, and NCO systems reported in [89] (see, also, [140]). The nature of these systems is such that the cations, namely CNC^+ and C_2N^+, can serve as the relevant closed-shell reference systems for CNC and C_2N, respectively, and hence the EA-EOMCC calculations were performed for these two molecules. Similarly, the anions, N_3^- and NCO^-, are the relevant closed-shell reference systems for N_3 and NCO, respectively, and so the

Table 2.11: Equilibrium geometries (Å), adiabatic excitation energies (eV), and approximate excitation levels relative to the ground states of the corresponding reference cations for the low-lying valence excited states of C_2N and CNC.

		Excitation		EA-EOM			
Molecule	State	Level	Geometry	CCSD(2p-1h)	CCSD(3p-2h)	CCSDt[a]	Expt.[b]
CNC			(R_{CN})				
	$X\ ^2\Pi_g$	1p	1.253				
	$A\ ^2\Delta_u$	2p-1h	1.256	7.206	4.105	4.085	3.761
	$B\ ^2\Sigma_u^+$	2p-1h	1.259	7.639	4.718	4.704	4.315
C_2N			(R_{CC},R_{CN})				
	$X\ ^2\Pi$	1p	1.400,1.185				
	$A\ ^2\Delta$	2p-1h	1.315,1.207	6.190	3.055	3.028	2.636
	$B\ ^2\Sigma^-$	2p-1h[c]	1.302,1.223	7.856	3.677	3.648	2.779
	$C\ ^2\Sigma^+$	2p-1h	1.311,1.214	6.722	3.809	3.788	3.306

[a] The active space consisted of the four lowest unoccupied molecular orbitals of CNC^+ and C_2N^+.
[b] Taken from [202]
[c] The $B\ ^2\Sigma^-$ state of C_2N also has small, but non-negligible 3p-2h contributions.

IP-EOMCC methods were applied in these two cases. All calculations utilized the double zeta basis set of Dunning augmented by one set of polarization functions, DZP[4s2p1d] [197,198], and the ground-state RHF orbitals of the appropriate closed-shell reference system, as described above. The core orbitals that correlate with the 1s shells of the C, N, and O atoms were frozen in the correlated calculations. In this work, only linear geometries were considered, and the optimized bond lengths for each state were obtained using the analytic gradients of the EA SAC-CI(3p-2h) or IP SAC-CI(3h-2p) approach [84,199,200] within the perturbative selection (PS) approximation [201] (in the PS approximation the small higher-order components of the electron-attaching or ionizing operator that do not significantly perturb a suitably chosen zero-order wave function are eliminated from the calculation via numerical thresholds).

Table 2.11 provides the results for CNC and C_2N, for which the EA-EOMCC calculations were performed. Examination of the results of the EA-EOMCCSD(2p-

$1h$) calculations clearly demonstrates the inability of this lower-order EA-EOMCC approximation to accurately describe the low-lying states of these two systems. Indeed the errors in the EA-EOMCCSD($2p$-$1h$) adiabatic excitation energies relative to experiment are 3.324 – 5.077 eV. This failure is not surprising when we consider the approximate excitation level of each state relative to the ground state of the corresponding reference cation. Indeed, we see that each of the states considered here are predominantly of a $2p$-$1h$ nature, and as discussed in Section 2.2.2, such states require that $3p$-$2h$ excitations be included in the $R_\mu^{(N+1)}$ operator of EA-EOMCC in order to obtain a reasonable description.

The above analysis regarding the need for $3p$-$2h$ excitations is indeed correct, as the EA-EOMCCSD($3p$-$2h$) scheme offers substantial improvements in the results when compared to the poor description obtained when the electron-attaching $R_\mu^{(N+1)}$ operator is truncated at $2p$-$1h$ terms. With the exception of the $B\ ^2\Sigma^-$ state of C_2N the errors in the EA-EOMCCSD($3p$-$2h$) results relative to experiment are between 0.3 and 0.5 eV, which is a major improvement over the large errors produced with EA-EOMCCSD($2p$-$1h$). It is possible that the remaining 0.3 – 0.5 eV errors are a result of the relatively small basis set used in this preliminary study, a possibility that will be studied in the future. Unfortunately, the $B\ ^2\Sigma^-$ state of C_2N still proves to be problematic, even for the full EA-EOMCCSD($3p$-$2h$) scheme. Though the inclusion of $3p$-$2h$ terms in the calculation leads to dramatic improvements over the poor EA-EOMCCSD($2p$-$1h$) error of 5.077 eV, the error in the EA-EOMCCSD($3p$-$2h$) excitation energy relative to experiment is still about 0.9 eV, which is a significant deviation. An analysis of the excitation structure of this state reveals that it is characterized by small but non-negligble $3p$-$2h$ contributions. As discussed in Section 2.2.2, the presence of significant $3p$-$2h$ excitations in the wave function generally points to a need for including the $4p$-$3h$ contributions in the EA-EOMCC (or equivalent SAC-CI) scheme in order to obtain accurate results. As a result, it is likely that

Table 2.12: Equilibrium geometries (Å), adiabatic excitation energies (eV), and approximate excitation levels relative to the ground states of the corresponding reference anions for the low-lying valence excited states of N_3 and NCO.

		Excitation		IP-EOM			
Molecule	State	Level	Geometry	CCSD(2h-1p)	CCSD(3h-2p)	CCSDt[a]	Expt.[b]
N_3			(R_{NN})				
	$X\ ^2\Pi_g$	1h	1.188				
	$B\ ^2\Sigma_u^+$	1h	1.185	4.640	4.598	4.729	4.555
NCO			(R_{NC},R_{CO})				
	$X\ ^2\Pi$	1h	1.230,1.193				
	$A\ ^2\Sigma^+$	1h	1.191,1.190	2.900	2.864	3.078	2.821
	$B\ ^2\Pi$	1h	1.220,1.309	4.199	3.911	3.904	3.937

[a] The active space consisted of the two highest unoccupied molecular orbitals of N_3^- and NCO^-.
[b] Taken from [202]

the neglect of these effects is the source of the non-negligible discrepancy between the EA-EOMCCSD(3p-2h) and experimental results. This will be investigated in a future work.

Though the inclusion of 3p-2h effects in the EA-EOMCC calculation results in substantial improvements in the accuracy of the excitation energies when compared to EA-EOMCCSD(2p-1h), these improvements come at a large computational price, as discussed in the earlier sections. This is certainly a good motivation for examining if the much less expensive active-space variant of EA-EOMCCSD(3p-2h), i.e. EA-EOMCCSDt, can provide similar improvements. The results presented in Table 2.11 demonstrate that the active-space EA-EOMCCSDt scheme accurately mimics its considerably more expensive parent EA-EOMCCSD(3p-2h) approach. Indeed, for all states of CNC and C_2N studied here, the differences between the active-space EA-EOMCCSDt and full EA-EOMCCSD(3p-2h) excitation energies are less than 0.029 eV, even for the very challenging $B\ ^2\Sigma^-$ state of C_2N, where the difference between the EA-EOMCCSD(3p-2h) and experimental data is $\sim$ 0.9 eV.

Moving on to N_3 and NCO, it is clear from Table 2.12 that the low-lying states of these systems are not quite as complicated as the majority of states considered in this work. Indeed, Table 2.12 shows that the approximate excitation level of each of the states considered here relative to the ground state of the corresponding anion is only $1h$. As a result of the relatively simple structure of these states, even the basic IP-EOMCCSD($2h$-$1p$) approach is capable of providing accurate results, producing errors relative to experiment of 0.085, 0.079, and 0.262 eV for the $B\ ^2\Sigma_u^+$ state of N_3, and the $A\ ^2\Sigma^+$ and $B\ ^2\Pi$ states of NCO, respectively. Despite the high quality of these results, it is interesting to observe that even in this case the inclusion of $3h$-$2p$ effects in the calculation can provide further improvement. Indeed, the IP-EOMCCSD($3h$-$2p$) approach reduces the above IP-EOMCCSD($2h$-$1p$) errors for the $B\ ^2\Sigma_u^+$ state of N_3, and $A\ ^2\Sigma^+$ and $B\ ^2\Pi$ states of NCO down to 0.043, 0.043, and 0.026 eV, respectively. Ultimately, of course, we would like to know if these high accuracies can be reproduced with the less expensive IP-EOMCCSDt method in which the $3h$-$2p$ excitations are selected via active orbitals. As shown in Table 2.12, the discrepancies between the IP-EOMCCSDt excitation energies and those of its IP-EOMCCSD($3h$-$2p$) parent approximation are somewhat larger than the analogous differences between the EA-EOMCCSDt and EA-EOMCCSD($3p$-$2h$) excitation energies for CNC and C_2N, ranging from $\sim$ 0.1 to $\sim$ 0.2 eV. Although this agreement is still relatively good, one would prefer to see the IP-EOMCCSDt results to be closer to those of its parent IP-EOMCCSD($3h$-$2p$) scheme. It is likely that increasing the size of the active space used in the IP-EOMCCSDt calculations, which in the calculations presented here was very small, consisting of only the two highest occupied molecular orbitals, would improve the agreement between IP-EOMCCSDt and IP-EOMCCSD($3h$-$2p$), and we will explore this issue, along with the issues of the role $4h$-$3p$ excitations and basis sets in the future work.

Chapter 3

Noniterative Coupled-Cluster Methods for Open-Shell Systems

In the previous Chapter, the active-space EA- and IP-EOMCC methodologies, as well as the success of the basic approximations resulting from these methodologies in describing the low-lying states of radical and other open-shell systems, were discussed. Although it was shown that these methods can be extremely useful in studies of the excitation spectra of open-shell systems, producing high-quality results at low computational costs similar to CCSD or EOMCCSD calculations, as discussed in the Introduction no method is bullet-proof, and the active-space CC/EOMCC calculations depend on the choice of active orbitals, i.e., the active-space EA- and IP-EOMCC methods are not computational black-boxes of the type of conventional single-reference approaches. So in this chapter we consider an alternative, and perhaps even complimentary, method for studying open-shell systems, namely the open-shell extension of the so-called completely renormalized (CR) CC and EOMCC approaches based on the biorthogonal formulation of the MMCC formalism. Section 3.1 provides the theoretical details behind these CR-CC/CR-EOMCC schemes, including the basic elements of the biorthogonal MMCC theory that forms the formal basis

for these approaches, as described in [133–135, 138–140]. Section 3.2 provides the results of selected calculations that illustrate the performance of the CR-CC and CR-EOMCC approaches in studies of ground and excited states of open-shell systems, taken from [138–140, 150, 151].

3.1 Theory

3.1.1 The Biorthogonal Formulation of the Method of Moments of Coupled-Cluster Equations

The MMCC approach is based on the idea of adding a noniterative correction to the ground or excited state energy $E_\mu^{(A)}$, computed using some CC/EOMCC approximation abbreviated here as method A, in order to recover the corresponding exact (full CI) energy, E_μ. The CC/EOMCC method A refers to one of the standard CC/EOMCC approximations truncated at some excitation level m_A, such as, for example, the basic CCSD approach or its EOMCCSD analog, for which $m_A = 2$ (for CCSDT/EOMCCSDT, m_A would be 3, for CCSDTQ/EOMCCSDTQ, m_A would be 4, etc.). If we let $T^{(A)}$ (defined by Eq. (2.3) with $M_T = m_A$) represent the cluster operator characterizing the approximate CC method A, then replacing T with $T^{(A)}$ in Eq. (2.2) gives the ground-state CC wave function $|\Psi_0^{(A)}\rangle$ within this approximation. Using the EOMCC theory, the corresponding excited-state ($\mu > 0$) wave functions can then be expressed as:

$$|\Psi_\mu^{(A)}\rangle = R_\mu^{(A)}|\Psi_0^{(A)}\rangle = R_\mu^{(A)} e^{T^{(A)}}|\Phi\rangle, \tag{3.1}$$

where the excitation operator $R_\mu^{(A)}$ which transforms the CC ground state $|\Psi_0^{(A)}\rangle$ into the excited-state wave function $|\Psi_\mu^{(A)}\rangle$ is given by

$$R_\mu^{(A)} = R_{\mu,0}^{(A)} + R_{\mu,\text{open}}^{(A)} \equiv r_{\mu,0}\,\mathbf{1} + \sum_{n=1}^{m_A} R_{\mu,n}, \tag{3.2}$$

with

$$R_{\mu,n} = \left(\frac{1}{n!}\right)^2 r_{\mu,a_1\ldots a_n}^{i_1\ldots i_n}\, a^{a_1}\cdots a^{a_n} a_{i_n}\cdots a_{i_1}, \tag{3.3}$$

$\mathbf{1}$ representing the identity operator, and $r_{\mu,a_1\ldots a_n}^{i_1\ldots i_n}$ designating the corresponding excitation amplitudes of EOMCC. One may notice that the structure of the wave function ansatz given by Eq. (3.1) is very similar to the EA/IP-EOMCC wave function ansatz of Eq. (2.1), except that instead of an electron-attaching or ionizing operator, $R_\mu^{(A)}$ is a particle-conserving excitation operator. It should also be noted that although Eq. (3.1) is formally applicable to excited states, one can easily extend it to include the ground-state ($\mu = 0$) case if we adopt a convention in which $R_0^{(A)}$ is the identity operator. We use this convention throughout this work. The $R_0^{(A)} = \mathbf{1}$ condition for the $\mu = 0$ $R_\mu^{(A)}$ operator is equivalent to defining $r_{0,0} = 1$ and $r_{0,a_1\ldots a_n}^{i_1\ldots i_n} = 0$ for $n \geq 1$.

With the CC/EOMCC approximation A defined as above, the noniterative energy correction recovering the full CI energy from the CC/EOMCC energy, $\delta_\mu^{(A)}$, which defines the biorthogonal formulation of the MMCC theory, is given by the following

compact expression [133–137, 139, 140]

$$\begin{aligned}
\delta_{\mu}^{(A)} &\equiv E_{\mu} - E_{\mu}^{(A)} \\
&= \sum_{n=m_A+1}^{N_{\mu,A}} \langle \Phi | \mathscr{L}_{\mu,n} \, M_{\mu,n}(m_A) | \Phi \rangle \\
&= \sum_{n=m_A+1}^{N_{\mu,A}} \sum_{\substack{i_1 < \cdots < i_n \\ a_1 < \cdots < a_n}} \ell_{\mu,i_1 \ldots i_n}^{a_1 \ldots a_n} \, \mathfrak{M}_{\mu,a_1 \ldots a_n}^{i_1 \ldots i_n}(m_A). \qquad (3.4)
\end{aligned}$$

There are two fundamental contributions to this equation that must be discussed. The first,

$$M_{\mu,n}(m_A) = \left(\frac{1}{n!}\right)^2 \mathfrak{M}_{\mu,a_1 \ldots a_n}^{i_1 \ldots i_n}(m_A) \, a^{a_1} \cdots a^{a_n} a_{i_n} \cdots a_{i_1}, \qquad (3.5)$$

is a particle-hole excitation operator defined through the *generalized moments of the CC/EOMCC equations*, $\mathfrak{M}_{\mu,a_1 \ldots a_n}^{i_1 \ldots i_n}(m_A)$, which correspond to the projections of the CC/EOMCC equations for method A on the excited determinants that are normally disregarded in the standard CC/EOMCC calculations. Mathematically, this equates to the following definition for the moments $\mathfrak{M}_{\mu,a_1 \ldots a_n}^{i_1 \ldots i_n}(m_A)$:

$$\mathfrak{M}_{\mu,a_1 \ldots a_n}^{i_1 \ldots i_n}(m_A) = \langle \Phi_{i_1 \ldots i_n}^{a_1 \ldots a_n} | (\bar{H}^{(A)} R_{\mu}^{(A)}) | \Phi \rangle, \qquad (3.6)$$

where $n > m_A$, and $\bar{H}^{(A)}$ is the similarity-transformed Hamiltonian of CC method A given by Eq. (2.10) with $T = T^{(A)}$. Since it was established that $R_0^{(A)} = \mathbf{1}$, Eq. (3.6) is general and defines both the ground- and excited-state moments. If one specifically examines the ground-state case, then Eq. (3.6) reduces to the generalized moments

of the ground-state CC equations defining method A,

$$\mathfrak{M}^{i_1\ldots i_n}_{0,a_1\ldots a_n}(m_A) \equiv \mathfrak{M}^{i_1\ldots i_n}_{a_1\ldots a_n}(m_A) = \langle \Phi^{a_1\ldots a_n}_{i_1\ldots i_n} | \bar{H}^{(A)} | \Phi \rangle. \tag{3.7}$$

At this point it should be noted that for a given CC/EOMCC method A, not all of the moments $\mathfrak{M}^{i_1\ldots i_n}_{\mu,a_1\ldots a_n}(m_A)$ with $n > m_A$ are non-zero. Indeed, for a given approximation, there is generally a value of n above which all moments $\mathfrak{M}^{i_1\ldots i_n}_{\mu,a_1\ldots a_n}(m_A)$ are zero. This is the source of the upper summation limit $N_{\mu,A}$ in Eq. (3.4), which is equal to this value of n for the CC/EOMCC method A. For instance, in the case of CCSD (the $m_A = 2$ case), only the triply, quadruply, pentuply, and hextuply excited moments, i.e. moments with $n = 3 - 6$, are nonzero when the Hamiltonian contains pairwise interactions only, and thus $N_{0,A} = 6$ (the CCSD equations are solved by zeroing the singly and doubly excited moments, $\mathfrak{M}^{i}_{0,a}(2)$ and $\mathfrak{M}^{ij}_{0,ab}(2)$, respectively, hence the triply excited moments are the first to be nonzero). Similarly, in the EOMCCSD case with $\mu > 0$, $N_{\mu,A} = 8$.

The second fundamental contribution to the equation for the noniterative energy correction defining the biorthogonal MMCC approach, Eq. (3.4), are the operators $\mathscr{L}_{\mu,n}$ and the corresponding deexcitation amplitudes $\ell^{a_1\ldots a_n}_{\mu,i_1\ldots i_n}$. The $\mathscr{L}_{\mu,n}$ operators are the n-body components of the deexcitation operator $\mathscr{L}_\mu$ which is designed to give the following parameterization for the exact full CI "bra" wave function:

$$\langle \Psi_\mu | = \langle \Phi | \mathscr{L}_\mu \, e^{-T^{(A)}}, \tag{3.8}$$

where

$$\mathscr{L}_\mu = \sum_{n=0}^{N} \mathscr{L}_{\mu,n}, \quad \mathscr{L}_{\mu,n} = \left(\frac{1}{n!}\right)^2 \ell^{a_1\ldots a_n}_{\mu,i_1\ldots i_n} \, a^{i_1} \cdots a^{i_n} a_{a_n} \cdots a_{a_1}, \tag{3.9}$$

with N designating the number of correlated electrons. As can be seen from Eq.

(3.4), it is specifically the n-body components $\mathscr{L}_{\mu,n}$ with $n > m_A$ that contribute to the energy corrections $\delta_\mu^{(A)}$. As a result, it is useful to deconstruct the exact operator $\mathscr{L}_\mu$ in the following way:

$$\mathscr{L}_\mu = \mathscr{L}_\mu^{(A)} + \delta\mathscr{L}_\mu^{(A)}, \tag{3.10}$$

where the A part of $\mathscr{L}_\mu$ is given by

$$\mathscr{L}_\mu^{(A)} = \sum_{n=0}^{m_A} \mathscr{L}_{\mu,n}, \tag{3.11}$$

and the remainder corresponding to n-tuply deexcited contributions with $n > m_A$ by

$$\delta\mathscr{L}_\mu^{(A)} = \sum_{n=m_A+1}^{N} \mathscr{L}_{\mu,n}. \tag{3.12}$$

This helps in designing the approximate schemes based on Eq. (3.4), such as the CR-CC(2,3) or CR-EOMCC(2,3) approaches discussed in the next section.

It is also important to note that the validity of Eq. (3.4) depends on the normalization of $\mathscr{L}_\mu$. Indeed, Eq. (3.4) only gives the exact difference between the full CI and CC/EOMCC energies if the following normalization condition is used:

$$\langle\Phi|\mathscr{L}_\mu^{(A)} R_\mu^{(A)}|\Phi\rangle = 1. \tag{3.13}$$

Once again, we note that because of the convention in which $R_0^{(A)} = \mathbf{1}$ this equation is general, and in the ground-state case, reduces to

$$\langle\Phi|\mathscr{L}_0^{(A)}|\Phi\rangle = 1. \tag{3.14}$$

Inspection of Eq. (3.13) reveals that it is very similar to the biorthonormality

condition defining the CC/EOMCC bra states $\langle\tilde{\Psi}_\mu^{(A)}|$, namely,

$$\langle\tilde{\Psi}_\mu^{(A)}|\Psi_\nu^{(A)}\rangle = \langle\Phi|L_\mu^{(A)}\, R_\nu^{(A)}|\Phi\rangle = \delta_{\mu,\nu}. \tag{3.15}$$

Here, the CC/EOMCC bra state $\langle\tilde{\Psi}_\mu^{(A)}|$ corresponding to the ket state $|\Psi_\mu^{(A)}\rangle$ defined by Eq. (3.1) is given by

$$\langle\tilde{\Psi}_\mu^{(A)}| = \langle\Phi|L_\mu^{(A)} e^{-T^{(A)}} \tag{3.16}$$

(cf. [9, 10]), where $L_\mu^{(A)}$ is a deexcitation operator defined as

$$L_\mu^{(A)} = L_{\mu,0}^{(A)} + L_{\mu,\mathrm{open}}^{(A)}, \tag{3.17}$$

with

$$L_{\mu,0}^{(A)} = \delta_{\mu,0}\,\mathbf{1} \tag{3.18}$$

and

$$L_{\mu,\mathrm{open}}^{(A)} = \sum_{n=1}^{m_A} L_{\mu,n}, \quad L_{\mu,n} = \left(\frac{1}{n!}\right)^2 l_{\mu,i_1\ldots i_n}^{a_1\ldots a_n}\, a^{i_1}\cdots a^{i_n} a_{a_n}\cdots a_{a_1}. \tag{3.19}$$

Examination of the above equations reveals obvious similarities between the standard EOMCC deexcitation operator $L_\mu^{(A)}$ Eq. (3.17) and the A part $\mathscr{L}_\mu^{(A)}$ of the operator $\mathscr{L}_\mu$ Eq. (3.11), but it is important to stress that these are two different objects. Indeed, the bra states $\langle\Phi|L_\mu^{(A)}$ are the left eigenstates of the non-Hermitian similarity-transformed Hamiltonian $\bar{H}^{(A)}$, which are obtained by solving the left eigenvalue problem for the CC/EOMCC method A,

$$\begin{aligned}\delta_{\mu,0}\,\langle\Phi|\bar{H}_{\mathrm{open}}^{(A)}|\Phi_{i_1\ldots i_n}^{a_1\ldots a_n}\rangle \;+\; &\langle\Phi|L_{\mu,\mathrm{open}}^{(A)}\bar{H}_{\mathrm{open}}^{(A)}|\Phi_{i_1\ldots i_n}^{a_1\ldots a_n}\rangle \\ &= \omega_\mu^{(A)}\, l_{\mu,i_1\ldots i_n}^{a_1\ldots a_n}, \\ &i_1 < \cdots < i_n,\; a_1 < \cdots < a_n,\end{aligned} \tag{3.20}$$

where $\omega_\mu^{(A)} = E_\mu^{(A)} - E_0^{(A)}$ is the corresponding vertical excitation energy obtained with method A ($\omega_0^{(A)} = 0$), in the subspace of the N-electron Hilbert space spanned by the excited determinants $|\Phi_{i_1\ldots i_n}^{a_1\ldots a_n}\rangle$ with $n = 1, \ldots, m_A$. These left eigenstates are the bra counterparts of the ket eigenstates $R_\mu^{(A)}|\Phi\rangle$ of $\bar{H}^{(A)}$ which are obtained by solving the EOMCC right eigenvalue problem,

$$\langle\Phi_{i_1\ldots i_n}^{a_1\ldots a_n}|(\bar{H}_{\rm open}^{(A)} R_{\mu,{\rm open}}^{(A)})_C|\Phi\rangle = \omega_\mu^{(A)} r_{\mu,a_1\ldots a_n}^{i_1\ldots i_n}, \tag{3.21}$$

in the space spanned by the excited determinants $|\Phi_{i_1\ldots i_n}^{a_1\ldots a_n}\rangle$ with n=1,. . .,m_A, followed by the determination of the zero-body amplitude $r_{\mu,0}$ using the equation

$$r_{\mu,0} = \langle\Phi|(\bar{H}_{\rm open}^{(A)} R_{\mu,{\rm open}}^{(A)})_C|\Phi\rangle/\omega_\mu^{(A)}. \tag{3.22}$$

On the other hand, the bra state $\langle\Phi|\mathscr{L}_\mu^{(A)}$ is only one of two contributions to the exact state $\langle\Phi|\mathscr{L}_\mu$, which is obtained by solving the eigenvalue problem

$$\langle\Phi|\mathscr{L}_\mu \bar{H}^{(A)} = E_\mu \langle\Phi|\mathscr{L}_\mu, \tag{3.23}$$

which is equivalent to the adjoint form of the Schrödinger equation, $\langle\Psi_\mu|H = E_\mu \langle\Psi_\mu|$, for the exact bra wave function $\langle\Psi_\mu|$ and exact energy E_μ in the entire N-electron Hilbert space. As a result, the two operators, $L_\mu^{(A)}$ and $\mathscr{L}_\mu^{(A)}$, are identical only in the special case of $m_A = N$, where N is the number of correlated electrons. However, despite the fact that the two operators are formally different, the observed similarities between them are useful in formulating approximate CC/EOMCC methods based on the biorthogonal MMCC theory, which is the subject of the next section.

As a final point, it is worth noting that the formula for the noniterative energy correction $\delta_\mu^{(A)}$, Eq. (3.4), originates from a consideration of the following asymmetric

energy functional [120, 122, 127, 129, 130, 133, 134]

$$\Lambda[\Psi] = \frac{\langle \Psi | H R_\mu^{(A)} e^{T^{(A)}} | \Phi \rangle}{\langle \Psi | R_\mu^{(A)} e^{T^{(A)}} | \Phi \rangle}. \tag{3.24}$$

The unique feature of this expression is that when Ψ is the exact, full CI state Ψ_μ, then the value of the $\Lambda[\Psi]$ functional is the full CI energy E_μ (i.e. $\Lambda[\Psi_\mu] = E_\mu$), regardless of the choice of $R_\mu^{(A)}$ or $e^{T^{(A)}}$ for the CC/EOMCC method A. This is a consequence of the Hermitian nature of the Hamiltonian, which results in the equation being unchanged if one applies the Hamiltonian to the bra state $\langle \Psi_\mu |$ in Eq. (3.24) rather than to the ket state $R_\mu^{(A)} e^{T^{(A)}} | \Phi \rangle$. It is the invariance of this expression with respect to the CC/EOMCC truncation m_A that makes it such a good starting point for the derivation of the noniterative correction $\delta_\mu^{(A)}$, Eq. (3.4). For a derivation of the formula for $\delta_\mu^{(A)}$, Eq. (3.4), see Appendix B.

3.1.2 The CR-CC(2,3)/CR-EOMCC(2,3) and CR-CC(2,4)/CR-EOMCC(2,4) Approaches

Equation (3.4) provides one with a well-defined procedure for correcting the CC/EOMCC energy for the ground or excited state of a given molecular system in order to obtain a good approximation to the exact energy. By applying a series of systematic approximations to Eq. (3.4), it is possible to generate a class of practical and highly accurate CC/EOMCC methods, referred to as the completely renormalized (CR) CC/EOMCC approaches. This section discusses the systematic approximations that generate the so-called CR-CC(m_A, m_B)/CR-EOMCC(m_A, m_B) schemes, with a particular focus on the CR-CC(2,3)/CR-EOMCC(2,3) and CR-CC(2,4)/CR-EOMCC(2,4) approximations utilized in this work.

When attempting to generate practical computational approaches from Eq. (3.4) the first issue faced is that of the summation over n and the upper summation limit $N_{\mu,A}$. With the exception of small molecular systems consisting of only a few correlated electrons, it is not feasible to consider all the terms up to $N_{\mu,A}$ in electronic structure calculations. Indeed, as discussed in Section 3.1.1, if one starts from the basic CCSD/EOMCCSD approach, then $N_{0,A} = 6$ and $N_{\mu,A} = 8$ for $\mu > 0$, which means that terms involving up to hextuply excited moments of the CCSD equations and up to octuply excited moments of the EOMCCSD equations would have to be included. Such high-order moments are computationally too expensive to be included in calculations for all but the smallest systems. In order to overcome this difficulty, one can truncate the summation over n in Eq. (3.4) at some value m_B, where $m_A < m_B < N_{\mu,A}$. This leads to a systematic hierarchy of approximate CC methods, referred to as the MMCC(m_A, m_B)$_{\mathscr{L}}$ schemes, for which the total electronic energy is calculated as [133–137, 139, 140]

$$E_\mu(m_A, m_B) = E_\mu^{(A)} + \delta_\mu(m_A, m_B), \tag{3.25}$$

where the noniterative correction $\delta_\mu(m_A, m_B)$ is given by:

$$\begin{aligned}\delta_\mu(m_A, m_B) &= \sum_{n=m_A+1}^{m_B} \langle\Phi|\mathscr{L}_{\mu,n}\, M_{\mu,n}(m_A)|\Phi\rangle \\ &= \sum_{n=m_A+1}^{m_B} \sum_{\substack{i_1<\cdots<i_n \\ a_1<\cdots<a_n}} \ell^{a_1\ldots a_n}_{\mu,i_1\ldots i_n}\, \mathfrak{M}^{i_1\ldots i_n}_{\mu,a_1\ldots a_n}(m_A). \end{aligned} \tag{3.26}$$

Of particular interest to this work are the MMCC(2,3)$_{\mathscr{L}}$ and MMCC(2,4)$_{\mathscr{L}}$ truncations, which are defined by

$$E_\mu(2,3) = E_\mu^{(\mathrm{CCSD})} + \delta_\mu(2,3), \tag{3.27}$$

and

$$E_\mu(2,4) = E_\mu^{(\mathrm{CCSD})} + \delta_\mu(2,4), \tag{3.28}$$

where the noniterative energy corrections to the CCSD ($\mu = 0$) or EOMCCSD ($\mu > 0$) energy are given by

$$\begin{aligned}\delta_\mu(2,3) &= \langle\Phi|\mathscr{L}_{\mu,3}\, M_{\mu,3}(2)|\Phi\rangle \\ &= \sum_{\substack{i<j<k \\ a<b<c}} \ell^{abc}_{\mu,ijk}\, \mathfrak{M}^{ijk}_{\mu,abc}(2) \end{aligned} \tag{3.29}$$

and

$$\begin{aligned}
\delta_\mu(2,4) &= \langle\Phi|\mathscr{L}_{\mu,3}M_{\mu,3}(2)|\Phi\rangle + \langle\Phi|\mathscr{L}_{\mu,4}M_{\mu,4}(2)|\Phi\rangle \\
&= \sum_{\substack{i<j<k \\ a<b<c}} \ell^{abc}_{\mu,ijk}\,\mathfrak{M}^{ijk}_{\mu,abc}(2) \\
&\quad + \sum_{\substack{i<j<k<l \\ a<b<c<d}} \ell^{abcd}_{\mu,ijkl}\,\mathfrak{M}^{ijkl}_{\mu,abcd}(2),
\end{aligned} \tag{3.30}$$

respectively. It is clear from the above equations that the MMCC(2,3)$_{\mathscr{L}}$ truncation scheme equates to the addition of a noniterative correction due to triple excitations to the standard CCSD or EOMCCSD energy. Similarly, the MMCC(2,4)$_{\mathscr{L}}$ approach equates to the addition of a noniterative correction due to triple and quadruple excitations to the CCSD or EOMCCSD energy.

Unfortunately the above truncation schemes alone do not, by themselves, lead to practical computational schemes. Indeed, as can be seen in Eqs. (3.29) and (3.30), in order to obtain the energies $E_\mu(2,3)$ and $E_\mu(2,4)$ defined above, one must be able to obtain the three- and four-body components of the exact operator $\mathscr{L}_\mu$. Since one would need to solve for the full CI bra state $\langle\Psi_\mu|$ to obtain these components, they are generally not accessible, and so an alternative, more practical means of obtaining approximate three- and four-body components of $\mathscr{L}_\mu$ is required. In order to derive such approximations we will make use of the inherent similarities between $\mathscr{L}^{(A)}_\mu$ and $L^{(A)}_\mu$ discussed in Section 3.1.1. Although it was stressed that $\mathscr{L}^{(A)}_\mu$ and $L^{(A)}_\mu$ are mathematically different operators, their similarities are big enough to make it possible to replace $\mathscr{L}^{(A)}_\mu$ by $L^{(A)}_\mu$ in the definition of $\mathscr{L}_\mu$ in order to obtain approximate formulas for the higher-order components of $\mathscr{L}_\mu$ which enter Eqs. (3.29) and (3.30). In particular, if one is interested in developing a practical approximation based on

the MMCC(2,3)$_{\mathscr{L}}$ scheme, in which we want to determine the triples correction to the CCSD or EOMCCSD energy, then the following approximate form for $\mathscr{L}_\mu$ can be used:

$$\mathscr{L}_\mu \approx L_\mu^{(\mathrm{CCSD})} + \tilde{\mathscr{L}}_{\mu,3}, \tag{3.31}$$

where

$$L_\mu^{(\mathrm{CCSD})} = \delta_{\mu,0} + L_{\mu,1} + L_{\mu,2} = \delta_{\mu,0} + l_{\mu,i}^{a}\, a^i a_a + \tfrac{1}{4} l_{\mu,ij}^{ab}\, a^i a^j a_b a_a \tag{3.32}$$

are the deexcitation operators defining the left eigenstates of the CCSD similarity-transformed Hamiltonian (see Eqs. (3.17) - (3.19) with $m_A = 2$). In order to determine the approximate three-body component of $\mathscr{L}_\mu$, i.e., $\tilde{\mathscr{L}}_{\mu,3}$, the expression for $\mathscr{L}_\mu$ given by Eq. (3.31) can be substituted into Eq. (3.23) written for the $m_A = 2$ case. The resulting expression is then right-projected on the triply excited determinants $|\Phi_{ijk}^{abc}\rangle$ to obtain

$$\begin{aligned} &\langle\Phi|L_\mu^{(\mathrm{CCSD})}\,\bar{H}^{(\mathrm{CCSD})}|\Phi_{ijk}^{abc}\rangle + \langle\Phi|\tilde{\mathscr{L}}_{\mu,3}\,\bar{H}^{(\mathrm{CCSD})}|\Phi_{ijk}^{abc}\rangle \\ &= E_\mu\,\langle\Phi|\tilde{\mathscr{L}}_{\mu,3}|\Phi_{ijk}^{abc}\rangle \equiv E_\mu\,\tilde{\ell}_{\mu,ijk}^{abc}. \end{aligned} \tag{3.33}$$

By replacing the exact energy E_μ by the CCSD/EOMCCSD energy $E_\mu^{(\mathrm{CCSD})}$, approximating the triples-triples block of $\bar{H}^{(\mathrm{CCSD})}$ by its diagonal, and solving for the amplitudes defining $\tilde{\mathscr{L}}_{\mu,3}$, $\tilde{\ell}_{\mu,ijk}^{abc}$, one obtains the quasiperturbative expression

$$\tilde{\ell}_{\mu,ijk}^{abc} = \langle\Phi|L_\mu^{(\mathrm{CCSD})}\,\bar{H}^{(\mathrm{CCSD})}|\Phi_{ijk}^{abc}\rangle / D_{\mu,abc}^{ijk}, \tag{3.34}$$

where the Epstein-Nesbet-like denominator $D^{ijk}_{\mu,abc}$ is defined as

$$\begin{aligned} D^{ijk}_{\mu,abc} &= E^{(\mathrm{CCSD})}_{\mu} - \langle \Phi^{abc}_{ijk} | \bar{H}^{(\mathrm{CCSD})} | \Phi^{abc}_{ijk} \rangle \\ &= \omega^{(\mathrm{CCSD})}_{\mu} - \langle \Phi^{abc}_{ijk} | \bar{H}^{(\mathrm{CCSD})}_{1} | \Phi^{abc}_{ijk} \rangle \\ &\quad - \langle \Phi^{abc}_{ijk} | \bar{H}^{(\mathrm{CCSD})}_{2} | \Phi^{abc}_{ijk} \rangle \\ &\quad - \langle \Phi^{abc}_{ijk} | \bar{H}^{(\mathrm{CCSD})}_{3} | \Phi^{abc}_{ijk} \rangle . \end{aligned} \tag{3.35}$$

Here $\omega^{(\mathrm{CCSD})}_{\mu}$ represents the EOMCCSD vertical excitation energy,

$$\omega^{(\mathrm{CCSD})}_{\mu} = E^{(\mathrm{CCSD})}_{\mu} - E^{(\mathrm{CCSD})}_{0}, \tag{3.36}$$

and $\bar{H}^{(\mathrm{CCSD})}_{m}$ represents the m-body component of the CCSD similarity-transformed Hamiltonian. By substituting $\tilde{\ell}^{abc}_{\mu,ijk}$, defined through Eq. (3.34), into the equations defining the MMCC(2,3)$_{\mathscr{L}}$ approach, Eqs. (3.27) and (3.29), we obtain the formula for the total electronic energy defining the CR-CC(2,3) ($\mu = 0$) or CR-EOMCC(2,3) ($\mu > 0$) approach, namely,

$$\begin{aligned} E^{\mathrm{CR(2,3)}}_{\mu} &= E^{(\mathrm{CCSD})}_{\mu} + \delta^{\mathrm{CR(2,3)}}_{\mu} \\ &= E^{(\mathrm{CCSD})}_{\mu} + \sum_{\substack{i<j<k \\ a<b<c}} \tilde{\ell}^{abc}_{\mu,ijk}\, \mathfrak{M}^{ijk}_{\mu,abc}(2), \end{aligned} \tag{3.37}$$

with $\tilde{\ell}^{abc}_{\mu,ijk}$ given by Eq. (3.34) and the triply excited moments $\mathfrak{M}^{ijk}_{\mu,abc}(2)$ given by Eq. (3.6) in which $m_A = 2$ (A = CCSD) and $n = 3$. These moments are calculated using the T_1 and T_2 clusters obtained from the CCSD calculations and, in the excited-state ($\mu > 0$) case, the zero-, one-, and two-body components $R_{\mu,0}$, $R_{\mu,1}$, and $R_{\mu,2}$ obtained by solving the EOMCCSD eigenvalue problem. It is important to mention that the above expression for the $\tilde{\ell}^{abc}_{\mu,ijk}$ amplitudes, Eq. (3.34), may

have to be modified if one of the indices i, j, k, a, b, c corresponds to an orbital which is degenerate with some other orbitals. In that case, to make sure that the CR-CC(2,3)/CR-EOMCC(2,3) energies remain invariant with respect to rotations among degenerate orbitals, one should replace Eq. (3.34) by a more elaborate expression in which, instead of using the diagonal matrix elements $\langle\Phi^{abc}_{ijk}|\bar{H}^{(\mathrm{CCSD})}|\Phi^{abc}_{ijk}\rangle$ that enter the Epstein-Nesbet-like denominator $D^{ijk}_{\mu,abc}$, Eq. (3.35), one solves a small system of linear equations, similar to Eq. (3.33), where all amplitudes $\tilde{\ell}^{abc}_{\mu,ijk}$ involving indices of degenerate spin-orbitals are coupled together through the off-diagonal matrix elements $\langle\Phi^{def}_{lmn}|\bar{H}^{(\mathrm{CCSD})}|\Phi^{abc}_{ijk}\rangle$ involving the triply excited determinants that carry the indices of degenerate spin-orbitals [138]. Without taking care of this issue, the CR-EOMCC(2,3) energy correction $\delta^{\mathrm{CR(2,3)}}_{\mu}$ is not strictly invariant with respect to the rotations among degenerate orbitals, although the dependence of the $\delta^{\mathrm{CR(2,3)}}_{\mu}$ correction employing Eq. (3.34) to determine the $\tilde{\ell}^{abc}_{\mu,ijk}$ amplitudes on the rotations among degenerate orbitals is minimal. Indeed, as shown in [138], changes in the values of triples corrections due to the rotations among degenerate orbitals do not exceed 0.1 millihartree when one uses Eq. (3.34) to determine amplitudes $\tilde{\ell}^{abc}_{\mu,ijk}$. Thus, the issue of the lack of invariance of the CR-EOMCC(2,3) correction $\delta^{\mathrm{CR(2,3)}}_{\mu}$ employing Eq. (3.34) with respect to the rotations among degenerate orbitals is more of a formal problem than the practical one as long as one does not calculate energy derivatives for systems with orbital degeneracies. If the molecule has at most an Abelian symmetry or if the orbitals employed break the non-Abelian symmetry (for example, due to the use of symmetry-broken reference determinant or external fields), so that there are no orbital degeneracies, one can apply Eq. (3.34) to all amplitudes $\tilde{\ell}^{abc}_{\mu,ijk}$ as is.

The computational costs of the CR-CC(2,3)/CR-EOMCC(2,3) schemes are characterized by the iterative $n_o^2 n_u^4$ steps of the underlying CCSD/EOMCCSD approach plus a single noniterative step that scales as $n_o^3 n_u^4$. These scalings are similar to those that characterize CCSD(T), and so, like CCSD(T), CR-CC(2,3)/CR-EOMCC(2,3)

can be applied to systems with up to about 100 correlated electrons and a few hundred basis functions. Furthermore, the overall structure of the CR-CC(2,3)/CR-EOMCC(2,3) formulas for the energy given by Eqs. (3.34) – (3.37) is the same as that of CCSD(T). Indeed, the formula for the CCSD(T) energy can be obtained from Eq. (3.37) by approximating $\tilde{\ell}^{abc}_{0,ijk}$ and $\mathfrak{M}^{ijk}_{0,abc}(2)$ in the following manner: in the definition of $\tilde{\ell}^{abc}_{0,ijk}$, Eq. (3.34), we replace the denominator $D^{ijk}_{0,abc}$, Eq. (3.35), by the spin-orbital energy difference $(\epsilon_i+\epsilon_j+\epsilon_k-\epsilon_a-\epsilon_b-\epsilon_c)$, neglect the $(L_{0,2}\bar{H}^{(\mathrm{CCSD})})_{DC}$ contribution to the $\langle\Phi|L^{(\mathrm{CCSD})}_{\mu}\bar{H}^{(\mathrm{CCSD})}|\Phi^{abc}_{ijk}\rangle$ numerator of Eq. (3.34), which is at least a fourth-order term in many-body perturbation theory (MBPT) if the HF reference is used, replace $L_{0,1}$, $L_{0,2}$, and $\bar{H}^{(\mathrm{CCSD})}_2$ by $T^{\dagger}_1$, $T^{\dagger}_2$, and V_N in the remaining contributions to $\langle\Phi|L^{(\mathrm{CCSD})}_{\mu}\bar{H}^{(\mathrm{CCSD})}|\Phi^{abc}_{ijk}\rangle$, where V_N is the two-body part of the Hamiltonian in the normal ordered form relative to the Fermi vacuum and $T^{\dagger}_1$ and $T^{\dagger}_2$ are the adjoints of the T_1 and T_2 cluster operators determined by solving the CCSD equations, and replace the triply excited moments $\mathfrak{M}^{ijk}_{0,abc}(2)$, Eq. (3.7) with $n=3$ and $m_A=2$, by the lead term $\langle\Phi^{abc}_{ijk}|(V_NT_2)_C|\Phi\rangle$. As a result, the CR-CC(2,3) and CR-EOMCC(2,3) approaches maintain the same "black-box" nature and ease-of-use that CCSD(T) is known for. There are, however, many advantages of the CR-CC(2,3)/CR-EOMCC(2,3) methodology over CCSD(T). First of all, as shown in Section 3.2 and [138–140, 150] for the open-shell systems and [133–135, 137, 141–149] for singlet ground states, CR-CC(2,3) eliminates the failures of CCSD(T) in bond breaking and biradical situations, while being as accurate as CCSD(T) when the multi-reference character of the calculated state is small. Furthermore, CR-CC(2,3) has a natural extension to excited states in the CR-EOMCC(2,3) scheme, as described above, and there is no natural formal extension of CCSD(T) to excited states. The earlier CR-CCSD(T) approach of [127], which relies on the original MMCC formalism of [127, 130] that does not utilize the left eigenstates of the similarity-transformed Hamiltonian, has an extension to excited states as well [131, 132], but unlike CR-

CC(2,3), the earlier CR-CCSD(T) is not strictly size extensive. The CR-CC(2,3) approach and its higher-order CR-CC(2,4) analog are both size extensive.

A procedure similar to that used to derive the CR-CC(2,3) and CR-EOMCC(2,3) equations can be used to develop methods based on the MMCC(2,4)$_{\mathscr{L}}$ approximation. In this case, the approximate form of $\mathscr{L}_\mu$, given by

$$\mathscr{L}_\mu \approx L_\mu^{(\mathrm{CCSD})} + \tilde{\mathscr{L}}_{\mu,3} + \tilde{\mathscr{L}}_{\mu,4}, \tag{3.38}$$

is substituted into the adjoint form of the Schrödinger equation, Eq.(3.23), and then right-projected on the triply excited determinants $|\Phi_{ijk}^{abc}\rangle$ and quadruply excited determinants $|\Phi_{ijkl}^{abcd}\rangle$. In the CR-CC(2,4)/CR-EOMCC(2,4) approximation studied in this work, one then replaces the exact energy E_μ in the resulting system of equations for $\tilde{\mathscr{L}}_{\mu,3}$ and $\tilde{\mathscr{L}}_{\mu,4}$ by the CCSD/EOMCCSD energy $E_\mu^{(\mathrm{CCSD})}$ and approximates the triples-triples and quadruples-quadruples blocks of $\bar{H}^{(\mathrm{CCSD})}$ by their diagonals, while ignoring any coupling between triples and quadruples. As a result of these manipulations, one obtains the same mathematical expressions for $\tilde{\ell}_{\mu,ijk}^{abc}$ as in the CR-CC(2,3)/CR-EOMCC(2,3) case, Eqs. (3.34) and (3.35), and the following formula for $\tilde{\ell}_{\mu,ijkl}^{abcd}$:

$$\tilde{\ell}_{\mu,ijkl}^{abcd} = \langle\Phi|L_\mu^{(\mathrm{CCSD})}\bar{H}^{(\mathrm{CCSD})}|\Phi_{ijkl}^{abcd}\rangle / D_{\mu,abcd}^{ijkl}, \tag{3.39}$$

where the denominator $D_{\mu,abcd}^{ijkl}$ is defined as

$$\begin{aligned} D_{\mu,abcd}^{ijkl} &= E_\mu^{(\mathrm{CCSD})} - \langle\Phi_{ijkl}^{abcd}|\bar{H}^{(\mathrm{CCSD})}|\Phi_{ijkl}^{abcd}\rangle \\ &= \omega_\mu^{(\mathrm{CCSD})} - \langle\Phi_{ijkl}^{abcd}|\bar{H}_1^{(\mathrm{CCSD})}|\Phi_{ijkl}^{abcd}\rangle \\ &\quad -\langle\Phi_{ijkl}^{abcd}|\bar{H}_2^{(\mathrm{CCSD})}|\Phi_{ijkl}^{abcd}\rangle \\ &\quad -\langle\Phi_{ijkl}^{abcd}|\bar{H}_3^{(\mathrm{CCSD})}|\Phi_{ijkl}^{abcd}\rangle. \end{aligned} \tag{3.40}$$

By substituting $\tilde{\ell}^{abc}_{\mu,ijk}$, Eqs. (3.34) and (3.35), and $\tilde{\ell}^{abcd}_{\mu,ijkl}$, Eqs. (3.39) and (3.40), into the equations defining the MMCC(2,4)$_{\mathscr{L}}$ approach, Eqs. (3.28) and (3.30), we obtain the formula for the total energy that defines the CR-CC(2,4)/CR-EOMCC(2,4) approach,

$$\begin{aligned} E_\mu^{\mathrm{CR(2,4)}} &= E_\mu^{(\mathrm{CCSD})} + \delta_\mu^{\mathrm{CR(2,4)}} \\ &= E_\mu^{(\mathrm{CCSD})} + \sum_{\substack{i<j<k \\ a<b<c}} \tilde{\ell}^{abc}_{\mu,ijk}\, \mathfrak{M}^{ijk}_{\mu,abc}(2) \\ &\quad + \sum_{\substack{i<j<k<l \\ a<b<c<d}} \tilde{\ell}^{abcd}_{\mu,ijkl}\, \mathfrak{M}^{ijkl}_{\mu,abcd}(2). \end{aligned} \tag{3.41}$$

Examination of this result reveals that in this formulation of CR-CC(2,4)/CR-EOMCC(2,4), the total energy can be thought of as being obtained by adding a noniterative correction due to quadruple excitations, given by

$$\delta_\mu^{\mathrm{CR(2,4),Q}} = \sum_{\substack{i<j<k<l \\ a<b<c<d}} \tilde{\ell}^{abcd}_{\mu,ijkl}\, \mathfrak{M}^{ijkl}_{\mu,abcd}(2), \tag{3.42}$$

to the CR-CC(2,3)/CR-EOMCC(2,3) energy. The computer time scalings of the CR-CC(2,4)/CR-EOMCC(2,4) calculations are characterized by the $n_o^2 n_u^4$ iterative steps of CCSD/EOMCCSD, the noniterative $n_o^3 n_u^4$ steps of the triples correction and the $n_o^4 n_u^5$ noniterative steps characterizing the correction due to quadruples, Eq. (3.42). These costs are quite a bit higher than those of the CR-CC(2,3)/CR-EOMCC(2,3) approach, and so the CR-CC(2,4)/CR-EOMCC(2,4) scheme is much more limited in its applicability. However, this still represents a rather significant computational saving over the iterative $n_o^4 n_u^6$ steps that define the full CCSDTQ/EOMCCSDTQ

approach (to which CR-CC(2,4)/CR-EOMCC(2,4) is an approximation).

Let us also comment on neglecting the couplings between triple and quadruple excitations in deriving Eq. (3.41). A few test calculations have revealed that neglecting this coupling may be detrimental to the accuracy of the CR-CC(2,4)/CR-EOMCC(2,4) results. Because of this observation, the development of an alternative formulation of the CR-CC(2,4)/CR-EOMCC(2,4) energy correction may be necessary. In this work, however, we focus on the variant described by Eq. (3.41), which is sufficiently accurate for the applications discussed in this thesis.

It should be noted that the above equations describe the most complete variants of the CR-CC(2,3)/CR-EOMCC(2,3) and CR-CC(2,4)/CR-EOMCC(2,4) approaches, which are often labeled by the additional letter 'D' (e.g. CR-CC(2,3),D). One can certainly contemplate other variants by replacing the exact Epstein-Nesbet-like denominators $D^{ijk}_{\mu,abc}$ and $D^{ijkl}_{\mu,abcd}$, Eqs. (3.35) and (3.40), by various approximate forms. For example, variants C of CR-CC(2,3)/CR-EOMCC(2,3) and CR-CC(2,4)/CR-EOMCC(2,4) are obtained by neglecting the three-body components of the similarity-transformed Hamiltonian, i.e., the $\langle \Phi^{abc}_{ijk}|\bar{H}^{(\mathrm{CCSD})}_3|\Phi^{abc}_{ijk}\rangle$ and $\langle \Phi^{abcd}_{ijkl}|\bar{H}^{(\mathrm{CCSD})}_3|\Phi^{abcd}_{ijkl}\rangle$ terms in Eqs. (3.35) and (3.40), while variants B are obtained by neglecting both the two-body and three-body components of $\bar{H}^{(\mathrm{CCSD})}_3$, which leaves only the $\langle \Phi^{abc}_{ijk}|\bar{H}^{(\mathrm{CCSD})}_1|\Phi^{abc}_{ijk}\rangle$ term in the definition of $D^{ijk}_{\mu,abc}$ and the $\langle \Phi^{abcd}_{ijkl}|\bar{H}^{(\mathrm{CCSD})}_1|\Phi^{abcd}_{ijkl}\rangle$ term in the definition of $D^{ijkl}_{\mu,abcd}$. Finally, variant A is obtained by replacing the Epstein-Nesbet-like denominators $D^{ijk}_{\mu,abc}$ and $D^{ijkl}_{\mu,abcd}$ by the corresponding Møller-Plesset-like denominators, $[\omega^{(\mathrm{CCSD})}_\mu - (\epsilon_a+\epsilon_b+\epsilon_c-\epsilon_i-\epsilon_j-\epsilon_k)]$ for triple excitations, and $[\omega^{(\mathrm{CCSD})}_\mu - (\epsilon_a+\epsilon_b+\epsilon_c+\epsilon_d-\epsilon_i-\epsilon_j-\epsilon_k-\epsilon_l)]$ for quadruple excitations.

Finally, there are also relationships between the CR-CC(2,3)/CR-EOMCC(2,3) and CR-CC(2,4)/CR-EOMCC(2,4) approaches and other noniterative CC/EOMCC methods. For instance, the CR-EOMCC(2,4),A method is equivalent to the EOM-

CC(2)PT(2) of [203, 204] when the canonical Hartree-Fock orbitals are used. A similar equivalency exists between the CR-EOMCC(2,3),A approach and the triples correction of EOM-CC(2)PT(2). The ground-state CR-CC(2,3),A and CR-CC(2,4),A schemes are equivalent to the CCSD(2)$_{\mathrm{T}}$ and CCSD(2)$_{\mathrm{TQ}}$ methods of [205] when the canonical Hartree-Fock orbitals are used, and the analogous relationships exist between the CR-CC(2,3),B and CR-CC(2,4),B schemes and the CCSD(2) approach of [206–209]. For example, the CR-CC(2,3),B approach is equivalent, up to small details, to the triples correction of CCSD(2). As mentioned earlier, there is also a straightforward relationship between CR-CC(2,3) and CCSD(T).

3.1.3 Computer Implementation of the Open-Shell Variants of the CR-CC(2,3)/CR-EOMCC(2,3) and CR-CC(2,4)/CR-EOMCC(2,4) Approaches

Unlike the active-space EA/IP-EOMCC methods discussed in Chapter 2, which are built from the ground up specifically for open-shell valence systems, there is nothing about the CR-CC(2,3)/CR-EOMCC(2,3) or CR-CC(2,4)/CR-EOMCC(2,4) approaches that specifically depends on the open- or closed-shell nature of the molecular system of interest other than the choice of the reference determinant $|\Phi\rangle$. Indeed, the first computer implementation of the CR-CC(2,3)/CR-EOMCC(2,3) approach, developed by Professors Marta Włoch and Piotr Piecuch [133] and available in GAMESS, was written specifically for closed-shell references. As discussed in the Introduction, the early applications of this approach to singlet states of molecular systems [133–135, 137, 141–149] revealed its ability to provide highly accurate results at a reasonable low computer cost. In particular, CR-CC(2,3) proved to be very effective in calculations of the singlet states of biradical systems and single bond breaking on singlet potential energy surfaces, which are characterized by a significant multi-reference character. Though restricted to open-shell singlet states, these results offered the first glimpse of the potential applicability of the CR-CC(2,3) approach to general open-shell molecular systems.

As the overarching goal of this dissertation is the development of practical methods for studying open-shell systems, the original closed-shell CR-CC(2,3) work of [133] was followed up by the development of the general-purpose open-shell computer implementation of the CR-CC(2,3) and CR-EOMCC(2,3) approaches that are applicable to singlet as well as non-singlet states [138, 140]. Furthermore, in order to study the performance of higher-order CR-CC approximations based on the biorthogonal MMCC theory of [133, 134], the CR-CC(2,4)/CR-EOMCC(2,4) method was implemented by

the author of this dissertation as well (with the help of routines for quadruply excited moments provided by Dr. Maricris Lodriguito, reviewed in [210]), using a general formulation applicable to both singlet and high-spin non-singlet reference determinants. The resulting computer codes are highly efficient, fully vectorized codes which make use of recursively generated intermediates and fast matrix multiplication routines. The programs are general in the sense that they can work with any type of high-spin reference determinant, though currently they are used with the RHF and ROHF references generated by GAMESS. These codes utilize the standard spin-orbital basis of α and β spin-orbitals in performing calculations, and the most recent version of the open-shell ground-state CR-CC(2,3) program, which is specifically designed for non-relativistic molecules, is written in a spin-integrated form which avoids explicit calculations of terms that go to zero because of spin symmetry, making it as fast as possible [138]. This version of the CR-CC(2,3) code is available as part of the GAMESS package. Currently, the open-shell CR-EOMCC(2,3) and CR-CC(2,4)/CR-EOMCC(2,4) codes are stand-alone pilot programs that are only loosely interfaced with the integral transformation and RHF/ROHF routines of GAMESS, but work is under way to develop more efficient, spin-integrated implementations that will be fully included in GAMESS and thus available to the public. As already mentioned, the CR-CC(2,4)/CR-EOMCC(2,4) computer codes developed as part of this research benefitted from the thesis project of Dr. Maricris Lodriguito, who provided the author of this thesis with the routines for calculating the quadruply excited moments $\mathfrak{M}^{ijkl}_{\mu,abcd}(2)$ [210, 211].

As an illustration of the algorithmic details that are associated with the above method and code development efforts, we present the key details of the computer implementation of the CR-CC(2,3)/CR-EOMCC(2,3) method. The CR-CC(2,3)/CR-EOMCC(2,3) computer codes implemented as part of this work consist of four main parts. In the first part, as was the case in the EA-EOMCC and IP-EOMCC codes

discussed in Section 2.1.3, we solve the usual CCSD equations for the ground state in order to obtain the singly and doubly excited cluster amplitudes, t_a^i and t_{ab}^{ij}, respectively. In the next step, again in analogy to the EA-EOMCC and IP-EOMCC codes, we use these amplitudes to construct the one- and two-body matrix elements of the CCSD similarity-transformed Hamiltonian, $\bar{h}_p^q$ and $\bar{h}_{pq}^{rs}$, respectively. As a reminder, the explicit equations for these matrix elements in terms of the one- and two-electron integrals, f_p^q and v_{pq}^{rs}, respectively, and the cluster amplitudes t_a^i and t_{ab}^{ij} can be found in Table 2.1. In the third step, we construct and solve the EOMCCSD equations. In executing this step, we must distinguish between two situations. If our interest is in the noniterative corrections $\delta_\mu^{\mathrm{CR(2,3)}}$ for the ground ($\mu = 0$) and excited ($\mu > 0$) states, we must construct and solve both the right and left EOMCCSD equations, Eq. (3.21), augmented by Eq. (3.22), and Eq. (3.20), respectively, in which A = CCSD and $m_A = 2$. The right eigenstates $R_\mu^{(\mathrm{CCSD})}|\Phi\rangle$ needed to construct the EOMCCSD moments $\mathfrak{M}_{\mu,abc}^{ijk}(2)$ with $\mu > 0$, Eq. (3.6) in which $m_A = 2$ and $n = 3$, whereas the left eigenstates $L_\mu^{(\mathrm{CCSD})}|\Phi\rangle$ are needed to construct the deexcitation amplitudes $\tilde{\ell}_{\mu,ijk}^{abc}$, Eq. (3.34). If our interest is in the ground-state correction $\delta_0^{\mathrm{CR(2,3)}}$ only, we must solve the CCSD left eigenvalue problem obtained by setting $\mu = 0$, A = CCSD, and $m_A = 2$ in Eq. (3.20). The right EOMCCSD eigenvalue problem for the excited-state ($\mu > 0$) case is solved using the Hirao-Nakatsuji generalization [176] of the Davidson diagonalization algorithm [177] to non-Hermitian eigenvalue problems and is generally solved for first. Once the excitation energy $\omega_\mu^{(\mathrm{CCSD})}$ is known (in the ground-state case, $\omega_0^{(\mathrm{CCSD})} = 0$), it is substituted into the left (EOM)CCSD eigenvalue problem, Eq. (3.20), which converts it into a system of linear equations for the $l_{\mu,i}^a$ and $l_{\mu,ij}^{ab}$ amplitudes, which we can solve with the same DIIS solver [212–214] that we normally use to solve the ground-state CC equations. As the focus of this work is the CR-CC(2,3)/CR-EOMCC(2,3) approach, we will not go into further details of the above steps in this dissertation and rather focus on the final step, which is the

determination of the $\delta_{\mu}^{\mathrm{CR(2,3)}}$ triples correction.

From Eq. (3.37), we know that in order to calculate $\delta_{\mu}^{\mathrm{CR(2,3)}}$ we must first express the deexcitation amplitudes $\tilde{\ell}_{\mu,ijk}^{abc}$ and the triply excited moments $\mathfrak{M}_{\mu,abc}^{ijk}(2)$ in terms of the molecular integrals f_p^q and v_{pq}^{rs}, CCSD cluster amplitudes t_a^i and t_{ab}^{ij}, right EOMCCSD excitation amplitudes $r_{\mu,0}$, $r_{\mu,a}^i$ and $r_{\mu,ab}^{ij}$ (when $\mu > 0$ only), and left EOMCCSD deexcitation amplitudes $l_{\mu,i}^a$ and $l_{\mu,ij}^{ab}$ ($\mu = 0$ and $\mu > 0$). To that end we begin by reexpressing the $\tilde{\ell}_{\mu,ijk}^{abc}$ amplitudes as follows:

$$\tilde{\ell}_{\mu,ijk}^{abc} = N_{\mu,ijk}^{abc} / D_{\mu,abc}^{ijk}. \tag{3.43}$$

Here the denominator $D_{\mu,abc}^{ijk}$ is still defined by Eq. (3.35) and the numerator is given by (cf. Eq. (3.34))

$$\begin{aligned} N_{\mu,ijk}^{abc} &= \langle \Phi | L_{\mu}^{(\mathrm{CCSD})} \bar{H}^{(\mathrm{CCSD})} | \Phi_{ijk}^{abc} \rangle \\ &= \mathscr{A}_{abc} \Gamma_{\mu,ijk}^{abc}, \end{aligned} \tag{3.44}$$

where the partially antisymmetric quantity $\Gamma_{\mu,ijk}^{abc}$ is defined as

$$\Gamma_{\mu,ijk}^{abc} = \mathscr{A}^{i/jk} [\tfrac{1}{2} l_i^a v_{jk}^{bc} + \tfrac{1}{2} l_{jk}^{bc} \bar{h}_i^a + \tfrac{1}{2} l_{jk}^{ec} \bar{h}_{ie}^{ab} - \tfrac{1}{2} l_{im}^{ab} \bar{h}_{jk}^{mc}] \tag{3.45}$$

(we dropped the symbol μ representing the electronic state of interest from $l_{\mu,i}^a$ and $l_{\mu,ij}^{ab}$ for clarity reasons). Inspection of Eq. (3.35) reveals that the determination of the $D_{\mu,abc}^{ijk}$ denominators requires the calculation of the diagonal matrix elements $\left\langle \Phi_{ijk}^{abc} \right| \bar{H}_m^{(\mathrm{CCSD})} \left| \Phi_{ijk}^{abc} \right\rangle$ with $m = 1$, 2, and 3. These three quantities can be computed using the following expressions:

$$\begin{aligned} \left\langle \Phi_{ijk}^{abc} \right| \bar{H}_1^{(\mathrm{CCSD})} \left| \Phi_{ijk}^{abc} \right\rangle &= -\bar{h}_i^i - \bar{h}_j^j - \bar{h}_k^k \\ &\quad + \bar{h}_a^a + \bar{h}_b^b + \bar{h}_c^c, \end{aligned} \tag{3.46}$$

$$\begin{aligned}
\left\langle \Phi_{ijk}^{abc} \right| \bar{H}_2^{(\mathrm{CCSD})} \left| \Phi_{ijk}^{abc} \right\rangle \;=\; & -\bar{h}_{ai}^{ai} - \bar{h}_{bi}^{bi} - \bar{h}_{ci}^{ci} \\
& -\bar{h}_{aj}^{aj} - \bar{h}_{bj}^{bj} - \bar{h}_{cj}^{cj} \\
& -\bar{h}_{ak}^{ak} - \bar{h}_{bk}^{bk} - \bar{h}_{ck}^{ck} \\
& +\bar{h}_{ij}^{ij} + \bar{h}_{ik}^{ik} + \bar{h}_{jk}^{jk} \\
& +\bar{h}_{ab}^{ab} + \bar{h}_{ac}^{ac} + \bar{h}_{bc}^{bc},
\end{aligned} \tag{3.47}$$

and

$$\begin{aligned}
\left\langle \Phi_{ijk}^{abc} \right| \bar{H}_3^{(\mathrm{CCSD})} \left| \Phi_{ijk}^{abc} \right\rangle \;=\; & -\bar{h}_{aij}^{iaj} - \bar{h}_{aik}^{iak} - \bar{h}_{ajk}^{jak} \\
& -\bar{h}_{bij}^{ibj} - \bar{h}_{bik}^{ibk} - \bar{h}_{bjk}^{jbk} \\
& -\bar{h}_{cij}^{icj} - \bar{h}_{cik}^{ick} - \bar{h}_{cjk}^{jck} \\
& +\bar{h}_{aib}^{iab} + \bar{h}_{aic}^{iac} + \bar{h}_{bic}^{ibc} \\
& +\bar{h}_{ajb}^{jab} + \bar{h}_{ajc}^{jac} + \bar{h}_{bjc}^{jbc} \\
& +\bar{h}_{akb}^{kab} + \bar{h}_{akc}^{kac} + \bar{h}_{bkc}^{kbc},
\end{aligned} \tag{3.48}$$

where the one- and two-body matrix elements $\bar{h}_p^q$ and $\bar{h}_{pq}^{rs}$ are defined in Table 2.1 and the specialized three-body matrix elements entering Eq. (3.48) are defined as

$$\bar{h}_{aib}^{iab} = -\sum_m v_{im}^{ab} t_{ab}^{im}, \tag{3.49}$$

and

$$\bar{h}_{aij}^{iaj} = \sum_e v_{ij}^{ae} t_{ae}^{ij}. \tag{3.50}$$

For the triply excited moments $\mathfrak{M}_{\mu,abc}^{ijk}(2)$ that multiply the amplitudes $\tilde{\ell}_{\mu,ijk}^{abc}$ to produce the correction $\delta_\mu^{\mathrm{CR(2,3)}}$ (cf. Eq. (3.37)), we can write

$$\mathfrak{M}_{\mu,abc}^{ijk}(2) = \mathscr{A}_{abc}\, \mathfrak{T}_{\mu,abc}^{ijk}(2), \tag{3.51}$$

where the partially antisymmetric $\mathfrak{T}^{ijk}_{\mu,abc}(2)$ quantities are defined by

$$\begin{aligned}\mathfrak{T}^{ijk}_{\mu,abc}(2) &= \mathscr{A}^{i/jk}\,[\,(\tfrac{1}{2}\bar{h}^{ie}_{ab}r^{jk}_{ec} - \tfrac{1}{2}\bar{h}^{jk}_{mc}r^{im}_{ab} - \tfrac{1}{2}I^{jk}_{mc}t^{im}_{ab} + I^{ie}_{ab}t^{jk}_{ec}) \\ &\quad + \tfrac{1}{2}r_0\,(\bar{h}^{ie}_{ab}t^{jk}_{ec} - I'^{jk}_{mc}t^{im}_{ab})\,] \qquad (3.52)\end{aligned}$$

(again, we dropped the symbol μ from $r_{\mu,0}$, $r^i_{\mu,a}$ and $r^{ij}_{\mu,ab}$ for the sake of clarity). The intermediates that enter the above expression for $\mathfrak{T}^{ijk}_{\mu,abc}(2)$ are defined as

$$I^{ic}_{ab} = \tfrac{1}{2}\bar{h}^{ec}_{ab}r^i_e - \bar{h}^{ec}_{bm}r^{im}_{ae} + \tfrac{1}{4}\bar{h}^{ic}_{mn}r^{mn}_{ab} - \bar{h}^{ic}_{mb}r^m_a, \qquad (3.53)$$

$$I^{jk}_{ia} = I^e_i t^{kj}_{ae} + \tfrac{1}{2}\bar{h}^{ef}_{ai}r^{kj}_{ef} - \bar{h}^{jk}_{im}r^m_a + \mathscr{A}^{jk}(\bar{h}^{je}_{im}r^{km}_{ae} + \bar{h}^{je}_{ia}r^k_e), \qquad (3.54)$$

$$I'^{jk}_{ia} = \bar{h}^{jk}_{ia} - t^{jk}_{ea}\bar{h}^e_i, \qquad (3.55)$$

and

$$I^a_i = -r^m_e v^{ae}_{mi} \qquad (3.56)$$

while the antisymmetrizers that enter several of the above equations are given by

$$\mathscr{A}_{pqr} \equiv \mathscr{A}^{pqr} = 1 - (pq) - (pr) - (qr) + (pqr) + (prq), \qquad (3.57)$$

$$\mathscr{A}_{p/qr} \equiv \mathscr{A}^{p/qr} = 1 - (pq) - (pr), \qquad (3.58)$$

and

$$\mathscr{A}_{pq} \equiv \mathscr{A}^{pq} = 1 - (pq), \qquad (3.59)$$

with (pq) and (pqr) representing the cyclic permutations of two and three indices, respectively. As in the earlier equations, the one- and two-body matrix elements of $\bar{H}^{(\mathrm{CCSD})}$, $\bar{h}^q_p$ and $\bar{h}^{rs}_{pq}$, respectively, that enter Eqs. (3.52) – (3.56) can be found in Table 2.1. If the object of the calculation is the ground-state ($\mu = 0$) correction $\delta_0^{\mathrm{CR(2,3)}}$, we modify Eqs. (3.52) – (3.56) by replacing r_0 by 1 while zeroing all amplitudes r^i_a

```
SUM = 0.0
LOOP OVER i<j<k
   Calculate Γ^{abc}_{μ,ijk} for all values of a, b, c using Eq. (3.45)
   Calculate N^{abc}_{μ,ijk} by antisymmetrizing Γ^{abc}_{μ,ijk}, as in Eq. (3.44)
   Calculate 𝔗^{ijk}_{μ,abc}(2) for all values of a, b, c using Eq. (3.52)
   Calculate 𝔐^{ijk}_{μ,abc}(2) by antisymmetrizing 𝔗^{ijk}_{μ,abc}(2), as in Eq. (3.51)
   LOOP OVER a<b<c
      Calculate D^{ijk}_{μ,abc}, Eqs. (3.35) and (3.46)–(3.48)
      Calculate ℓ̃^{abc}_{μ,ijk}, Eq. (3.43)
      SUM = SUM + ℓ̃^{abc}_{μ,ijk} * 𝔐^{ijk}_{μ,abc}(2)
   END OF LOOP OVER a<b<c
END OF LOOP OVER i<j<k
δ_μ^{CR(2,3)} = SUM
```

Figure 3.1: The key elements of the algorithm used to compute $\delta_\mu^{\mathrm{CR(2,3)}}$ in the efficient open-shell implementation of CR-CC(2,3)/CR-EOMCC(2,3).

and r_{ab}^{ij}.

The CR-CC(2,3)/CR-EOMCC(2,3) computer programs developed in this work use the above expressions, Eqs. (3.43) – (3.59) and Eq. (3.37), to compute the noniterative corrections $\delta_\mu^{\mathrm{CR(2,3)}}$. The key elements of the corresponding computer algorithm are presented in Figure 3.1. As one can see, we use external loops over the occupied indices $i < j < k$ to compute the entire set of $N_{\mu,ijk}^{abc}$ and $\mathfrak{M}_{\mu,abc}^{ijk}(2)$ values for a given combination of the indices $i < j < k$ and for all values of a, b, and c. This is accomplished by first calculating the partially antisymmetric quantities $\Gamma_{\mu,ijk}^{abc}$ and $\mathfrak{T}_{\mu,abc}^{ijk}(2)$ with the help of fast matrix multiplication routines, which are subsequently antisymmetrized with respect to a, b, and c to produce the final result. In this way, we avoid explicit, and long, loops over a, b, and c in determining $N_{\mu,ijk}^{abc}$ and $\mathfrak{M}_{\mu,abc}^{ijk}(2)$,

which greatly speeds up the calculations. Once $N^{abc}_{\mu,ijk}$ and $\mathfrak{M}^{ijk}_{\mu,abc}(2)$ are determined for a given set of $i < j < k$ values and all a, b, and c, we enter the loops over $a < b < c$ in which the denominator $D^{ijk}_{\mu,abc}$ is computed to complete the evaluation of the desired $\tilde{\ell}^{abc}_{\mu,ijk}$ amplitude. At this point the $\tilde{\ell}^{abc}_{\mu,ijk}$ and $\mathfrak{M}^{ijk}_{\mu,abc}(2)$ values for a specific combination of $i < j < k$ and $a < b < c$ in the loops over these indices are multiplied to obtain a contribution to $\delta^{\mathrm{CR(2,3)}}_{\mu}$. The reason we use this algorithm is that it allows us to maximize the benefits of using fast matrix multiplication routines while eliminating the need to store the long $\tilde{\ell}^{abc}_{\mu,ijk}$ and $\mathfrak{M}^{ijk}_{\mu,abc}(2)$ vectors of the $n_o^3 n_u^3$ type in memory or on disk. As a result, the memory and disk requirements are quite similar to those of the underlying CCSD or EOMCCSD calculations (for memory $\sim n_o n_u^3$ times a small prefactor).

3.2 Applications

The CR-CC(2,3)/CR-EOMCC(2,3) approach has been used in calculations for a variety of molecular problems involving closed- and open-shell species, both as part of this work and outside of it, including (but not limited to) determination of the singlet-triplet gaps in biradical systems [138, 139, 151], studies of the stereoelectronic effects on geometries, singlet, and triplet state energies of copper-dioxygen and dicopper-dioxygen complexes (which function as models for copper containing metalloenzymes) [142–144], calculations for the barrier heights of reactions [148, 149], studies of the potential surfaces for bond breaking reactions [133–135, 137, 138, 145–147, 150], studies of reaction mechanisms involving biradical transition states [133, 134, 141], and examination of low-lying excited states of closed-shell molecules [135, 136] and radicals [89, 140]. To illustrate the performance of the CR-CC(2,3) and CR-EOMCC(2,3) schemes in studies of open-shell systems, only a few representative examples will be discussed here. Section 3.2.1 examines single bond-breaking reactions, specifically the

dissociation of H_2C-X and H_2Si-X into ^3H_2C + X and ^3H_2Si + X, respectively, where X = H, Cl, CH_3 and SiH_3. In Section 3.2.2, the results of calculations for the singlet-triplet gaps of several biradicals, specifically CH_2, $(HFH)^-$, and BN, will be discussed. Finally, Section 3.2.3 reexamines the triatomic molecules C_2N, CNC, N_3, and NCO discussed in Section 2.2.3 in order to examine the performance of CR-EOMCC(2,3) in studies of the excitation spectra of radicals, as well as to see how it performs relative to the active-space EA/IP-EOMCC methods of the previous chapter.

3.2.1 Bond Breaking in Radical Species: H_2C-X and H_2Si-X

The first test case for the open-shell CR-CC(2,3) approach examined here is a set of single bond breaking reactions in radical systems. Specifically, in collaboration with Dr. Yingbin Ge and Professor Mark Gordon at Iowa State University, the potential energy surfaces describing the representative bond-breaking reactions of H_2C–X $\longrightarrow$ H_2C + X and H_2Si–X $\longrightarrow$ H_2Si + X (X = H, Cl, CH_3 and SiH_3), were studied using CR-CC(2,3) [150]. One of the interesting features of these radical reactions is that they are of importance in high temperature chemical vapor deposition (CVD) processes, such as the silicon carbide CVD process [215,216]. In order to evaluate the performance of the ROHF-based CR-CC(2,3) method, either the full CI method or the internally contracted MRCI(Q) [181,182] scheme (depending on the size of the basis) was used to provide benchmark potential energy surfaces. Furthermore, the results were compared with those obtained with the UHF-based CCSD(T) approach, which is often used in high accuracy studies of radical species, and the multi-reference second-order perturbation theory (MRMP2) [217,218].

Calculations of the potential surfaces for all eight of the reactions described above were performed. To save space, two of these reactions, namely H_2C–H $\longrightarrow$ $^3CH_2$ + H and H_2Si–H $\longrightarrow$ $^1SiH_2$ + H, will be described in detail and the remaining ones will only be summarized. Five different basis sets were utilized in the calculations,

namely, MINI [219], 6-31G [194, 195], 6-31g(d) [195], cc-pVDZ [178, 220] and cc-pVTZ [178,220]. Full CI is used as the benchmark for calculations utilizing the MINI basis set, while the remaining calculations use MRCI(Q) to provide the reference results. All five basis sets were used for each reaction, except for the CH_2–Cl and SiH_2–Cl reactions, for which the MINI basis set was replaced by a mixed basis set, abbreviated as MIX, in which MINI is used for C, Si, and Cl and 6-311G is used for H, and for the $H_2C(Si)$–$C(Si)H_3$ reactions, for which the 6-31G(d), cc-pVDZ, and cc-pVTZ basis sets could not be applied due to the excessive computational cost of the MRCI(Q) calculations. The potential energy surfaces were constructed by sampling the breaking bond distances from slightly shorter than the equilibrium bond length (R_e) to roughly $3R_e$ in 0.2 Å increments. In order to ensure that the two fragments on the product side of each reaction have negligible interaction, so that the bond can be considered to be 'broken', if the last two structures at $3R_e$ had an energy difference of more than 0.16 millihartree (0.1 kcal/mol), then more structures with longer bond lengths would be computed until the energy difference was below the 0.16 millihartree threshold. For all eight reactions with the MINI (or MIX as the case may be) basis set, as well as for the $H_2C(Si)$–H reaction with the 6-31G and 6-31G(d) basis sets, full CI was used to optimize the structures on the one-dimensional bond-breaking reaction surface. In all other calculations, the full-valence CASSCF was used for the structure optimizations. Finally, it should be noted that the frozen core approximation was used in all calculations, and the full valence CASSCF was used as the zero-order wave function for all MRCI and MRMP2 calculations.

Figure 3.2 shows the CCSD, CR-CC(2,3), CCSD(T), and MRMP2 error curves relative to MRCI(Q) for the H_2C–H $\longrightarrow$ $^3CH_2$ + H reaction as computed with the cc-pVTZ basis set. Inspection of these error curves reveals that the CR-CC(2,3) results are either as accurate as or more accurate than CCSD(T) for all geometries considered. Indeed we can observe that the error in CCSD(T) begins to increase

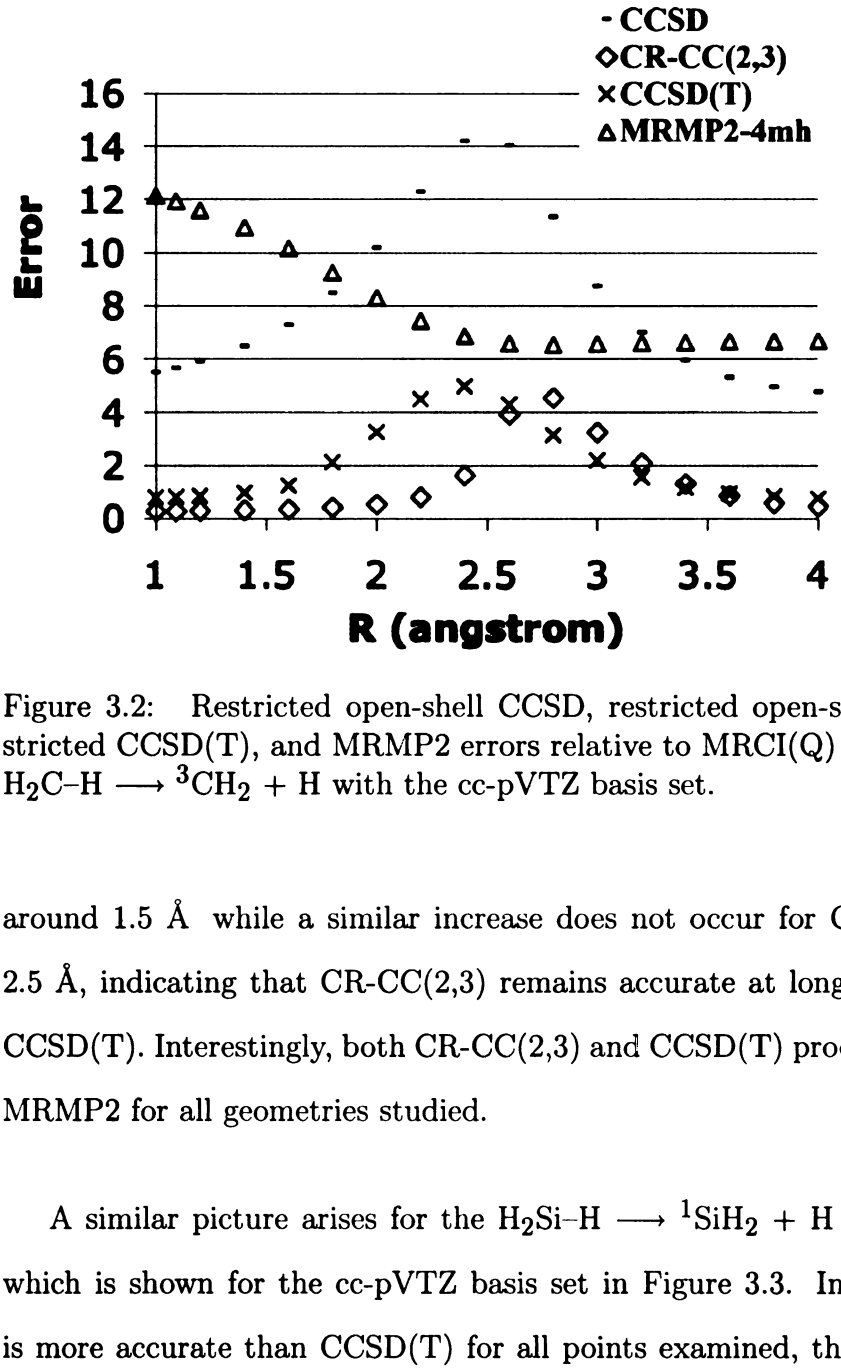

Figure 3.2: Restricted open-shell CCSD, restricted open-shell CR-CC(2,3), unrestricted CCSD(T), and MRMP2 errors relative to MRCI(Q) for H_2C–H $\longrightarrow$ $^3CH_2$ + H with the cc-pVTZ basis set.

around 1.5 Å while a similar increase does not occur for CR-CC(2,3) until about 2.5 Å, indicating that CR-CC(2,3) remains accurate at longer bond distances than CCSD(T). Interestingly, both CR-CC(2,3) and CCSD(T) produce smaller errors than MRMP2 for all geometries studied.

A similar picture arises for the H_2Si–H $\longrightarrow$ $^1SiH_2$ + H potential energy curve, which is shown for the cc-pVTZ basis set in Figure 3.3. In this case, CR-CC(2,3) is more accurate than CCSD(T) for all points examined, though for the very short distances and very long distances the discrepancy between the two is relatively small. Once again, a bump in the error curve of CCSD(T) is observed, with the rise in the error beginning at roughly 2 Å. As was the case for H_2C–H, a similar rise in the error of the CR-CC(2,3) result does not occur until about 2.6 Å, once again indicating that CR-CC(2,3) remains accurate at longer bond distances than CCSD(T). Furthermore, the bump in the CR-CC(2,3) error curve at about 2.6 Å is considerably smaller

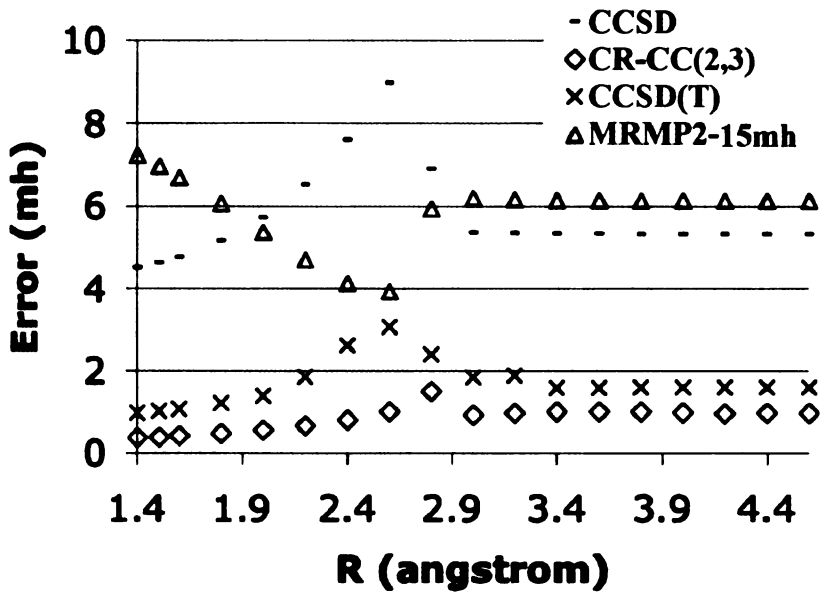

Figure 3.3: Restricted open-shell CCSD, restricted open-shell CR-CC(2,3), unrestricted CCSD(T), and MRMP2 errors relative to MRCI(Q) for $H_2Si–H \longrightarrow {}^1SiH_2 + H$ with the cc-pVTZ basis set.

than that of CCSD(T), leading to a smoother and overall consistently more accurate potential energy surface. Once again, both methods are significantly more accurate than MRMP2 at all geometries considered.

Rather than analyzing all of the remaining potential energy surfaces generated in a similar fashion, the rest of this discussion will focus on summarizing the result through the use of three fundamental quantities that serve as valuable indicators of the accuracy of the potential energy surfaces, namely the nonparallelity error (NPE), the standard deviation error (STD), and the reaction energy error (REE). As described earlier in this thesis, NPE is defined as the difference between the most positive and the most negative signed errors along the surface, and thus is a measure of how closely the shape of the potential energy surface matches that of the benchmark surface. As the name implies, REE measures the error in the reaction energy and is defined as the difference between the error at the longest bond distance (i.e. the 'broken bond'

distance) and the error at the equilibrium geometry. Finally, STD is defined as

$$\mathrm{STD} = \sqrt{\frac{1}{N}\left(\sum_{i=1}^{N}[\mathrm{Err}(R_i)]^2 - \left[\sum_{i=1}^{N}|\mathrm{Err}(R_i)|\right]^2\right)}, \tag{3.60}$$

where N is the number of geometries, and $\mathrm{Err}(R_i)$ is the error at the bond length R_i. Table 3.1 gives the NPE, STD, and REE values for all eight potential energy surfaces determined in this study.

Analysis of Table 3.1 reveals that for all reactions other than H_2C–Cl, the CR-CC(2,3) NPE values for the various basis set calculations are less than (in many cases, much less than), or in a few cases virtually identical to, the corresponding CCSD(T) value. Similarly, the average CR-CC(2,3) NPE as computed with 6-31G (the largest basis set that all reactions were computed with) is 0.4 millihartree less than that of CCSD(T), while the average CR-CC(2,3) NPE for the cc-pVTZ basis (the largest basis set considered) is 0.3 millihartree less than CCSD(T). Thus it would seem that, at least in terms of NPE, the ROHF-based CR-CC(2,3) scheme is capable of outperforming the frequently used UHF-based CCSD(T) approach in these reactions. Interestingly, the situation is a little different when CR-CC(2,3) and MRMP2 are compared, as neither is clearly superior with regards to NPE. Indeed, for half of the reactions, namely H_2C–H, H_2Si–H, H_2Si–Cl, and H_2Si–CH_3, the CR-CC(2,3) NPE values are smaller than the corresponding MRMP2 values, while for the remaining reactions it is the other way around. Looking at the average NPE values, we see that for 6-31G, the CR-CC(2,3) average NPE is higher than that of MRMP2 by roughly 0.5 millihartree, whereas for cc-pVTZ the CR-CC(2,3) value is actually lower by 0.4 millihartree.

Moving on, Table 3.1 reveals that the STD patterns observed are quite similar to those observed for the NPE values. Indeed, it turns out that with the exception of

Table 3.1: Restricted open-shell CR-CC(2,3), unrestricted CCSD(T) and MRMP2 NPE, STD, and REE values relative to MRCI(Q). Units are millihartree.[a]

	NPE			STD			REE		
Basis	CR-CC(2,3)	CCSD(T)	MR-MP2	CR-CC(2,3)	CCSD(T)	MR-MP2	CR-CC(2,3)	CCSD(T)	MR-MP2
				H_2C–H					
MINI	0.366	1.093	N.A.	0.146	0.431	N.A.	-0.313	0.851	N.A.
6-31G	1.725	2.081	1.883	0.565	0.766	0.627	0.104	-0.035	-1.507
6-31G(d)	3.279	3.339	3.447	1.072	1.160	1.226	0.152	-0.052	-3.114
cc-pVDZ	3.621	3.699	4.807	1.162	1.286	1.832	0.170	-0.040	-4.529
cc-pVTZ	4.256	4.223	5.613	1.365	1.455	2.181	0.181	-0.062	-5.276
				H_2C–Cl					
MIX	2.022	1.965	0.436	0.624	0.754	0.125	-0.840	-1.118	-0.114
6-31G	3.772	2.674	0.832	1.175	0.957	0.293	0.111	-0.421	0.123
6-31G(d)	6.787	6.146	2.694	1.919	1.956	0.777	0.583	0.248	-1.519
cc-pVDZ	7.112	6.705	2.875	2.029	2.072	0.855	0.643	0.423	-1.653
cc-pVTZ	8.367	7.794	4.646	2.398	2.327	1.410	0.582	1.165	-2.879
				H_2C–CH_3					
MINI	0.301	2.543	N.A.	0.197	0.849	N.A.	-0.326	0.300	N.A.
6-31G	3.126	4.023	1.176	0.981	1.401	0.401	0.160	-0.039	-0.753
				H_2C–SiH_3					
MINI	0.412	1.814	N.A.	0.127	0.666	N.A.	0.064	0.017	N.A.
6-31G	2.681	3.142	1.553	0.821	1.069	0.539	-0.136	-0.236	-1.272
				H_2Si–H					
MINI	0.237	0.443	N.A.	0.063	0.142	N.A.	0.049	0.063	N.A.
6-31G	0.526	0.801	0.697	0.151	0.277	0.228	0.041	0.035	-0.059
6-31G(d)	1.061	1.450	2.271	0.239	0.366	0.767	0.300	0.509	0.585
cc-pVDZ	0.923	1.100	3.128	0.212	0.315	0.847	0.245	0.236	-0.822
cc-pVTZ	1.132	2.092	3.310	0.295	0.547	0.873	0.584	0.577	-0.842
				H_2Si–Cl					
MIX	0.744	1.377	0.478	0.225	0.406	0.163	-0.114	-0.342	0.294
6-31G	0.682	2.094	1.917	0.175	0.592	0.565	0.463	0.346	-1.870
6-31G(d)	1.917	3.616	3.302	0.583	0.842	1.308	0.054	0.474	2.034
cc-pVDZ	1.833	3.661	4.170	0.543	0.814	1.688	0.068	0.499	2.823
cc-pVTZ	2.705	3.600	4.472	0.801	0.764	1.604	-1.013	0.221	2.006
				H_2Si–CH_3					
MINI	0.392	0.696	N.A.	0.127	0.235	N.A.	-0.040	-0.110	N.A.
6-31G	0.434	0.765	1.288	0.114	0.226	0.321	-0.054	-0.031	-0.740
				H_2Si–SiH_3					
MINI	0.485	1.991	N.A.	0.158	0.571	N.A.	-0.046	0.000	N.A.
6-31G	1.510	2.048	0.797	0.357	0.545	0.184	-0.077	-0.115	0.103
				Unsigned Average					
6-31G	1.807	2.204	1.268	0.542	0.729	0.395	0.143	0.157	0.803
cc-pVTZ	4.115	4.427	4.510	1.215	1.273	1.517	0.590	0.506	2.751

[a] Full CI is the benchmark method with the MINI basis set.

the CR-CC(2,3) MINI surface for H_2C–CH_3, the STD values are roughly 20–30% of the corresponding NPE values. As result, much of the previous NPE discussion also applies in the STD case. However, in the REE case, such patterns are not observed, and a more detailed analysis is useful. Upon inspection of Table 3.1, it becomes clear that both CR-CC(2,3) and CCSD(T) significantly outperform MRMP2 in terms of REE. Indeed, in some cases the MRMP2 REE values exceed those of CR-CC(2,3) and CCSD(T) by as much as 5 millihartree. This is further illustrated by the average REE values, for which the MRMP2 result exceeds those of CR-CC(2,3) and CCSD(T) by roughly 0.7 and 2.2 millihartree for the 6-31G and cc-pVTZ basis sets, respectively. A more direct comparison of just CR-CC(2,3) and CCSD(T) reveals that these two methods perform very similarly to each other with respect to average REE values. In fact, the average CR-CC(2,3) REE value is less than that of CCSD(T) by only 0.01 millihartree for the 6-31G basis set, while it is greater than that of CCSD(T) by only 0.09 millihartree with the cc-pVTZ basis.

Based on these results, it is clear that the ROHF-based CR-CC(2,3) approach is a promising alternative for performing high accuracy calculations of single-bond breaking processes in radicals. Indeed, these results indicate that for H_2C–X and H_2Si–X reactions, CR-CC(2,3) outperforms the popular UHF-based CCSD(T) and MRMP2 approaches, which are traditionally considered the recommended options for high accuracy, low-cost calculations of bond breaking in radicals. In particular, we see that CR-CC(2,3) produces NPE values that are notably smaller than those of CCSD(T) and which are comparable to those of MRMP2, while producing REE values that are comparable to the small values produced by CCSD(T) and significantly smaller than those of MRMP2. Thus, the CR-CC(2,3) approach provides a more balanced description of the radical potential energy surfaces than CCSD(T) or MRMP2 in spite of the use of the ROHF reference, which does not dissociate as well as the UHF reference used in the CCSD(T) calculations, and in spite of being a single-reference

black-box approach, which is much easier to use than MRMP2. Furthermore, the ROHF-based CR-CC(2,3) approach is able to provide such accurate results while avoiding the pitfalls associated with unrestricted or multi-reference formalisms, such as errors in relative energies resulting from spin contamination of UHF in the former case or the intruder state problem and the need for carefully selecting active orbitals in the latter.

3.2.2 Singlet-Triplet Gaps in Biradicals

The description of the singlet-triplet gaps in biradical systems represents a significant challenge for many electronic structure methods. The difficulty stems from the fact that the singlet and the triplet states, which result from the parallel or antiparallel coupling of the two unpaired electrons forming the radical centers, are often primarily characterized by consistently different correlation effects, particularly when the radical centers are separated by some distance. Indeed, the non-degenerate, high-spin triplet state is dominated by dynamical correlations, while the singlet state often shows a strong contribution from nondynamical correlations, and thus has a more multi-reference nature. As a result, the accurate description of the gap between these states requires an electronic structure method capable of accurately balancing both types of correlations. It has generally been thought that the genuine multi-reference methods of the MRCI or MRCC type are needed to produce accurate results under such conditions, but, as it turns out, the single-reference CR-CC(2,3) scheme employing the RHF reference for the singlet state and ROHF reference for the triplet state is also capable of accurately describing such systems, being very competitive with genuine multi-reference methods. To illustrate this, we consider several systems which are characterized by varying degrees of a biradical nature.

We begin with methylene, which is well known for being the subject of controversies between theory and experiment (cf., e.g., [221–226], and references therein). As

a first test, we performed calculations of the adiabatic singlet-triplet gap using the same DZP-type basis sets and geometries that were used in the well-known benchmark calculations of Bauschlicher and Taylor [227]. The results are presented in Table 3.2, along with the exact full CI results of Bauschlicher and Taylor. As can clearly be seen, the most complete CR-CC(2,3),D approach provides the best description of the singlet-triplet gap out of all the triples-type CC methods considered, producing an error relative to full CI of only 0.21 kcal/mol. This is a notable improvement over the 0.32, 0.44, and 0.41 kcal/mol errors obtained with CCSD(T), CR-CCSD(T), and CCSD(2)$_{\mathrm{T}}$ (=CR-CC(2,3),A), respectively. Furthermore, only the more complete variants C and D of CR-CC(2,3) are capable of providing a singlet-triplet gap that is more accurate than that of CCSD(T). Variants A and B, which are equivalent to the CCSD(2)$_{\mathrm{T}}$ methods of [205–209] are not as effective. It also important to note that the high accuracy of the CR-CC(2,3),D singlet-triplet gap value is not the result of a fortuitous cancellation of errors. Looking at the total energies for the singlet and triplet states, we see that the CR-CC(2,3) values are in excellent agreement with those of full CI. Indeed, the errors in the singlet and triplet energies are only 0.333 and -0.001 millihartree, respectively, which represent substantial improvements over the CCSD(T), CR-CCSD(T), and CCSD(2)$_{\mathrm{T}}$ triplet-state errors of 0.367, 0.516, and 0.469 millihartree and singlet-state errors of 0.873, 1.213, and 1.125 millihartree, respectively.

In order to further explore methylene, we performed a sequence of calculations using the aug-cc-pCVxZ (x=T, Q, and 5) basis sets [178, 179, 228] and compared the results with the Quantum Monte Carlo (QMC) [229–231] calculations of Umrigar [232]. Two different variants of QMC were used in Umrigar's calculations, namely variational Monte Carlo (VMC) and diffusion Monte Carlo (DMC). The trial functions for both variants consisted of Jastrow-Slater multi-determinant CAS wave functions which were optimized using the linear optimization method [233–235]. Three different

Table 3.2: The adiabatic $A\ ^1A_1 - X\ ^3B_1$ splitting in CH_2 obtained with full CI and various CC approaches, and the DZP basis set.[a]

	$E(X\ ^3B_1)$	$E(A\ ^1A_1)$	$E(A\ ^1A_1) - E(X\ ^3B_1)$
Method	(hartree)	(hartree)	(kcal/mol)
Full CI[a]	-39.046 260	-39.027 183	11.97
CCSD	-39.044 111	-39.023 639	12.85
CCSD(T)	-39.045 893	-39.026 310	12.29
CR-CCSD(T)	-39.045 744	-39.025 970	12.41
CR-CC(2,3),A[b]	-39.045 791	-39.026 058	12.38
CR-CC(2,3),B[c]	-39.045 743	-39.025 960	12.41
CR-CC(2,3),C	-39.046 267	-39.026 864	12.18
CR-CC(2,3),D	-39.046 261	-39.026 850	12.18

[a] The basis sets, geometries, and full CI energies were taken from [227]. As in [227], in all correlated calculations, the lowest occupied orbital was kept frozen and Cartesian components of the carbon d orbital were employed.
[b] Equivalent to the $CCSD(2)_T$ approach of [205].
[c] Equivalent to the triples part of the (2) correction of the CCSD(2) method of [206–209].

active spaces were used to generate CAS trial functions, specifically the (2,2), (4,4) and (6,6) active spaces (recall that (n, m) denotes an active space of n electrons and m orbitals). Rather than restricting ourselves to the ground $X\ ^3B_1$ and first excited $A\ ^1A_1$ states, as was done in the DZP calculations discussed above, we follow the calculations of Umrigar and also compute the higher-energy $B\ ^1B_1$ and $C\ ^1A_1$ states. It should be noted that since the $X\ ^3B_1$ and $A\ ^1A_1$ states are the lowest-energy states of their respective symmetries, they can be computed using the ground-state CR-CC(2,3) formalism, which is how both the DZP and this set of calculations were performed. The $B\ ^1B_1$ and $C\ ^1A_1$ states were calculated using the excited-state CR-EOMCC(2,3) approach of Section 3.1.2, with the $A\ ^1A_1$ state acting as the correlated ground state for the EOMCC ansatz (see Eq. (3.1)). The $C\ ^1A_1$ state is particularly important here, since this is a strongly multi-reference state of the same symmetry as the $A\ ^1A_1$ state. In both the CC and QMC calculations, the geometries for each state were taken from [236], where they were generated using the full CI

calculations with the [5s3p/2s] triple zeta basis set of Dunning [237] augmented with two sets of polarization functions (TZ2P). Finally, since QMC is derived using the first quantization formalism, and so does not utilize the concept of a basis set, a proper comparison between QMC and CC requires the determination of the complete basis set (CBS) limit for the CC results. This can be done through extrapolation from the aug-cc-pCVxZ data. In order to verify the stability of the CBS results, two different extrapolation schemes were utilized in this work. In the first scheme, the CBS total energy of the $X\ ^3B_1$ state was determined by first extrapolating the correlation energy using the formula

$$\Delta E(x) = \Delta E_\infty + Ax^{-3}, \tag{3.61}$$

with $x = 3, 4, 5$. Here x is the cardinal number of the aug-cc-pCVxZ basis set, $\Delta E(x)$ is the correlation energy obtained with the aug-cc-pCVxZ basis, and ΔE_∞ is the correlation energy in the CBS limit. The resulting extrapolated correlation energy was then added to the aug-cc-pCV5Z reference energy, which, due to the fast (exponential) convergence of the RHF/ROHF energy with respect to the basis set, is equivalent to the CBS reference energy to an extremely high (0.1 millihartree) accuracy. The CBS total energies of the remaining states were subsequently obtained by adding the aug-cc-pCV5Z excitation energy to the extrapolated total energy of the $X\ ^3B_1$ state. This approach was designed based on the assumption that with aug-cc-pCV5Z the excitation energies were essentially converged with respect to the basis set. The validity of this assumption will be discussed below. In the second extrapolation scheme, the CBS total energy of each state was extrapolated using the formula

$$E(x) = E_\infty + Be^{-(x-1)} + Ce^{-(x-1)^2}, \tag{3.62}$$

with $x = 3, 4, 5$. Here x is again the cardinal number of the aug-cc-pCVxZ basis set,

$E(x)$ is the total energy of the state as computed with the aug-cc-pCVxZ basis, and E_∞ is the total energy of the state in the CBS limit. Throughout the rest of this discussion, we will refer to the results obtained using the first extrapolation scheme as CBS-A and those obtained using the second as CBS-B. It should also be noted that since the CR-CC(2,3)/CR-EOMCC(2,3) programs are part of the GAMESS package, as mentioned in Section 3.1.3, and since the integral codes in GAMESS are currently restricted to g-functions, the h-functions of the aug-cc-pCV5Z basis set were omitted in these calculations. Furthermore, all electrons were correlated and the spherical components of the d, f, and g orbitals were employed in all CC calculations.

Table 3.3 shows the results of the methylene CC and QMC calculations. We begin by analyzing the stability of the CBS extrapolations. As mentioned above, the CBS-A extrapolation scheme was based on an assumption that although the total CC/EOMCC energies are not converged to the CBS limit with the aug-cc-pCV5Z basis, the excitation energies are. An analysis of Table 3.3 reveals that for this system this is indeed a valid assumption, as the EOMCCSD and CR-EOMCC(2,3) excitation energies do not significantly change when moving from the aug-cc-pCVQZ to aug-cc-pCV5Z basis sets, with the largest change of 0.02 eV occurring for the $C\ ^1A_1$ state. Moving on to a direct comparison of the two types of CBS CR-CC(2,3)/CR-EOMCC(2,3) total energies for each state, we see that the two extrapolation schemes produce results that are in reasonably good agreement. Indeed, the discrepancies between the two sets of results do not exceed 2.8 millihartree. The situation for the CCSD/EOMCCSD total energies is similar. The agreement between the two different CBS schemes for the adiabatic excitation energies is even better. For the $A\ ^1A_1$ and $B\ ^1B_1$ excitation energies, the two CBS CR-EOMCC(2,3) values differ by 0.001 eV or less, while in the case of the $C\ ^1A_1$ state, the discrepancy in the excitation energies is 0.013 eV. Again, similar observations apply to the EOMCCSD approach. We can conclude that the CBS CCSD/EOMCCSD and CR-CC(2,3)/CR-EOMCC(2,3)

Table 3.3: Comparison of the total energies (in hartree) and adiabatic excitation energies (in eV) for the low-lying states of CH_2 as obtained with various CC approaches, using the aug-cc-pCVxZ (x=T, Q, 5) basis sets and extrapolating to the CBS limit, with various QMC results.[a]

		Total Energy (Hartree)				Adiabatic Excitation Energy (eV)		
Method	Basis Set	$X\,^3B_1$	$A\,^1A_1$	$B\,^1B_1$	$C\,^1A_1$	$A\,^1A_1$ - $X\,^3B_1$	$B\,^1B_1$ - $X\,^3B_1$	$C\,^1A_1$ - $X\,^3B_1$
EOMCCSD	x=T	-39.126 182	-39.108 786	-39.072 643	-38.978 950	0.473	1.457	4.006
	x=Q	-39.137 932	-39.120 739	-39.085 176	-38.988 201	0.468	1.436	4.074
	x=5	-39.140 567	-39.123 385	-39.087 917	-38.990 384	0.468	1.433	4.087
	CBS-A	-39.144 329	-39.127 147	-39.091 680	-38.994 146	0.468	1.433	4.087
	CBS-B	-39.142 082	-39.124 905	-39.089 492	-38.991 641	0.467	1.431	4.094
CR-EOMCC(2,3)	x=T	-39.130 497	-39.114 493	-39.075 964	-39.034 496	0.435	1.484	2.612
	x=Q	-39.142 544	-39.126 736	-39.088 654	-39.046 556	0.430	1.466	2.612
	x=5	-39.145 196	-39.129 390	-39.091 392	-39.048 426	0.430	1.464	2.633
	CBS-A	-39.149 079	-39.133 273	-39.095 275	-39.052 309	0.430	1.464	2.633
	CBS-B	-39.146 720	-39.130 914	-39.092 964	-39.049 486	0.430	1.463	2.646
DMC: CAS(2,2)		-39.1406(1)	-39.1255(1)	-39.0890(1)	-39.0451(1)	0.412(4)	1.405(4)	2.600(4)
DMC: CAS(4,4)		-39.1408(1)	-39.1257(1)	-39.0891(1)	-39.0465(1)	0.412(4)	1.408(4)	2.566(4)
DMC: CAS(6,6)		-39.1428(1)	-39.1279(1)	-39.0908(1)	-39.0501(1)	0.406(4)	1.416(4)	2.524(4)
VMC: CAS(2,2)		-39.1273(2)	-39.1124(2)	-39.0755(2)	-39.0311(2)	0.407(8)	1.411(8)	2.620(8)
VMC: CAS(4,4)		-39.1279(2)	-39.1126(2)	-39.0758(2)	-39.0334(2)	0.416(8)	1.417(8)	2.573(8)
VMC: CAS(6,6)		-39.1327(2)	-39.1169(2)	-39.0790(2)	-39.0389(2)	0.430(8)	1.460(8)	2.550(8)

[a] The geometries were taken from [236] and were generated using full CI with the TZ2P basis set. In CC calculations, all electrons were correlated and the spherical components of the d, f, and g orbitals were employed. The calculations were performed using the GAMESS package, and so the aug-cc-pCV5Z basis set used neglects the h functions. All DMC and VMC results are taken from [232].

values are accurate to the level of approximately 2 millihartree in total energies, and approximately 0.01 eV in excitation energies.

We now turn our attention to the comparison of the CC results with those of QMC. Beginning with the basic CCSD/EOMCCSD calculations, we see that the results for the $A\ ^1A_1 - X\ ^3B_1$ and $B\ ^1B_1 - X\ ^3B_1$ gaps are in reasonably good agreement with the various QMC results. Furthermore, accounting for the effects of triples through CR-CC(2,3)/CR-EOMCC(2,3) does not significantly alter the values for these gaps, changing the excitation energies for the $A\ ^1A_1$ and $B\ ^1B_1$ states in the CBS limit by only about 0.03–0.04 eV. The situation is quite a bit different for the $C\ ^1A_1 - X\ ^3B_1$ excitation energy. For this gap, the EOMCCSD excitation energies differ from those generated by CR-EOMCC(2,3) and the various QMC approaches by roughly 1.4 – 1.5 eV, thus indicating that this is the most challenging state considered here, which is characterized by a significant multi-reference or two-electron excitation nature. Looking at the total energies of each state, we see that for the $X\ ^3B_1$, $A\ ^1A_1$, and $B\ ^1B_1$ states, which correspond to the states for which the EOMCCSD excitation energies were reasonable, CCSD/EOMCCSD produces errors relative to CR-CC(2,3)/CR-EOMCC(2,3) on the order of 3.5 to 6.1 millihartree, i.e. errors which are relatively small. The EOMCCSD calculation for the $C\ ^1A_1$ state, however, generates a huge 58 millihartree error relative to CR-EOMCC(2,3), illustrating the much larger role of triply excited clusters in the description of this multi-reference state.

Moving on, it can be seen from Table 3.3 that the CR-CC(2,3)/CR-EOMCC(2,3) results for the adiabatic excitation energies are in very good agreement with the various QMC results. Indeed, depending on the size of the CAS for the trial function, the discrepancies between the DMC and CR-CC(2,3)/CR-EOMCC(2,3) excitation energies range from 0.018–0.024, 0.047–0.059, and 0.033–0.122 eV for the $A\ ^1A_1$, $B\ ^1B_1$, and $C\ ^1A_1$ states, respectively. Interestingly, the agreement of the CR-

CC(2,3)/CR-EOMCC(2,3) excitation energies with the corresponding VMC data is even better, with the discrepancy ranges reducing to 0.000–0.023, 0.003–0.053, and 0.013–0.096 eV for the $A\ ^1A_1$, $B\ ^1B_1$, and $C\ ^1A_1$ states, respectively. It is worth noting, however, that the improvements in the excitation energy when going from DMC to VMC are not dramatic, and so we can conclude that the two QMC variants produce comparable results in this regard. The total energies, however, paint a somewhat different picture. The discrepancies between the VMC and DMC results are on the order of 10 millihartree, which is a rather substantial disagreement. Looking at the CR-CC(2,3)/CR-EOMCC(2,3) total energies, it is clear that they agree much more strongly with the DMC results than with the VMC results. If we focus on the largest CAS(6,6) QMC calculations, then the CBS-A CR-CC(2,3)/CR-EOMCC(2,3) energies differ from the DMC results by 2.2–6.3 millihartree while the CBS-B energies differ by only 0.6–3.9 millihartree, which represents an excellent level of agreement. The discrepancy with the VMC energies, on the other hand, is an order of magnitude worse, ranging from 13.4 to 16.4 millihartree for the CBS-A results and 10.6 to 14.0 millihartree for the CBS-B values. Given the agreement between the independent CR-CC(2,3)/CR-EOMCC(2,3) and DMC results, it is safe to conclude that the VMC results are the ones in larger error, producing total energies that are too high. However, given the fact that the increase in the VMC energies relative to the CR-CC(2,3)/CR-EOMCC(2,3) and DMC approaches is nearly constant for all four states, the resulting adiabatic excitation energies are still highly accurate and in very good agreement with those of the latter two methods.

In summary, we see that by using the aug-cc-pCVxZ series of basis sets to extrapolate the CBS limit of the CR-CC(2,3)/CR-EOMCC(2,3) energies for the low-lying states of methylene, the results are on the level of highly accurate, yet computationally expensive, QMC calculations, which implicitly produce CBS results. This is a very encouraging result that illustrates the large potential of CR-CC(2,3)/CR-

EOMCC(2,3) in describing the low-lying states of biradical species.

The methylene system, though a challenging case, is a relatively weak biradical. In order to investigate the performance of the CR-CC(2,3) scheme in describing the singlet-triplet gaps in systems characterized by a larger degree of biradical character, we consider the $(HFH)^-$ species. This $D_{\infty,h}$-symmetric linear molecule, which consists of two unpaired spins, represented by the hydrogen atoms, separated by a polarizable, diamagnetic bridge, namely F^-, is not only a strong biradical, but also a simple, yet informative, model for many magnetic systems. The singlet-triplet gap in such magnetic systems is particularly important as it provides information about the magnetic exchange coupling constant. In the case of $(HFH)^-$, this corresponds to the gap between the ground $X\ ^1\Sigma_g^+$ and the first-excited $A\ ^3\Sigma_u^+$ states. To test the performance of CR-CC(2,3) as a function of the degree of biradical character, calculations for the $A\ ^3\Sigma_u^+ - X\ ^1\Sigma_g^+$ gap of the $D_{\infty h}$-symmetric linear $(HFH)^-$ system were performed for various values of the H-F distance R_{H-F} [138, 139]. All calculations were performed using the 6-31G(d,p) basis set [194, 195], employing the spherical components of the d orbitals, and the lowest-energy molecular orbital correlating to the $1s$ orbital of F was kept frozen. To gauge the performance of the RHF/ROHF-based CR-CC(2,3) calculations, performed using the codes discussed in Section 3.1.3, the results are compared with full CI data obtained with GAMESS [173] and MOLPRO [183], and with the UHF-based CCSD and CCSD(T) results obtained with Gaussian 98 [238].

The $(HFH)^-$ system is a strong biradical, particularly for larger H-F distances. This can be seen quantitatively in Table 3.4, which gives the absolute value of the ratio of the full CI coefficients at the doubly excited $(HOMO)^2 \rightarrow (LUMO)^2$ determinant (c_2) and the RHF ground-state determiant (c_0) for the ground $X\ ^1\Sigma_g^+$ state. As is the case for the H_2 molecule, the symmetries of the HOMO and LUMO in $(HFH)^-$ are σ_g and σ_u, respectively, and the ratio c_2/c_0 is equivalent to the full CI value of the

Table 3.4: The $A\ ^3\Sigma_u^+ - X\ ^1\Sigma_g^+$ gap for the linear, $D_{\infty h}$-symmetric $(HFH)^-$ system (in cm^{-1}) described by the 6-31G(d,p) basis set [194, 195], as a function of the H–F distance R_{H-F} (in Å).

	RHF Reference								UHF Reference			
$R_{H\text{-}F}$	Full CI	SCF	CCSD	CCSD(T)	CR-CC(2,3),A[a]	CR-CC(2,3),B[b]	CR-CC(2,3),C	CR-CC(2,3),D	SCF	CCSD	CCSD(T)	$\lvert c_2/c_0\rvert$[c]
1.500	9525	-7169	7320	9468	8886	8759	9441	9355	3024	7398	8418	0.3768
1.625	7008	-12006	4372	7066	6279	6108	6965	6834	1641	4981	5776	0.4274
1.750	4911	-16708	1838	5179	4117	3891	4943	4752	718	3156	3693	0.4846
1.875	3304	-21135	-172	3902	2482	2193	3450	3183	186	1913	2244	0.5458
2.000	2147	-25229	-1656	3212	1345	988	2445	2087	-67	1122	1323	0.6082
2.125	1353	-28970	-2668	3023	615	189	1823	1370	-151	638	766	0.6698
2.250	827	-32363	-3282	3225	182	-303	1461	916	-150	350	438	0.7292
2.375	488	-35424	-3572	3714	-54	-581	1249	628	-118	182	247	0.7858
2.500	277	-38172	-3605	4394	-171	-718	1106	435	-81	88	137	0.8392
3.000	17	-46460	-2369	7370	-230	-634	601	43	-8	1	10	1.0174
4.000	0	-53986	-230	8899	-34	-92	55	-33	0	0	0	1.1727

[a] Equivalent to the $CCSD(2)_T$ approach of [205], when the canonical Hartree Fock orbitals are employed.

[b] Equivalent, up to small details, to the triples part of the (2) correction of the CCSD(2) method of [206–209].

[c] The absolute value of the ratio of the coefficients at the doubly excited $(HOMO)^2 \rightarrow (LUMO)^2$ determinant (c_2) and the RHF ground-state determinant (c_0) characterizing the full CI expansion of the $X\ ^1\Sigma_g^+$ state.

T_2 cluster amplitude corresponding to the $(\text{HOMO})^2 \rightarrow (\text{LUMO})^2$ double excitation. The magnitude of this T_2 amplitude is an indicator of the biradical character of the system, with values around zero representing essentially no biradical character and values around 1 representing a virtually pure biradical. From Table 3.4 we see that even for small values of $R_{\text{H-F}}$, the $(\text{HFH})^-$ system shows a large degree of biradical character. Furthermore, as the H-F distance is increased the degree of biradical nature steadily increases until the molecule becomes an essentially pure biradical at the largest distances. As a result of this strong biradical character, we expect the $A\ ^3\Sigma_u^+$ - $X\ ^1\Sigma_g^+$ gap to be relatively small, and thus very sensitive to the electron correlation treatment, even for the relatively small values of $R_{\text{H-F}}$, and steadily approach zero as the H-F distance is increased. As can be seen in Table 3.4, this behavior is displayed by the exact full CI results.

Analyzing the performance of the various CC approximations based on adding a noniterative correction due to triples to the CCSD energy, we see from Table 3.4 that the only method to provide a uniformly accurate description of the singlet-triplet gap across all values of $R_{\text{H-F}}$ is CR-CC(2,3) (with the complete variant D of CR-CC(2,3) offering the best results). Indeed, if we focus specifically on the CCSD(T) scheme, it is clear that it has severe difficulties in uniformly describing the $(\text{HFH})^-$ system regardless of which type of reference determinant is utitlized. With the RHF/ROHF reference, CCSD(T) does provide reasonably accurate results for the singlet-triplet gap at $R_{\text{H-F}} = 1.5$ and 1.625 Å, generating errors relative to full CI of approximately 60 cm^{-1}. However, this accuracy quickly breaks down as the H-F distance, and thus the biradical character, increases. The RHF/ROHF-based CCSD(T) approach does not produce the correct dependence of the gap on $R_{\text{H-F}}$, with the energy actually increasing after $R_{\text{H-F}} = 2.25$ Å rather than systematically approaching zero as the H-F distance is increased. The resulting errors relative to full CI are significant, growing from 268 cm^{-1} at $R_{\text{H-F}} = 1.75$ Å to 8900 cm^{-1} at $R_{\text{H-F}} = 4.00$ Å. This

behavior is easily understandable if we analyze the behavior of CCSD(T) with respect to each state (see Tables 3.5 and 3.6). Table 3.6 reveals that CCSD(T) provides accurate results for the $A\ ^3\Sigma_u^+$ state, producing errors relative to full CI of less than 0.7 millihartree for all geometries considered. This excellent performance makes sense since the $A\ ^3\Sigma_u^+$ state is a nondegenerate high-spin triplet state and so it is characterized primarily by dynamical correlations, which CCSD(T) describes well. However, as shown in Table 3.5, the situation is considerably different for the $X\ ^1\Sigma_g^+$ state. Because this state is characterized by strong nondynamical correlation effects, which CCSD(T) has difficulty describing, the results are not nearly so accurate. Indeed, though CCSD(T) performs well for small H-F distances where the biradical character of the state is not as large, producing errors relative to full CI that are less than 0.8 millihartree, the performance of CCSD(T) quickly breaks down as $R_{\mathrm{H-F}}$ increases, with the errors relative to full CI growing from 2 millihartree at $R_{\mathrm{H-F}} = 1.875$ Å to 40 millihartree at $R_{\mathrm{H-F}} = 4.000$ Å. Thus, we see that the problems in the RHF/ROHF based CCSD(T) description of the singlet-triplet gap stem from the unbalanced treatment of the two states, where the triplet is described very well but the description of the singlet is problematic. Switching to an unrestricted UHF reference for the CCSD(T) calculations improves the situation, but the description of the singlet-triplet gap is still problematic. Though the gap approaches zero as the H-F distance is increased when the UHF-based CCSD(T) approach is used, it decays too fast as well as a result of the considerable mixing of singlet and triplet contributions in the spin-contaminated CCSD(T)/UHF calculation. Furthermore, the results for shorter H-F distances, for which the restricted CCSD(T) calculations were quite successful, are considerably worse now. Indeed, the 57 and 58 cm^{-1} errors in the restricted CCSD(T) results relative to full CI for $R_{\mathrm{H-F}} = 1.5$ and 1.625 Å increase to 1107 and 1232 cm^{-1}, respectively, when the UHF-based CCSD(T) approach is employed.

Table 3.5: A comparison of the total energies obtained with various electronic structure methods for the $X\ ^1\Sigma_g^+$ state of the linear, $D_{\infty h}$-symmetric $(HFH)^-$ system described by the 6-31G(d,p) basis set [194, 195], as a function of the H–F distance R_{H-F} (in Å). The full CI energies are given in hartree, while the remaining energies are given in millihartree relative to the corresponding full CI values.

		RHF Reference							UHF Reference		
R_{H-F}	Full CI	SCF	CCSD	CCSD(T)	CR-CC(2,3),A[a]	CR-CC(2,3),B[b]	CR-CC(2,3),C	CR-CC(2,3),D	SCF	CCSD	CCSD(T)
1.500	-100.589392	277.056	12.674	0.827	3.471	4.113	0.519	0.919	226.127	12.240	5.580
1.625	-100.584704	285.951	14.501	0.330	3.881	4.718	0.364	0.967	219.120	11.667	6.165
1.750	-100.577669	296.141	16.351	-0.594	4.178	5.257	0.050	0.927	212.251	10.319	6.116
1.875	-100.570151	307.260	18.045	-2.071	4.291	5.655	-0.456	0.768	206.070	8.554	5.408
2.000	-100.563055	318.849	19.398	-4.177	4.185	5.858	-1.141	0.491	200.817	6.789	4.354
2.125	-100.556686	330.443	20.261	-6.914	3.876	5.855	-1.926	0.143	196.486	5.276	3.292
2.250	-100.551083	341.671	20.546	-10.225	3.432	5.676	-2.680	-0.192	192.950	4.089	2.405
2.375	-100.546222	352.284	20.224	-14.003	2.944	5.379	-3.267	-0.432	190.056	3.208	1.739
2.500	-100.542059	362.150	19.328	-18.084	2.500	5.020	-3.584	-0.524	187.679	2.578	1.274
3.000	-100.531336	393.748	12.346	-32.964	1.558	3.423	-2.485	0.060	181.950	1.579	0.568
4.000	-100.526513	425.698	2.518	-40.115	0.585	0.879	-0.089	0.321	179.720	1.472	0.433

[a] Equivalent to the $CCSD(2)_T$ approach of [205], when the canonical Hartree Fock orbitals are employed.

[b] Equivalent, up to small details, to the triples part of the (2) correction of the CCSD(2) method of [206–209].

Table 3.6: A comparison of the total energies obtained with various electronic structure methods for the $A\ ^3\Sigma_u^+$ state of the linear, $D_{\infty h}$-symmetric $(HFH)^-$ system described by the 6-31G(d,p) basis set [194, 195], as a function of the H–F distance R_{H-F} (in Å). The full CI energies are given in hartree, while the remaining energies are given in millihartree relative to the corresponding full CI values.

	RHF Reference								UHF Reference		
$R_{H\text{-}F}$	Full CI	SCF	CCSD	CCSD(T)	CR-CC(2,3),A[a]	CR-CC(2,3),B[b]	CR-CC(2,3),C	CR-CC(2,3),D	SCF	CCSD	CCSD(T)
1.500	-100.545993	200.994	2.628	0.569	0.559	0.620	0.136	0.143	196.505	2.547	0.537
1.625	-100.552773	199.318	2.492	0.595	0.561	0.617	0.168	0.175	194.668	2.430	0.549
1.750	-100.555291	197.638	2.349	0.624	0.557	0.609	0.196	0.202	193.145	2.320	0.564
1.875	-100.555097	195.908	2.206	0.652	0.546	0.594	0.211	0.216	191.865	2.216	0.580
2.000	-100.553271	194.114	2.068	0.677	0.531	0.574	0.213	0.218	190.730	2.117	0.598
2.125	-100.550520	192.280	1.940	0.694	0.512	0.551	0.215	0.219	189.633	2.017	0.616
2.250	-100.547315	190.446	1.824	0.699	0.492	0.528	0.209	0.213	188.498	1.914	0.630
2.375	-100.543996	188.656	1.722	0.692	0.473	0.505	0.199	0.202	187.293	1.812	0.638
2.500	-100.540796	186.962	1.637	0.672	0.457	0.487	0.190	0.193	186.047	1.717	0.634
3.000	-100.531257	181.982	1.476	0.537	0.430	0.457	0.174	0.178	181.834	1.503	0.534
4.000	-100.526513	179.722	1.472	0.434	0.431	0.459	0.164	0.169	179.720	1.473	0.434

[a] Equivalent to the $CCSD(2)_T$ approach of [205], when the canonical Hartree Fock orbitals are employed.

[b] Equivalent, up to small details, to the triples part of the (2) correction of the CCSD(2) method of [206–209].

Moving on to variants A and B of CR-CC(2,3), which, as discussed in Section 3.1.2, are equivalent, up to small details, to the CCSD(2)$_{\mathrm{T}}$ approach of [205] and the triples part of the CCSD(2) method of [206–209], respectively, it is clear that they too have some difficulties describing this system, although they are not nearly as big as in the CCSD(T) case. The singlet-triplet gaps generated by the CR-CC(2,3),A and CR-CC(2,3),B methods decrease too fast, and, as a result, end up passing zero and becoming negative. Thus, for the larger geometries both approaches predict the wrong ordering of states. Eventually, a turnover occurs and the gap begins to increase again back towards zero, but this does not happen until the value of the gap reaches -230 and -718 cm^{-1} for the A and B variants, respectively. Furthermore, the discrepancies in the singlet-triplet gap energies relative to full CI remain substantial for all values of the H-F distance besides $R_{\mathrm{H-F}} = 4.0$ Å, with errors ranging from 247–822 cm^{-1} in the CR-CC(2,3),A case and 651–1164 cm^{-1} in the CR-CC(2,3),B case.

The full variant D of CR-CC(2,3), which, from now on, will simply be referred to as CR-CC(2,3), does not suffer from such difficulties in describing the $A\ ^3\Sigma_u^+ - X\ ^1\Sigma_g^+$ gap. Indeed, we see clearly from Table 3.4 that CR-CC(2,3) reproduces the systematic decay of the energy gap accurately. Though it does overshoot zero slightly at $R_{\mathrm{H-F}} = 4.0$ Å, it is only by the very small value of 33 cm^{-1}. Quantitatively, the errors in the CR-CC(2,3) results relative to full CI never excced the relatively small value of 174 cm^{-1} regardless of the value of the H-F distance. Looking at Tables 3.5 and 3.6, it is clear that this excellent description in the singlet-triplet gap is not a result of a fortuitous cancellation of errors. In fact, CR-CC(2,3) provides a highly accurate description of the total energies of both the $A\ ^3\Sigma_u^+$ and $X\ ^1\Sigma_g^+$ states, with errors relative to full CI ranging from 0.143 to 0.219 millihartree for the former, and from 0.060 to 0.967 millihartree in the latter. Thus, we see that of the various approximate triples methods that have similar computational costs and ease of use, only CR-

CC(2,3) (specifically the complete variant D of it) is capable of properly balancing the dynamical and nondynamical correlation effects in a way necessary to accurately describe the singlet-triplet gap in $(HFH)^-$ as a function of the H-F distance.

As a final example in this section, we consider the BN molecule. This is an extremely challenging biradical system that is seemingly characterized by a large contribution from connected quadruply excited clusters (i.e T_4 clusters). Indeed, a calculation [239] of the singlet-triplet separation using the full CCSDT approach with the cc-pVQZ basis set [178, 220] generated a value that was significantly larger than experiment. Given the challenging nature of this biradical and the large T_4 effects, the CR-CC(2,3) approach, which only accounts for the effects of up to T_3 clusters, is not expected to accurately describe the singlet-triplet gap in this system, and so a higher-order method such as CR-CC(2,4), which accounts for the combined effect of T_3 and T_4 clusters, is likely to be necessary to produce high quality results.

In order to study the role of T_4 clusters in the description of the adiabatic singlet-triplet gap of BN, T_e, as well as to examine the performance of the CR-CC(2,4) approach in an application involving a biradical system, CR-CC and reduced multi-reference (RMR) CC calculations for T_e were performed in collaboration with Dr. Xiangzhu Li and Professor Josef Paldus. The RMR CCSD approach [240] is based on solving the so-called externally corrected CCSD equations, which include all terms of the standard CCSD equations plus correction terms involving the most important (i.e. primary) T_3 and T_4 clusters [241, 242]. In the RMR CCSD scheme, the T_3 and T_4 amplitudes that enter the T_3 plus T_4 corrected CCSD equations are obtained from the cluster analysis of a modest-size MRCISD wave function. As a result of this procedure, the T_3 and T_4 clusters that are accounted for in this scheme primarily describe nondynamical correlations. In order to provide a more balanced description of the correlation effects, a standard noniterative perturbative correction due to the remaining triply excited clusters can be added to the RMR CCSD energy to account

for those T_3 components that describe the missing dynamical correlation effects (this correction has the same form as that of the standard CCSD(T) approach, except that one uses it only for the dynamical T_3 contributions, i.e. those T_3 contributions that are not captured by MRCISD). This gives rise to the RMR CCSD(T) scheme [243].

In this study, all calculations were performed using the cc-pVxZ (x = D, T, Q, 5) basis sets. As was the case for the methylene study discussed above, the h-functions were omitted from the cc-pV5Z basis set due to the restriction of the integral routines of GAMESS to g-functions. These results were then used to extrapolate the CBS value of the singlet-triplet gap, T_e(CBS), using the following formula (cf. Eq. (3.62)):

$$T_e(x) = T_e(\mathrm{CBS}) + Be^{-(x-1)} + Ce^{-(x-1)^2} (x = 2, 3, 4, 5), \tag{3.63}$$

where $T_e(x)$ is the value of the singlet-triplet gap as computed with the cc-pVxZ basis set. In addition to the adiabatic singlet-triplet gap T_e, the equilibrium bond lengths R_e and harmonic vibrational frequencies ω_e, as obtained with the cc-pV5Z basis, were computed as well. Due to the pilot nature of the CR-CC(2,4) code that we have developed, as mentioned in Section 3.1.3, only variant A of CR-CC(2,4) was used to perform the calculations. As discussed in Section 3.1.2, CR-CC(2,4),A is equivalent to the CCSD(2) approach of [205] when the canonical RHF orbitals are used. As a further consequence of the pilot implementation, the cc-pV5Z CR-CC(2,4) calculations could not be performed, and thus Eq. (3.63) was used to extrapolate this value from the cc-pVxZ, x = D, T, and Q, data. For the RMR CC calculations, two different model (or reference) spaces were considered for the underlying MRCI calculations, which lead to what will be referred to here as the A- and B-type RMR CC calculations. The $a\ ^1\Sigma^+$ state, which is the more multi-reference, and thus more difficult, state to calculate, is described by a model space spanned by four symmetry-adapted determinants in the A-type and B-type RMR CC calculations. The ground

$X\ ^3\Pi$ state uses a single reference determinant in the A-type RMR CC calculations while a two determinant model space is used in the B-type RMR CC calculations.

Table 3.7 gives the results of the various calculations. We begin by considering the results for R_e and ω_e. Both types of RMR CCSD calculations produce a bond length that is too short and a harmonic frequency that is too large relative to the experimental values for the $X\ ^3\Pi$ state. On the other hand, the CCSD(T) aproach, which neglects T_4 completely and primarily describes only the dynamical T_3 effects, produces R_e and ω_e values that are in very good agreement with experiment. Furthermore, the results of the CR-CC(2,3) and RMR CCSD(T),B calculations do not significantly differ from those of CCSD(T) in this case (recall that for the triplet state, RMR CCSD(T),A uses a single reference and thus is identical to CCSD(T)). These data suggest that the $X\ ^3\Pi$ state is primarly characterized by dynamical correlation effects with little contribution from connected quadruples, which makes sense given the single-reference nature of this state. The $a\ ^1\Sigma^+$ state, on the other hand, has a strongly multi-reference nature, and thus the emerging picture is quite a bit different. CCSD(T) produces R_e and ω_e values that are somewhat too short and too large, respectively, relative to experiment. The CR-CC(2,3) approach, which has already been shown to better balance the dynamical and nondynamical correlation effects, performs better but still has difficulty, producing a bond length that is slightly too long and an oscillator frequency that is somewhat too small. This indicates that accounting for both the dynamical and nondynamical triples is not enough to accurately describe the spectroscopic properties of the $a\ ^1\Sigma^+$ state, and the T_4 effects must also be included. This is supported by the RMR CCSD(T) results, which show good agreement with experiment for both the bond length and harmonic frequency.

Moving on to the $a\ ^1\Sigma^+ - X\ ^3\Pi$ gap, T_e, we see that the standard CCSD approach dramatically fails, producing errors relative to experiment of more 4000 cm^{-1}. Using the RMR CCSD scheme, which incorporates the primary T_3 and T_4 correlation effects

Table 3.7: Equilibrium bond lengths R_e (in Å) and harmonic frequencies ω_e (in cm^{-1}) for the lowest triplet and singlet states of BN, as obtained with cc-pV5Z basis set, and the adiabatic singlet-triplet splittings T_e (in cm^{-1}) as obtained with the cc-pVxZ (x = D, T, Q, and 5) basis sets, as well as the extrapolated CBS limit values.

	$X\,^3\Pi$		$a^1\Sigma$		T_e				
Method	R_e	ω_e	R_e	ω_e	x=D	x=T	x=Q	x=5	CBS
CCSD	1.317	1586	1.272	1705	4196	4391	4459	4471	4488 ± 6
RMR CCSD,A[a]	1.317	1586	1.273	1727	1259	1357	1450	1490	1512 ± 1
RMR CCSD,B[b]	1.321	1559	1.273	1727	1677	1756	1827	1863	1878 ± 3
CCSD(T)	1.329	1510	1.269	1739	-34	-92	-94	-87	-88 ± 3
CCSDT[c]	1.330	1512	1.277	1702	–	–	844	–	–
CR-CC(2,3)	1.329	1518	1.281	1686	404	666	817	919	946 ± 19
CR-CC(2,4),A[d]	–	–	–	–	253	289	323	(337)	(345)
RMR CCSD(T),A[a]	1.329	1510	1.277	1691	361	264	267	269	271 ± 1
RMR CCSD(T),B[b]	1.330	1501	1.277	1691	548	422	408	406	404 ± 1
Experiment	1.329[e]	1519.2[f]	1.275[g]	1705.4[g]			15–182[f]		
		1496[e]	1.274[h]	1700.9[f]			153[h]		

[a] A-Type RMR CC calculations were based on the (2,2) active space, which leads to a four-dimensional model space for the singlet and a one-dimensional model space for the triplet [244].

[b] B-Type RMR CC calculations utilized a four-dimensional model space for the singlet and a two-dimensional model space for the triplet [244].

[c] From [239] using the cc-pVQZ basis set.

[d] Due to the pilot nature of the CR-CC(2,4),A code used in this work, gradient calculations were not possible. As a result, the CR-CC(2,3) optimized geometries were employed. The cc-pV5Z and CBS values for the singlet-triplet gap are extrapolated values obtained using Eq. (3.63).

[e] r_0 and ω_0 values from [245].

[f] From [246].

[g] From [247].

[h] From [248].

captured by MRCISD, does significantly improve the results, reducing the error in the calculated gap by a factor of more than two. Unfortunately, the error relative to experiment is still sizable, pointing to the importance of dynamical connected triples in the description of the singlet-triplet gap of BN missing in the RMR CCSD calculations. CCSD(T), on the other hand, produces negative values for T_e, meaning that it gives the wrong ordering of states. This results from CCSD(T) accurately treating the single-reference triplet state, while overshooting the energy of the multi-reference singlet state. The CR-CC(2,3) method produces the proper ordering of states as well an error reduction compared to RMR CCSD. In fact, for the cc-pVDZ basis set, the results look promising and are in reasonable agreement with the CR-CC(2,4) and RMR CCSD(T) results. Unfortunately, the error in the calculated gap increases as the size of the basis set increases, and so both the larger basis set and CBS CR-CC(2,3) values show sizable errors relative to experiment. It is important to note, however, that for the cc-pVQZ basis set, the CR-CC(2,3) value of T_e is in excellent agreement with the full CCSDT value of [239], differing by less than 30 cm^{-1}. This suggests that CR-CC(2,3) is accurately and properly describing the T_3 effects, and is unable to provide a reasonable description of the gap due to missing quadruply excited clusters.

The above data all suggests that both a properly balanced description of dynamical and nondynamical triples as well as the inclusion of connected quadruply excited clusters is necessary to accurately describe the singlet-triplet gap of BN. Table 3.7 reveals that this is indeed the case, as both the CR-CC(2,4) and RMR CCSD(T) approaches produce significantly better values for T_e, which are in good, although not perfect, agreement with the available experimental data, which are not well-established either, due to the smallness of the $a\ ^1\Sigma^+ - X\ ^3\Pi$ gap. Additionally it is encouraging to see that these two completely different methods of including the effects of T_3 and T_4 clusters in the CC calculations are in very good agreement with

each other.

3.2.3 Excitation Energies of C_2N, CNC, N_3, and NCO

As a final example of the performance of the left-eigenstate CR-CC/CR-EOMCC schemes in studies of open-shell systems, we once again examine the low-lying states of C_2N, CNC, N_3, and NCO, which were studied using the active-space EA-EOMCCSDt and IP-EOMCCSDt approaches in Section 2.2.3. Not only do these representative radical systems provide an interesting and informative test case for the open-shell CR-EOMCC(2,3) implementation, but they also allow us to directly compare the performance of both of the new approaches for studying open-shell systems developed in this research. To that end, the computational details, including basis set and equilibrium geometries used, are the same as those defining the calculations of Section 2.2.3 and will not be repeated here.

Table 3.8 shows the results of the calculations for CNC and C_2N. The EA-EOMCC results discussed in detail in Section 2.2.3 are also included to facilitate comparisons with the CR-EOMCC(2,3) data. One of the first things apparent from these results is that the basic EOMCCSD approach performs reasonably well for the $A\,^2\Delta_u$ state of CNC and the $A\,^2\Delta$ state of C_2N, producing results that are in reasonable agreement with both experiment and the high quality EA-EOMCCSD(3p-2h) results. Indeed, the difference between the EOMCCSD and EA-EOMCCSD(3p-2h) results are only 0.186 and 0.136 eV for the $A\,^2\Delta_u$ state of CNC and the $A\,^2\Delta$ state of C_2N, respectively. Furthermore, it is clear that including the effects of triples has little impact on these states, as all four variants of CR-EOMCC(2,3) provide similar values for the excitation energies that do not differ substantially from those of EOMCCSD. This is not too surprising given the relatively simple structure of these two states. Indeed, the so-called reduced excitation level (REL) values are 1.099 and 1.090 for the $A\,^2\Delta_u$ state of CNC and the $A\,^2\Delta$ state of C_2N, respectively. The REL diagnostic, intro-

duced in [132], is a quantitative measure of the nature of an excited state relative to the corresponding ground state, with values close to 1.0 indicating the state is dominated by single excitations and values close to 2.0 indicate domination by double excitations. It is well known that EOMCCSD performs well for states dominated by single excitations, and so it is not surprising to see the reasonable performance of this scheme for these two states.

The situation is different for the remaining states of CNC and C_2N, however. Indeed, the REL values characterizing the $B\ ^2\Sigma_u^+$ state of CNC, and the $B\ ^2\Sigma^-$ and $C\ ^2\Sigma^+$ states of C_2N are 1.979, 1.856, and 1.897, respectively, indicating that all of these states are dominated by two-electron transistions. Not surprisingly, given this observation, EOMCCSD fails to accurately describe the excitation energies, producing errors of 2.7 – 3.0 eV relative to experiment. When variant A of CR-EOMCC(2,3), which, as mentioned in Section 3.1.2, is equivalent to the EOM-CC(2)PT(2) scheme of [203,204] when the canonical RHF orbitals are employed, is used to calculate the excitation energies for the above three states, the errors are reduced but are still substantial. Indeed, the discrepancies with experiment are 1.117, 1.239, and 1.435 eV for the $B\ ^2\Sigma_u^+$ state of CNC, and the $B\ ^2\Sigma^-$ and $C\ ^2\Sigma^+$ states of C_2N, respectively. Variant B, which, as a reminder, replaces the orbital energies of the Møller-Plesset-like denominators of CR-EOMCC(2,3),A with the one-body diagonal elements of the similarity-transformed Hamiltonian (the latter essentially corresponding to 'dressed' orbital energies), shows essentially equivalent performance.

In contrast to variants A and B, the full variant D of CR-EOMCC(2,3) produces accurate results for the $B\ ^2\Sigma_u^+$ state of CNC, and the $B\ ^2\Sigma^-$ and $C\ ^2\Sigma^+$ states of C_2N. Indeed, the errors relative to experiment for the $B\ ^2\Sigma_u^+$ state of CNC, and the $B\ ^2\Sigma^-$ and $C\ ^2\Sigma^+$ states of C_2N are 0.284, 0.331, and 0.518 eV, respectively, which is a substantial improvement over the results of variants A and B (not to mention, EOMCCSD). Furthermore, the CR-EOMCC(2,3),D excitation

Table 3.8: Adiabatic excitation energies (eV) and reduced excitation level (REL) values of the low-lying valence excited states of CNC and C_2N.[a]

			EA-EOM				CR-EOMCC(2,3)				
Molecule	State	REL	CCSD(2p-1h)	CCSD(3p-2h)	CCSDt[b]	EOMCCSD	A	B	C	D	Experiment[c]
CNC	$A\,^2\Delta_u$	1.099	7.206	4.105	4.085	4.291	4.400	4.397	4.395	4.395	3.761
	$B\,^2\Sigma_u^+$	1.979	7.639	4.718	4.704	7.123	5.432	5.595	4.582	4.599	4.315
C_2N	$A\,^2\Delta$	1.090	6.190	3.055	3.028	3.191	3.377	3.368	3.389	3.388	2.636
	$B\,^2\Sigma^-$	1.856	7.856	3.677	3.648	5.514	4.018	4.160	3.091	3.110	2.779
	$C\,^2\Sigma^+$	1.897	6.722	3.809	3.788	6.358	4.741	4.901	3.799	3.824	3.306

[a] Linear geometries are used with optimized bond lengths obtained with the analytic gradients of the EA SAC-CI(3p-2h) approach. These bond lengths are the same as those presented in Table 2.11.
[b] The active space consisted of the four lowest unoccupied molecular orbitals of CNC^+ or C_2N^+.
[c] Taken from [202].

Table 3.9: Adiabatic excitation energies (eV) and reduced excitation level (REL) values of the low-lying valence excited states of N_3 and NCO.[a]

			IP-EOM				CR-EOMCC(2,3)				
Molecule	State	REL	CCSD($2h$-$1p$)	CCSD($3h$-$2p$)	CCSDt[b]	EOMCCSD	A	B	C	D	Experiment[c]
N_3	$B\,^2\Sigma_u^+$	1.087	4.640	4.598	4.729	4.804	4.948	4.941	4.971	4.968	4.597
NCO	$A\,^2\Sigma^+$	1.060	2.900	2.864	3.078	2.931	3.123	3.111	3.161	3.158	2.821
	$B\,^2\Pi$	1.073	4.199	3.911	3.904	4.053	4.093	4.106	4.061	4.068	3.937

[a] Linear geometries are used with optimized bond lengths obtained with the analytic gradients of the EA SAC-CI($3p$-$2h$) approach. These bond lengths are the same as those presented in Table 2.11.
[b] The active space consisted of the two highest unoccupied molecular orbitals of N_3^- or NCO^-.
[c] Taken from [202].

energies agree very well with the high-level EA-EOMCCSD(3*p*-2*h*) results. Indeed, for the $B\ ^2\Sigma_u^+$ state of CNC and the $C\ ^2\Sigma^+$ state of C_2N, the discrepancies between the CR-EOMCC(2,3),D and EA-EOMCCSD(3*p*-2*h*) data are only 0.119 and 0.015 eV, respectively. For the $B\ ^2\Sigma^-$ state, which poses some difficulty for the EA-EOMCCSD(3*p*-2*h*) scheme and likely requires 4*p*-3*h* excitations to properly describe it, the discrepancy between CR-EOMCC(2,3),D and EA-EOMCCSD(3*p*-2*h*) is somewhat larger, with CR-EOMCC(2,3),D improving the result by 0.567 eV, which is a remarkable improvement considering the black-box nature of the CR-EOMCC(2,3) theory.

Turning to the low-lying states of N_3 and NCO, Table 3.9 reveals that all three states included in it are dominated by single excitations. Thus, not surprisingly, the basic EOMCCSD approach provides accurate results for all of these states, with errors relative to experiment ranging from 0.110 to 0.207 eV. As observed earlier for the states of CNC and C_2N dominated by singles, all four variants of CR-EOMCC(2,3) provide essentially equivalent results, with differences among the results of less than 0.05 eV, and with small changes in excitation energies when going from EOMCCSD to CR-EOMCC(2,3). Finally, it should be noted that the CR-EOMCC(2,3) results are in good agreement with those of the high-level IP-EOMCCSD(3*h*-2*p*) calculations, with discrepancies of approximately 0.1 – 0.4 eV between the CR-EOMCC(2,3) and IP-EOMCCSD(3*h*-2*p*) data.

Thus, it is clear that the excited-state CR-EOMCC(2,3) approach performs very well for the low-lying states of open-shell systems, with the capability to produce results of similar quality as that provided by the high-level EA-EOMCCSD(3*p*-2*h*) and IP-EOMCCSD(3*h*-2*p*) approaches discussed in Chapter 2. More specifically, for states dominated by single-excitations, all variants of CR-EOMCC(2,3) perform equally well, and offer only minor improvements over the already satisfactory EOMCCSD results. For the more challenging states dominated by double excitations, only

the more complete variants C and D are able to successfully describe the excitation energies, providing results of the same quality as those of EA-EOMCCSD($3p$-$2h$) and IP-EOMCCSD($3h$-$2p$). From these results it is clear that the full CR-EOMCC(2,3) scheme, which has costs on the order of the popular ground-state CCSD(T) scheme, is capable of providing high-quality results for both the simple singly excited and more complicated doubly excited low-lying states of open-shell systems, and thus is a promising approach for studying the excitation spectra of radicals.

Chapter 4

Coupled-Cluster Calculations for Nuclei

In this chapter, the application of various CC approaches, in particular those detailed in Chapters 2 and 3, to the study of nuclear structure is discussed. In Section 4.1, a description of the main elements associated with performing CC calculations for nuclei, particularly those related to how nuclear CC calculations differ from molecular CC calculations, are presented. The rest of the chapter presents and discusses the results of some representative nuclear CC calculations performed as part of this research.

4.1 Details of Coupled-Cluster Calculations for Nuclei

Despite the many differences between nuclei and molecules, it turns out that the underlying physics describing the motion of the nucleons and electrons, all of which are spin 1/2 fermions, within the nuclear and molecular potentials, respectively, is essentially identical. Indeed, the time-independent, many-particle Schrödinger equations

for these two types of physical systems only differ in the form of the potential. Since the formulation of various CC methods in quantum chemistry makes virtually no assumptions about the form of the potential (the major exception will be discussed in detail below), they can be applied to calculations of nuclear structure, at least for Hamiltonians with pairwise nucleon-nucleon interactions, without any theoretical reformulation. For example, the explicit equations defining the EA-EOMCCSDt, IP-EOMCCSDt, and CR-CC(2,3)/CR-EOMCC(2,3) approaches, presented in Sections 2.1.3 and 3.1.3, utilize the integrals $v_{pq}^{rs} = \langle pq|v|rs\rangle - \langle pq|v|sr\rangle$, but, besides the requirement that integrals are real and not complex, make no assumptions regarding the functional form of v nor the values of v_{pq}^{rs}. Thus, the CC methods developed in quantum chemistry require no substantial theoretical reformulation in order to be applied to nuclear physics (though some changes in the details of the implementation of the methods may be necessary). The fundamental difference between running nuclear CC calculations and molecular CC calculations is the form of the operator v, and thus the resulting values of the matrix elements v_{pq}^{rs}, defining the second-quantized form of the Hamiltonian, that enter the equations defining the CC approximation of choice. Having stated all of the above, there are some complications in using the nucleon-nucleon potentials in CC calculations that may need out attention. We discuss them now.

Since it is the electrostatic force that governs the interaction between electrons, as well as their motion in the field of the nuclei, Coulomb's law defines the potential in nonrelativistic molecular calculations. The interactions between nucleons, on the other hand, are described primarily by the strong force, with small contribution from the Coulomb force through the mutual repulsion of protons. Unfortunately, there is no Coulomb's law analog known for the strong force, and as a result generating the Hamiltonian for nuclear calculations is not as simple or straightforward as in quantum chemistry. Because of this, a great deal of research has gone toward the development

of realistic nucleon-nucleon interactions, and, as a result, there are a variety of potentials to choose from, such as the well-known Argonne V_{18} [249] and CD-Bonn [250] potentials or the more recent interactions generated within the framework of chiral effective field theory [251, 252], such as Idaho-A or N^3LO [253, 254] to name a few. Because of this choice of interactions, the nuclear CC calculations performed as part of this work, and discussed in this dissertation, were based on several different interactions, both semi-empirical and *ab initio*, in order to gauge how the performance of the CC methods varies with regard to the choice of potential.

Besides the lack of an exact analytical expression for the nucleon-nucleon interaction, there is yet another complication that arises with this potential. Whereas electrons are point particles, and so the resulting interaction between them is two-body at most, nucleons have an underlying structure in terms of quarks. As a result, the interactions between nucleons are effective and not fundamental, and as such can be characterized by three-body and higher many-body components (to find an analogy in chemistry, the description of intermolecular forces that originate from the underlying electron-electron, electron-nucleus, and nucleus-nucleus interactions is characterized by a similar situation). This issue is important when attempting to apply the CC methods developed in quantum chemistry to nuclear structure theory because, although the quantum chemistry CC formulations make *virtually* no assumptions on the form of the potential, they do in fact assume that it is at most two-body in nature. There is nothing intrinsic in the CC theory that requires this assumption, and indeed a formulation of the basic CCSD approach based on three-body Hamiltonians has recently been derived and implemented [171]. However, the resulting calculations are considerably more expensive than those based on a two-body Hamiltonian. Furthermore, if one wants to explore more advanced methods, such as those described in this dissertation that have already been derived and implemented for two-body Hamiltonians, they would have to be rederived and re-implemented, with the result-

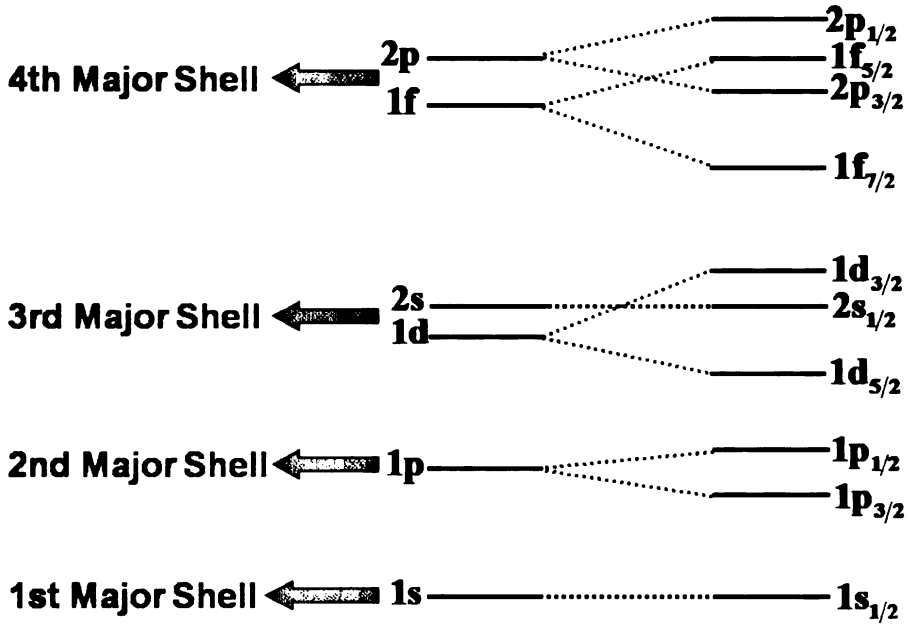

Figure 4.1: Pictorial illustration of the nuclear shell structure.

ing equations being considerably more complicated than their two-body Hamiltonian counterparts, before they could be used to study nuclei. Of course, it is possible to avoid these issues by simply restricting the calculations to two-body Hamiltonians only, which allows for a direct application of the quantum chemistry CC formulations to nuclear calculations, which is the route chosen for this research. In fact, two of the goals of this work are to explore the effect of neglecting three-body components of the Hamiltonian as well as the possibility of generating an accurate description of these effects within an effective two-body interaction. The latter makes a lot of sense since, as shown in [171], once the Hamiltonian is written in the normal-ordered form, as is usually done in CC considerations any way, the "true" three-body interactions play a negligible role. The main role of the three-body interactions is to modify the two-body interactions through the effective density-dependent terms that originate from the normal-ordered form of the Hamiltonian in a natural way, providing additional justification for focusing on effective pairwise potentials.

A final element of performing nuclear CC calculations that should be discussed before considering some examples is that of the basis set. The structure of the nuclear Hamiltonian written in internal coordinates is, in part, reminiscent of a harmonic oscillator potential and, as such, single-particle, three-dimensional harmonic oscillator functions are generally used as the basic one-nucleon basis functions. A key parameter for defining such a basis is the energy gap between adjacent oscillator energy levels, $\hbar\omega$, which is generally chosen such that it minimizes the ground-state energy of interest. These functions can be used directly in the CC or other correlated calculations, or a mean-field calculation, such as Hartree-Fock, can be performed first to optimize the nuclear orbitals represented as linear combinations of harmonic oscillator basis functions. As is the case for atoms and molecules, these nuclear orbitals form a shell structure when arranged according to energy. The first four shells within this structure are illustrated in Figure 4.1. As can be seen, the shell structure is closer to that of atoms than of molecules. However, unlike atoms, the magnitude of spin-orbit splitting is very large, and so even for light nuclei it must be accounted for. Thus the energy level splittings on the right-hand side of Figure 4.1 are the ones that should be used in calculations. Both protons and neutrons each have an identical energy level diagram, and so the number of basis functions associated with a given energy level is $2 * (2j + 1)$, where j is the total angular momentum for the spin-orbit coupled function. Generally, when building a basis set for use in a CC or other type of correlated calculation, basis functions are added entire shells at a time, and so the number of major shells is used to indicate the size of the basis. Unfortunately, due to the hard core of the nucleon-nucleon potential, the convergence of quantum calculations with respect to the number of major shells is very slow if the bare interaction is used, and so extremely large basis sets are needed to produce accurate results in such calculations. In order to improve the convergence with the size of the basis set, and thus reduce the corresponding computational cost, the Hamiltonian is generally

renormalized in order to soften the potential. Several of the calculations performed in this and related work [157–167] made use of the no-core G-matrix procedure described in [255,256], whereas our most recent calculations for ^{16}O [169,170] made use of the renormalized two-body interaction that accounts, to some extent, for three-body interactions, called V_{UCOM} [257–260]. The effective semi-empirical Hamiltonians, such as those used in our CC calculations for heavy nuclei [167,168], are generally soft and need no renormalization.

Last, but not least, we must remember that unlike atoms or molecules, that consist of electrons moving in a fairly rigid framework of nuclei creating an external potential, nuclei are self-bound systems, which introduces a new layer of complexity absent in electronic structure calculations. The exact nuclear wave function factorizes into the intrinsic part and the center-of-mass part, but this is no longer true for approximate methods, such as those based on CC theory. This issue becomes particularly dramatic for light nuclei where one can easily produce center-of-mass contaminated results, although our recent study shows that the issue does not automatically disappear when heavier nuclei are examined [170]. The issue of center-of-mass contamination is not discussed here and we refer the reader to the literature, including some of our recent work [169,170]. Needless to say, we will mention our ways of addressing the issue, as appropriate, in the next sections, without going into details.

It is virtually impossible to describe all of our nuclear CC applications to date [157–171]. Thus, in the following section we focus on a few representative examples only.

4.2 Low-lying States of ^{16}O and the Surrounding Valence Systems

One of this project's first applications of CC approaches to nuclear physics was the calculation of the ground and first excited $J = 3^-$ states of ^{16}O [157, 161–164]. Two different Hamiltonians, both derived from chiral effective field theory, were used in these calculations, namely Idaho-A and N^{3}LO [253, 254]. The former includes up to chiral-order three diagrams, while the latter includes up to chiral-order four diagrams as well as charge-symmetry and charge-independence breaking terms. Additionally, the proton-proton Coulomb repulsion is included in the N^{3}LO interaction [253, 254]. In order to soften the potential, the Idaho-A and N^{3}LO Hamiltonians were renormalized using the no-core G-matrix approach [255, 256]. Each of the resulting renormalized effective two-body Hamiltonians was subsequently corrected by adding the $\beta H_{\rm CM}$ term to it, where $H_{\rm CM}$ is the center-of-mass Hamiltonian and β is the Lagrange multiplier that are optimized to minimize that center-of-mass contaminations. Finally, once the final form of the renormalized, center-of-mass-corrected Hamiltonian was generated, we determined the relevant one- and two-body matrix elements, f_p^q and v_{pq}^{rs}, in the basis set consisting of the standard harmonic oscillator single-particle functions (i.e. no mean-field optimization of orbitals was performed). We refer the reader to [160–164] for the details of the procedure used to define the final form of the Hamiltonian from the Idaho-A and N^{3}LO interactions that was used in the CC calculations ^{16}O.

The CC methods used in the calculations for ^{16}O reported in [157, 161–164] included the basic CCSD/EOMCCSD approach, for which basis sets with up to 8 major oscillator shells (480 single-particle functions) were used for the ground state and with up to 7 major shells (336 single-particle functions) for the 3^- state, and the completely renormalized CR-CCSD(T)/CR-EOMCCSD(T) scheme [120, 122, 123, 126–128, 131,

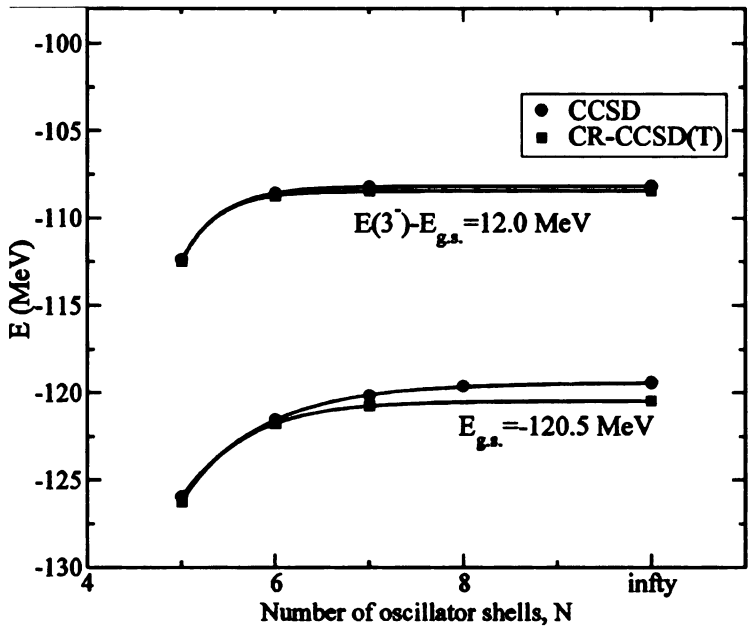

Figure 4.2: The CC energies of the ground-state (g.s.) and first-excited 3^- state of ^{16}O as functions of the number of major oscillator shells N obtained with the Idaho-A interaction.

132], for which basis sets with up to 7 oscillator shells were used for both states. The latter scheme is essentially an older variant of CR-CC(2,3)/CR-EOMCC(2,3) discussed in Chapter 3 based on the original formulation of the MMCC theory [120–123, 126–129] (as opposed to the biorthogonal formulation CR-CC(2,3)/CR-EOMCC(2,3) is based on). For the calculations with 7 and 8 major oscillator shells, $\hbar\omega$ was set at 11 MeV, to minimize the CCSD energy. It should be noted, however, that the results were virtually independent of the value of $\hbar\omega$, when the larger basis sets were employed, which is a typical behavior since the dependence of the results on the basis set parameter $\hbar\omega$ disappears in the CBS limit.

Figure 4.2 shows the CCSD/EOMCCSD and CR-CCSD(T)/CR-EOMCCSD(T) energies as functions of the number of major oscillator shells, N, for both the ground and excited 3^- states. The symbols correspond to the actual CC energies, while the

lines were generated by fitting the energies to the following formula:

$$E(N) = E_{\infty} + ae^{(-bN)}, \tag{4.1}$$

where the extrapolated infinite basis set (quantum chemists' CBS) energy, E_{∞}, as well as the parameters a and b are determined by the fit. It is clear from Figure 4.2 that this is an excellent fit to the calculated energies, and as such the extrapolated CC energies should be an accurate representation of the infinite basis set results.

For the ground-state case, the CCSD scheme generates an extrapolated binding energy of -7.46 MeV/nucleon with the Idaho-A interaction, whereas the extrapolated CR-CCSD(T) binding energy is -7.53 MeV/nucleon. It is immediately clear that the inclusion of the effects of triply excited clusters has very little effect on the result, changing the binding energy by only 0.9 %. It is also clear from Figure 4.2 that the discrepancy between the two results is consistently small for all basis sets for which both calculations were performed. This small effect due to connected triply excited clusters would suggest that all of the important correlation effects are already included at the CCSD and CCSD(T) levels, and that the inclusion of higher-order clusters would have little impact on the resulting binding energies. This is not too surprising since ^{16}O is a strongly closed-shell nucleus, or "doubly magic" system as it is called in nuclear physics, and so the role of T_3 and higher-order clusters cannot be significant. Before comparing the above CCSD and CR-CCSD(T) results to experiment, however, we must remember that, as mentioned above, the Idaho-A interaction used in these calculations does not include the effects of Coulomb repulsion of the protons. The effect of Coulomb repulsion is known to add approximately 0.7 MeV/nucleon to the binding energy, and so adding this value to the converged CR-CCSD(T) binding energy obtained with Idaho-A gives an approximate final CR-CCSD(T) binding energy of -6.8 MeV/nucleon. As shown in [164], this value is in

excellent agreement with the extrapolated N^{3}LO CR-CCSD(T) binding energy of -7.0 MeV/nucleon (the N^{3}LO interaction includes the Coulomb repulsion). Comparing these results with the experimental value of -8.0 MeV/nucleon, we see that the CC calculations underbind ^{16}O by about 1.0 MeV/nucleon. This result immediately begs the question of where this discrepancy comes from. Indeed, as illustrated by Figure 4.2, the above results appear to be fully converged with the basis set. Furthermore, based on the above discussion, it is safe to conclude that the CR-CCSD(T) method has saturated the particle correlations describing this system. Thus, it would appear, at least at first glance, that our CC calculations for ^{16}O not missing any fundamental physics, and should reproduce the experimental result with much better accuracy. However, we must not forget that the Hamiltonians used in our calculations included only up to two-body interactions, and all three-body and higher interactions and their effect on pairwise interactions were neglected. Thus, we conclude that the three-body interactions in the Hamiltonian neglected in our calculations should provide an additional 1.0 MeV/nucleon in the binding for the ^{16}O nucleus. We will return to this interesting aspect of our calculations in a later part of this section.

Turning to the 3^- state, the basic EOMCCSD approach provides an extrapolated excitation energy of 11.3 MeV with Idaho-A, while the extrapolated Idaho-A CR-EOMCCSD(T) excitation energy is $\sim$ 12.0 MeV. N^{3}LO produces essentially equivalent results. This 3^- state is thought to be dominated by single (i.e. $1p$-$1h$) excitations [261] (specifically, a single excitation from the $1p_{1/2}$ orbital to the $1d_{5/2}$ orbital; see Figure 4.1). As discussed in Chapter 3, it is the experience of quantum chemistry that even the basic EOMCCSD approach is capable of providing an accurate description of states with such a structure, and the incorporation of T_3 effects has little impact on the overall result if the Hamiltonian contains two-body interactions only (as would be the case in quantum chemistry). It is clear from Figure 4.2 that the inclusion of triply excited clusters through CR-EOMCCSD(T) causes only a slight

change in the excitation energy of the 3^- state, in agreement with quantum-chemist intuition. The experience of quantum chemistry is telling us then that it is safe to conclude that CR-EOMCCSD(T) provides an essentially exact solution (from the point-of-view of many-body correlation effects) for the 3^- state of ^{16}O. The creates a real puzzle, since our converged EOMCCSD and CR-EOMCCSD(T) results for the excitation energy of the 3^- state significantly differ from the experimental excitation energy of 6.12 MeV. Once again, we believe that the discrepancy between CC and experiment is due to missing three-body forces in the Hamiltonian.

In order to expand the above study to include open-shell nuclei, a number of CC calculations were performed for the valence systems surrounding ^{16}O, namely ^{15}O, ^{15}N, ^{17}O, and ^{17}F [165]. Given that these systems are all one-nucleon away from ^{16}O, which is a closed-shell system, they are excellent candidates for EA-type and IP-type EOMCC calculations. Of course, the names 'electron-attached' and 'ionized' make no sense in the context of nuclear physics, so we will describe the nuclear analogs of the EA- and IP-EOMCC methods as the particle-attached (PA) and particle-removed (PR) EOMCC schemes. Thus, we performed the basic PA-EOMCCSD(2p-1h) calculations for ^{17}O and ^{17}F and the PR-EOMCCSD(2h-1p) calculations for ^{15}O and ^{15}N. We used the chiral N^{3}LO interaction from the above ^{16}O study as well the phenomenological Argonne V_{18} and CD-Bonn potential mentioned in Section 4.1. For ^{15}O and ^{15}N, the ground and first-excited $(3/2)^-_1$ states were computed, while for ^{17}O and ^{17}F, the ground, $(3/2)^+_1$ and $(1/2)^+_1$ states were calculated. As in the ^{16}O case, a basis of harmonic oscillator states was utilized. Although the calculations reported in [165] include basis sets with various numbers of oscillator shells, in this discussion we focus on the largest $N = 8$ basis set only. Furthermore, because there is almost no dependence of the results on the value of $\hbar\omega$ when the large $N = 8$ basis set is employed, we focus on the results with $\hbar\omega = 11$ MeV for N^{3}LO and CD-Bonn, and $\hbar\omega = 10$ MeV for Argonne V_{18}. The discussion of the results for other $\hbar\omega$ values

Table 4.1: A comparison of the binding energies per particle for ^{15}O and ^{15}N (the PR-EOMCCSD(2h-1p) values), ^{16}O (the CCSD values), and ^{17}O and ^{17}F (the PA-EOMCCSD(2p-1h) values), obtained with the N^{3}LO [253,254], CD-Bonn [250], and V_{18} [249] potentials, and eight major oscillator shells, with the experimental data taken from [262]. All entries are in MeV. For the CD-Bonn and N^{3}LO interactions, we used $\hbar\omega = 11$ MeV. For V_{18}, we used $\hbar\omega = 10$ MeV.

	Interaction			
Nucleus	N^{3}LO	CD-Bonn	V_{18}	Expt
^{15}O	6.643	7.584	5.246	7.464
^{15}N	6.824	7.751	5.414	7.699
^{16}O	7.406	8.327	5.897	7.976
^{17}O	7.150	8.032	5.617	7.751
^{17}F	6.987	7.879	5.462	7.542

and basis sets with $N \leq 7$ can be found in [165].

Table 4.1 gives PA-EOMCCSD(2p-1h) and PR-EOMCCSD(2h-2p) results for the binding energies per particle for ^{15}O, ^{15}N, ^{17}O and ^{17}F. Focusing on the results obtained with the N^{3}LO interaction, we see that the PA-EOMCCSD(2p-1h) and PR-EOMCCSD(2h-1p) energies differ from the experimental values by roughly 0.5 to 0.8 MeV/nucleon. One potential source for this discrepancy could be that the most basic PA-EOMCCSD(2p-1h) and PR-EOMCCSD(2h-1p) schemes do not include all of the relevant correlation effects necessary to describe the ground states of these nuclei. In particular, they lack the 3p-2h/3h-2p components of the particle-attaching and particle-removing operators, which, as discussed in Chapter 2, are in some cases essential for obtaining accurate results for the low-lying states of open-shell systems. However, it is known that the ground states of all four of these valence nuclei are dominated by 1p (^{17}O, ^{17}F) or 1h (^{15}O, ^{15}N) transitions relative to the ground-state of ^{16}O. As illustrated in Section 2.2.3 for molecular applications, the basic PA-EOMCCSD(2p-1h) and PR-EOMCCSD(2h-1p) schemes perform quite well for states dominated by 1p or 1h transitions, and improvements resulting from using the higher-order PA-EOMCCSD(3p-2h) and PR-EOMCCSD(3h-2p) approaches was minimal

in those situations. Thus, it is safe to conclude that the higher-order components of the cluster, particle-attaching, and particle-removing operators play a relatively small role in the structure of the ground states of ^{15}O, ^{15}N, ^{17}O and ^{17}F, and so PA-EOMCCSD(2p-1h) and PR-EOMCCSD(2h-1p) accurately describe the relevant many-body correlations. As a result of this analysis, we once again conclude that the discrepancy with experiment is likely due to the inadequate treatment of the nucleon-nucleon interaction resulting from neglecting three-body forces. In fact, the 0.5 to 0.8 MeV/nucleon differences between the PA-EOMCCSD(2p-1h)/PR-EOMCCSD(2h-1p) results and experiment for the valence nuclei are in good agreement with the 0.6 or 1.0 MeV/nucleon differences between the 8-shell N^{3}LO CCSD (Table 4.1) or infinite-basis set CR-CCSD(T) binding energies, respectively, and experiment, observed earlier. This relatively consistent discrepancy with experiment across all five nuclei around ^{16}O indicates that the role of three-body forces is approximately the same in each case.

Turning to a comparison of the results obtained with different potentials, Table 4.1 shows that the binding energies obtained with the N^{3}LO and CD-Bonn interactions, both of which are based on a nonlocal model for the interaction defined in momentum space, are in reasonable agreement with each other, although the binding is greater with the CD-Bonn potential. On the other hand, the results obtained with the Argonne V_{18} potential, which is based on a local parameterization in coordinate space, shows a much larger deviation, underbinding the nuclei by approximately 1.4 to 1.5 MeV/nucleon relative to N^{3}LO. Since the above arguments regarding the convergence of the CC calculations and the potential role three-body interactions apply to a lesser or larger extent, to any interaction, our calculations strongly suggest that the role of three-body forces depends on what interaction model is used, and so every potential needs its own unique three-body interaction. This is an important finding, since it has been a tendency of the nuclear physics community for quite some time to

add some form of three-body interaction to some form of two-body interaction in the Hamiltonian without realizing the possible inconsistency in such an ad hoc treatment.

Before moving on to an analysis of the CC results for the low-lying excited states of the ^{15}O, ^{15}N, ^{17}O and ^{17}F nuclei, it is useful at this point to return to the discussion of the potential role of three-body interactions in the case of the lowest excited state of ^{16}O of the 3^- symmetry. As mentioned above, a zero-order description of this state is that of a $1p$-$1h$ excitation from the $1p_{1/2}$ orbital to the $1d_{5/2}$ orbital. The approximate energy associated with such an excitation, relative to the ground state of ^{16}O, can easily be estimated using the formulas

$$\begin{aligned} \Delta\epsilon_\pi &= \epsilon_\pi(1d_{5/2}) - \epsilon_\pi(1p_{1/2}) \\ &= [\mathrm{BE}(^{16}\mathrm{O}) - \mathrm{BE}(^{17}\mathrm{F})] + [\mathrm{BE}(^{16}\mathrm{O}) - \mathrm{BE}(^{15}\mathrm{N})] \end{aligned} \tag{4.2}$$

and

$$\begin{aligned} \Delta\epsilon_\nu &= \epsilon_\nu(1d_{5/2}) - \epsilon_\nu(1p_{1/2}) \\ &= [\mathrm{BE}(^{16}\mathrm{O}) - \mathrm{BE}(^{17}\mathrm{O})] + [\mathrm{BE}(^{16}\mathrm{O}) - \mathrm{BE}(^{15}\mathrm{O})] \end{aligned} \tag{4.3}$$

for the proton (π) and neutron (ν) excitations, respectively, where BE represents the relevant total binding energy for the labeled nucleus. Using the results presented in Table 4.1, Eqs. (4.2) and (4.3) can be used to calculate both CC and experimental values for $\Delta\epsilon_\pi$ and $\Delta\epsilon_\nu$, which give a zeroth-order estimate for the excitation energy of the 3^- state of ^{16}O. The resulting zeroth-order CC values are $\Delta\epsilon_\pi = 15.846$ MeV and $\Delta\epsilon_\nu = 15.789$ MeV, whereas the corresponding experimentally derived values are $\Delta\epsilon_\pi = 11.526$ MeV and $\Delta\epsilon_\nu = 11.521$ MeV. Thus, regardless of whether a proton or a neutron is excited from the $1p_{1/2}$ orbital to the $1d_{5/2}$ orbital, there is a discrepancy between the zeroth-order CC and experimental estimates of the 3^- excitation energy of about 4.3 MeV, which is a large fraction of the missing 6 MeV

Table 4.2: A comparison of the energies of the low-lying excited states of ^{15}O, ^{15}N, ^{17}O and ^{17}F, relative to the corresponding ground-state energies (the $(1/2)^-_1$ states of ^{15}O and ^{15}N and the $(5/2)^+_1$ states of ^{17}O and ^{17}F) obtained with the PR-EOMCCSD(2h-1p) (^{15}O and ^{15}N) and PA-EOMCCSD(2p-1h) (^{17}O and ^{17}F) methods, the N^{3}LO [253,254], CD-Bonn [250], and Argonne V_{18} [249] potentials, and eight major oscillator shells, with the experimental data taken from [263]. All entries are in MeV. For the CD-Bonn and N^{3}LO interactions, we used $\hbar\omega = 11$ MeV. For V_{18}, we used $\hbar\omega = 10$ MeV.

	Interaction			
Excited state	N^{3}LO	CD-Bonn	V_{18}	Expt
^{15}O $(3/2)^-_1$	6.264	7.351	4.452	6.176
^{15}N $(3/2)^-_1$	6.318	7.443	4.499	6.323
^{17}O $(3/2)^+_1$	5.675	6.406	3.946	5.084
^{17}O $(1/2)^+_1$	-0.025	0.311	-0.390	0.870
^{17}F $(3/2)^+_1$	5.891	6.677	4.163	5.000
^{17}F $(1/2)^+_1$	0.428	0.805	0.062	0.495

in the CR-EOMCCSD(T) excitation energy for this state. Based on this analysis, it appears that the discrepancy between the CC and experimental results for the 3^- state is primarily due to a relatively poor reproduction of the shell structure of ^{16}O, in particular, an incorrect energy gap between the 1p and 2s1d shells (see Figure 4.1), which is known to be affected by three-nucleon forces. This is a strong evidence that it is the lack of three-body forces in the Hamiltonian, and not any intrinsic deficiencies in our CC/EOMCC calculations for ^{16}O, that is largely responsible for the ~ 6 MeV discrepancy between the converged EOMCCSD or CR-EOMCCSD(T) and experimental excitation energies for the 3^- state of ^{16}O.

Moving on to the excited states of the ^{15}O, ^{15}N, ^{17}O and ^{17}F systems, Table 4.2 reveals that the N^{3}LO PA-EOMCCSD(2p-1h) and PR-EOMCCSD(2h-1p) results for the lowest $(3/2)^-_1$ states of ^{15}O and ^{15}N and the $(1/2)^+_1$ state of ^{17}F are in good agreement with the experimental values, differing by less than 0.1 MeV. The description for the remaining states is not as good, but it is still reasonable, with the errors relative to experiment increasing to 0.6 to 0.9 MeV. It is important to note

that the $(3/2)_1^+$ states of ^{17}O and ^{17}F are known to be resonances, which cannot be treated properly by the CC codes utilized in this work since they are designed for the bound states only. This fact is likely one of the main contributions to the discrepancy between the CC and experimental results for these particular states. Finally, it is worth noting that once again there are significant differences between the results obtained with different potentials. Indeed, the CD-Bonn interaction produces excitation energies that are notably higher than the experimental values in most cases, while Argonne V_{18} consistently underestimated the excitation energies in the ^{15}O, ^{15}N, ^{17}O and ^{17}F systems. Of the potentials used in our calculation, it appears that N^{3}LO provides the best overall results.

Based on the above analysis, it seems that the three-body contributions to the nucleon-nucleon interaction may have a significant effect on calculated nuclear properties. However, as already mentioned above, the explicit inclusion of three-body interactions in the nuclear Hamiltonian is not the best way to proceed, as it increases the computational costs of the many-body nuclear structure calculations, and requires the rederivation of the equations defining various correlated methodologies that are typically formulated for pairwise potentials. This certainly applies to all quantum-chemistry-inspired CC theories discussed in this thesis. Furthermore, as shown in [171], where the CCSD calculations for the two- and three-body interactions were presented, the main contribution of the three-body force is in the density-dependent zero-, one-, and two-body terms that result from using the normal-ordered form of the Hamiltonian. The "true" three-body terms of the normal-ordered Hamiltonian can safely be neglected with minimum impact on the accuracy of the CC results. In other words, the most important three-body interactions can be expressed in the form of effective two-body matrix elements. This is an important finding as it points to the possibility of incorporating the effects of three-body forces within an effective two-body Hamiltonian, allowing for a straightforward application of quantum

chemistry inspired CC methods such as the ones utilized above. An example of a modern interaction that attempts to effectively account for three-body and higher many-body interactions within a two-body Hamiltonian is the V_{UCOM} potential [257–260]. This is a pure two-body interaction derived from Argonne V_{18} through a clever unitary transformation to account for short-range central and tensor correlations, which is adjusted to reproduce the experimental binding energies of three- and four-particle nuclei.

In order to gauge whether V_{UCOM} offers any improvements over the standard two-body interactions considered above when used in CC calculations of nuclei, as well as to further test the performance of the CC theory in studies of nuclear structure, we performed extensive CR-CC(2,3) calculations for the ground state of ^{16}O using the V_{UCOM} potential [169]. In addition, importance-truncated configuration interaction (IT-CI) [264] calculations were performed in order to further examine the strengths and weaknesses of both the CC methodology and the IT-CI formalism through direct comparisons [169]. The IT-CI approach is based on the idea of truncating the CI model space in which the Hamiltonian is diagonalized through the use of an importance measure for the individual configurations derived from perturbation theory followed by the numerical extrapolation to the limit corresponding to all configurations of a given CI scheme. For instance, the IT-CI($4p$-$4h$) method, which is the IT-CI scheme used in our study [169], is an approximation to CISDTQ (CI with singles, doubles, triples, and quadruples), in which configurations with an importance measure less than a given threshold are neglected from the calculation. This reduces the large computational costs of CISDTQ without sacrificing accuracy. We then repeat the IT-CI($4p$-$4h$) calculations with increasingly smaller thresholds for selecting configurations and extrapolate the results to the zero-threshold limit (which is equivalent to full CISDTQ). For the calculations summarized in this dissertation, all taken from [169], a Hartree-Fock basis was used. This decision is based on comparisons

of the IT-CI and CC results with both the the harmonic oscillator and Hartree-Fock (HF) bases, which show that, unlike the CC results which are almost insensitive to the choice of the basis set type, the IT-CI results for the harmonic oscillator basis become poor for larger $\hbar\omega$ values (for the complete details of this analysis see [169]). Basis sets consisting of 5, 6, 7, and 8 major oscillator shells, which can also be identified by the quantum numbers e_{max} = 4, 5, 6, and 7, respectively, were utilized.

Figure 4.3 displays the results of the CCSD, CR-CC(2,3), and IT-CI calculations for the binding energy of ^{16}O using V_{UCOM}. In addition to considering basic IT-CI(4p-4h) results, calculations were also performed in which a multi-reference Davidson correction [265–269] was added to the IT-CI(4p-4h) energies (which will be referred to as IT-CI(4p-4h)+MRD). This correction is meant to estimate the effect of higher-than-4p-4h configurations as well as to approximately restore size extensivity (unlike CC, truncated CI methods, including IT-CI, are not size extensive). As can be seen from panel (a) of Figure 4.3, the effect of the Davidson correction is fairly small regardless of the size of the basis set or the value of the basis set parameter $\hbar\omega$, maintaining a value of $\sim$ 1 MeV. This implies that with the HF basis, the contributions of higher-than-4p-4h configurations to the ground-state wave function are small. Panel (b) shows a comparison of the CCSD and CR-CC(2,3) results. It is clear from these results that the effect of connected triply excited clusters is quite significant, particularly for larger values of $\hbar\omega$. Quantitatively, the shift in energy when moving from CCSD to CR-CC(2,3) can be as large as 6 MeV, indicating that the inclusion of T_3 effects is important for obtaining an accurate description of the binding energies of ^{16}O with the V_{UCOM} interaction. Turning to a direct comparison of the CR-CC(2,3) and IT-CI(4p-4h) results, Figure 4.3 (c) reveals that the agreement between the two methodologies is remarkable. Indeed, for all but the largest basis set, the two plots are virtually on top of each other. Though the agreement is slightly worse for the largest e_{max} = 7 basis, it is still very good, with discrepancies between CR-CC(2,3) and IT-

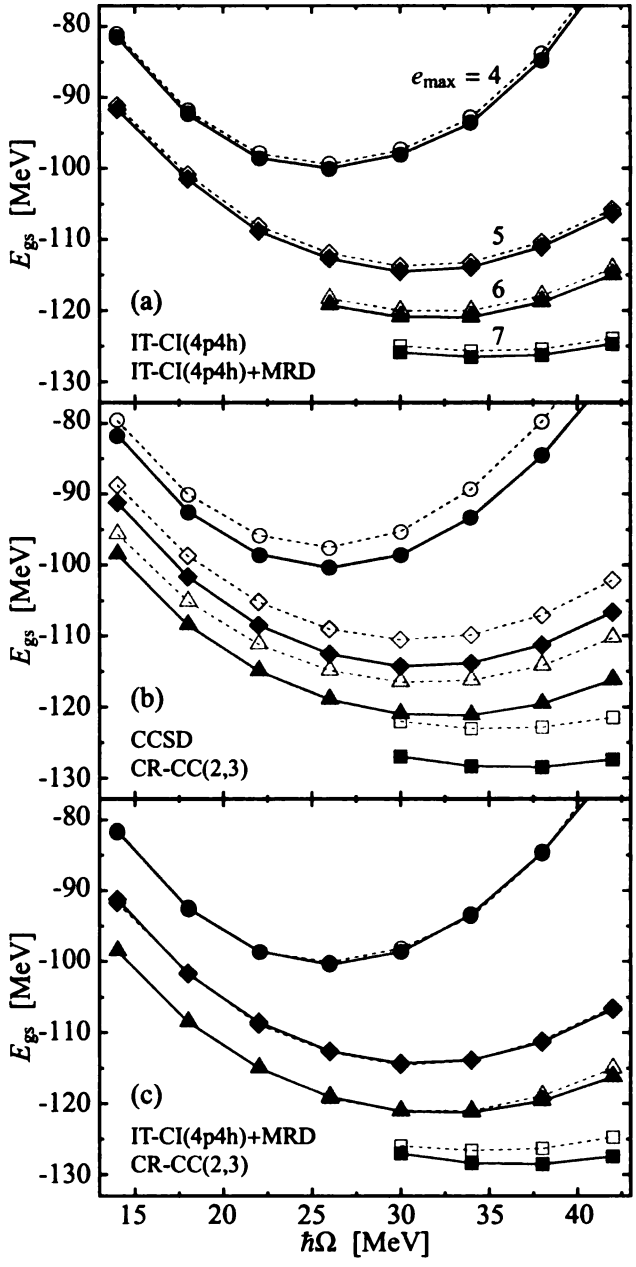

Figure 4.3: Systematic comparison of IT-CI and CC results for the ground-state energy of ^{16}O using HF-optimized single-particle bases with e_{max} = 4, 5, 6, and 7. (a) Comparison of IT-CI(4p-4h) (open symbols) with IT-CI(4p-4h)+MRD (filled symbols). (b) Comparison of CCSD (open symbols) with CR-CC(2,3) (filled symbols). (c) Comparison of IT-CI(4p-4h)+MRD (open symbols) with CR-CC(2,3) (filled symbols).

CI($4p$-$4h$)+MRD on the order of 1-2 MeV only. This is an important finding, which demonstrates that the relatively inexpensive CC theory with singles, doubles, and noniterative triples, represented here by CR-CC(2,3), is as accurate as the considerably more expensive CISDTQ-like IT-CI($4p$-$4h$)+MRD calculations. We do not have to worry about the Davidson extensivity corrections since the CCSD, CR-CC(2,3), and most of the other CC approximations are automatically size extensive and, as mentioned earlier, the CC results are almost insensitive to the choice of the basis set type (harmonic oscillator or HF) due to the presence of the e^{T_1} component in the CC wave function that makes CC calculations approximately invariant with respect to orbital rotations (Thouless' theorem). As demonstrated in [169], the IT-CI results for the harmonic oscillator basis are considerably worse than their HF counterparts shown in Figure 4.3, which is another strong argument in favor of using CC methods in nuclear applications (in addition to the computer costs which are lower in the CC case compared to CI aimed at similar accuracies). We refer the reader to [169] for further analysis.

As a final element of the $^{16}\mathrm{O}/V_{\mathrm{UCOM}}$ study, we extrapolate the CR-CC(2,3) results to the infinite basis set limit in order to compare the resulting binding energies with experiment. Unfortunately, there are a couple of issues that complicate such an extrapolation. First, the V_{UCOM} interaction has a harder core than in an interaction transformed by the G-matrix approach used in our earlier work [164], and as a result a basis set including up to 8 shells is still relatively far from convergence. In addition, the HF and, in consequence, correlation energies do not change uniformly when increasing the size of the basis set through the addition of the next major oscillator shell. As a consequence of these issues and due to the limited amount of data obtained in our study, we could only conclude that the extrapolated infinite basis set CR-CC(2,3) energies fall within the range of -131 to -141 MeV. Comparing this range of values with the experimental binding energy of -127.6 MeV reveals

that using the V_{UCOM} interaction in the CC calculations does improve the results over the purely two-body N^{3}LO interaction [164]. Indeed, the error in the binding energy per nucleon for the very roughly extrapolated CR-CC(2,3) results is 0.21 to 0.84 MeV/nucleon (-0.5 MeV/nucleon on average), which represents an improvement over the $\sim$ 1.0 MeV/nucleon error obtained in the N^{3}LO CR-CCSD(T) calculations for the ^{16}O ground state [164] or $\sim$ 2 MeV/nucleon error obtained with Argonne V_{18} and CCSD [165] (see Table 4.1). The latter observation is important since V_{UCOM} is based on transforming Argonne V_{18}. Given that the CR-CCSD(T) and CR-CC(2,3) approaches should yield similar accuracies for small or medium size closed-shell systems, we can conclude that the observed improvement is the result of the improved interaction. These results are certainly promising, though further calculation to help improve the extrapolation would be useful. The remaining potential errors in the CR-CC(2,3) V_{UCOM} binding energy is likely the result of contamination from the center-of-mass motion. Indeed, unlike in quantum chemistry, where thanks to the Born-Oppenheimer approximation there is a rigid nuclear framework in which the electrons move, the self-bound nucleus has translational degrees of freedom, and in truncated CC or CI calculations there may be spurious contributions induced by a coupling between the translational and intrinsic degrees of freedom. Such contamination can introduce errors into the CC results for the intrinsic energy of the nuclear state of interest. For a more detailed analysis of the center-of-mass problem in CC calculations of nuclei, see [169, 170].

4.3 Ground and Excited States of ^{55}Ni, ^{56}Ni, and ^{57}Ni

In order to analyze the performance of the CC theory in studies of heavy nuclei, we performed CR-CC(2,3)/CR-EOMCC(2,3) and CR-CC(2,4)/CR-EOMCC(2,4) calcu-

lations for the ground and low-lying excited states of ^{56}Ni [167]. Besides being an example of a heavier nucleus for which all non-CC high-level methodologies, such as the Green's function Monte Carlo [152] and no-core shell-model [153–156] approaches, are prohibitively expensive, it is also an example of what can be described as a 'semi-closed shell' nucleus. Indeed, the lowest-energy configuration for the ground state of ^{56}Ni completely fills all energy levels up to and including the $1f_{7/2}$ level (see Figure 4.1). Although there is a notable energy gap between this level and the lowest unoccupied $2p_{3/2}$ level, the $1f_{7/2} - 2p_{3/2}$ gap in ^{56}Ni is not as large as what would be found in a perfectly closed-shell system and not as small as what would be found in a typical quasidegenerate open-shell system. This means that the degree of non-dynamical correlations in ^{56}Ni is larger than in a typical closed-shell system in spite of the completely filled highest occupied $1f_{7/2}$ subshell. As a result, this is a very interesting test case for the CR-CC approaches discussed in this work, which have been shown to perform well for molecular systems with significant nondynamical correlations, and smaller HOMO-LUMO gaps. In order to extend these considerations and further explore the performance of the CR-CC(2,3) and CR-CC(2,4) schemes in studies of nuclei characterized by varying degrees of nondynamical character, we performed calculations in which the value of the $1f_{7/2} - 2p_{3/2}$ energy gap was varied through the shifting of the energies of the $2p_{3/2}$, $1f_{5/2}$, and $2p_{1/2}$ levels relative to the $1f_{7/2}$ level by an amount ΔG. Both negative values of ΔG, for which the gap is reduced and thus the degree of nondynamical correlation is increased, and positive values, for which the gap is increased and the nucleus becomes more closed-shell, were considered [167]. $\Delta G = 0$ is the original gap in a realistic description of ^{56}Ni.

The ^{56}Ni calculations in this study utilized the semi-empirical GXPF1A effective Hamiltonian [270], which is derived from a microscopic calculation based on the renormalized G-Matrix theory with the Bonn-C interaction [255], and then parameterized to fit experimental data for the low-lying states in nuclei from $A = 47$ to

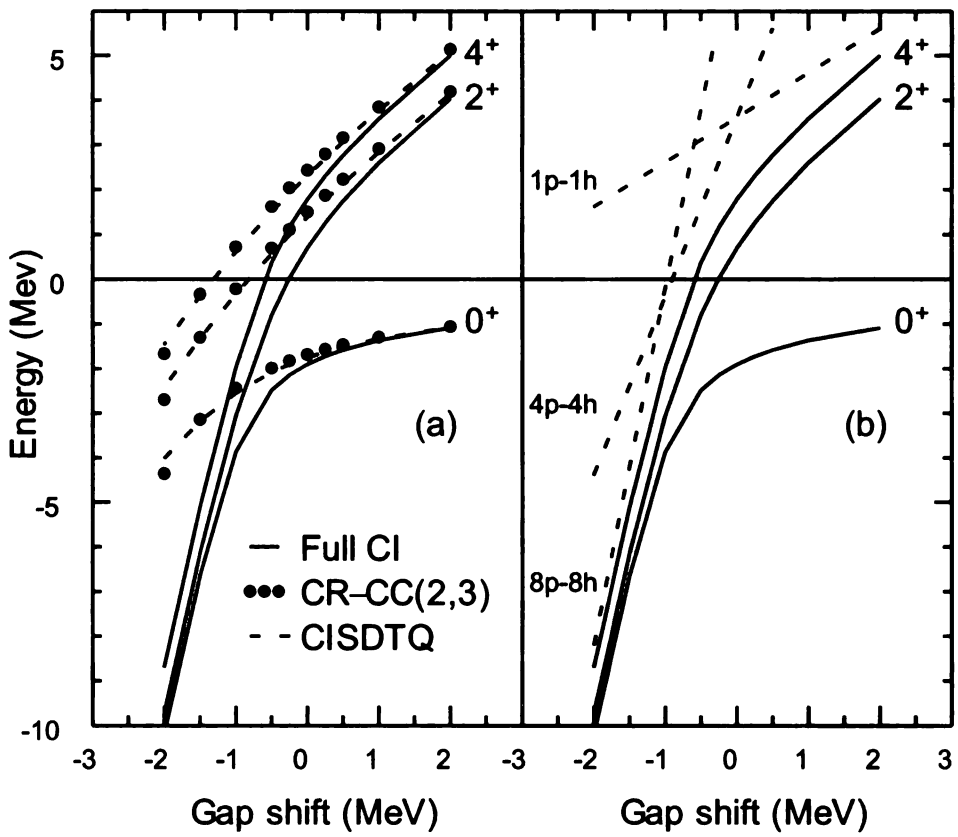

Figure 4.4: (a) The full CI, CISDTQ, and CR-CC(2,3) energies of ^{56}Ni as functions of the shell-gap shift ΔG. (b) Comparison of full CI energies with the trends expected for the $1p$-$1h$, $4p$-$4h$, and $8p$-$8h$ configurations as functions of ΔG.

$A = 66$ [270–272] (A is the mass number). In order to accurately gauge the accuracy of the CR-CC(2,3)/CR-EOMCC(2,3) and CR-CC(2,4)/CR-EOMCC(2,4) schemes in describing the correlations within this system, we wanted to perform full CI calculations as well as a sequence of truncated CI calculations for benchmarking purposes. Since ^{56}Ni is too large for no-core full CI calculations, the full CI and all CC and other CI calculations were performed within a valence model space consisting of only the pf shell (the highest shell depicted in Figure 4.1), with the nucleons occupying the lower shells being accounted for in an effective manner through the GXPF1A effective Hamiltonian.

Figure 4.4 depicts the results of our CR-CC(2,3)/CR-EOMCC(2,3) calculations and their comparison with the CISDTQ and full CI data. Focusing on the results for the ground 0^+ state, panel (a) shows that the CR-CC(2,3) energies agree very well with those of full CI for positive values of ΔG. This is confirmed quantitatively in Table 4.3, which shows that for this ΔG region, the difference between CR-CC(2,3) and full CI ranges from 0.07 to 0.09 MeV. This excellent agreement is not surprising given the predominantly closed-shell nature of the nucleus for $\Delta G < 0$. Indeed, as seen in Table 4.3, the value of $S_0 = |\langle \Phi_0 | \Psi_0^{\text{Full-CI}} \rangle|$, which measures the overlap of the reference determinant $|\Phi_0\rangle$ with the exact, full CI wave function $|\Psi_0^{\text{Full-CI}}\rangle$, is over 0.9 the $\Delta G > 0$ region. This indicates that the wave function is dominated by the reference configuration, and, as such, is mostly single reference in nature. For the physical value of the gap (i.e., $\Delta G = 0$), the S_0 value drops to 0.825, indicating a somewhat stronger multi-reference character, and thus a more open-shell nature. However, even in this case, CR-CC(2,3) performs very well, producing an error relative to full CI of 0.22 MeV which is almost nothing on the scale of binding energies of heavier nuclei. It is when ΔG becomes negative that CR-CC(2,3) begins to have more trouble, as can be clearly seen from Figure 4.4. Quantitatively, one finds discrepancies between CR-CC(2,3) and full CI of 1.43 and 5.84 MeV for $\Delta G = -1$ and -2 MeV, respectively. This is certainly a result of the much more strongly open-shell or quasidegenerate nature of the nucleus for this ΔG region. Indeed, $S_0 = 0.332$ and 0.022 for $\Delta G = -1$ and -2 MeV, respectively. Such small overlaps between the reference determinant and the exact wave function indicate that the ground state is characterized very strong nondynamical correlations, similar to those found in metallic-like systems, that even CR-CC(2,3) has difficulty with.

Interestingly, even in the strongly correlated multi-reference $\Delta G < 0$ region, where CR-CC(2,3) has difficulty reproducing the full CI results, the CR-CC(2,3) energies are in excellent agreement with those of the much more expensive CISDTQ approach.

Indeed, the two differ by less than 0.34 MeV for all values of ΔG. This is a very encouraging result given that the most expensive computational steps of CR-CC(2,3) scale as $n_o^2 n_u^4$ in the iterative CCSD part and $n_o^3 n_u^4$ in the noniterative triples correction part (see Section 3.1.2), whereas CISDTQ is characterized by iterative steps that scale as $n_o^4 n_u^6$. As in the case of ^{16}O, the CR-CC(2,3) approach offers substantial savings in the computer effort compared to CI with minimal loss in accuracy. This would not be surprising if ^{56}Ni was a closed-shell system. What is surprising and certainly very promising here is the fact that the inexpensive CR-CC(2,3) approach accurately describes all correlations among nucleons up to quadruple excitation independent of the $1f_{7/2} - 2p_{3/2}$ gap, i.e., independent of the degree of quasidegenerate character of our ^{56}Ni model system and independent of the strength of the correlations. The fact that the agreement between CR-CC(2,3) and CISDTQ holds in a metallic-like region where the reference determinant $|\Phi_0\rangle$ contributes only a few percent of the wave function is unheard of, demonstrating the great utility of CR-CC(2,3). It is also interesting to observe that quadruple excitations are largely dominated by disconnected $\frac{1}{2}T_2^2$ contributions. This is verified by the CR-CC(2,4) results which only differ from the CR-CC(2,3) binding energies in Table 4.3 by 0.001-0.102 MeV. Such small changes when moving from CR-CC(2,3) to CR-CC(2,4) indicates that there is very little contribution from the connected quadruply excited clusters T_4.

Turning to the excited 2^+ and 4^+ states of our ^{56}Ni model, Figure 4.4 and Table 4.3 reveal that the trends displayed by the results for the ground state apply to the excited states as well, with CR-EOMCC(2,3) mimicking full CI for $\Delta G = 0$, 1 and 2 MeV, but diverging from the full CI results for $\Delta G = -2$ and -1 MeV. Furthermore, as was true for the ground state, the CR-EOMCC(2,3) results are practically identical to those of CISDTQ, and the role of T_4 and $R_{\mu,4}$, as indicated by the CR-EOMCC(2,4) energies, is small regardless of the ΔG value. One interesting observation, however, is that the REL values for these two states are less than 1.33 independent of ΔG,

Table 4.3: Energies (in MeV) of ^{56}Ni as functions of the shell-gap shift ΔG (also in MeV), relative to the reference energy $\langle\Phi_0|H|\Phi_0\rangle = -203.800$ MeV. S_0 is defined as $|\langle\Phi_0|\Psi_0^{\text{Full-CI}}\rangle|$.

	ΔG	-2	-1	0	1	2
State	S_0	0.022	0.332	0.825	0.917	0.949
0^+	CCSD	-3.218	-2.048	-1.509	-1.202	-1.002
	CR-CC(2,3)	-4.355	-2.437	-1.686	-1.298	-1.060
	CR-CC(2,4)	-4.253	-2.415	-1.679	-1.295	-1.059
	CISD	-2.148	-1.652	-1.327	-1.104	-0.943
	CISDT	-2.706	-1.946	-1.488	-1.199	-1.004
	CISDTQ	-4.013	-2.548	-1.758	-1.334	-1.079
	Full CI	-10.198	-3.868	-1.909	-1.370	-1.091
2^+	CCSD	-2.440	-0.065	1.595	2.983	4.241
	CR-CC(2,3)	-2.695	-0.218	1.496	2.915	4.192
	CR-CC(2,4)	-2.700	-0.222	1.493	2.913	4.190
	CISD	0.864	2.000	3.093	4.162	5.215
	CISDT	-1.227	0.359	1.771	3.066	4.283
	CISDTQ	-2.426	-0.335	1.378	2.833	4.137
	Full CI	-9.728	-3.054	0.689	2.594	4.027
	REL	1.309	1.178	1.114	1.080	1.060
4^+	CCSD	-1.373	0.910	2.551	3.942	5.211
	CR-CC(2,3)	-1.667	0.720	2.420	3.848	5.141
	CR-CC(2,4)	-1.626	0.736	2.428	3.852	5.144
	CISD	1.554	2.743	3.884	4.994	6.082
	CISDT	-0.271	1.301	2.713	4.017	5.248
	CISDTQ	-1.465	0.606	2.308	3.769	5.087
	Full CI	-8.700	-1.974	1.778	3.581	4.999
	REL	1.333	1.215	1.152	1.115	1.090

which indicates that regardless of the quasidegenerate nature, the excited states are dominated by single excitations relative to the ground state. As discussed in Section 3.2.3, the CR-EOMCC(2,3) approach describes such states accurately. Thus, it is likely that the excitation process that generates the 2^+ and 4^+ excited states of ^{56}Ni is described correctly regardless of the choice of ΔG, and that the discrepancies between CR-EOMCC(2,3) and full CI in the negative ΔG region are due to the propagation of errors from the ground-state calculations.

Given the above analysis, the remaining issue is the physical nature of the source

of the discrepancy between CR-CC(2,3)/CR-EOMCC(2,3) and full CI in the negative ΔG region. Panel (b) of Figure 4.4 gives some insights into this issue. In this figure, the full CI results for the three states of ^{56}Ni, as a function of ΔG, are plotted and compared to the trends expected for the $1p$-$1h$ (single), $4p$-$4h$ (quadruple), and $8p$-$8h$ (octuple) configurations. By comparing the slopes of the full CI curves against the slopes of the mp-mh lines, it is clear that as ΔG approaches zero from the positive side, the role of $4p$-$4h$ configurations increases, but there is little contribution from higher-than $4p$-$4h$ configurations. This explains why CR-CC(2,3)/CR-EOMCC(2,3) and CISDTQ perform so well in this region. They both capture all nucleon correlations up to $4p$-$4h$ excitation almost perfectly. However, as the gap is decreased further, it is clear that $8p$-$8h$ configurations begin to dominate the wave function. Now since the CR-CC methods used in this study neglect the effect of T_n clusters with $n > 4$, they are incapable of describing the entire set of $8p$-$8h$ excitations. The exponential nature of CC means that some $8p$-$8h$ correlations are accounted for via disconnected product terms, such as $\frac{1}{24}T_2^4$. However, because of the noniterative nature of the CR-CC schemes used here, some important $8p$-$8h$ disconnected product terms involving T_3, such as $\frac{1}{2}T_3^2T_2$ are more or less neglected, and so only product terms involving T_1 and T_2 are included in CR-CC(2,3). Clearly, given our results, these are not enough to describe the $8p$-$8h$ correlations dominating the low-lying states of ^{56}Ni when ΔG is negative and the $1f_{7/2} - 2p_{3/2}$ gap becomes small.

As a further extension of the ^{56}Ni study, we performed PA-EOMCCSD($3p$-$2h$) and PR-EOMCCSD($3h$-$2p$) calculations for the ground $\frac{7}{2}^-$ state of ^{55}Ni and the ground $\frac{3}{2}^-$ and excited $\frac{5}{2}^-$ and $\frac{1}{2}^-$ states of ^{57}Ni, using ^{56}Ni as the "closed-shell" reference system. As this was a continuation of the above ^{56}Ni study, these calculations were again performed within the pf model space, using the same GXPF1A effective Hamiltonian as that used in the ^{56}Ni calculations. It should only be noted that the two-body matrix elements of the GXPF1A interaction have a smooth mass

Table 4.4: Binding energies (in MeV) of ^{55}Ni and ^{57}Ni relative to the corresponding reference energies $\langle\Phi_0^{(A)}(j)|H|\Phi_0^{(A)}(j)\rangle$, $A = 55$ and 57, respectively, as functions of the shell gap shift ΔG (in MeV). $S_0^{(A)}(j)$ is defined as $|\langle\Phi_0^{(A)}(j)|\Psi_{0,A}^{\text{Full-CI}}(j)\rangle|$.

ΔG	-2	-1	0	1	2
^{55}Ni					
PR-EOMCC($2h$-$1p$)	-3.649	-2.459	-1.884	-1.542	-1.313
PR-EOMCC($3h$-$2p$)	-3.844	-2.567	-1.951	-1.587	-1.344
CI($2p$-$2h$)	-2.505	-2.013	-1.672	-1.427	-1.244
CI($3p$-$3h$)	-3.295	-2.449	-1.922	-1.580	-1.344
CI($4p$-$4h$)	-4.457	-2.967	-2.150	-1.693	-1.406
CI($6p$-$6h$)	-6.397	-3.519	-2.262	-1.723	-1.417
Full-CI	-9.091	-3.920	-2.279	-1.725	-1.417
$S_0^{(55)}(\frac{7}{2})$	0.0362	0.4023	0.8015	0.8919	0.9287
^{57}Ni					
PA-EOMCC($2p$-$1h$)	-3.868	-2.671	-2.080	-1.721	-1.476
PA-EOMCC($3p$-$2h$)	-4.295	-2.871	-2.186	-1.783	-1.516
CI($2p$-$2h$)	-2.692	-2.192	-1.840	-1.584	-1.389
CI($3p$-$3h$)	-3.622	-2.717	-2.146	-1.772	-1.513
CI($4p$-$4h$)	-4.697	-3.217	-2.370	-1.884	-1.575
CI($6p$-$6h$)	-6.534	-3.768	-2.493	-1.918	-1.588
Full-CI	-9.391	-4.151	-2.511	-1.921	-1.588
$S_0^{(57)}(\frac{3}{2})$	0.0335	0.4062	0.7802	0.8774	0.9182

dependence that scales as $(42/A)^{1/3}$, and so we had to scale them to the mass number of the nucleus of interest (i.e. $A = 55$ or $A = 57$). As was done in the ^{56}Ni study, the $1f_{7/2} - 2p_{3/2}$ shell gap is varied by an amount ΔG in order to study the performance of the PA- and PR-EOMCC methods for differing degrees of nondynamical correlation effects.

Table 4.4 gives the results for the binding energies of ^{55}Ni and ^{57}Ni. As was the case for the ground state of ^{56}Ni, it is clear that the PA-EOMCCSD($3p$-$2h$) and PR-EOMCCSD($3h$-$2p$) schemes perform very well in the positive ΔG region, producing discrepancies relative to full CI for both states of about 0.07 MeV for $\Delta G = 2$ MeV and 0.14 MeV for $\Delta G = 1$ MeV. This result is not unexpected as the ground states of both ^{55}Ni and ^{57}Ni show a predominantly single-reference nature, with an overlap between the CI reference determinant and the full CI wave function, $S_0^{(A)}(j)$, of about 0.9 (please note that the CI calculations treat the nuclei of interest, ^{55}Ni or ^{57}Ni, directly rather than attempting to build them out of ^{56}Ni through particle attachment or particle removal as is the case in PA/PR-EOMCC). The more interesting question is how the PA- and PR-EOMCC schemes perform when the multi-reference character of a nucleus increases. For the physical energy gap corresponding to $\Delta G = 0$ MeV, for which $S_0^{(55)}(\frac{7}{2}) \approx 0.80$ and $S_0^{(57)}(\frac{3}{2}) \approx 0.78$, the PA-EOMCCSD($3p$-$2h$) and PR-EOMCCSD($3h$-$2p$) approaches still produce accurate results for the ground states of ^{55}Ni and ^{57}Ni, differing from full CI by only 0.33 MeV in both cases. However, similar to what was observed for ^{56}Ni, the agreement begins to break down for negative ΔG values. Indeed, for $\Delta G = -1$ MeV, for which the CI reference determinant makes up less than half of the full CI wave function, the CC and full CI energies differ by 1.35 MeV and 1.28 MeV for ^{55}Ni and ^{57}Ni, respectively. For $\Delta G = -2$ MeV, where the CI reference $|\Phi_0^{(A)}(j)\rangle$ is virtually orthogonal to the corresponding full CI wave function, there is a breakdown in accuracy, with the PA-EOMCCSD($3p$-$2h$) and PR-EOMCCSD($3h$-$2p$) errors of 5.10 and 5.24 MeV respectively.

Despite the difficulties the ^{57}Ni and ^{55}Ni model systems pose to the PA- and PR-EOMCC methods when $\Delta G < 0$ MeV, we once again see that there is a nice correlation between the CC and CISDTQ (labelled by the equivalent CI($4p$-$4h$) designation in Table 4.4) results regardless of the value of ΔG. Indeed, although CISDTQ is slightly more accurate than PA-EOMCCSD($3p$-$2h$) and PR-EOMCCSD($3h$-$2p$) in describing the ground states of ^{57}Ni and ^{55}Ni, there is a reasonable agreement between these CI and CC results, with discrepancies that are only about 0.06 MeV for the largest $\Delta G = 2$ MeV gap, and $\sim 0.4 - 0.6$ MeV for the smallest $\Delta G = -2$ MeV energy gap. Furthermore, the PA-EOMCCSD($3p$-$2h$) and PR-EOMCCSD($3h$-$2p$) results are consistently more accurate than those of CISDT. This result is encouraging because these PA- and PR-EOMCC schemes with up to $3p$-$2h$ and $3h$-$2p$ excitations are characterized by iterative steps that scale as $n_o^2 n_u^5$ and $n_o^3 n_u^4$, respectively, which are both considerably less expensive than the the $n_o^3 n_u^5$ and $n_o^4 n_u^6$ steps that characterize CISDT and CISDTQ. Furthermore, if one were to consider the active-space variants of the PA- and PR-EOMCC schemes discussed above, the associated computer costs would be even lower (see Section 2.1.2).

Looking at the excited $(5/2)^-$ and $(1/2)^-$ states of ^{57}Ni, Table 4.5 reveals that the observed accuracy patterns are similar to those seen for the ground-state calculations, with the accuracy of the PA-EOMCCSD($3p$-$2h$) approach declining as the energy gap is decreased. Furthermore, there is again a good agreement between the PA-EOMCCSD($3p$-$2h$) and CISDTQ results. In fact, the agreement observed for the excitation energies of the $(5/2)^-$ and $(1/2)^-$ states of ^{57}Ni is superior to what was observed for the binding energies, with the PA-EOMCCSD($3p$-$2h$) and CISDTQ excitation energies differing by less than 0.1 MeV for all values of ΔG. Again, this is an excellent result given the large savings in computational effort provided by the PA-EOMCCSD($3p$-$2h$) approach when compared to CISDTQ.

Table 4.5: Excitation energies (in MeV) of the low-lying states of ^{57}Ni as functions of the shell gap shift ΔG (in MeV). $S_0^{(A)}(j)$ is defined as $|\langle\Phi_0^{(A)}(j)|\Psi_{0,A}^{\text{Full-CI}}(j)\rangle|$.

ΔG	-2	-1	0	1	2
$(5/2)^-$					
PA-EOMCC($2p$-$1h$)	0.658	0.819	0.895	0.937	0.961
PA-EOMCC($3p$-$2h$)	0.625	0.771	0.856	0.908	0.939
CI($2p$-$2h$)	0.812	0.856	0.897	0.927	0.948
CI($3p$-$3h$)	0.781	0.827	0.878	0.917	0.944
CI($4p$-$4h$)	0.692	0.776	0.852	0.904	0.937
CI($6p$-$6h$)	0.360	0.658	0.832	0.900	0.936
Full CI	-0.118	0.402	0.825	0.900	0.936
$S_0^{(57)}(\frac{5}{2})$	0.0193	0.2640	0.7443	0.8596	0.9077
$(1/2)^-$					
PA-EOMCC($2p$-$1h$)	1.259	1.494	1.639	1.739	1.813
PA-EOMCC($3p$-$2h$)	0.669	1.071	1.366	1.562	1.694
CI($2p$-$2h$)	1.279	1.451	1.592	1.699	1.781
CI($3p$-$3h$)	1.009	1.218	1.426	1.588	1.706
CI($4p$-$4h$)	0.763	1.021	1.312	1.530	1.676
CI($6p$-$6h$)	0.395	0.739	1.211	1.499	1.665
Full CI	0.050	0.434	1.184	1.496	1.665
$S_0^{(57)}(\frac{1}{2})$	0.0293	0.2561	0.6577	0.8049	0.8701

Chapter 5

Summary and Future Perspectives

In this dissertation, two new *ab initio* methodologies designed specifically to address the challenges posed by open-shell many-fermion systems within a single-reference formalism have been developed and tested. The active-space EA- and IP-EOMCC theories (and their PA- and PR-EOMCC extensions to non-electronic systems) are based on the idea of building an open-shell system, such as a radical, through the direct addition or removal of a particle to or from the related closed-shell species. Additionally, these new schemes are characterized by the use of active orbitals to *a priori* select the dominant higher-than $2p$-$1h$ and higher-than $2h$-$1p$ components of the electron-attaching and ionizing operators, respectively, which greatly reduces the computational cost of higher-level EA- and IP-EOMCC approximations without sacrificing any of the associated accuracy. The performance of these schemes was illustrated through benchmark calculations for adiabatic or vertical excitation energies of the low-lying states of CH, SH, C_2N, CNC, N_3, and NCO. All of these molecular examples revealed that the most basic active-space EA- and IP-EOMCC approaches, the EA-EOMCCSDt and IP-EOMCCSDt methods which include up to $3p$-$2h$ and $3h$-$2p$ components in the electron-attaching and ionizing operators, respectively, were able to provide a highly accurate description of the electronic excitation spectra while

requiring computational costs that are only a small prefactor times those characterizing the basic and widely applicable CCSD method. Additionally, calculations for the potential energy curves of the low-lying states of the OH radical revealed that while the IP-EOMCCSDt approach performs well in the spectroscopic Franck-Condon region, the inclusion of the higher-order $4h$-$3p$ effects is needed in order to accurately break chemical bonds in excited states. It was then demonstrated that the active-space SAC-CI($4h$-$3p$) scheme, which includes the dominant $3h$-$2p$ and $4h$-$3p$ effects selected via a small subset of active orbitals and which is essentially equivalent to the active-space IP-EOMCC method with up to $4h$-$3p$ "excitations" produces essentially identical accuracies as its substantially more expensive parent approach while requiring a significantly less computational effort, while enabling us to obtain a perfect description of the entire ground- and excited-state potential energy surfaces of OH, including the Franck-Condon and asymptotic regions. Similar statements apply to the active-space EA-EOMCC and EA SAC-CI schemes.

The second methodology discussed in this dissertation was the CR-CC/CR-EOMCC formalism based on the biorthogonal MMCC theory. In particular, the CR-CC(2,3)/CR-EOMCC(2,3) and CR-CC(2,4)/CR-EOMCC(2,4) approaches, in which noniterative corrections due to triply or triply and quadruply excited clusters are added to the energies obtained with the basic CCSD/EOMCCSD scheme, were extended to general open-shell references of the high-spin ROHF type, implemented, and tested. In order to gauge the performance of CR-CC(2,3) in a variety of scenarios involving open-shell molecular systems, calculations for single-bond breaking reactions in radicals and for singlet-triplet gaps in biradical systems were performed. These calculations revealed that CR-CC(2,3) is able to provide highly accurate results for these types of problems, producing values that are as good as or, particularly for states or geometries characterized by a large degree of nondynamical correlation, superior to those of both the restricted and unrestricted CCSD(T) methods that are often referred to as the

'gold standard' of quantum chemistry (a somewhat problematic classification in view of our findings). Furthermore, the CR-CC(2,3) approach produces these excellent results while maintaining the relatively low computational costs and the ease-of-use that have made CCSD(T) so popular. Through calculations for the unusually small singlet-triplet gap in the BN molecule, which is an extreme case characterized by strong T_4 effects, it was shown that the CR-CC(2,4) approach is capable of accurately describing the effects of quadruply excited clusters without requiring the high computational costs characterizing the full CCSDTQ method. Finally, calculations for the low-lying excited states of radicals revealed that the extension of CR-CC(2,3) to excited states, CR-EOMCC(2,3), offers same balance of high accuracy and low computational cost demonstrated for the ground-state CR-CC(2,3) scheme when the excitation spectra of radicals and other open-shell species are examined.

Although a great deal of progress was made in regards to the development and implementation of the above quantum chemistry methodologies, there remains a large amount of future development work to be done. Indeed, in the case of the active-space EA- and IP-EOMCC schemes, higher-order approximations, such as the EA-EOMCCSDtq and IP-EOMCCSDtq schemes, which include up to triples in the cluster operator defining the closed-shell reference system, and up to $4p$-$3h$ or $4h$-$3p$ components in the electron-attaching and ionizing operators, respectively, should be implemented. This is especially important given the conclusion that $4p$-$3h$ and $4h$-$3p$ effects are important in accurately describing bond-breaking processes, particularly in the excited states of radicals. Furthermore, the development and computer implementation of the active-space DEA- and DIP-EOMCC schemes, which build the wave function for an open-shell system by adding two particles to, or removing two particles from the related closed shell, would be a valuable development as it would make it possible to study biradicals within this formalism. In terms of the CR-CC schemes, further development of the CR-CC(2,4) approach with regards to the cou-

pling between triples and quadruples, which was neglected in the CR-CC(2,4) scheme described in this dissertation but may be important for obtaining accurate results for some systems, is needed. Additionally the development of higher-order CR-CC approximations, such as the CR-CC(3,4) method, which corrects the CCSDT energy for the effect of connected quadruply excited clusters, would be useful. Clearly it would be great to develop the analogous CR-EOMCC(3,4) scheme that corrects the EOMCCSDT results for excited states for the quadruple excitations.

In addition to the above work, an important development that would be useful with respect to the active-space CC/EOMCC and CR-CC/CR-EOMCC methodologies discussed in this thesis is the extension of these approaches to very large systems through an appropriate local correlation approximation. Indeed, there has already been significant progress in this area as local variants of the CR-CC(2,3) scheme and its CCSD and CCSD(T) counterparts, based on the so-called "cluster-in-molecule" [38, 39] framework, have already been developed [40–44]. This is an important development as it extends the applicability of these types of CC methods to much larger systems that generally are the regime of inexpensive, low-order approximations or semi-empirical schemes by replacing the $\mathcal{N}^6 - \mathcal{N}^7$ scalings of the CPU time with the system size $\mathcal{N}$ by a linear scaling.

As a final component of this dissertation, the CC methods developed in this work, as well as other quantum chemistry inspired CC approaches, have been used in calculations of the structure of nuclei. The basis of this work is that the fundamental many-body physics underlying the structures of both molecular and nuclear systems is the same, with essentially only the form of the interaction changing, and thus the CC approaches developed in quantum chemistry can also work within the context of nuclear physics. The methodologies developed in this dissertation are of particular value in nuclear structure theory as, thanks to the atom-like shell structure of nuclei characterized by a large amount of degeneracy, the majority of nuclei are in

fact open-shell systems. Indeed, in a study of ^{55}Ni, ^{56}Ni, and ^{57}Ni, the size of the energy gap between the highest occupied and lowest unoccupied levels was varied in order to test the performance of the CC methods as a function of the degree of the open-shell character of the nucleus of interest. This study revealed that regardless of the degree of open-shell character and strength of the correlation effects, the CR-CC(2,3)/CR-EOMCC(2,3) (^{56}Ni), PA-EOMCCSD(3p-2h) (^{57}Ni), and PR-EOMCCSD(3h-2p) (^{55}Ni) methods were capable of producing results of essentially the same quality as those of the much more expensive CISDTQ scheme. In a separate set of calculations involving ^{16}O and the surrounding valence systems, it was found that the three-body components of the nucleon-nucleon interaction, which are not present in the Coulomb interaction between electrons, plays a significant role, and cannot be ignored if one wants to obtain results in agreement with experiment. However, it was also demonstrated that it is possible to reasonably accurately include the effects of three-body forces through an effective two-body interaction. Finally, as was the case for ^{56}Ni, the CR-CC(2,3) results for ^{16}O are in excellent agreement with those of CI schemes including up to quadruple excitations without the need to worry about orbital optimization or size extensivity. Some potential further developments that can be pursued as part of this work include the further refinement and testing of two-body Hamiltonians that effectively account for three-body forces and the extension of genuine MRCC methods to nuclear calculations as midshell nuclei and some excited states in closed- and open-shell nuclei may require such a treatment in order to be properly described. Finally, there is still an open issue of how to deal with contaminations from the translational degrees of freedom in the CC calculations for nuclei. Indeed such a problem does not exist in quantum chemistry as, in the Born-Oppenheimer approximation, the nuclei create a fixed framework within which the electrons move. Although some investigation of the degree to which such contamination is an issue in CC and CI calculations has already been performed [170], further

study as well as the development of ways to overcome this issue in CC calculations is needed.

Appendix A

Factorized Form of the EA-EOMCCSD($3p$-$2h$) and IP-EOMCCSD($3h$-$2p$) Equations

In this appendix, we present the fully factorized form of the equations defining the EA-EOMCCSD($3p$-$2h$) and IP-EOMCCSD($3h$-$2p$) eigenvalue problems, exploited in this study, in terms of the one- and two-electron molecular integrals, $f_p^q = \langle p|f|q\rangle$ (f is the Fock operator) and $v_{pq}^{rs} = \langle pq|v|rs\rangle - \langle pq|v|sr\rangle$, respectively, defining the Hamiltonian, T_1 and T_2 cluster amplitudes defining the underlying N-electron ground-state CCSD problem, and the $R_{\mu,1p}$, $R_{\mu,2p\text{-}1h}$, and $R_{\mu,3p\text{-}2h}$ and $R_{\mu,1h}$, $R_{\mu,2h\text{-}1p}$, and $R_{\mu,3h\text{-}2p}$ amplitudes defining the electron attaching and electron removing operators, $R_\mu^{(N+1)}$ and $R_\mu^{(N-1)}$, respectively. The EA-EOMCCSD($3p$-$2h$) equations can be given the following form:

$$\begin{aligned}\langle\Phi^a|(\bar{H}^{(\mathrm{CCSD})}_{N,\mathrm{open}} R_\mu^{(N+1)})_C|\Phi\rangle &= \bar{h}_a^e r_e + \bar{h}_m^e r_{ae}^{\ m} + \tfrac{1}{2}\bar{h}_{am}^{ef} r_{ef}^{\ m} \\ &+ \tfrac{1}{4} v_{mn}^{ef} r_{aef}^{\ mn} = \omega_\mu^{(N+1)} r_a, \end{aligned} \tag{A.1}$$

$$\begin{aligned}\langle\Phi^{ab}_{\ j}|(\bar{H}^{(\mathrm{CCSD})}_{N,\mathrm{open}}R^{(N+1)}_{\mu})_C|\Phi\rangle &= \mathscr{A}_{ab}[-\tfrac{1}{2}\bar{h}^{je}_{ab}r_e + \bar{h}^{e}_{a}r^{\ j}_{eb} \\ &\quad -\tfrac{1}{2}\bar{h}^{j}_{m}r^{\ m}_{ab} + \tfrac{1}{4}\bar{h}^{ef}_{ab}r^{\ j}_{ef} - \bar{h}^{je}_{ma}r^{\ m}_{eb} - \tfrac{1}{2}I_m t^{mj}_{ab} \\ &\quad +\tfrac{1}{2}\bar{h}^{e}_{m}r^{\ jm}_{abe} + \tfrac{1}{2}\bar{h}^{ef}_{bm}r^{\ jm}_{aef} - \tfrac{1}{4}\bar{h}^{je}_{mn}r^{\ mn}_{abe}] \\ &= \omega^{(N+1)}_{\mu}\, r^{\ j}_{ab}, \end{aligned} \tag{A.2}$$

$$\begin{aligned}&\langle\Phi^{abc}_{\ jk}|(\bar{H}^{(\mathrm{CCSD})}_{N,\mathrm{open}}R^{(N+1)}_{\mu})_C|\Phi\rangle \\ &= \mathscr{A}_{bc}\mathscr{A}^{jk}[-\tfrac{1}{2}\bar{h}^{ke}_{bc}r^{\ j}_{ae} + \bar{h}^{ke}_{ac}r^{\ j}_{be} - \tfrac{1}{4}\bar{h}^{jk}_{ma}r^{\ m}_{bc} - \tfrac{1}{2}\bar{h}^{jk}_{mc}r^{\ m}_{ab} \\ &\quad +\tfrac{1}{4}\bar{h}^{e}_{a}r^{\ jk}_{ebc} + \tfrac{1}{2}\bar{h}^{e}_{c}r^{\ jk}_{abe} + \tfrac{1}{2}\bar{h}^{j}_{m}r^{\ km}_{abc} + \tfrac{1}{8}\bar{h}^{ef}_{bc}r^{\ jk}_{aef} \\ &\quad -\tfrac{1}{4}\bar{h}^{ef}_{ac}r^{\ jk}_{bef} + \tfrac{1}{8}\bar{h}^{jk}_{mn}r^{\ mn}_{abc} - \tfrac{1}{2}\bar{h}^{je}_{ma}r^{\ mk}_{bce} - \bar{h}^{je}_{mc}r^{\ mk}_{abe} \\ &\quad -\tfrac{1}{2}I^{\ j}_{am}t^{mk}_{bc} + I^{\ j}_{bm}t^{mk}_{ac} - \tfrac{1}{4}I^{\ f}_{bc}t^{jk}_{af} + \tfrac{1}{2}I^{\ f}_{ac}t^{jk}_{bf}] \\ &= \omega^{(N+1)}_{\mu}\, r^{\ jk}_{abc}, \end{aligned} \tag{A.3}$$

where, in addition to one- and two-body matrix elements of the similarity-transformed Hamiltonian $\bar{H}^{(\mathrm{CCSD})}_{N,\mathrm{open}}$ of the CCSD approach, $\bar{h}^{q}_{p}$ and $\bar{h}^{rs}_{pq}$, respectively, which have been defined in Table 2.1 we define the following intermediates:

$$I_m = \tfrac{1}{2}v^{ef}_{mn}r^{\ n}_{ef}, \tag{A.4}$$

$$I^{\ j}_{am} = \bar{h}^{je}_{ma}r_e + \tfrac{1}{2}\bar{h}^{ef}_{am}r^{\ j}_{ef} + \bar{h}^{je}_{mn}r^{\ n}_{ae} + \tfrac{1}{2}v^{ef}_{mn}r^{\ jn}_{aef}, \tag{A.5}$$

$$I^{\ f}_{bc} = \bar{h}^{ef}_{bc}r_e - \mathscr{A}_{bc}\bar{h}^{ef}_{cm}r^{\ m}_{be} - \tfrac{1}{2}v^{ef}_{mn}r^{\ mn}_{bec}. \tag{A.6}$$

The IP-EOMCCSD($3h$-$2p$) equations used in this work are:

$$\begin{aligned}\langle\Phi_i|(\bar{H}^{(\mathrm{CCSD})}_{N,\mathrm{open}}R^{(N-1)}_{\mu})_C|\Phi\rangle &= -\bar{h}^{i}_{m}r^{m} + \bar{h}^{e}_{m}r^{im}_{\ \ e} \\ &\quad -\tfrac{1}{2}\bar{h}^{ie}_{mn}r^{mn}_{\ \ e} + \tfrac{1}{4}v^{ef}_{mn}r^{imn}_{\ \ ef} = \omega^{(N-1)}_{\mu}\, r^{i}, \end{aligned} \tag{A.7}$$

$$\begin{aligned}\langle\Phi_{ij}^{\ b}|(\bar{H}^{(\mathrm{CCSD})}_{N,\mathrm{open}}R^{(N-1)}_{\mu})_C|\Phi\rangle &= \mathscr{A}^{ij}[-\tfrac{1}{2}\bar{h}^{ij}_{mb}r^{m} - \bar{h}^{i}_{m}r^{mj}_{\ \ b} \\ &+\tfrac{1}{2}\bar{h}^{e}_{b}r^{ij}_{\ \ e} + \tfrac{1}{4}\bar{h}^{ij}_{mn}r^{mn}_{\ \ b} - \bar{h}^{ie}_{mb}r^{mj}_{\ \ e} + \tfrac{1}{2}I^{e}t^{ij}_{eb} \\ &+\tfrac{1}{2}\bar{h}^{e}_{m}r^{ijm}_{\ \ be} + \tfrac{1}{2}\bar{h}^{je}_{mn}r^{imn}_{\ \ eb} + \tfrac{1}{4}\bar{h}^{ef}_{bm}r^{ijm}_{\ \ ef}] \\ &= \omega^{(N-1)}_{\mu}\, r^{ij}_{\ \ b}, \end{aligned} \tag{A.8}$$

$$\begin{aligned}&\langle\Phi_{ijk}^{\ bc}|(\bar{H}^{(\mathrm{CCSD})}_{N,\mathrm{open}}R^{(N-1)}_{\mu})_C|\Phi\rangle \\ &= \mathscr{A}^{jk}\mathscr{A}_{bc}[\tfrac{1}{2}\bar{h}^{jk}_{mb}r^{im}_{\ \ c} + \bar{h}^{ij}_{mb}r^{km}_{\ \ c} - \tfrac{1}{4}\bar{h}^{ie}_{bc}r^{jk}_{\ \ e} - \tfrac{1}{2}\bar{h}^{ke}_{bc}r^{ij}_{\ \ e} \\ &\quad -\tfrac{1}{4}\bar{h}^{i}_{m}r^{mjk}_{\ \ bc} - \tfrac{1}{2}\bar{h}^{k}_{m}r^{ijm}_{\ \ bc} + \tfrac{1}{2}\bar{h}^{e}_{c}r^{ijk}_{\ \ be} + \tfrac{1}{8}\bar{h}^{ef}_{bc}r^{ijk}_{\ \ ef} \\ &\quad +\tfrac{1}{8}\bar{h}^{jk}_{mn}r^{imn}_{\ \ bc} - \tfrac{1}{4}\bar{h}^{ik}_{mn}r^{jmn}_{\ \ bc} - \tfrac{1}{2}\bar{h}^{ie}_{mc}r^{mjk}_{\ \ be} - \bar{h}^{ke}_{mc}r^{ijm}_{\ \ be} \\ &\quad +\tfrac{1}{4}I^{jk}_{\ \ n}t^{in}_{bc} - \tfrac{1}{2}I^{ik}_{\ \ n}t^{jn}_{bc} + \tfrac{1}{2}I^{if}_{\ \ c}t^{jk}_{bf} + I^{kf}_{\ \ c}t^{ij}_{bf}] \\ &= \omega^{(N-1)}_{\mu}\, r^{ijk}_{\ \ bc}, \end{aligned} \tag{A.9}$$

where

$$I^{e} = -\tfrac{1}{2}v^{ef}_{mn}r^{mn}_{\ \ f}, \tag{A.10}$$

$$I^{if}_{\ \ c} = -\bar{h}^{if}_{mc}r^{m} + \tfrac{1}{2}\bar{h}^{if}_{mn}r^{mn}_{\ \ c} - \bar{h}^{ef}_{cm}r^{im}_{\ \ e} - \tfrac{1}{2}v^{ef}_{mn}r^{imn}_{\ \ ec}, \tag{A.11}$$

$$I^{jk}_{\ \ n} = -\bar{h}^{jk}_{mn}r^{m} - \mathscr{A}^{jk}\bar{h}^{ke}_{mn}r^{jm}_{\ \ e} + \tfrac{1}{2}v^{ef}_{mn}r^{jmk}_{\ \ ef}. \tag{A.12}$$

The antisymmetrizer $\mathscr{A}_{pq} = \mathscr{A}^{pq}$, which enter Eqs. (A.2), (A.3), (A.6), (A.8), (A.9), and (A.12), is defined as

$$\mathscr{A}_{pq} \equiv \mathscr{A}^{pq} = 1 - (pq), \tag{A.13}$$

respectively, with (pq) representing a transposition of two indices.

Appendix B

Derivation of the Noniterative Energy Correction Defining the Biorthogonal MMCC Theory

In this appendix, we present the derivation of the formula for the noniterative energy correction $\delta_\mu^{(A)}$ that when added to the CC/EOMCC energy $E_\mu^{(A)}$ generates the full CI energy E_μ within the biorthogonal MMCC formalism [134]. We begin the derivation by replacing the generic function Ψ in Eq. (3.24) with the exact full CI wave function Ψ_μ, which gives rise to the following expression for the full CI energy E_μ:

$$E_\mu = \frac{\langle \Psi_\mu | H R_\mu^{(A)} e^{T^{(A)}} | \Phi \rangle}{\langle \Psi_\mu | R_\mu^{(A)} e^{T^{(A)}} | \Phi \rangle}. \tag{B.1}$$

Recall that $T^{(A)}$ and $R_\mu^{(A)}$ are the cluster and linear excitation operators that define the wave function in the truncated CC/EOMCC method A. We replace the exact bra state $\langle \Psi_\mu |$ in Eq. (B.1) by the ansatz given by Eq. (3.8) and use the fact that $T^{(A)}$ and $R_\mu^{(A)}$ commute. We obtain,

$$E_\mu = \frac{\langle \Phi | \mathscr{L}_\mu \bar{H}^{(A)} R_\mu^{(A)} | \Phi \rangle}{\langle \Phi | \mathscr{L}_\mu R_\mu^{(A)} | \Phi \rangle}, \tag{B.2}$$

where $\bar{H}^{(A)}$ is the similarity-transformed Hamiltonian of CC method A defined by Eq. (2.10). By imposing the normalization condition given in Eq. (3.13), the denominator in Eq. (B.2) goes to one, leaving the following expression for the full CI energy of state μ:

$$E_\mu = \langle\Phi|\mathscr{L}_\mu \bar{H}^{(A)} R_\mu^{(A)}|\Phi\rangle. \tag{B.3}$$

At this point, we insert the resolution of the identity in the N-electron Hilbert space,

$$P + Q^{(A)} + Q^{(R)} = \mathbf{1}, \tag{B.4}$$

where

$$P = |\Phi\rangle\langle\Phi|, \tag{B.5}$$

$$Q^{(A)} = \sum_{n=1}^{m_A} \sum_{\substack{i_1 < \cdots < i_n \\ a_1 < \cdots < a_n}} |\Phi_{i_1\ldots i_n}^{a_1\ldots a_n}\rangle\langle\Phi_{i_1\ldots i_n}^{a_1\ldots a_n}|, \tag{B.6}$$

and

$$Q^{(R)} = \sum_{n=m_A+1}^{N} \sum_{\substack{i_1 < \cdots < i_n \\ a_1 < \cdots < a_n}} |\Phi_{i_1\ldots i_n}^{a_1\ldots a_n}\rangle\langle\Phi_{i_1\ldots i_n}^{a_1\ldots a_n}|, \tag{B.7}$$

in between $\mathscr{L}_\mu$ and $\bar{H}^{(A)}$, and use the decomposition of $\mathscr{L}_\mu$ into $\mathscr{L}_\mu^{(A)}$ (3.11) and $\delta\mathscr{L}_\mu^{(A)}$ (3.12) defined by Eq. (3.10), while utilizing the property that $\langle\Phi|\mathscr{L}_\mu^{(A)}Q^{(R)} = 0$. This gives

$$E_\mu = \langle\Phi|\mathscr{L}_\mu^{(A)}(P + Q^{(A)})\bar{H}^{(A)}R_\mu^{(A)}|\Phi\rangle + \langle\Phi|\delta\mathscr{L}_\mu^{(A)}Q^{(R)}\bar{H}^{(A)}R_\mu^{(A)}|\Phi\rangle. \tag{B.8}$$

Since the EOMCCSD eigenvalue problem, Eqs. (3.21) and (3.22) can be written as

$$(P + Q^{(A)})\bar{H}^{(A)}R_\mu^{(A)}|\Phi\rangle = E_\mu^{(A)}R_\mu^{(A)}|\Phi\rangle, \tag{B.9}$$

we can simplify Eq. (B.8) to

$$E_\mu = E_\mu^{(A)}\langle\Phi|\mathscr{L}_\mu^{(A)}R_\mu^{(A)}|\Phi\rangle + \langle\Phi|\delta\mathscr{L}_\mu^{(A)}Q^{(R)}\bar{H}^{(A)}R_\mu^{(A)}|\Phi\rangle. \tag{B.10}$$

Substituting the normalization condition given by Eq. (3.13) and the explicit form of $Q^{(R)}$ given by Eq. (B.7) into Eq. (B.10) yields

$$E_\mu = E_\mu^{(A)} + \sum_{n=m_A+1}^{N} \sum_{\substack{i_1<\cdots<i_n \\ a_1<\cdots<a_n}} \langle\Phi|\delta\mathscr{L}_\mu^{(A)}|\Phi_{i_1\ldots i_n}^{a_1\ldots a_n}\rangle\langle\Phi_{i_1\ldots i_n}^{a_1\ldots a_n}|\bar{H}^{(A)}R_\mu^{(A)}|\Phi\rangle. \tag{B.11}$$

We know that the $\langle\Phi|\delta\mathscr{L}_\mu^{(A)}|\Phi_{i_1\ldots i_n}^{a_1\ldots a_n}\rangle$ term that enters Eq. (B.11) simply represents the amplitudes defining the $\mathscr{L}_\mu$ deexcitation operator, $\ell_{\mu,i_1\ldots i_n}^{a_1\ldots a_n}$, with $n > m_A$. Furthermore, comparison of Eq. (B.11) with Eq. (3.6) reveals the presence of the generalized moments of the CC/EOMCC equations $\mathfrak{M}_{\mu,a_1\ldots a_n}^{i_1\ldots i_n}(m_A) = \langle\Phi_{i_1\ldots i_n}^{a_1\ldots a_n}|\bar{H}^{(A)}R_\mu^{(A)}|\Phi\rangle$. By taking advantage of these observations, along with the fact that the moments are zero for $n > N_{\mu,A}$, Eq. (B.11) can be rewritten as

$$\delta_\mu^{(A)} \equiv E_\mu - E_\mu^{(A)} = \sum_{n=m_A+1}^{N_{\mu,A}} \sum_{\substack{i_1<\cdots<i_n \\ a_1<\cdots<a_n}} \ell_{\mu,i_1\ldots i_n}^{a_1\ldots a_n}\mathfrak{M}_{\mu,a_1\ldots a_n}^{i_1\ldots i_n}(m_A) \tag{B.12}$$

which completes the derivation.

REFERENCES

[1] F. Coester, Nucl. Phys. **7**, 421 (1958).

[2] F. Coester and H. Kümmel, Nucl. Phys. **17**, 477 (1960).

[3] J. Čížek, J. Chem. Phys. **45**, 4256 (1966).

[4] J. Čížek, Adv. Chem. Phys. **14**, 35 (1969).

[5] J. Čížek and J. Paldus, Int. J. Quantum Chem. **5**, 359 (1971).

[6] K. Emrich, Nucl. Phys. A **351**, 379 (1981).

[7] J. Geertsen, M. Rittby, and R. J. Bartlett, Chem. Phys. Lett. **164**, 57 (1989).

[8] D. C. Comeau and R. J. Bartlett, Chem. Phys. Lett. **207**, 414 (1993).

[9] J. F. Stanton and R. J. Bartlett, J. Chem. Phys. **98**, 7029 (1993).

[10] P. Piecuch and R. J. Bartlett, Adv. Quantum Chem. **34**, 295 (1999).

[11] H. Nakatsuji and K. Hirao, Chem. Phys. Lett. **47**, 569 (1977).

[12] H. Nakatsuji and K. Hirao, J. Chem. Phys. **68**, 4279 (1978).

[13] H. Nakatsuji and K. Hirao, J. Chem. Phys. **68**, 4279 (1978).

[14] H. Nakatsuji, In *Computational Chemistry: Reviews of Current Trends*, edited by J. Leszczyński, vol. 2, pages 62–124 (World Scientific, Singapore, 1997), and references therein.

[15] H. Nakatsuji, Bull. Chem. Soc. Jpn. **78**, 1705 (2005), and references therein.

[16] H. Monkhorst, Int. J. Quantum Chem. Symp. **11**, 421 (1977).

[17] E. Dalgaard and H. Monkhorst, Phys. Rev. A **28**, 1217 (1983).

[18] M. Takahashi and J. Paldus, J. Chem. Phys. **85**, 1486 (1986).

[19] H. Koch and P. Jørgensen, J. Chem. Phys. **93**, 3333 (1990).

[20] H. Koch, H. J. A. Jensen, P. Jørgensen, and T. Helgaker, J. Chem. Phys. **93**, 3345 (1990).

[21] G. D. Purvis, III and R. J. Bartlett, J. Chem. Phys. **76**, 1910 (1982).

[22] J. M. Cullen and M. C. Zerner, J. Chem. Phys. **77**, 4088 (1982).

[23] G. E. Scuseria, A. C. Scheiner, T. J. Lee, J. E. Rice, and H. F. Schaefer, III, J. Chem. Phys. **86**, 2881 (1987).

[24] P. Piecuch and J. Paldus, Int. J. Quantum Chem. **36**, 429 (1989).

[25] K. Raghavachari, G. W. Trucks, J. A. Pople, and M. Head-Gordon, Chem. Phys. Lett. **102**, 479 (1989).

[26] J. Noga and R. J. Bartlett, J. Chem. Phys. **86**, 7041 (1987), **89**, 3401 (1988) [Erratum].

[27] G. E. Scuseria and H. F. Schaefer, III, Chem. Phys. Lett. **152**, 382 (1988).

[28] K. Kowalski and P. Piecuch, J. Chem. Phys. **115**, 643 (2001).

[29] K. Kowalski and P. Piecuch, Chem. Phys. Lett. **347**, 237 (2001).

[30] S. A. Kucharski, M. Włoch, M. Musiał, and R. J. Bartlett, J. Chem. Phys. **115**, 8263 (2001).

[31] S. Hirata, J. Chem. Phys. **121**, 51 (2004).

[32] C. Hampel and H.-J. Werner, J. Chem. Phys. **104**, 6286 (1996).

[33] M. Schütz and H.-J. Werner, J. Chem. Phys. **114**, 661 (2001).

[34] M. Schütz, J. Chem. Phys. **113**, 9986 (2000).

[35] M. Schütz and H.-J. Werner, Chem. Phys. Lett. **318**, 370 (2000).

[36] M. Schütz, J. Chem. Phys. **116**, 8772 (2002).

[37] M. Schütz, Phys. Chem. Chem. Phys. **4**, 3941 (2002).

[38] S. Li, J. Ma, and Y. Jian, J. Comput. Chem. **23**, 237 (2002).

[39] S. Li, J. Shen, W. Li, and Y. Jiang, J. Chem. Phys. **125**, 074109 (2006).

[40] W. Li, P. Piecuch, and J. R. Gour, In *Theory and Applications of Computational Chemistry - 2008*, edited by D.-Q. Wei and X.-J. Wang, vol. 1102 of *AIP Conference Proceedings*, pages 68–113 (American Institute of Physics, Melville, NY, 2009).

[41] W. Li, P. Piecuch, and J. R. Gour, In *Advances in the Theory of Atomic and Molecular Systems: Chemistry*, edited by P. Piecuch, J. Maruani, G. Delgado-Barrio, and S. Wilson, vol. 19 of *Progress in Theoretical Chemistry and Physics*, pages 131–195 (Springer, Dordrecht, 2009).

[42] W. Li, J. R. Gour, P. Piecuch, and S. Li, J. Chem. Phys. **131**, 114109 (2009).

[43] W. Li and P. Piecuch, J. Chem. Phys. In press; Articles ASAP; Publication Date (Web): April 7, 2010; DOI:.1021/jp100782u.

[44] W. Li and P. Piecuch, J. Phys. Chem. A Submitted.

[45] I. Lindgren and D. Mukherjee, Phys. Rep. **151**, 93 (1987).

[46] D. Mukherjee and S. Pal, Adv. Quantum Chem. **20**, 291 (1989).

[47] B. Jeziorski and H. J. Monkhorst, Phys. Rev. A **24**, 1668 (1995).

[48] K. Kowalski and P. Piecuch, Phys. Rev. A **61**, 052506 (2000).

[49] J. Paldus, P. Piecuch, L. Pylypow, and B. Jeziorski, Phys. Rev. A **47**, 2738 (1993).

[50] K. Kowalski and P. Piecuch, Int. J. Quantum Chem. **80**, 757 (2000).

[51] P. Piecuch, R. Toboła, and J. Paldus, Chem. Phys. Lett. **210**, 243 (1993).

[52] P. Piecuch and J. Paldus, Phys. Rev. A **49**, 3479 (1994).

[53] K. Jankowski, J. Paldus, I. Grabowski, and K. Kowalski, J. Chem. Phys. **97**, 7600 (1992).

[54] K. Jankowski, J. Paldus, I. Grabowski, and K. Kowalski, J. Chem. Phys. **101**, 3085 (1994).

[55] P. Piecuch and K. Kowalski, Int. J. Mol. Sci. **3**, 676 (2002).

[56] K. R. Shamsundar and S. Pal, J. Chem. Phys. **114**, 1981 (2001), **115**, 1979 (2001).

[57] P. Piecuch and J. I. Landman, Parallel Comp. **26**, 913 (2000).

[58] K. Kowalski and P. Piecuch, Chem. Phys. Lett. **334**, 89 (2001).

[59] K. Kowalski and P. Piecuch, J. Molec. Struct.: Theochem **547**, 191 (2001).

[60] K. Kowalski and P. Piecuch, Mol. Phys. **102**, 2425 (2004).

[61] X. Li and J. Paldus, J. Chem. Phys. **119**, 5320 (2003).

[62] X. Li and J. Paldus, J. Chem. Phys. **119**, 5334 (2003).

[63] X. Li and J. Paldus, J. Chem. Phys. **110**, 5346 (2003).

[64] X. Li and J. Paldus, J. Chem. Phys. **120**, 5890 (2004).

[65] M. Musiał and R. J. Bartlett, J. Chem. Phys. **121**, 1670 (2004).

[66] M. Musiał, L. Meissner, S. A. Kucharski, and R. J. Bartlett, J. Chem. Phys. **122**, 224110 (2005).

[67] M. Hanrath, J. Chem. Phys. **123**, 084102 (2005).

[68] M. Nooijen and R. J. Bartlett, J. Chem. Phys. **102**, 3629 (1995).

[69] M. Nooijen and R. J. Bartlett, J. Chem. Phys. **102**, 6735 (1995).

[70] M. Musiał and R. J. Bartlett, J. Chem. Phys. **119**, 1901 (2003).

[71] R. J. Bartlett and J. F. Stanton, In *Reviews in Computational Chemistry*, edited by K. B. Lipkowitz and D. B. Boyd, vol. 5, pages 65–169 (VCH Publishers, New York, 1994).

[72] M. Nooijen and J. G. Snijders, Int. J. Quantum Chem. Symp. **26**, 55 (1992).

[73] M. Nooijen and J. G. Snijders, Int. J. Quantum Chem. **48**, 15 (1993).

[74] J. F. Stanton and J. Gauss, J. Chem. Phys. **101**, 8938 (1994).

[75] M. Musiał, S. A. Kucharski, and R. J. Bartlett, J. Chem. Phys. **118**, 1128 (2003).

[76] M. Musiał and R. J. Bartlett, Chem. Phys. Lett. **384**, 210 (2004).

[77] Y. J. Bomble, J. C. Saeh, J. F. Stanton, P. G. Szalay, and M. Kállay, J. Chem. Phys. **122**, 154107 (2005).

[78] H. Nakatsuji and K. Hirao, Int. J. Quantum Chem. **20**, 1301 (1981).

[79] H. Nakatsuji, K. Ohta, and K. Hirao, J. Chem. Phys. **75**, 2952 (1981).

[80] H. Nakatsuji, K. Ohta, and T. Yonezawa, J. Phys. Chem. **87**, 3068 (1983).

[81] H. Nakatsuji, Chem. Phys. Lett. **177**, 331 (1991).

[82] H. Nakatsuji and M. Ehara, J. Chem. Phys. **98**, 7179 (1993).

[83] H. Nakatsuji, M. Ehara, and T. Momose, J. Chem. Phys. **100**, 5821 (1994).

[84] M. Ishida, K. Toyota, M. Ehara, H. Nakatsuji, and M. J. Frisch, J. Chem. Phys. **120**, 2593 (2004).

[85] J. R. Gour, P. Piecuch, and M. Włoch, J. Chem. Phys. **123**, 134113 (2005).

[86] J. R. Gour, P. Piecuch, and M. Włoch, Int. J. Quantum Chem. **106**, 2854 (2006).

[87] J. R. Gour and P. Piecuch, J. Chem. Phys. **125**, 234107 (2006).

[88] Y. Ohtsuka, P. Piecuch, J. R. Gour, M. Ehara, and H. Nakatsuji, J. Chem. Phys. **126**, 164111 (2007).

[89] M. Ehara, J. R. Gour, and P. Piecuch, Mol. Phys. **107**, 871 (2009).

[90] M. Kamiya and S. Hirata, J. Chem. Phys. **125**, 074111 (2006).

[91] M. Nooijen and R. J. Bartlett, J. Chem. Phys. **106**, 6441 (1997).

[92] M. Wladyslawski and M. Nooijen, In *Low-Lying Potential Energy Surfaces*, edited by M. R. Hoffmann and K. G. Dyall, vol. 828 of *ACS Symposium Series*, pages 65–92 (American Chemical Society, Washington, D.C., 2002).

[93] M. Nooijen, Int. J. Mol. Sci. **3**, 656 (2002).

[94] N. Oliphant and L. Adamowicz, J. Chem. Phys. **94**, 1229 (1991).

[95] N. Oliphant and L. Adamowicz, J. Chem. Phys. **96**, 3739 (1992).

[96] N. Oliphant and L. Adamowicz, Int. Rev. Phys. Chem. **12**, 339 (1993).

[97] P. Piecuch, N. Oliphant, and L. Adamowicz, J. Chem. Phys. **99**, 1875 (1993).

[98] P. Piecuch and L. Adamowicz, J. Chem. Phys. **100**, 5792 (1994).

[99] P. Piecuch and L. Adamowicz, Chem. Phys. Lett. **221**, 121 (1993).

[100] P. Piecuch and L. Adamowicz, J. Chem. Phys. **102**, 898 (1995).

[101] K. B. Ghose, P. Piecuch, and L. Adamowicz, J. Chem. Phys. **103**, 9331 (1995).

[102] K. B. Ghose and L. Adamowicz, J. Chem. Phys. **103**, 9324 (1995).

[103] V. Alexandrov, P. Piecuch, and L. Adamowicz, J. Chem. Phys. **102**, 3301 (1995).

[104] K. B. Ghose, P. Piecuch, S. Pal, and L. Adamowicz, J. Chem. Phys. **104**, 6582 (1996).

[105] L. Adamowicz, P. Piecuch, and K. B. Ghose, Mol. Phys. **94**, 225 (1998).

[106] P. Piecuch, S. A. Kucharski, and R. J. Bartlett, J. Chem. Phys. **110**, 6103 (1999).

[107] P. Piecuch, S. A. Kucharski, and V. Špirko, J. Chem. Phys. **111**, 6679 (1999).

[108] K. Kowalski and P. Piecuch, Chem. Phys. Lett. **344**, 165 (2001).

[109] K. Kowalski and P. Piecuch, J. Chem. Phys. **113**, 8490 (2000).

[110] K. Kowalski, S. Hirata, M. Włoch, P. Piecuch, and T. L. Windus, J. Chem. Phys. **123**, 074319 (2005).

[111] P. Piecuch, S. Hirata, K. Kowalski, P.-D. Fan, and T. L. Windus, Int. J. Quantum Chem. **106**, 79 (2006).

[112] M. Kállay and J. Gauss, J. Chem. Phys. **121**, 9257 (2004).

[113] L. Adamowicz, J.-P. Malrieu, and V. V. Ivanov, J. Chem. Phys. **112**, 10075 (2000).

[114] V. V. Ivanov and L. Adamowicz, J. Chem. Phys. **112**, 9258 (2000).

[115] D. I. Lyakh, V. V. Ivanov, and L. Adamowciz, J. Chem. Phys. **122**, 024108 (2005).

[116] J. Olsen, J. Chem. Phys. **113**, 7140 (2000).

[117] J. W. Krogh and J. Olsen, Chem. Phys. Lett. **344**, 578 (2001).

[118] M. Kállay, P. G. Szalay, and P. G. Surján, J. Chem. Phys. **117**, 980 (2002).

[119] A. Köhn and J. Olsen, J. Chem. Phys. **125**, 174110 (2006).

[120] P. Piecuch, K. Kowalski, I. S. O. Pimienta, and M. J. McGuire, Int. Rev. Phys. Chem. **21**, 527 (2002).

[121] P. Piecuch, K. Kowalski, I. S. O. Pimienta, and S. A. Kucharski, In *Low-Lying Potential Energy Surfaces*, edited by M. R. Hoffman and K. G. Dyall, vol. 828 of *ACS Symposium Series*, pages 31–64 (American Chemical Society, Washington D.C., 2002).

[122] P. Piecuch, K. Kowalski, P.-D. Fan, and I. S. O. Pimienta, In *Advanced Topics in Theoretical Chemical Physics*, edited by J. Maruani, R. Lefebvre, and E. Brändas, vol. 12 of *Progress in Theoretical Chemistry and Physics*, pages 119–206 (Kluwer, Dordrecht, 2003).

[123] P. Piecuch, K. Kowalski, I. S. O. Pimienta, P.-D. Fan, M. Lodriguito, M. J. McGuire, S. A. Kucharski, T. Kuś, and M. Musiał, Theor. Chem. Acc. **112**, 349 (2004).

[124] P.-D. Fan, K. Kowalski, and P. Piecuch, Mol. Phys. **103**, 2191 (2005).

[125] P.-D. Fan and P. Piecuch, Adv. Quantum Chem. **51**, 1 (2006).

[126] P. Piecuch and K. Kowalski, In *Computational Chemistry: Reviews of Current Trends*, edited by J. Leszczyński, vol. 5, pages 1–104 (World Scientific, Singapore, 2000).

[127] K. Kowalski and P. Piecuch, J. Chem. Phys. **113**, 18 (2000).

[128] K. Kowalski and P. Piecuch, J. Chem. Phys. **113**, 5644 (2000).

[129] K. Kowalski and P. Piecuch, J. Chem. Phys. **122**, 074107 (2005).

[130] K. Kowalski and P. Piecuch, J. Chem. Phys. **115**, 2966 (2001).

[131] K. Kowalski and P. Piecuch, J. Chem. Phys. **120**, 1715 (2004).

[132] M. Włoch, J. R. Gour, K. Kowalski, and P. Piecuch, J. Chem. Phys. **122**, 214107 (2005).

[133] P. Piecuch and M. Włoch, J. Chem. Phys. **123**, 224105 (2005).

[134] P. Piecuch, M. Włoch, J. R. Gour, and A. Kinal, Chem. Phys. Lett. **418**, 463 (2005).

[135] M. Włoch, M. D. Lodriguito, P. Piecuch, and J. R. Gour, Mol. Phys. **104**, 2149 (2006).

[136] P. Piecuch, M. Włoch, M. Lodriguito, and J. R. Gour, In *Recent Advances in the Theory of Chemical and Physical Systems*, edited by S. Wilson, J.-P. Julien, J. Maruani, E. Brändas, and G. Delgado-Barrio, vol. 15 of *Progress in Theoretical Chemistry and Physics*, pages 45–106 (Springer, Berlin, 2006).

[137] P. Piecuch, M. Włoch, and A. J. C. Varandas, In *Topics in the Theory of Chemical and Physical Systems*, edited by S. Lahmar, J. Maruani, S. Wilson, and G. Delgado-Barrio, vol. 16 of *Progress in Theoretical Chemistry and Physics*, pages 63–121 (Springer, Dordrecht, 2007).

[138] M. Włoch, J. R. Gour, and P. Piecuch, J. Phys. Chem. A **111**, 11359 (2007).

[139] P. Piecuch, J. R. Gour, and M. Włoch, Int. J. Quantum Chem. **108**, 2128 (2008).

[140] P. Piecuch, J. R. Gour, and M. Włoch, Int. J. Quantum Chem. **109**, 3268 (2009).

[141] A. Kinal and P. Piecuch, J. Phys. Chem. A **111**, 734 (2007).

[142] C. J. Cramer, M. Włoch, P. Piecuch, C. Puzzarini, and L. Gagliardi, J. Phys. Chem. A **110**, 1991 (2006).

[143] C. J. Cramer, A. Kinal, M. Włoch, P. Piecuch, and L. Gagliardi, J. Phys. Chem. A **110**, 11557 (2006).

[144] C. J. Cramer, J. R. Gour, A. Kinal, M. Włoch, P. Piecuch, A. R. M. Shahi, and L. Gagliardi, J. Phys. Chem. A **112**, 3754 (2008).

[145] P. Piecuch, M. Włoch, and A. J. C. Varandas, Theor. Chem. Acc. **120**, 59 (2008).

[146] Y. Z. Song, A. Kinal, P. J. S. B. Caridade, A. J. C. Varandas, and P. Piecuch, J. Mol. Struc.: Theochem **859**, 22 (2008).

[147] Y. B. Ge, M. S. Gordon, and P. Piecuch, J. Chem. Phys. **127**, 174106 (2007).

[148] J. J. Zheng, J. R. Gour, J. J. Lutz, M. Włoch, P. Piecuch, and D. G. Truhlar, J. Chem. Phys. **128**, 044108 (2008).

[149] Y. Zhao, O. Tishchenko, J. R. Gour, W. Li, J. J. Lutz, P. Piecuch, and D. G. Truhlar, J. Phys. Chem. A **113**, 5786 (2009).

[150] Y. B. Ge, M. S. Gordon, P. Piecuch, M. Włoch, and J. R. Gour, J. Phys. Chem. A **112**, 11873 (2008).

[151] X. Li, J. R. Gour, J. Paldus, and P. Piecuch, Chem. Phys. Lett. **461**, 321 (2008).

[152] R. B. Wiringa and S. C. Pieper, Phys. Rev. Lett. **89**, 182501 (2002).

[153] P. Navrátil and W. E. Ormand, Phys. Rev. C **68**, 034305 (2003).

[154] P. Navrátil and W. E. Ormand, Phys. Rev. Lett. **88**, 152502 (2002).

[155] P. Navrátil and E. Caurier, Phys. Rev. C **69**, 014311 (2004).

[156] S. Aroua, P. Navrátil, L. Zamick, M. S. Fayache, B. R. Barrett, J. P. Vary, and K. Heyde, Nucl. Phys. A **720**, 71 (2004).

[157] P. Piecuch, M. Włoch, J. R. Gour, D. J. Dean, M. Hjorth-Jensen, and T. Papenbrock, In *Nuclei and Mesoscopic Physics: Workshop on Nuclei and Mescopic Physics WNMP 2004*, edited by V. Zelevinsky, vol. 777 of *AIP Conference Proceedings*, pages 28–45 (American Institute of Physics, Melville, New York, 2005).

[158] D. J. Dean, M. Hjorth-Jensen, K. Kowalski, T. Papenbrock, M. Włoch, and P. Piecuch, In *Key Topics in Nuclear Structure*, edited by A. Covello, Proceedings of the 8th International Spring Seminar on Nuclear Physics, pages 147–157 (World Scientific, Singapore, 2005).

[159] D. J. Dean, M. Hjorth-Jensen, K. Kowalski, P. Piecuch, and M. Włoch, In *Condensed Matter Theories*, edited by J. W. Clark and R. M. Panoff, vol. 20 (Nova Science Publishers, 2006).

[160] K. Kowalski, D. J. Dean, M. Hjorth-Jensen, T. Papenbrock, and P. Piecuch, Phys. Rev. Lett. **92**, 132501 (2004).

[161] D. J. Dean, J. R. Gour, G. Hagen, M. Hjorth-Jensen, K. Kowalski, T. Papenbrock, P. Piecuch, and M. Włoch, Nucl. Phys. A **752**, 299 (2005).

[162] M. Włoch, D. J. Dean, J. R. Gour, P. Piecuch, M. Hjorth-Jensen, T. Papenbrock, and K. Kowalski, Eur. Phys. J. A **25**, 485 (2005).

[163] M. Włoch, J. R. Gour, P. Piecuch, D. J. Dean, M. Hjorth-Jensen, and T. Papenbrock, J. Phys. G: Nucl. Part. Phys. **31**, S1291 (2005).

[164] M. Włoch, D. J. Dean, J. R. Gour, M. Hjorth-Jensen, K. Kowalski, T. Papenbrock, and P. Piecuch, Phys. Rev. Lett. **94**, 212501 (2005).

[165] J. R. Gour, P. Piecuch, M. Hjorth-Jensen, M. Włoch, and D. J. Dean, Phys. Rev. C **74**, 024310 (2006).

[166] T. Papenbrock, D. J. Dean, J. R. Gour, G. Hagen, M. Hjorth-Jensen, P. Piecuch, and M. Włoch, Int. J. Mod. Phys. B **20**, 5338 (2006).

[167] M. Horoi, J. R. Gour, M. Włoch, M. D. Lodriguito, B. A. Brown, and P. Piecuch, Phys. Rev. Lett. **98**, 112501 (2007).

[168] J. R. Gour, M. Horoi, P. Piecuch, and B. A. Brown, Phys. Rev. Lett. **101**, 052501 (2008).

[169] R. Roth, J. R. Gour, and P. Piecuch, Phys. Rev. C **79**, 054325 (2009).

[170] R. Roth, J. R. Gour, and P. Piecuch, Phys. Lett. B **679**, 334 (2009).

[171] G. Hagen, T. Papenbrock, D. J. Dean, A. Shwenk, A. Nogga, M. Włoch, and P. Piecuch, Phys. Rev. C **76**, 034302 (2007).

[172] S. Hirata, M. Nooijen, and R. J. Bartlett, Chem. Phys. Lett. **328**, 459 (2000).

[173] M. W. Schmidt, K. K. Baldridge, J. A. Boatz, S. T. Elbert, M. S. Gordon, J. H. Jensen, S. Koseki, N. Matsunaga, K. A. Nguyen, S. J. Su, T. L. Windus, M. Dupuis, and J. A. Montgomery, J. Comput. Chem. **14**, 1347 (1993).

[174] P. Piecuch, S. A. Kucharski, K. Kowalski, and M. Musiał, Comp. Phys. Commun. **149**, 71 (2002).

[175] J. Gauss, In *Encyclopedia of Computational Chemistry*, edited by P. v. R. Schleyer, N. L. Allinger, J. G. T. Clark, P. A. Kollman, H. F. Schaefer, III, and P. R. Schreiner, vol. 1, pages 615–636 (Wiley, Chichester, U.K., 1998).

[176] K. Hirao and H. Nakatsuji, J. Comput. Phys. **45**, 246 (1982).

[177] E. R. Davidson, J. Comput. Phys. **17**, 87 (1975).

[178] T. H. Dunning, Jr., J. Chem. Phys. **90**, 1007 (1989).

[179] R. A. Kendall, T. H. Dunning, Jr., and R. J. Harrison, J. Chem. Phys. **96**, 6769 (1992).

[180] Basis sets were obtained from the Extensible Computational Chemistry Environment Basis Set Database, Version 02/25/04, as developed and distributed by the Molecular Science Computing Facility, Environmental and Molecular Sciences Laboratory which is part of the Pacific Northwest Laboratory, P.O. Box 999, Richland, Washington 99352, USA, and funded by the U.S. Department of Energy. The Pacific Northwest Laboratory is a multi-program laboratory operated by Battelle Memorial Institute for the U.S. Department of Energy under contract DE-AC06-76RLO 1830. Contact David Feller or Karen Schuchardt for further information.

[181] H.-J. Werner and P. J. Knowles, J. Chem. Phys. **89**, 5803 (1988).

[182] P. J. Knowles and H.-J. Werner, Chem. Phys. Lett. **145**, 514 (1988).

[183] H.-J. Werner, P. J. Knowles, R. Lindh, F. R. Manby, M. Schütz, P. Celani, T. Korona, G. Rauhut, R. D. Amos, A. Bernhardsson, A. Berning, D. L. Cooper, M. J. O. Deegan, A. J. Dobbyn, F. Eckert, C. Hampel, G. Hetzer, A. W. Lloyd, S. J. McNicholas, W. Meyer, M. E. Mura, A. Nicklass, P. Palmieri, R. Pitzer, U. Schumann, H. Stoll, A. J. Stone, R. Tarroni, and T. Thorsteinsson. MOLPRO, version 2006.1, a package of ab initio programs.

[184] The active-space used in the CASSCF-based MRCI(Q) calculations for CH consisted of 4 electrons and 14 orbitals (the 2σ - 7σ orbitals and the orbitals constituting the 1π - 3π and 1δ shells of CH were used). The active-space used in the CASSCF-based MRCI(Q) calculations for SH included 7 electrons and 10 orbitals (the 4σ - 9σ orbitals and the orbitals constituting the 2π - 3π shells of SH were used). In the MRCI(Q) calculations the lowest-energy core orbitals ($\sim 1s$ orbitals of C and S) were kept frozen.

[185] M. Zachwieja, J. Mol. Spectrosc. **170**, 285 (1995).

[186] T. Nelis, J. M. Brown, and K. M. Evenson, J. Chem. Phys. **92**, 4067 (1990).

[187] R. Kepa, A. Para, M. Rytel, and M. Zachwieja, J. Mol. Spectrosc. **178**, 189 (1996).

[188] K. P. Huber and G. Herzberg. *Molecular Spectra and Molecular Structure: Constants of Diatomic Molecules* (Van Nostrand Reinhold, New York), 1979).

[189] A. Kasdan, E. Herbst, and W. C. Lineberger, Chem. Phys. Lett. **31**, 78 (1975).

[190] C. E. Smith, R. A. King, and T. D. Crawford, J. Chem. Phys. **122**, 054110 (2005).

[191] A. Kalemos, A. Mavridis, and A. Metropoulos, J. Chem. Phys. **111**, 9536 (1999).

[192] K. P. Huber and G. Herzberg. *Constants of Diatomic Molecules*. NIST Chemistry WebBook, NIST Standard Reference Database Number 69, June 2005. National Institute of Standards and Technology, Gaithersburg MD, 20899, http://webbook.nist.gov.

[193] T. H. Dunning, Jr., K. A. Peterson, and A. K. Wilson, J. Chem. Phys. **114**, 9244 (2001).

[194] W. J. Hehre, R. Ditchfield, and J. A. Pople, J. Chem. Phys. **56**, 2257 (1972).

[195] P. C. Hariharan and J. A. Pople, Theor. Chim. Acta **28**, 213 (1973).

[196] A. V. Nemukhin and B. L. Grigorenko, Chem. Phys. Lett. **276**, 171 (1997).

[197] T. H. Dunning, Jr., J. Chem. Phys. **53**, 2823 (1970).

[198] T. H. Dunning, Jr. and P. J. Hay, In *Methods of Electronic Structure Theory*, edited by H. F. Schaefer, III, vol. 2, pages 1–28 (Plenum, New York, 1977).

[199] T. Nakajima and H. Nakatsuji, Chem. Phys. Lett. **79**, 280 (1997).

[200] M. Ishida, K. Toyota, M. Ehara, and H. Nakatsuji, Chem. Phys. Lett. **347**, 493 (2001).

[201] H. Nakatsuji, Chem. Phys. **75**, 425 (1983).

[202] G. Herzberg. *Molecular Spectra and Molecular Structure 1: Spectra of Diatomic Molecules* (Van Nostrand, London, 1967).

[203] S. Hirata, M. Nooijen, I. Grabowski, and R. J. Bartlett, J. Chem. Phys. **114**, 3919 (2001).

[204] T. Shiozaki, K. Hirao, and S. Hirata, J. Chem. Phys. **126**, 224106 (2007).

[205] S. Hirata, P.-D. Fan, A. A. Auer, M. Nooijen, and P. Piecuch, J. Chem. Phys. **121**, 12197 (2004).

[206] S. R. Gwaltney and M. Head-Gordon, Chem. Phys. Lett. **323**, 21 (2000).

[207] S. R. Gwaltney, C. D. Sherrill, M. Head-Gordon, and A. I. Krylov, J. Chem. Phys. **113**, 3548 (2000).

[208] S. R. Gwaltney and M. Head-Gordon, J. Chem. Phys. **115**, 2014 (2001).

[209] S. R. Gwaltney, E. F. C. Byrd, T. V. Voorhis, and M. Head-Gordon, Chem. Phys. Lett. **353**, 359 (2002).

[210] M. Lodriguito and P. Piecuch, In *Frontiers in Quantum Systems in Chemistry and Physics*, edited by S. Wilson, P. Grout, J. Maruani, G. Delgado-Barrio, and P. Piecuch, vol. 18 of *Progress in Theoretical Chemistry and Physics*, pages 67–174 (Springer, Dordrecht, 2008).

[211] M. D. Lodriguito. *Single-Reference Coupled-Cluster Methods Employing Multi-Reference Perturbation Theory*. Ph.D. thesis, Michigan State University (2007).

[212] P. Pulay, Chem. Phys. Lett. **73**, 393 (1980).

[213] P. Pulay, J Comput. Chem. **3**, 556 (1982).

[214] T. P. Hamilton and P. Pulay, J. Chem. Phys. **84**, 5728 (1986).

[215] Y. B. Ge, M. S. Gordon, F. Battaglia, and R. O. Fox, J. Phys. Chem. A **111**, 1475 (2007).

[216] Y. B. Ge, M. S. Gordon, F. Battaglia, and R. O. Fox, J. Phys. Chem. A **111**, 1462 (2007).

[217] K. Hirao, Chem. Phys. Lett. **190**, 374 (1992).

[218] K. Hirao, Chem. Phys. Lett. **196**, 397 (1992).

[219] S. Huzinaga, J. Andzelm, M. Klobukowski, E. Radzio-Andzelm, Y. Sakai, and H. Tatewaki. *Guassian Basis Sets for Molecular Calculations* (Elsevier, Amsterdam, 1984).

[220] D. E. Woon and T. H. Dunning, Jr., J. Chem. Phys. **98**, 1358 (1993).

[221] J. F. Harrison, Accts of Chem. Res. **7**, 378 (1974).

[222] I. Shavitt, Tetrahedron **41**, 1531 (1985).

[223] W. A. Goddard, III, Science **227**, 917 (1985).

[224] H. F. Schaefer, III, Science **231**, 1100 (1986).

[225] P. R. Bunker, In *Comparison of Ab Initio Quantum Chemistry with Experiment for Small Molecules*, edited by R. J. Bartlett, page 141 (Reidel, Dordrecht, The Netherlands, 1985).

[226] P. Jensen and P. R. Bunker, J. Chem. Phys. **89**, 1327 (1988).

[227] C. W. Bauschlicher and P. R. Taylor, J. Chem. Phys. **85**, 6510 (1986).

[228] D. E. Woon and T. H. Dunning, Jr., J. Chem. Phys. **103**, 4572 (1995).

[229] W. M. C. Foulkes, L. Mitas, R. J. Needs, and G. Rajagopal, Rev. Mod. Phys. **73**, 33 (2001).

[230] M. P. Nightingale and C. J. Umrigar, editors. *Quantum Monte Carlo Methods in Physics and Chemistry*, vol. 525 of *NATO ASI Ser. C* (Kluwer, Dordrecht, 1999).

[231] S. Zhang and H. Krakauer, Phys. Rev. Lett. **90**, 136401 (2003).

[232] P. M. Zimmerman, J. Toulouse, Z. Zhang, C. B. Musgrave, and C. J. Umrigar, J. Chem. Phys. **131**, 124103 (2009).

[233] J. Toulouse and C. J. Umrigar, J. Chem. Phys. **126**, 084102 (2007).

[234] C. J. Umrigar, J. Toulouse, C. Filippi, S. Sorella, and R. G. Hennig, Phys. Rev. Lett. **98**, 110201 (2007).

[235] J. Toulouse and C. J. Umrigar, J. Chem. Phys. **128**, 174101 (2008).

[236] C. D. Sherrill, M. L. Leininger, T. J. V. Huis, and H. F. Schaefer, III, J. Chem. Phys. **108**, 1040 (1998).

[237] T. H. Dunning, Jr., J. Chem. Phys. **55**, 716 (1971).

[238] M. J. Frisch, G. W. Trucks, H. B. Schlegel, G. E. Scuseria, M. A. Robb, J. R. Cheeseman, V. G. Zakrzewki, J. A. Montgomery, Jr., R. E. Stratmann, J. C. Burant, S. Dapprich, J. M. Millam, A. D. Daniels, K. N. Kudin, M. C. Strain, O. Farkas, J. Tomasi, V. Barone, M. Cossi, , R. Cammi, B. Mennucci, C. Pomelli, C. Adamo, S. Clifford, J. Ochterski, G. A. Petersson, P. Y. Ayala, Q. Cui, K. Morokuma, K. Malick, A. D. Rabuck, K. Raghavachari, J. B. Foresman, J. Cioslowski, J. V. Ortiz, B. B. Stefanov, G. Liu, A. Liashenko, P. Piskorz, I. Komaromi, , R. Gomperts, R. L. Martin, D. J. Fox, T. Keith, M. A. Al-Laham, C. Peng, C. Y. Peng, A. Nanayakkara, C. Gonazalez, M. Challacombe, P. M. W. Gill, B. Johnson, W. Chen, M. W. W. J. L. Andres, M. Head-Gordon, E. S. Replogle, and J. A. Pople. *GAUSSIAN*98, revision A.5 (Gaussian Inc., Pittsburgh, PA, 1998).

[239] J. D. Watts, In *Computational Chemistry: Reviews of Current Trends*, edited by J. Leszczynski, vol. 7, pages 65–169 (World Scientific, Singapore, 2002).

[240] X. Li and J. Paldus, J. Chem. Phys. **107**, 6257 (1997).

[241] J. Paldus and J. Planelles, Theor. Chem. Acta **89**, 13 (1994).

[242] X. Li, G. Peris, J. Planelles, F. Rajadell, and J. Paldus, J. Chem. Phys. **107**, 90 (1997).

[243] X. Li and J. Paldus, J. Chem. Phys. **124**, 174101 (2006).

[244] X. Li and J. Paldus, Chem. Phys. Lett. **431**, 179 (2006).

[245] H. Bredohl, I. Dubois, Y. Houbrechts, and P. Nzohabonayo, J. Mol. Spectrosc. **112**, 430 (1985).

[246] M. Lorenz, J. Agreiter, A. M. Smith, and V. E. Bondybey, J. Chem. Phys. **104**, 3143 (1996).

[247] R. S. Ram and P. F. Bernath, J. Mol. Spectrosc. **180**, 414 (1996).

[248] K. R. Asmis, T. R. Taylor, and D. M. Neumark, Chem. Phys. Lett. **295**, 75 (1998).

[249] R. B. Wiringa, V. G. J. Stoks, and R. Schiavilla, Phys. Rev. C **51**, 38 (1995).

[250] R. Machleidt, Phys. Rev. C **63**, 024001 (2001).

[251] S. Weinberg, Phys. Lett. **B251**, 288 (1990).

[252] U. van Kolck, Prog. Part. Nucl. Phys. **43**, 337 (1999).

[253] D. R. Entem and R. Machleidt, Phys. Rev. Lett. B **524**, 93 (2002).

[254] D. R. Entem and R. Machleidt, Phys. Rev. C **68**, 41001 (2003).

[255] M. Hjorth-Jensen, T. T. S. Kuo, and E. Osnes, Phys. Rep. **261**, 125 (1995).

[256] D. J. Dean and M. Hjorth-Jensen, Phys. Rev. C **69**, 054320 (2004).

[257] R. Roth, H. Hergert, P. Papakonstantinou, T. Neff, and H. Feldmeier, Phys. Rev. C **72**, 034002 (2005).

[258] R. Roth, T. Neff, H. Hergert, and H. Feldmeier, Nucl. Phys. A **745**, 3 (2004).

[259] H. Feldmeier, T. Neff, R. Roth, and J. Schnack, Nucl. Phys. A **632**, 61 (1998).

[260] T. Neff and H. Feldmeier, Nucl. Phys. A **713**, 311 (2002).

[261] E. K. Warburton and B. A. Brown, Phys. Rev. C **46**, 923 (1992).

[262] G. Audi, A. H. Wapstra, and C. Thibault, Nucl. Phys. A **729**, 337 (2003).

[263] R. B. Firestone, V. S. Shirley, C. M. Baglin, S. Y. F. Chu, and J. Zipkin. *Table of Isotopes, 8th Ed.* (Wiley Interscience, New York, 1996).

[264] R. Roth and P. Navratil, Phys. Rev. Lett. **99**, 092501 (2007).

[265] P. J. Bruna and S. D. Peyerimhoff, Adv. Chem. Phys. **67**, 1 (1987).

[266] J. Paldus, In *New Horizons in Quantum Chemistry*, edited by P.-O. Löwdin and B. Pullman, pages 31–60 (Reidel, Dordrecht, 1983).

[267] R. Buenker and S. Peyerimhoff, In *New Horizons in Quantum Chemistry*, edited by P.-O. Löwdin and B. Pullman, pages 183–220 (Reidel, Dordrecht, 1983).

[268] P. J. Bruna, S. D. Peyerimhoff, and R. J. Buenker, Chem. Phys. Lett. **72**, 278 (1980).

[269] K. Jankowski, L. Meissner, and J. Wasilewksi, Int. J. Quantum Chem. **28**, 931 (1985).

[270] M. Honma, T. Otsuka, B. A. Brown, and T. Mizusaki, Eur. Phys. Jour. A **25**, 499 (2005).

[271] M. Honma, T. Otsuka, B. A. Brown, and T. Mizusaki, Phys. Rev. C **65**, 061301 (2002).

[272] M. Honma, T. Otsuka, B. A. Brown, and T. Mizusaki, Phys. Rev. C **69**, 034335 (2004).